

ResQProp

DSE Group 28 - Affordable eVTOL Ambulance

Final Report

Author Name:

Leonhard Justus Balster

Mihai Alexandru Coman

Qingyi Chen

Gaia Ejlal Moghari

Noam Hendriks

Zian Liu

Job de Steenhuijsen Piters

Olivers Vasilevskis

Shilang Wang

Patrycja Wiczorowska

Student Number:

5737354

5706734

5713943

5466687

5764327

5750334

5736021

5739039

5689015

5764793

Delft University of Technology



[This page is intentionally left blank.]

Preface

This report builds on the conceptual design developed in the Midterm Report, as well as the project strategy and design ambition outlined in the Project Plan and the Baseline Report. It represents the culmination of ten weeks of dedicated effort by a design team composed of ten Bachelor students in Aerospace Engineering at Delft University of Technology.

The successful completion of this project would not have been possible without the exceptional support from the Aerospace Engineering faculty staff. We extend our heartfelt thanks to the AE3200 teaching assistants, and the members of the OSCC, who played a crucial role in organizing this year's spring Design Synthesis Exercise. Special gratitude is owed to our tutors, Prof.Dr.ir. Fulvio Scarano and Prof.Dr. Stefan Hickel, and our project coaches, Till Blaha and Ehshan ul-Haq, who gave essential insights and paved the way for the team to be creative and deliver a meaningful project.

Lastly the team is very grateful for the external experts and professors for their extensive knowledge and guidance during the project, namely Dr.ir. Saullo Castro, Dr.ir. Marilena Pavel, Dr.ir. Calvin Rans and Ir. Joris Melkert. Additionally, special thanks go to Frans Rutten for providing the team with his knowledge and expertise on emergency medical procedures, and to Dr. Marco Stuhlpfarrer for the mentorship offered on eVTOL design from industry.

We hope this design project will help push forward the boundaries of technology and emergency services of today, such that more people in need can receive assistance in difficult situations.

DSE Group 28

Supervisors:

Prof.dr. Fulvio Scarano
Prof.dr. Stefan Hickel

Coaches:

PhD Candidate Till Blaha
PhD Candidate Ehshan ul-Haq

External Expert:

Dr. Marco Stuhlpfarrer

Executive Overview

Project Definition

Emergency missions are performed in most countries by either using an ambulance, an emergency helicopter, or a combination. The emergency helicopter provides a fast and versatile option for reaching the location of an emergency, as it does not depend so much on the state of the road and can fly over and around mountains and valleys. The helicopter is mostly used for exceptional cases and is not scaled to replace ground ambulances. This provides a gap for the eVTOL ambulance, which is to make a scalable system by being low-cost and socially accepted, and to be faster than on road infrastructure relying systems. This is stated by the mission need statement, which afterwards provided a project objective statement:

Mission Need Statement: Design an affordable eVTOL ambulance that provides emergency medical assistance for small and medium communities in Central Europe and is a scalable competitor to emergency helicopters, and a substitute for ground-based ambulances.

Project Objective Statement: Design an eVTOL ambulance capable of transporting two medical staff to the site, as well as having the ability to transport the patient back to the hospital.

These statements functioned as the red line through this project, and decisions were made adhering to these statements.

Market Analysis

A market analysis has been conducted that analyzed regions in Europe to find regions with a high GDP per capita where, annually, a high number of emergencies are not reached within 15 minutes. Of all of these regions, Bavaria has been selected as a potential beachhead market since it has a high GDP per capita and achievable range requirements. A geographic analysis of the region showed that a potential eVTOL system requires an operational range of 50 km with a cruise velocity of 200 km/h if stationed directly at the hospitals

Competition is fueled by a high projected compound annual growth rate (CAGR) of 9.8% of the ambulance services market in Germany until 2030. Potential competitors of an eVTOL ambulance system include established emergency medical service systems, such as ground ambulances and helicopters, but also existing eVTOL systems. Ambulances offer a relatively low mission cost and easy accessibility, but are highly dependent on road and traffic risk, and must travel further due to being constrained to roads. Helicopters are not as dependent on infrastructure and can access remote and difficult terrains quickly. Their issue is that they are expensive to operate and have high maintenance demands. eVTOL systems have the potential to combine the benefits of both systems, but cause their challenges, such as regulatory compliance challenges, high battery degradation rates, and limited flight range. The SWOT analysis of an existing eVTOL ambulance concept is shown in Table 1

Table 1: SWOT analysis of Volocity (eVTOL ambulance)

	Helpful	Harmful
Internal	<ul style="list-style-type: none">• Low noise emission• Low operational cost• Short emergency response time	<ul style="list-style-type: none">• Limited flight range• Requires new infrastructures (charging)
External	<ul style="list-style-type: none">• Growth of urban air mobility (UAM)• Increasing eVTOL investments• Future autonomous possibilities	<ul style="list-style-type: none">• Regulatory compliance challenges• High battery degradation rates

Mission Profile and Operations

In addition to the gap found for the mission need statement, it was discovered that the eVTOL ambulance can simplify the operations process from emergency call to bringing the patient to the hospital. Figure 1 presents the sequential phases of operation, from mission start to system readiness for the next deployment.

The process is divided into four primary functional stages: Mission Launch, Patient Pick-up and Transport, Landing and Handoff, and Vehicle Recharge.

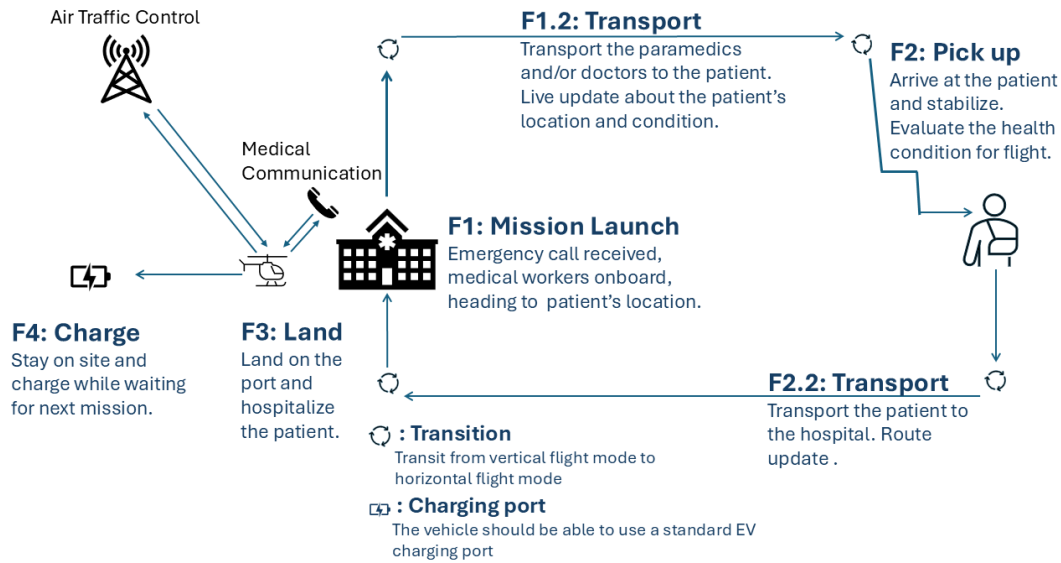


Figure 1: Operation Diagram

The mission profile and the respective time for each mission phase are illustrated by Figure 2. The same one-way flight profile is performed again for the return leg, which was the most critical scenario and was closely considered for energy budgeting.

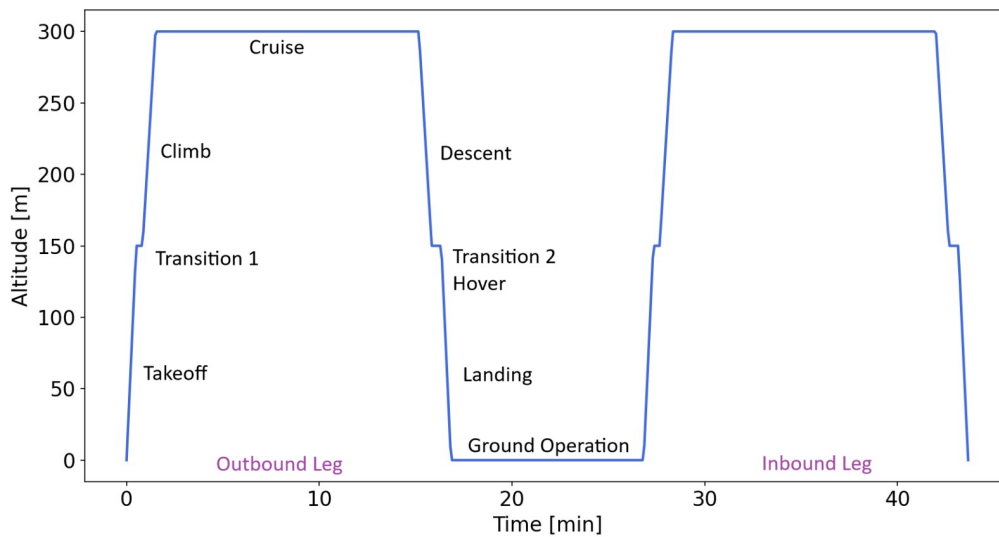


Figure 2: Standard mission profile

In the mission, the complete flight phase, the two legs combined, takes 34 minutes and including the ground operation, it takes 44 minutes. For ease of use and quick response, it was decided that the emergency vehicle would be stationed at hospitals, or when this is not possible, the necessary elements will be accommodated near the hospital. For this type of mission, multiple components are necessary:

1. Landing pad: Due to the nature of the vehicle, the pad will not need to be as big and resilient as one used for helicopters, and ideally, normal road pavement can be used.
2. eVTOL hangar: To facilitate maintenance and reduce the impact from rain, snow, or other natural phenomena, a dedicated hangar for storing the vehicle has to be used.

3. Power infrastructure: To power up the batteries, a standard connection to the power grid can be equipped with a DC charger or existing EV chargers can be used.
4. Handling equipment: The landing gear selected uses wheels, which provides a trivial way to move the eVTOL wherever needed.

Stakeholder Requirements

The stakeholder requirements are the top level requirements of the system. They have been further broken down into subsystem requirements later during the systems engineering process. The stakeholder requirements for ResQProp are given in Table 2.

Table 2: *Stakeholder Requirements*

Requirement ID	Requirement
REQ-STK-01	The mass of the payload shall be no less than 400 kg.
REQ-STK-02	The indicative maximum footprint on the ground shall not exceed a diameter of 12 m.
REQ-STK-03	The aircraft shall respond to an emergency in 50km radius in 15 minutes from its base.
REQ-STK-04	The new vehicle shall respect European noise emissions over urban areas.
REQ-STK-05	The cabin noise level shall not exceed 60 dB.
REQ-STK-06	The vehicle shall have electric power autonomy for 100 km operation radius with take-off and landing at 2 sites, plus a reasonable reserve.
REQ-STK-07	The vehicle shall be able to operate at 5m distance from people and 3m from any object.
REQ-STK-08	The aircraft shall be able to fly in windy conditions, up to 8 Beaufort, also in case of rain or snow.
REQ-STK-09	The vehicle shall be able to land and take-off at unprepared and uneven sites.
REQ-STK-10	The propulsive system shall offer redundancies in case of failure of any main component.
REQ-STK-11	The vehicle shall be able to transport the patient safely to a hospital.
REQ-STK-12	The main structure shall have a lifetime equal or longer than a helicopter ambulance.
REQ-STK-13	If battery-electric propulsion is chosen, then the battery should be easily replaceable.
REQ-STK-14	The main structure shall be recyclable.
REQ-STK-15	The cost of the vehicle shall not exceed 2M Euros.
REQ-STK-16	The cost of operation, including distributed hubs and vehicles, shall not exceed 1000 Euro/flight.
REQ-STK-17	The aircraft shall comply with EASA regulations.
REQ-STK-18	The aircraft shall be able to fly in mountainous regions.
REQ-STK-19	The aircraft shall be designed to allow efficient and straightforward maintenance operations.
REQ-STK-20	The aircraft shall be able to fly during day-time and night-time.
REQ-STK-21	The aircraft shall be capable of rapid deployment to respond to emergencies.

Concept Design

It was found that with the required range, a wing was needed for lift generation. Additionally, to ensure a low-complexity infrastructure, it was decided to power the VTOL electrically using batteries. After a trade-off was performed considering the performance of the concepts for five diverging criteria, it was found that a tilting wing eVTOL was optimal to perform the mission as shown by Figure 3. Later, it was found that a wing with a downward kink, called a gull wing, was beneficial for pitch control because it spaces out the engines.

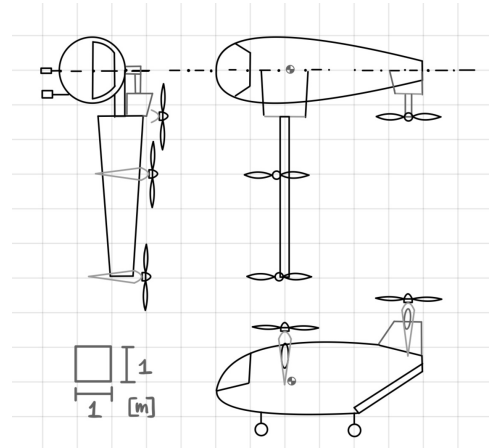


Figure 3: Concept 3: TiltWing

Subsystem Design

Aerodynamics

For aerodynamics, first, the wing is designed by optimizing for an elliptical lift distribution and changing the airfoil type, chord, and twist angle as a consequence. Also, the stall behavior of the wing is considered to allow for gradual stall starting from the wing root. This resulted in an optimized wing whose lift-over-drag value is more than 25% higher than the non-optimized older wing design. The performance characteristics of the wing are shown in Figure 3. Note that the interference between the wing and other components of the aircraft is not taken into account here.

Table 3: Performance of optimized wing design

Specification	After optimization
Maximum C_L [-]	1.92
Cruise L/D [-]	24.8
Cruise AoA [deg]	6.5
Oswald factor [-]	0.748
Cruise C_m [-]	0.115

After the wing was designed, the tail was sized to make sure the aircraft is statically stable in cruise flight. The decision was made to design it as a T-tail to have the least interference with the fuselage, wing, and propellers. It is found that the horizontal tail size should be at least 28% of the wing size to achieve both longitudinal stability and controllability. Additionally, the minimum vertical tail size is 22% of the wing size to achieve static directional stability. The final wing platform design including the aileron sizing is visualized by Figure 4.

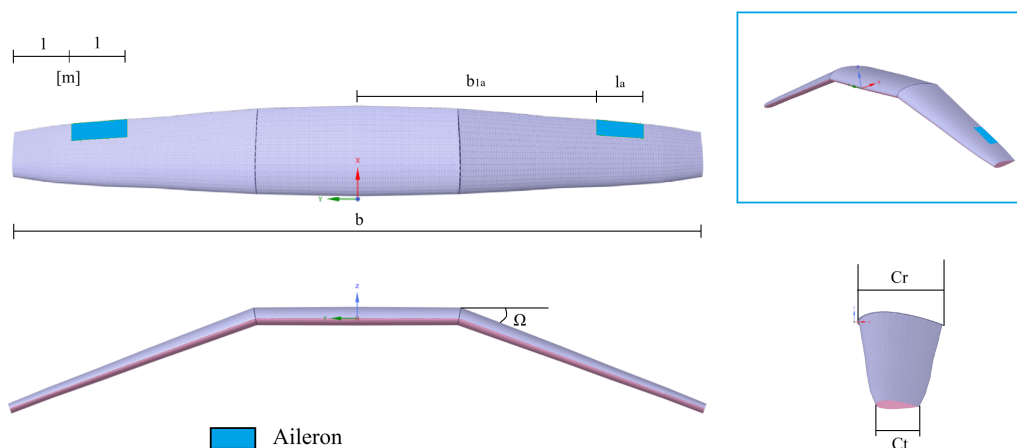


Figure 4: Final wing platform design

Propulsion and Power

The most critical aspect of the design of the propulsion system was the battery choice. Available batteries are always a compromise between power and energy density and their durability. Semi-Solid State NMC811 battery cells have been chosen since they offer sufficient power and energy density while having an acceptable durability.

Cruise Current [A]	Takeoff Current [A]	Nom. Voltage [V]	Capacity [kWh]	Charging Time [min]
216	746	800	155	31

Table 4: HV battery parameters.

The batteries will be configured such that ResQProp is compatible with the existing 400V EV charging structure. Furthermore, a thermal control system will ensure adequate performance over a broad range of ambient temperatures ranging from -20 to $+40^{\circ}\text{C}$.

The propellers have not been optimized for hover or cruise but rather over the full flight profile and thus offering a good compromise between hover and cruise performance. Variable pitch propellers are used to allow them to operate more optimally in the different flight conditions and to increase the responsiveness of their thrust. The propeller size is designed to ensure that the propeller tips travel outside of the transonic region to reduce noise.

Control and Avionics

A Simulink model has been developed to represent the system dynamics throughout hover, transition, and cruise conditions. A control system has been created that allows ResQProp to be controllable throughout all of its mission stages, including transition and potential wind gust rejections in hover flight.

In addition to that, it has been considered how different failure modes impact the controllability of the vehicle and what control strategies could be used to ensure a safe landing in these cases. Furthermore, a suite of sensors and data processing devices has been presented that will allow the control system to run smoothly by providing it with the required measurements at the required data rate and with a sufficient amount of redundancy.

Structures and Materials

After optimizing the wingbox materials selection process for low-cost, lightweight, and good strength and deflection performance, it was found that Al2024-T6 was the best performing material and was thus selected. Also the fuselage frame is made from this material, in contrary to the fuselage skin which is selected to be produced using the cheaper material Al6061-T6.

After a load analysis was performed the wingbox design was optimized by optimizing its thickness to obtain a lightweight wingbox design that is within the requirements. The wingbox is designed as a cone with a downwards kink corresponding with the wing. The symmetrical circular cross-section of this wingbox is

beneficial considering the rotating wing. The resulting optimized thickness for the wingbox and the final thickness that was decided upon are visualized by Figure 5.

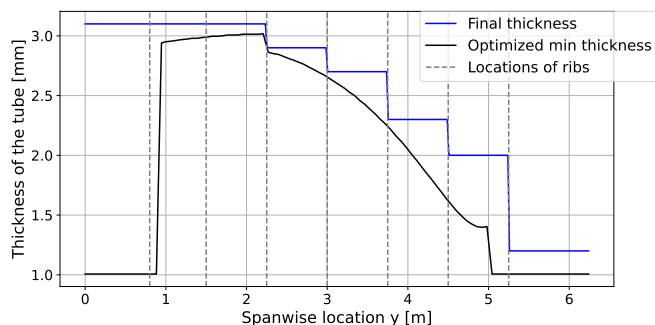


Figure 5: Cone thickness at each interval compared to optimal thickness distribution for all the load cases

The ResQProp can transition between vertical and horizontal flight by rotating its wing. This requires a hinge mechanism on the wingbox, which is designed to be actuated by a worm and helical gear combination. As the wingbox is designed as a tube it can be directly rotated around its axis. The hinge assembly is visualized by Figure 6. The hinge is capable of withstanding a torque of 30 kNm, it can rotate the wingbox by 45° in one second and the complete mechanism weighs 67 kilograms. The conical shape of the tube can be manufactured using a combination of rolling the metal sheet and stir welding.

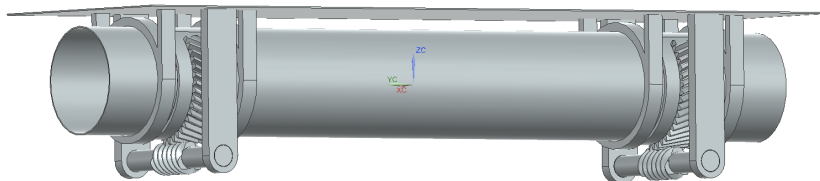


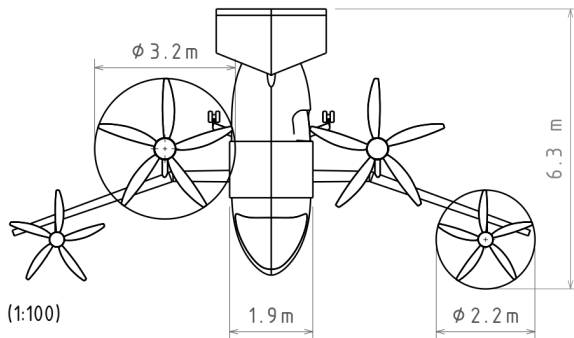
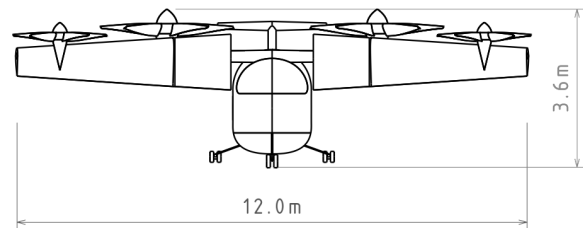
Figure 6: Hinge assembly

Final Design

The final design of ResQProp is based on a tiltwing concept with a novel wing design featuring an anhedral layout offering control capabilities that are similar to those of a multi rotor. The design of the aircraft is heavily requirement driven to allow it to fulfill both ground footprint requirements and offer sufficient payload space. The most important design aspects can be found in Table 5. The final design of the vehicle is shown in Figure 7. The most important dimensions can be found in Figure 8 and Figure 9.

Table 5: Most important design aspects

Parameter	Value
MTOW [kg]	2600
Payload mass [kg]	456
Maximum mission radius (round trip) [km]	60
Cruise speed [km/h]	200
Rate of climb [m/s]	5
Cabin volume [m ³]	11
Ground footprint [m]	12 x 6
Battery capacity [kWh]	155

**Figure 7:** ResQProp in cruise flight configuration**Figure 8:** Dimensioned top view of the final design**Figure 9:** Dimensioned front view of the final design

Risk Management

To assess possible incidents that might occur during the operational life of the product, a risk management analysis was performed. By considering all possible threats, we can effectively prevent or mitigate the risks on time. After identifying the risks, the team established mitigation strategies, which are actions that prevent the risks from occurring, as well as contingency strategies, ensuring that if a risk does occur, its impact is minimized. Mitigation strategies may involve important design considerations or highlight the need for maintenance and testing. These actions moved the risks outside of the high risk zone by decreasing the probability of their occurrence or their impact on the system or mission.

Sustainability

Sustainability of ResQProp has been assessed using the 3P-framework, which combines profit, planet and people. It has been expanded including strategic risks as an additional measure of sustainability.

As shown in Figure 10, ResQProp falls between ambulances and helicopters for most sustainability measures. The most significant sustainability improvement over helicopters is achieved in terms of greenhouse gas emissions, where the ResQProp system offers an 85% reduction.

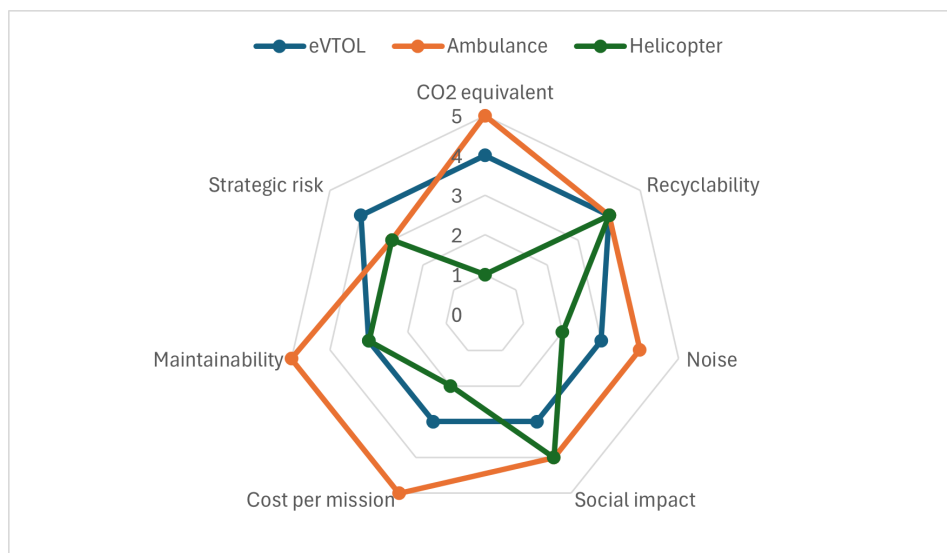


Figure 10: Sustainability spider plot

Cost Breakdown

A cost analysis was performed to break down the costs for the subsystems and to find the total program cost, the direct operational cost, and the retail price, followed by the return on investment. First, the cost was estimated for the subsystems as shown in Table 14.6.

Table 6: Estimated eVTOL subsystem costs (in 2019 EUR)

Subsystem	Estimated Cost (€)
Propulsion System	390,000
Energy Storage (Battery)	136,500
Avionics and Flight Control	150,000
Airframe Structure	287,000
Total Estimated Cost	965,000

The total cost of ResQProp is the sum of all subsystem costs and the RDT&E cost divided by the total production quantity. With a 5% margin included, the estimated unit cost is approximately €1.9 million .

The operational cost for the ResQProp is estimated to be around 910 EUR in 2025; this number means the cost of one flight. Lastly, the profitability of the eVTOL was established. For this, comparisons were made using the prices of existing medical helicopters, and the government budget for hospital infrastructure in Bavaria was considered. The final retail price of the ResQProp is set at 2.5 million (2025 EUR). With this retail price, the return on investment will be 32%, which indicates a highly favorable financial outcome for the eVTOL investment.

Future steps

Until ResQProp can be taken to market, certain additional steps have to be performed in the future. These include finalizing the detailed eVTOL design until Q2 2026, Manufacturing prototypes until Q4 2026, Testing them until Q2 2028 and certifying the design until Q2 of 2034. These steps will prepare the system for mass production and market entry in 2036.

Contents

Executive Overview	iv		
List of Symbols	xiii		
1 Introduction	1		
2 Market Analysis	2		
2.1 Identification and Analysis of Market Gap	2		
2.2 Competitors	4		
2.3 Cost Requirements	6		
3 Mission Profile and Operations	8		
3.1 Mission Objective	8		
3.2 Mission Profile	9		
3.3 Architecture Management	10		
3.4 Communications	11		
3.5 Functional Breakdown and Flow	11		
4 Sustainable Development Strategy	17		
4.1 Strategic Goals	17		
4.2 Embedding Sustainability in Project Phases	18		
5 Concept Design	19		
5.1 Concepts for Design	19		
5.2 Concept Trade-Off	20		
6 Concept Sizing	21		
6.1 Internal Design	21		
6.2 External Layout	25		
6.3 Technical Resource Allocations	28		
7 Aerodynamics	33		
7.1 Wing Design and Optimization	33		
7.2 Tail Sizing	36		
7.3 Control Surfaces Sizing	38		
7.4 Specifications	38		
7.5 Sensitivity analysis	40		
8 Propulsion and Power	41		
8.1 Required Power and Energy	41		
8.2 List of Components	42		
8.3 Propulsion Motors	43		
8.4 High Voltage Batteries	44		
8.5 Propeller Design	49		
9 Control and Avionics	54		
		9.1 Aircraft Model	55
		9.2 Motor Mixer	58
		9.3 Hover Control	58
		9.4 Cruise Control	59
		9.5 Transition	60
		9.6 Gust Rejection	62
		9.7 Controller Robustness	63
		9.8 Critical View on the Model	63
		9.9 Future considerations	63
		9.10 Failure	64
		9.11 Avionics	65
		10 Structures and Materials	66
		10.1 Material Selection	66
		10.2 Load Analysis	69
		10.3 Wingbox Design	73
		10.4 Hinge Design	78
		10.5 Landing Gear	81
		10.6 Crash Structure	84
		11 Final Design	85
		11.1 Final Design Overview	85
		11.2 Mass and Power Breakdown	85
		11.3 Performance Analysis	89
		11.4 Computational Fluid Dynamics	91
		12 Risk Management	93
		12.1 RAMS	93
		12.2 Technical Risks	95
		13 Sustainability Assessment	103
		13.1 Greenhouse Gas Emissions	103
		13.2 Strategic Goals Assessment	103
		13.3 Strategic Risks	104
		13.4 Sustainability Spider Map	105
		14 Cost Breakdown	106
		14.1 eVTOL Development and Procurement Cost	106
		14.2 eVTOL Direct Operational Costs	108
		14.3 Return on Investment	108
		14.4 Sensitivity Analysis	109
		15 Verification and Validation	110
		15.1 Tools and Models for V&V	110
		15.2 Compliance matrix	113
		15.3 Requirement Verification and Validation	116
		15.4 Verification and Validation of the Design	125
		16 Project Production and Development	127
		16.1 Project Design and Development Logic	127
		16.2 Production Plan	127
		17 Conclusion	132
		Bibliography	133

Nomenclature

Abbreviations

(e)VTOL (electric) Vertical Takeoff and Landing
AERO Aerodynamics
BJB Battery Junction Boxes
BMU Battery Management Units
CDTM Design To Maintain Coefficient
CFD Computational Fluid Dynamics
CFRP Carbon Fiber Reinforced Polymer
CG Center of Gravity
CMU Cell Monitoring Units
CO2 Carbon Dioxide
CTL Control
EASA European Union Aviation Safety Agency
EMI Electromagnetic Interference
EoM Equations of Motion
EU European Union
EV Electric Vehicle
FBD Functional Breakdown Diagram
FFD Functional Flow Diagram
FH Flight Hour
GPS Global Positioning System
HV High voltage
HVAC Heating, Ventilation, and Air Conditioning

IA Age Index
IC Complexity Index
IMU Inertial Measurement Unit
IR Role Index
IRM Maintenance Role Index
LV Low voltage
MEW Maximum Empty Weight
MMH Maintenance Man Hour
MTBF Mean Time Between Failures
MTOW Maximum Takeoff Weight
NDT Non-Destructive Testing
OPS Operations
PID Proportional Integral Derivative
PIV Particle Image Velocimetry
PPL Propulsion
PWM Pulse Width Modulation
RL Safety Role Index
SM Safety Margin
SPL Sound Pressure Level
STR Structures
TBD To Be Determined
TRL Technology Readiness Level
UAM Urban Air Mobility
UHF Ultra High Frequency
USD United States Dollar
V&V Verification & Validation

Introduction

In this report, an eVTOL solution will be presented that fills the gap between ground-based ambulances and emergency helicopters in Central Europe. Focusing on rural communities in Bavaria, Germany, major challenges for the healthcare system can be identified. These include arriving at the site of a medical emergency within 15 minutes and transporting critical patients to the nearest capable hospital quickly. In the current emergency architecture, ground ambulances and medical helicopters are used for medical emergencies in remote villages in Germany. This creates a gap in the market, as medical helicopters are expensive, cramped, and loud, both within the cabin and in the residential districts through which they operate. Cheaper ground ambulances, on the other hand, are slow and rely heavily on the presence of direct and unclogged roads. The ResQProp will offer the same response time as a medical helicopter, due to its ability to cruise at speeds of 200 km/h. It will be capable of transporting two medically trained staff to the site, as well as having the ability to transport the patient back to the hospital. Furthermore, it will be able to operate in a service radius of 60 km from the hospital where it is stationed, allowing it to cover the whole state of Bavaria. Its operational cost will be comparable to ground ambulances, therefore creating competition in the market.

From the baseline report, the mission scope, stakeholder needs, system-level requirements, and concept generation for an affordable eVTOL ambulance in Central Europe were defined. This was followed by a midterm report, which transitioned from conceptual understanding to a detailed design exploration. Multiple vehicle configurations were evaluated, and by comparing the concepts through both quantitative and qualitative criteria, was able to converge to one single design configuration to serve the purpose of this mission.

This report will present a detailed design of the ResQProp, as well as a complete picture of the market it aims to operate in and future development considerations. It will begin by first researching the market gap ResQProp is designed to fill, as will be presented in Chapter 2. From the market analysis an understanding what the eVTOL needs to provide follows. Then a mission profile and operations aspects such as infrastructure compatibility and communications, will be addressed in Chapter 3. In Chapter 4, a sustainable development strategy will be presented. Subsequently, the design concepts and the final decision from the midterm report will shortly be summarized in Chapter 5.

After this, the design of the ResQProp will truly commence. First in Chapter 6, the internal and external layout of the eVTOL, along with an overview of the technical resource allocations, will be presented. Chapter 7 will explore the wing design, tail design, and surface controls. Chapter 8, will go on to present the choices made in terms of powertrain systems, how resources are allocated, and a detailed propeller design. This is followed by Chapter 9, which will explore the controls side of the operations, delving deep into the different controllers required for cruise, transition, and hover flight. Chapter 10 will explore the material selection for different subsystems for eVTOL, design the wingbox of the wing, present a hinge design, and a conceptualize the landing gear. To wrap up the detailed design, Chapter 11 will bring all the subsystems together to present a complete picture of the ResQProp.

The detailed design is followed by a thorough risk assessment in Chapter 12, followed by the sustainability assessment of the project in Chapter 13. In Chapter 14, a cost breakdown is presented. Chapter 15 reports on the verification and validation of the design, as well as an outline of which requirements have been satisfied. Lastly, the project design and development logic, followed by the production plan, which includes manufacturing, assembly, and integration, is presented in Chapter 16.

2

Market Analysis

In this section, a market analysis will be conducted, starting from the broader European market and narrowing down to Germany. The market gaps will be identified in Section 2.1 and current competitors will be analyzed in Section 2.2, along with a SWOT analysis (Strengths, Weaknesses, Opportunities, and Threats) used to develop a comprehensive understanding of the competitive landscape. Then, a detailed cost and function analysis will be performed to guarantee competitiveness with air and ground ambulances in Section 2.3.

2.1. Identification and Analysis of Market Gap

In order to create a viable product, a market gap must be identified. This not only helps with placing the project in the financial landscape, but also provides the team with requirements and constraints that a useful design should meet. From the mission need statement, it follows that the design should be able to reach more places than a ground ambulance while being cheaper than a helicopter. These current capabilities can be illustrated by emergency response time statistics shown in Figure 2.1.

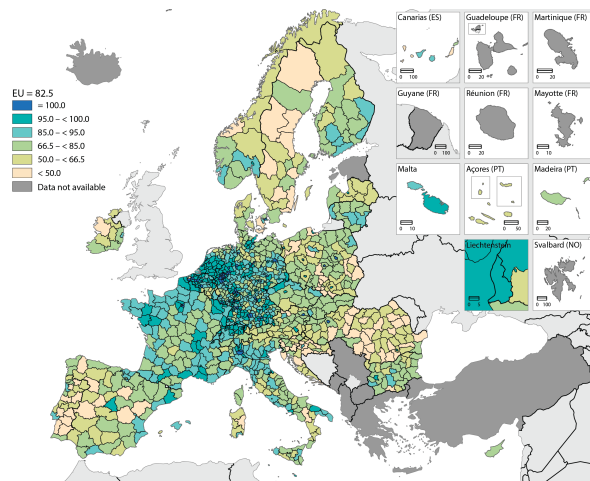


Figure 2.1: Population living within 15 minutes driving time of a hospital, 2020 (% , by NUTS3 regions)[1]

Figure 2.1 shows how large parts of central and eastern Europe are more than 15 minutes from a hospital by conventional ambulance. According to F. Rutten (personal communication, April 29, 2025), this has a significant impact on the chance of survival, making it vitally important to decrease the response time. This is where eVTOL technology can be applied, as it can achieve higher velocities and fly shorter paths.

The most desperate regions will be evaluated in more detail. *Desperate*, here, will be defined as the highest number of unreachable emergencies per area, as these regions would benefit the most from a single eVTOL with a finite range. Note that this does not apply to metropolitan areas, as all locations in such regions are typically reachable within a 15-minute driving range of a hospital. The number of emergencies per region can be estimated from the population size and emergency rate per person, where the age has to be taken into account, as emergency rates are much higher for the elderly [2].

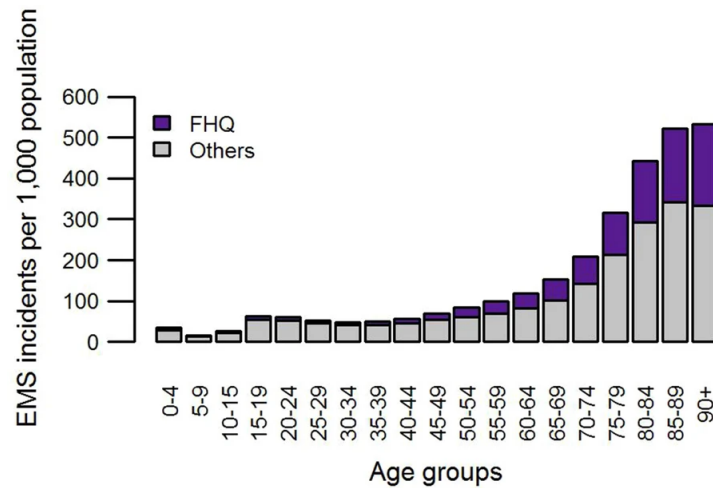


Figure 2.2: Emergency incident rates increase by age [2]

These emergency rates are combined with the Eurostat population data [3], and multiplied by the percentage of unreachable emergencies per region. If the data is then normalized by area, it results in a new map.

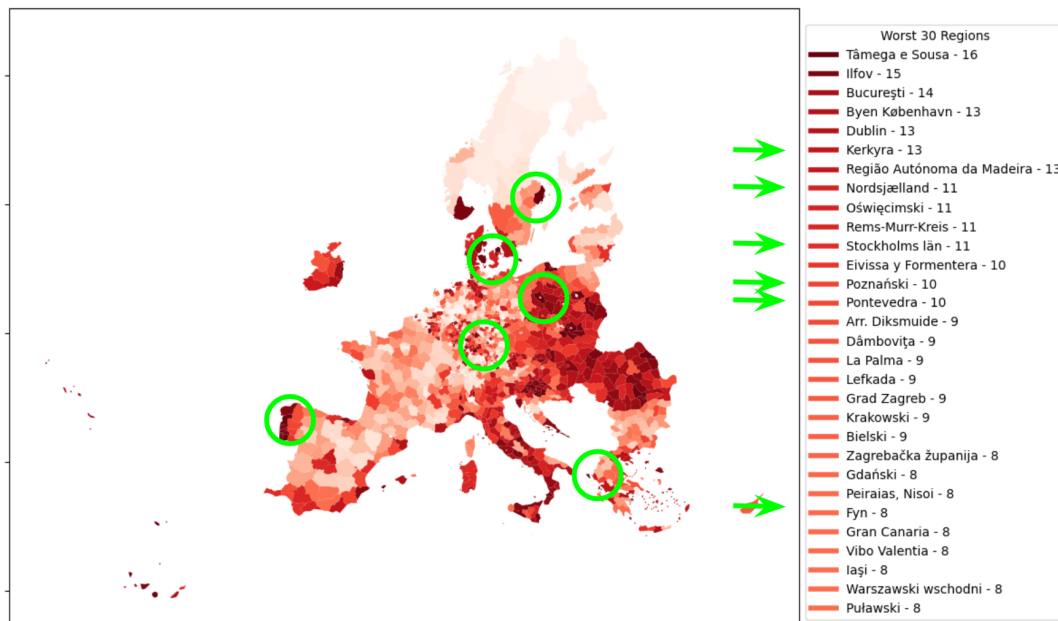


Figure 2.3: Annual number of emergencies not within 15 minutes of a hospital per square kilometer

From the worst 30 regions, the ones with a higher GDP per capita are selected as new technologies are more likely to be adopted there. Once it is proven, other regions can also implement this solution. Each of the 6 selected options is now assessed in more detail to derive operational requirements. For each region, all hospitals in and around the region are marked, and a circle is drawn such that the entire land area is covered. These circles then represent the required range of eVTOLs stationed at the hospital. This process is illustrated by Figure 2.4.

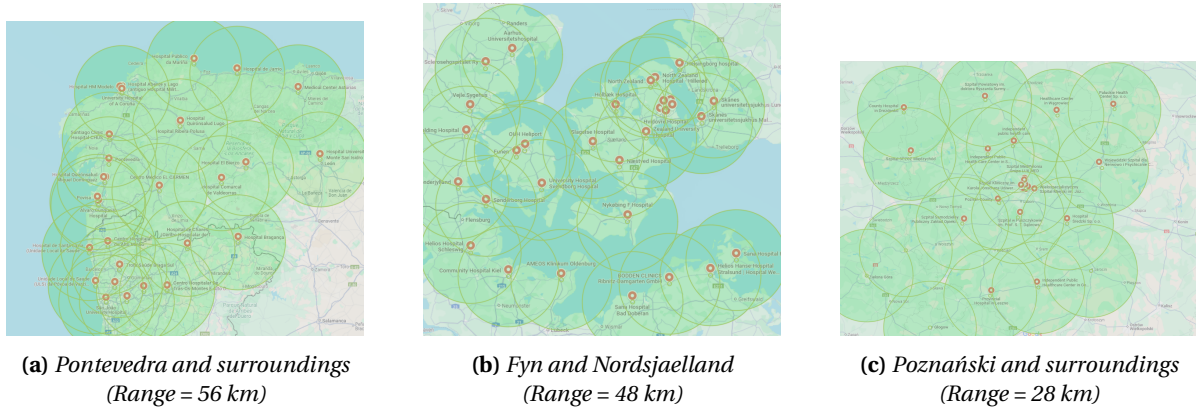


Figure 2.4: Three of the selected regions with hospital locations and required eVTOL ranges

From these maps it becomes clear that almost all land area can be reached with a range of 50 km, so to be able to return a patient, 100 km of range is needed. If the eVTOL wants to reach the majority of this area within 15 minutes, it needs to fly at least 200 km/h. Some regions will still be more demanding, but with this performance, the large majority is served. This is illustrated by Table 2.1.

Table 2.1: Speed and range requirements for the selected regions

Parameter	Poznański	Kerkyra	Fyn	Bavaria	Pontevedra	Stockholm
Total Range [km]	28	30	48	50	56	75
Flight Velocity [km/h]	112	120	192	200	224	300

For the rest of the market analysis, one region is chosen to save resources. As all regions are similar in terms of criticality, Bavaria is selected for its average range requirements and good economy, which will make it easier to implement a new technology. Once it has been tried and tested, the system can be introduced in other regions as well. Based on an average number 4 daily emergencies per eVTOL from the examined regions, a total number of around 7000 vehicles would be needed to serve all of the unreachable emergencies in Europe.

2.2. Competitors

This section will investigate what current methods are used to save people in need of help. Information on this is useful, as it might reveal flaws in the approach and give a guideline for the costs and performance required to be competitive.

2.2.1. Market Value

According to HORIZON [4], the ambulance services market in Europe is expected to reach approximately USD 19,341.1 million by 2030, with a projected compound annual growth rate (CAGR) of 8.8% between 2024 and 2030. This indicates a substantial market size and impressive annual growth. Focusing more specifically on Central Europe, particularly Germany, the ambulance services market in Germany is expected to reach a projected revenue of USD 3,450.5 million by 2030. A compound annual growth rate of 9.8% is expected for the German ambulance services market from 2024 to 2030. This reveals a rapid growth rate and potential market size, where more products need to fill in the gap.

2.2.2. Stakeholder Identification

Creating a stakeholder map is essential for the success of the project, since the product will be operated in a highly regulated and competitive market. Maintaining the relationships with the stakeholders is thus critical for both the acquisition of the product and its operational life. In Figure 2.5 the involved parties are identified and categorized.

The following entities can be observed:

1. Authorities/Policy Makers: These include the regulators of the air and medical spaces which dictate the performance needs of the design.

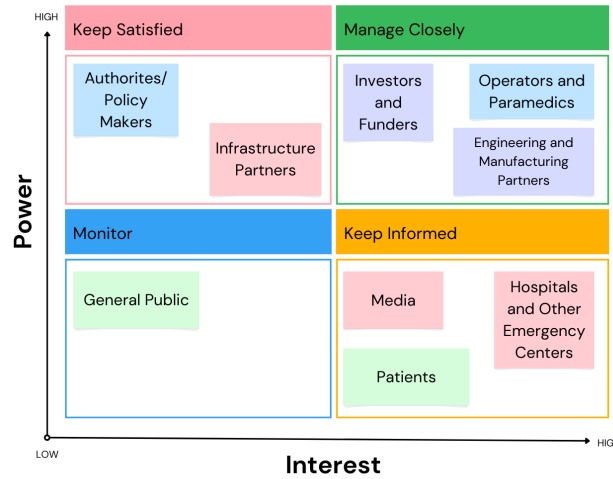


Figure 2.5: Stakeholder map

2. Infrastructure Partners: Heliport and general infrastructure developers which influence the usability and implementation of the design.
3. Investors and Funders: The customers of the design, such as governments and/or state owned companies. These are the stakeholders that will provide the funding of the project.
4. Engineering and Manufacturing Partners: Due to the project’s dependence on novel and optimized technology, the technical partners of the project play a big role in achieving the required performance metrics.
5. Patients: The individual beneficiaries should be monitored, especially in cases where the use of the emergency aircraft is more likely to be requested.
6. Media: Due to the media’s influence on public opinion and decisions made by the government, these parties need to be informed and a positive relation/image needs to be kept.
7. Operators and Paramedics: The emergency personnel required for the mission needs to be kept informed about the developments, strengths and shortcomings of the equipment for proper operation. Training and updating this personnel is crucial to the proper operation of the emergency vehicle.
8. Hospitals and Other Emergency Centers: These centers need to be adapted to this new emergency vehicle. Together with infrastructure partners, these health centers will be provided with all the necessary equipment, and communication for emergency operations needs to be defined and implemented.
9. General Public: Due to the necessity of using private airspace for operations, the negative effects towards the general public must be as small as possible. Failure to keep this stakeholder satisfied brings financial and operative risks.

2.2.3. Competitors Landscape

When looking into the existing solutions for emergency service, specifically in Germany, there are mainly three ways – ground ambulances, helicopters, and Volocity (German eVTOL company). The SWOT analysis is performed to identify the gap.

Table 2.2: SWOT analysis of ground ambulance

	Helpful	Harmful
Internal	<ul style="list-style-type: none"> • Cheap cost • Easy accessibility 	<ul style="list-style-type: none"> • Limited space • Slow over long distances • Dependent on traffic
External	<ul style="list-style-type: none"> • Integration with telemedicine • Electric ambulance innovation • AI-based route optimization 	<ul style="list-style-type: none"> • Car accidents risk • Road condition dependence

Table 2.3: SWOT analysis of helicopter ambulance

	Helpful	Harmful
Internal	<ul style="list-style-type: none"> • Reduces out-of-hospital transfer time • Access remote or difficult terrains quickly 	<ul style="list-style-type: none"> • Expensive operation • Weather-dependent
External	<ul style="list-style-type: none"> • Coverage expansion to rural areas • Improved weather forecasting • Development of hybrid helicopters 	<ul style="list-style-type: none"> • Risk of helicopter accidents • High maintenance demands

Table 2.4: SWOT analysis of Volocity (eVTOL ambulance)

	Helpful	Harmful
Internal	<ul style="list-style-type: none"> • Low noise emission • Low operational cost • Short emergency response time 	<ul style="list-style-type: none"> • Limited flight range • Requires new infrastructures (charging)
External	<ul style="list-style-type: none"> • Growth of urban air mobility (UAM) • Increasing eVTOL investments • Future autonomous possibilities 	<ul style="list-style-type: none"> • Regulatory compliance challenges • High battery degradation rates

2.3. Cost Requirements

With the competition clearly defined, it is now possible to establish the performance required to compete with it. This will be done based on three metrics: mission performance, initial cost, and operational costs.

2.3.1. Required Mission Performance

From the mission statement, it follows that the design should be able to replace air ambulances. As these are far more capable than ground ambulances, this section will only compare the new concept to helicopters.

According to literature [5], air ambulances have a typical cruise speed of 210 km/h. This is comparable to the cruise velocity found in Table 2.1 and will be adopted in the requirements.

A metric that is more difficult to meet is the range of air ambulances, which is around 700 km [5]. This far exceeds the capabilities of current eVTOL technology, but can be compensated for by stationing vehicles at more locations. The study from Section 2.1 found that a range of 50 km would suffice to serve all of Bavaria if eVTOLs were stationed at all 63 hospitals in the region.

One final thing left to consider is the reliability of the system as a whole. Since vehicles can only be used for one emergency at a time, multiple eVTOLs may have to be stationed at each hospital to match the reliability of emergency helicopters. To quantify this reliability, the chance of an emergency occurring while all vehicles of a station are deployed is calculated using the Erlang B formula [6] in (2.1), where N is the number of vehicles at a station and A the mission time over the time in between emergencies. It has been used to find the reliability of both air ambulances and two types of eVTOL arrangements.

$$B(N, A) = \frac{\frac{A^N}{N!}}{\sum_{k=0}^N \frac{A^k}{k!}} \quad (2.1)$$

Table 2.5: Reliability calculation for air ambulance and eVTOL systems

	Air Ambulances	1 eVTOL	2 eVTOLs
Mission time [min]	86	116	116
Missions from station per day	3.3	10.5	10.5
Mean time between emergencies [min]	438	138	138
A [Erlangs]	0.20	0.84	0.84
Reliability [%]	84	54	84

Column 1 of Table 2.5 is based on an average amount of about 1200 missions per DRF station, a German air ambulance operator [7]. This results in about 3 missions per day, with an average duration of 86 minutes

[8]. Columns 2 and 3 are based on the number of unreachable emergencies from Section 2.1, as these are the cases they would serve primarily. If the eVTOLs are stationed at every one of the 63 major hospitals in Bavaria, this results in an average of 10.5 emergencies per station. Next to this, the average turnaround time is also about 30 minutes longer due to battery charging. This results in a reliability of just 54% if only one eVTOL is stationed at each hospital. In this case, an eVTOL from any other hospital within 100 km could also be used, but this comes with a longer response time, and this eVTOL would also have to be returned to its own hospital eventually. Thus, to obtain a reliability figure similar to air ambulances, two eVTOLs are stationed at each hospital. This results in a total of 126 eVTOLs for the system to cover all of Bavaria.

2.3.2. Required Costs

With the mission performance equal to or better than air ambulances, it is time to consider costs. In order to be viable, the system has to be affordable for a German operator such as DRF or ADAC, so the initial costs of the system will be compared to the initial costs of their fleet, as well as the initial costs of regular ambulances for completeness.

DRF and ADAC combined currently operate about 20 air ambulances in Bavaria. Each one of these helicopters costs about 4.5 million euros [9], so the cost of the total system is about 90 million euros. Subsection 2.3.1 established that 126 eVTOLs would be needed to serve the same area. This means that if each eVTOL could be bought for 0.7 million euros, the systems would have the same initial costs. This is a rather optimistic price for an eVTOL, so it is more likely that the difference in price would have to be compensated for by a reduction in operating costs. In that case, an eVTOL of 2 million euros and a lifetime of 20 years would be 34 euros more expensive per flight to offset the difference in initial costs.

To put this in perspective, these initial costs will also be compared to the price of the ground ambulances in Bavaria. There are 506 of those, with a price of about 125,000 euros each. Combined this gives a total system cost of 63 million euros, and it should be noted that the eVTOL system will only replace part of these vehicles, as there are also a lot of emergencies within range of conventional ambulances. So, the initial costs of the eVTOL system will be 4 times as expensive as the ground ambulance system. However, this is only a small part of the total expenses of rescuing people. The most expensive part are the operational costs, so to determine whether eVTOLs are competitive with ground ambulances in terms of costs this should also be considered. The same could be done for air ambulances, but these have far higher operational costs and, according to the mission statement, the system has to compete with ground ambulances.

The majority of operational costs are the onboard personnel. These costs depend on their hourly wages and the time they spend on each mission. The former will likely be a bit higher for eVTOLs, as air operations require personell with advanced training. This is probably offset by a reduction in mission time as the air ambulance is able to travel a lot faster, thus reducing mission time. Next to this, there are also maintenance and energy costs. These are easier to quantify and have been listed in Table 2.6.

Table 2.6: Energy and maintenance costs for ground and eVTOL ambulances for a mission of 100 km

	Ground Ambulance	eVTOL
Energy costs	27	34
Maintenance costs	20	12
Battery costs	-	40
Total (€)	47	86

These numbers are based on a battery of 150 kWh, a typical value of large eVTOLs [10]. Maintenance costs are then derived from battery costs using an estimated relation by [11]. Lastly, energy costs are calculated using current electricity and fuel prices. Together, the eVTOL seems to be approximately 40 euros more expensive per mission. However, the total costs of an ambulance for a 100 km mission are on the order of 900 euros, with high-priority missions costing up to 1400 euros [12]. Compared to this, a 40 euro difference in energy and maintenance costs is negligible.

Mission Profile and Operations

In order to facilitate the use of the emergency eVTOL, the logistics of the missions need to be clearly defined in order to maintain consistency and cooperate with medical bodies and air traffic management. The operations will be discussed in the following order: firstly, the general mission aim and objective will be presented in Section 3.1. Next, the flight and mission profile will be defined in Section 3.2. Lastly, necessary architecture and communications channels will be presented in Section 3.3 and Section 3.4, respectively. Additionally, in Section 3.5, a workflow diagram and breakdown structure will be presented.

3.1. Mission Objective

As explained in Chapter 2, emergency missions are performed in most countries by either using a ground ambulance, an emergency helicopter, or a combination. The emergency helicopter provides a fast and versatile option for reaching the location of an emergency, as it does not depend on the state of the road and can fly over and around mountain terrains. However, currently, the helicopter is rarely used to transport the patient from the emergency scene to the hospital, and is only deployed for exceptional cases. It is known from experience that the helicopter improves the prospects for heavily injured patients (F. Rutten, personal communication, April 29, 2025); however, now it is not scalable or a replacement for ground ambulances. Their scalability is constrained by their high cost and lower social acceptance, due to noise generation and emission. This shows the opportunity for the eVTOL, which can provide a less noisy and more sustainable solution. Consequently, it can be used for more than exceptionally severe cases and possibly also be a replacement for ground ambulances due to its ability to avoid obstacles and reach more remote locations.

The goal of the mission is to fill the gap between the slower and more infrastructure-reliant ambulance and the less scalable emergency helicopter. This is phrased by the following mission need statement: *'Design an affordable eVTOL ambulance that provides emergency medical assistance for small and medium communities in Central Europe and is a scalable competitor to emergency helicopters, and a substitute for ground-based ambulances.'*

This mission need statement outlines the following key points: the eVTOL should be driven by a sustainable energy storage method and minimize costs to become scalable and compete with the current helicopters. It will provide emergency medical assistance targeting small and medium communities, as these are the rural areas where it is harder for ambulances to arrive at the scene quickly. It will provide medical assistance by transporting a specialized doctor to the location of the emergency. Additionally, it can also facilitate the transportation of patients to a nearby hospital instead of using an ambulance as the transportation method. This mission proposal increases the need for more trained paramedics specialized in these kinds of missions. Furthermore, additional pilots are required to manage the increasing number of eVTOLs, which highlights the importance of an easier-to-control aircraft to simplify pilot training.

To achieve these, the following operational decisions are taken:

- The eVTOL hangar will be inside the perimeter of the hospital or in the proximity. This allows for the swift dispatch and handling of the stretcher with the patient. Additionally, the distances to be traveled will be minimized due to not requiring the pickup of a paramedic from a third location, eliminating a landing and takeoff procedure.
- Paramedics and pilots will be stationed at the hangar, where they will be dispatched from. Again, this speeds up the response time and allows the staff to handle the vehicle and all associated equipment efficiently.
- Existing infrastructure will be used or repurposed for the eVTOL as much as possible. Being scalable is of utmost importance, and reducing costs by reusing existing infrastructure allows cutting costs in the case of many hospitals, which will host the eVTOLs. Examples of these can be using existing parking lots as landing pads and using EV chargers to fill the batteries.

3.2. Mission Profile

The operational framework for the proposed emergency medical air transport system is structured to enable fast, reliable, and coordinated responses to critical health emergencies. Figure 3.1 presents the sequential phases of operation, from mission start to system readiness for the next deployment. The process is divided into four primary functional stages: mission launch, patient pick-up and transport, landing and handoff, and vehicle recharge.

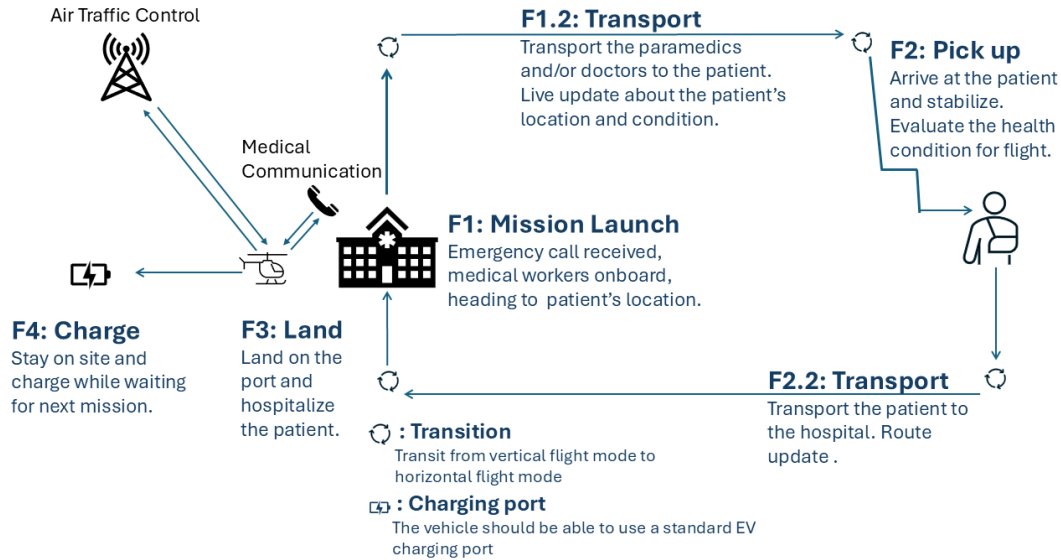


Figure 3.1: Operation Diagram

F1: Mission Launch

The operation is initiated upon receiving an emergency call. Medical personnel and a pilot are dispatched and assigned an eVTOL. The vehicle is launched from the base station and navigates towards the location of the patient, informed by real-time medical and logistical data. Effective coordination with Air Traffic Control and ongoing medical communication is essential during this phase to ensure a swift and safe dispatch and to provide all stakeholders with necessary information in the clinical and operational decision-making.

F2: Patient Pick-up and Medical Stabilization

Upon arrival at the scene, medical personnel conduct an immediate evaluation of the condition of the patient. The patient is stabilized to meet the safety requirements for aerial transport. This stage is crucial to minimize flying risks. Following stabilization, the patient is securely boarded and transported to the designated healthcare facility. The transport path is dynamically adjusted based on current airspace data and patient condition. Furthermore, the vehicle was sized and designed in order to accommodate harsh terrains, highways, and rural areas for possible landing locations. This was achieved through employing adequate requirements and technical decisions.

F3: Landing and Patient Handoff

Upon reaching the hospital, the aircraft transitions from horizontal to vertical flight mode and lands on the designated landing pad. The patient is then transferred into the care of hospital staff. This handoff is facilitated by prior communication and coordination during the transport phase.

F4: Recharge and Standby Mode

After patient delivery, the aircraft remains stationed at the hangar of the hospital, where it connects to a charging port. During this phase, the aircraft recharges and remains in standby mode, ready to respond to the next emergency call.

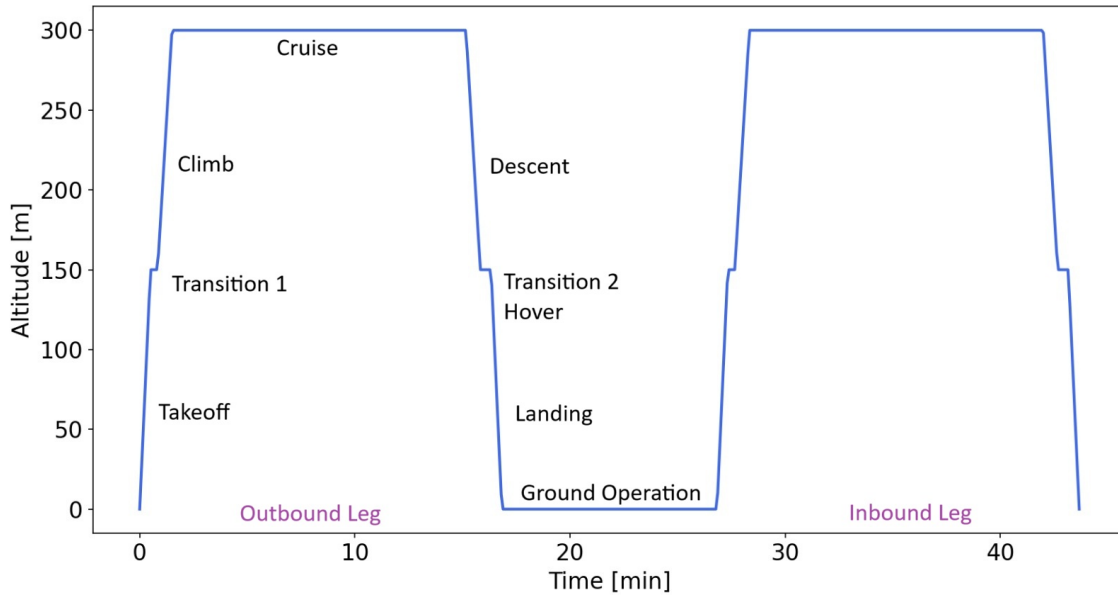


Figure 3.2: Standard mission profile

Table 3.1: Mission phases for a standard flight for an emergency 50 km away (limit)

Mission Phase	Duration (sec)	Notes
Takeoff	30	Climb to 150 m
Transition 1	20	eVTOL transition to forward flight
Climb	40	Until 300 m altitude
Cruise	820	Cruise over 50 km
Descent	40	Until 150 m altitude
Transition 2	20	eVTOL transition to hover
Hover	10	Final approach to landing site
Landing	30	Final touchdown
One Leg	1010	Half of a mission
Flight Total	2020	Total time in flight
Mission Total	2620	Including ground operation

The typical one-way trip of the eVTOL consists of takeoff, first transition, climb, cruise, descent, second transition, hover, and landing. The typical mission profile consists of two one-way trips, as can be seen in Figure 3.2. In detail, the aircraft takes off to 150 m in 30 s. It then spends 20 s in transition (1st) to forward flight without changing altitude. Next, it climbs at 3.75 m/s for 40 s. At 300 m, it cruises at 200 km/h for 820 s or 13.7 min. It then undergoes a power-off descent to 150 m in 40 s. The 2nd transition takes 20 s, putting the aircraft in hover mode. Before landing, a short 10 s hovering phase is added to search for a possible landing site. After touchdown, ground operation at the location of the patient is assumed to have a duration of 10 minutes. The same one-way flight profile is carried again for the return leg. It is to be noted that this is the most critical scenario, which will be considered for energy budgeting. After production and full-scale testing, more efficient operational altitudes and velocities could be defined based on performance as well as the patient and hospital location.

3.3. Architecture Management

For ease of use and quick response, it was decided that the emergency vehicle would be stationed at hospitals, or when this is not possible, the necessary elements will be accommodated near the hospital. For this type of mission, multiple components are necessary:

1. Landing pad: This provides the vehicle with a place to land and bring the patient to the hospital. Due to the nature of the vehicle, the pad will not need to be as big and resilient as one used for helicopters,

and ideally, normal road pavement can be used. However, to not interfere with other activities next to the hospital, this landing site needs to be clearly defined, equipped with lights, and kept clear for landing. Only authorized personnel should be allowed next to this landing pad, due to the downwash of the propellers.

2. eVTOL hangar: In order to facilitate maintenance and reduce the impact from rain, snow, or other natural phenomena, a dedicated hangar for storing the vehicle is to be used. This structure needs to provide shelter to the technicians and operators of the eVTOL for maintenance, charging, medical equipment storage, and fast dispatch.
3. Power infrastructure: In order to power up the batteries, a standard connection to the power grid can be equipped with a DC charger. Additionally, if the hospital is equipped with an EV charger, it can be used without needing to build unnecessary infrastructure.
4. Handling equipment: The landing gear selected uses wheels, which provide a trivial way to move the eVTOL wherever needed. However, to block the wheels, aviation-grade wheel chocks will be necessary. Furthermore, due to the low OEW, car jacks will be present in the hangar as well in order to provide a handling method in case of wheel failure and or lockage.

3.4. Communications

A robust communications system is essential for the safe and effective operation of an eVTOL ambulance. The vehicle must maintain continuous contact with air traffic control, hospital networks, and Urban Air Mobility networks. This is achieved through a combination of VHF/UHF radio, 5G, and satellite links, ensuring reliable air-to-ground communication throughout the mission.

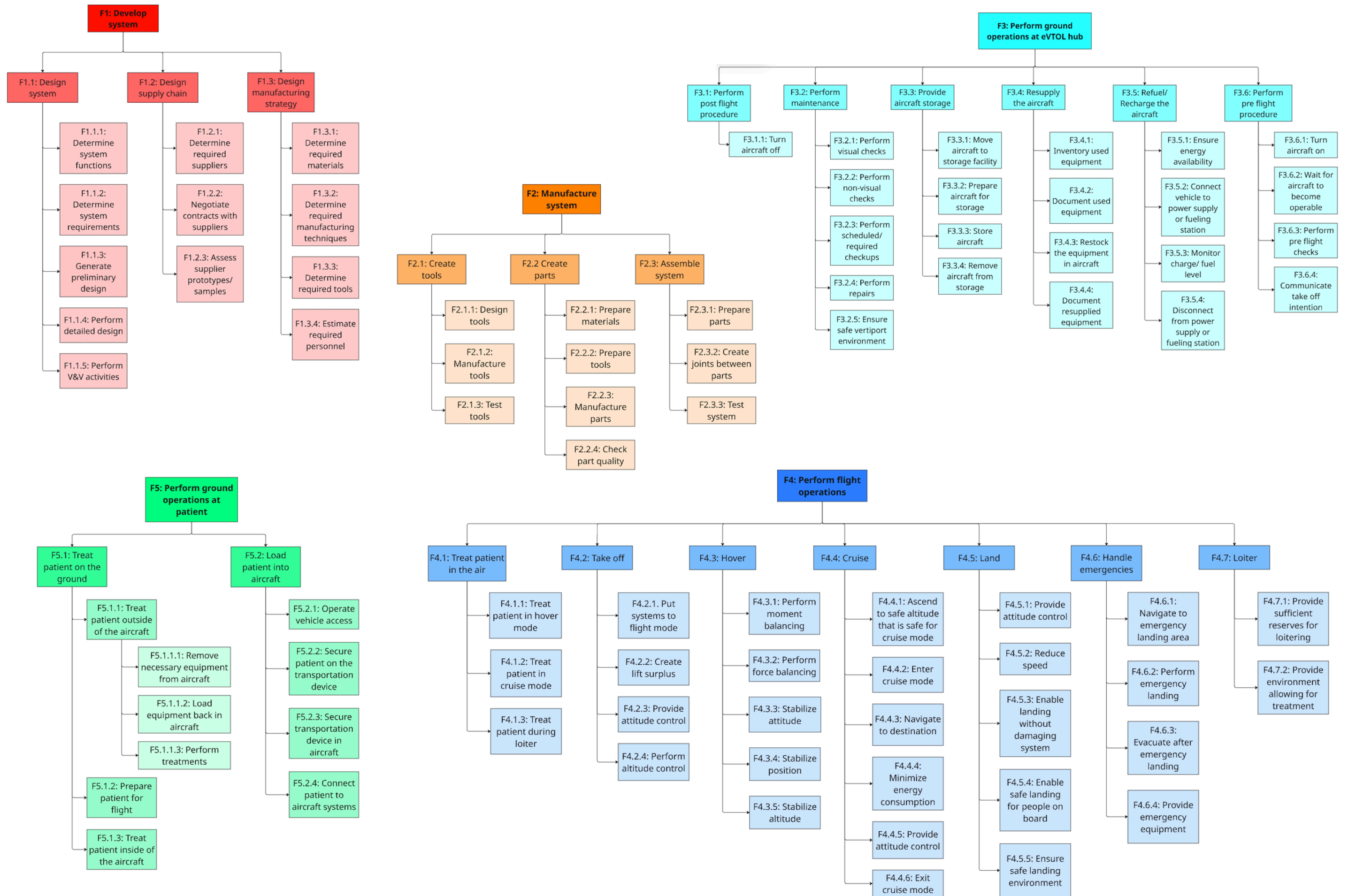
These systems support real-time updates on patient status, route changes, and coordination with hospital staff to prepare for arrival. In emergencies, automated alerts can transmit the health of the vehicle and mission status to ground teams, enabling timely responses to technical issues or diversions.

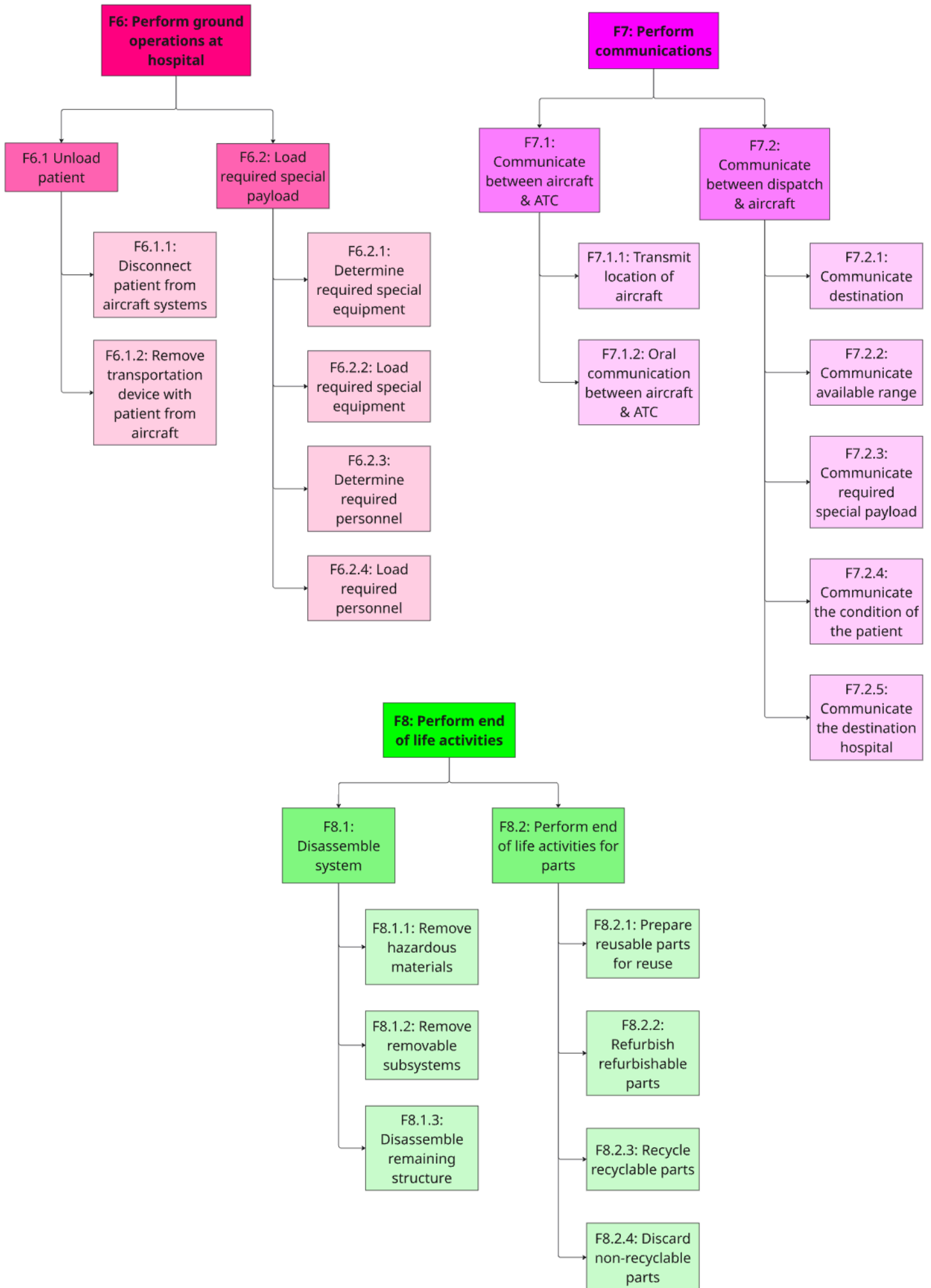
Within the cabin, noise-canceling headsets enable clear communication between the pilot and paramedics, as well as with external parties. These systems are fully integrated and tested during the deployment phase of the vehicle to ensure readiness from day one.

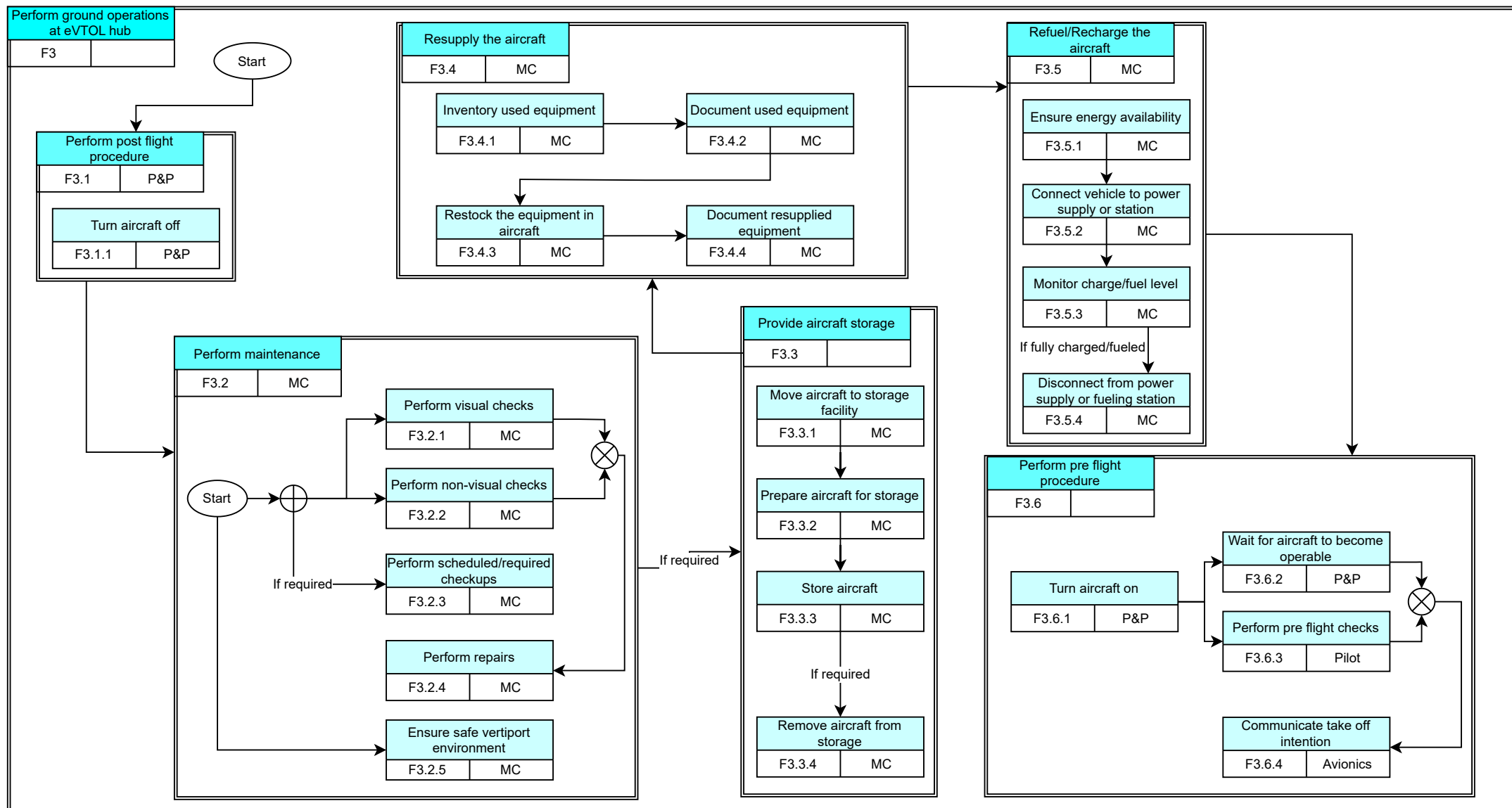
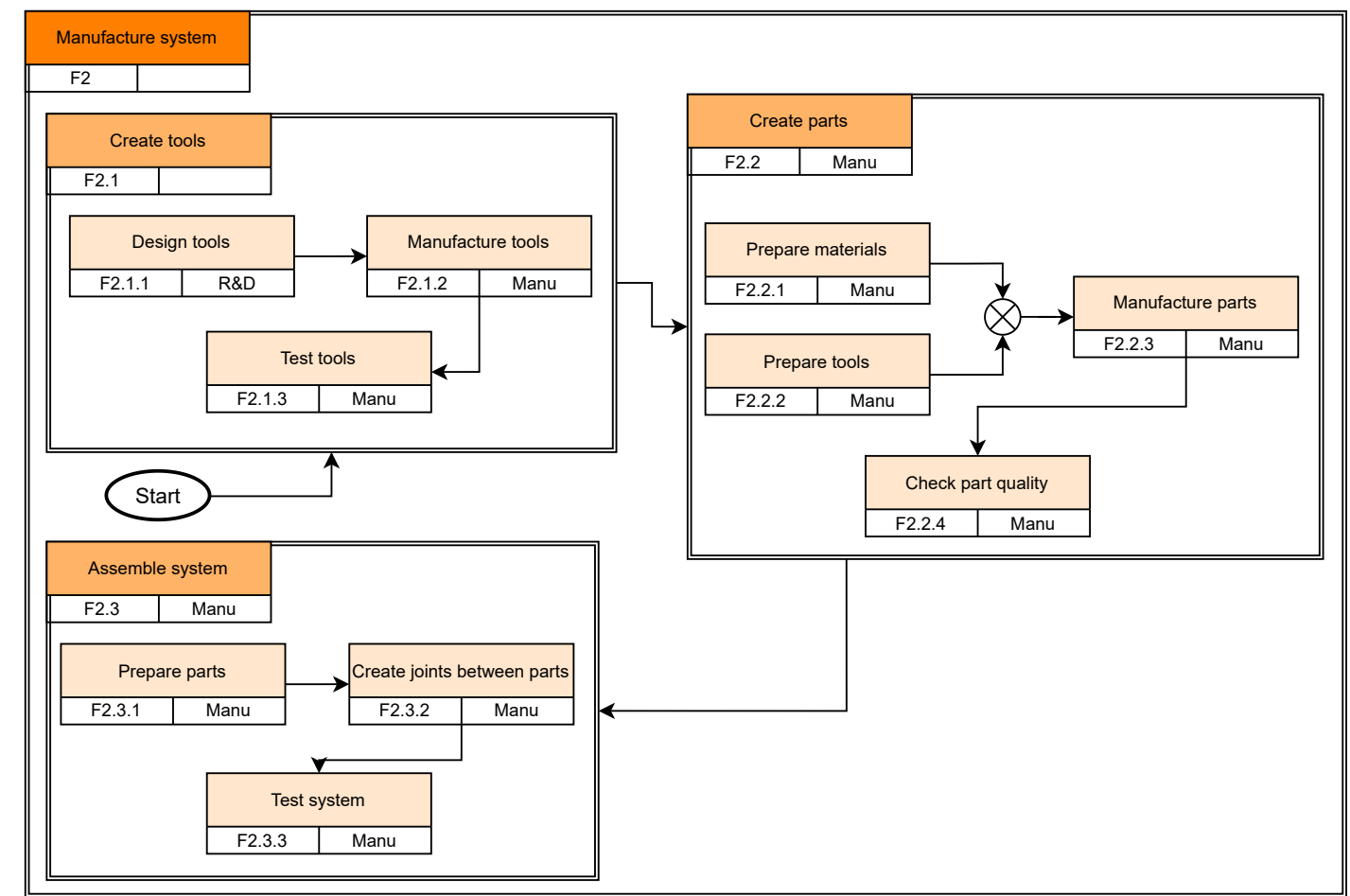
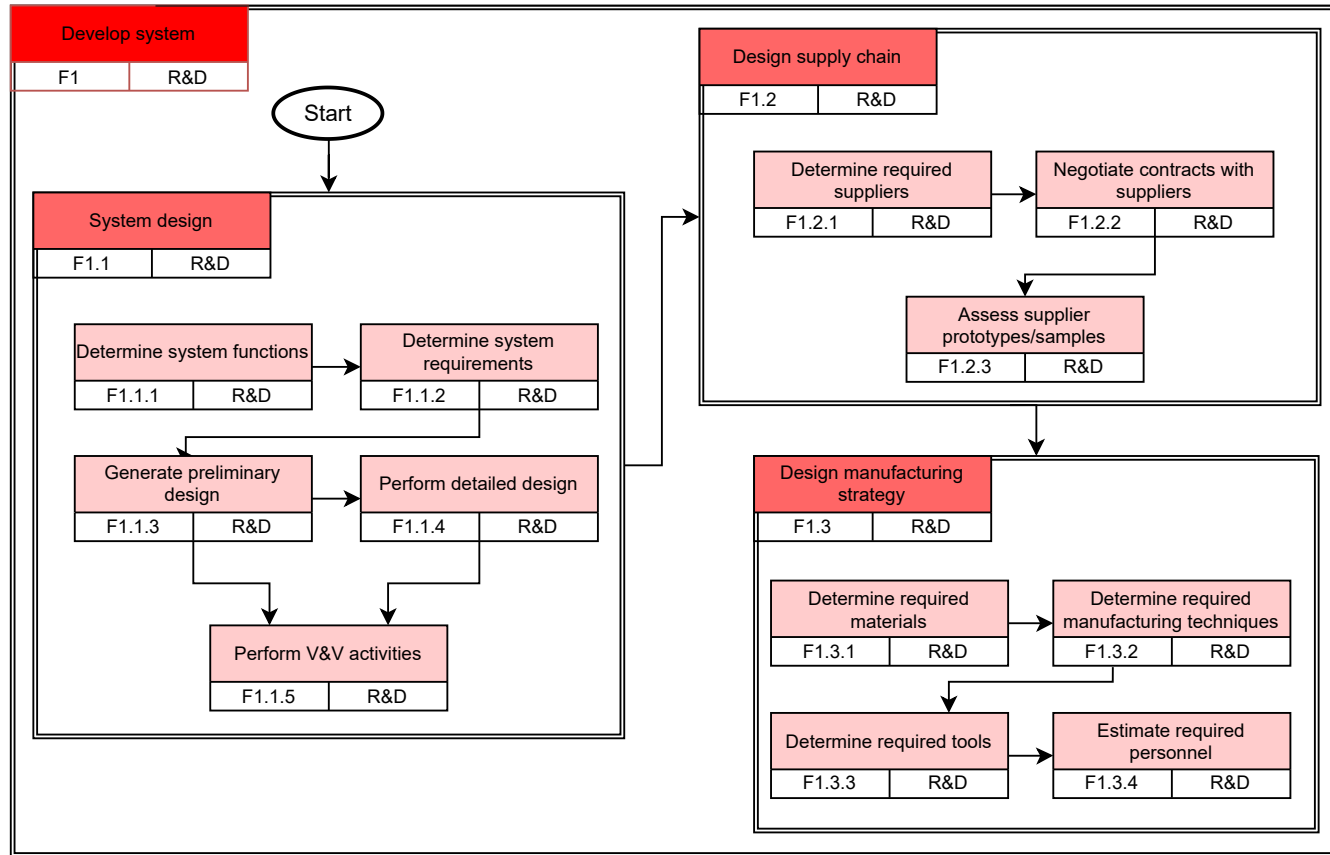
3.5. Functional Breakdown and Flow

The Functional Breakdown Diagram (FBD) is used to discover the different functions that are supposed to be fulfilled during the mission and life cycle. The main functions and life cycle stages of the system are accommodated on the first level of the diagram. These are: "Develop system", "Manufacture system", "Perform ground operations at eVTOL hub", "Perform flight operations", "Perform ground operations at patient", "Perform ground operations at hospital", "Perform communications", and "Perform end of life activities". "Perform ground operations at eVTOL hub" and "Perform ground operations at hospital" are separated, since the eVTOLs might be stationed at a separate hub or at a hub that is integrated into the hospital. Top-level functions are further broken down to generate all of the low-level functions without making assumptions about the system. If adequate performance in these functions is guaranteed through the requirements, the system will be able to perform its mission.

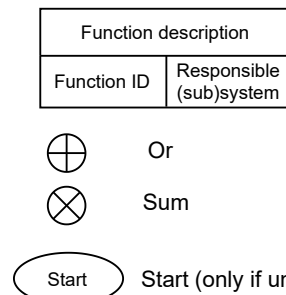
The functions are also presented in the Functional Flow Diagram (FFD). This diagram not only shows the functions but also gives insights into which functions can be completed in parallel and which must be completed in sequence. An FFD is created for each top-level function. The IDs that are specified in the FBD and the FFD are consistent. The FFD also shows the specific system or subsystem that carries the main responsibility for each low-level function. If all the low-level functions within a higher-level function are handled by the same system or subsystem, it is also responsible for the higher-level function. The aircraft has been broken down into subsystems, while the other systems that are performing functions, such as the maintenance crew, have not been further refined.





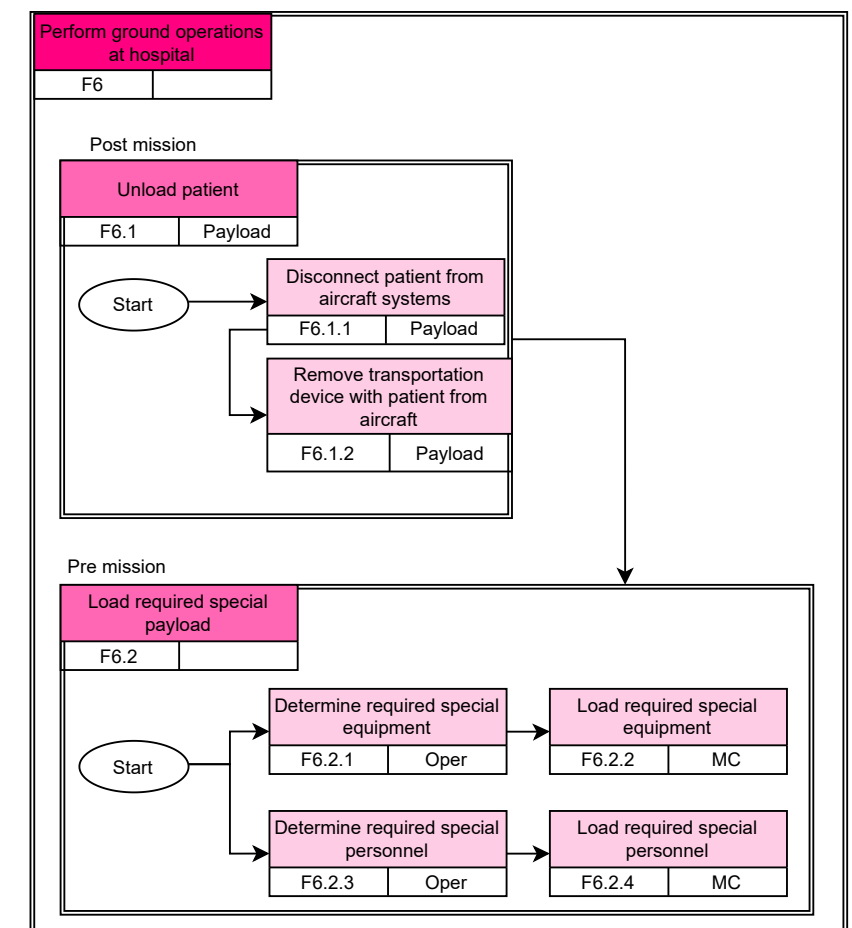
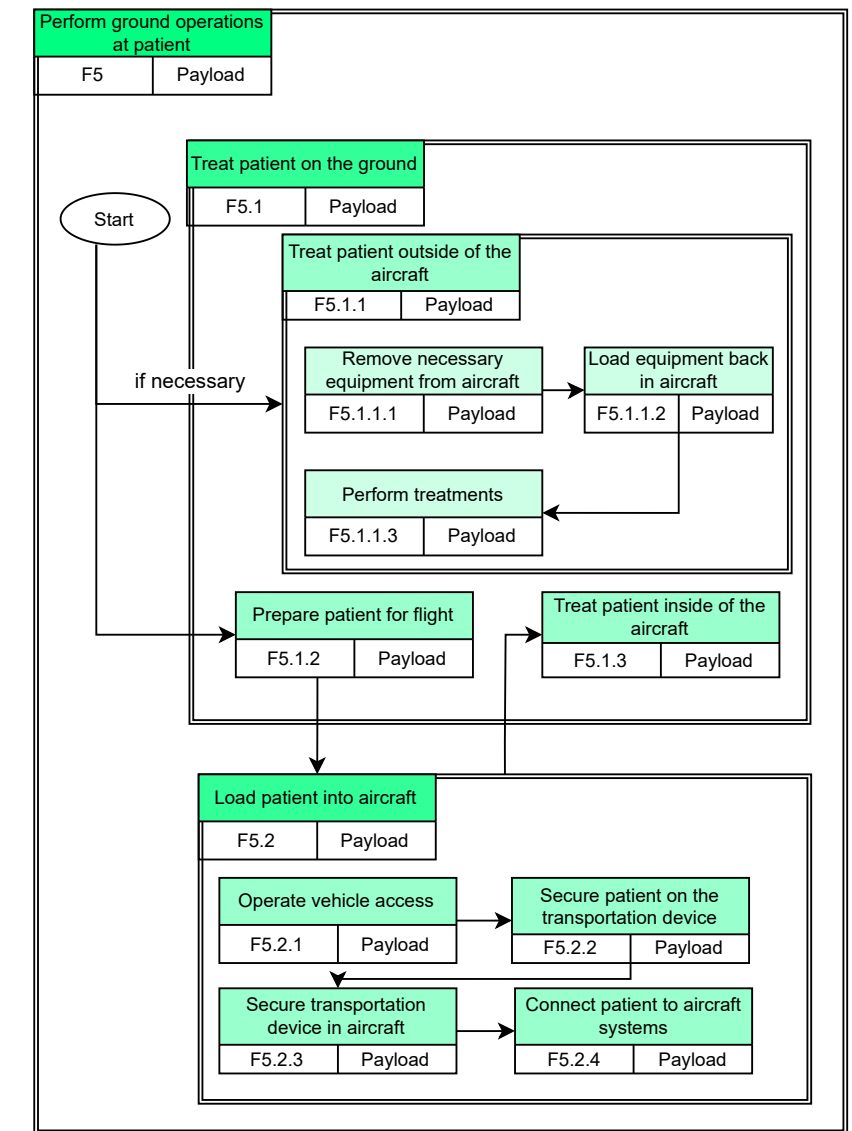
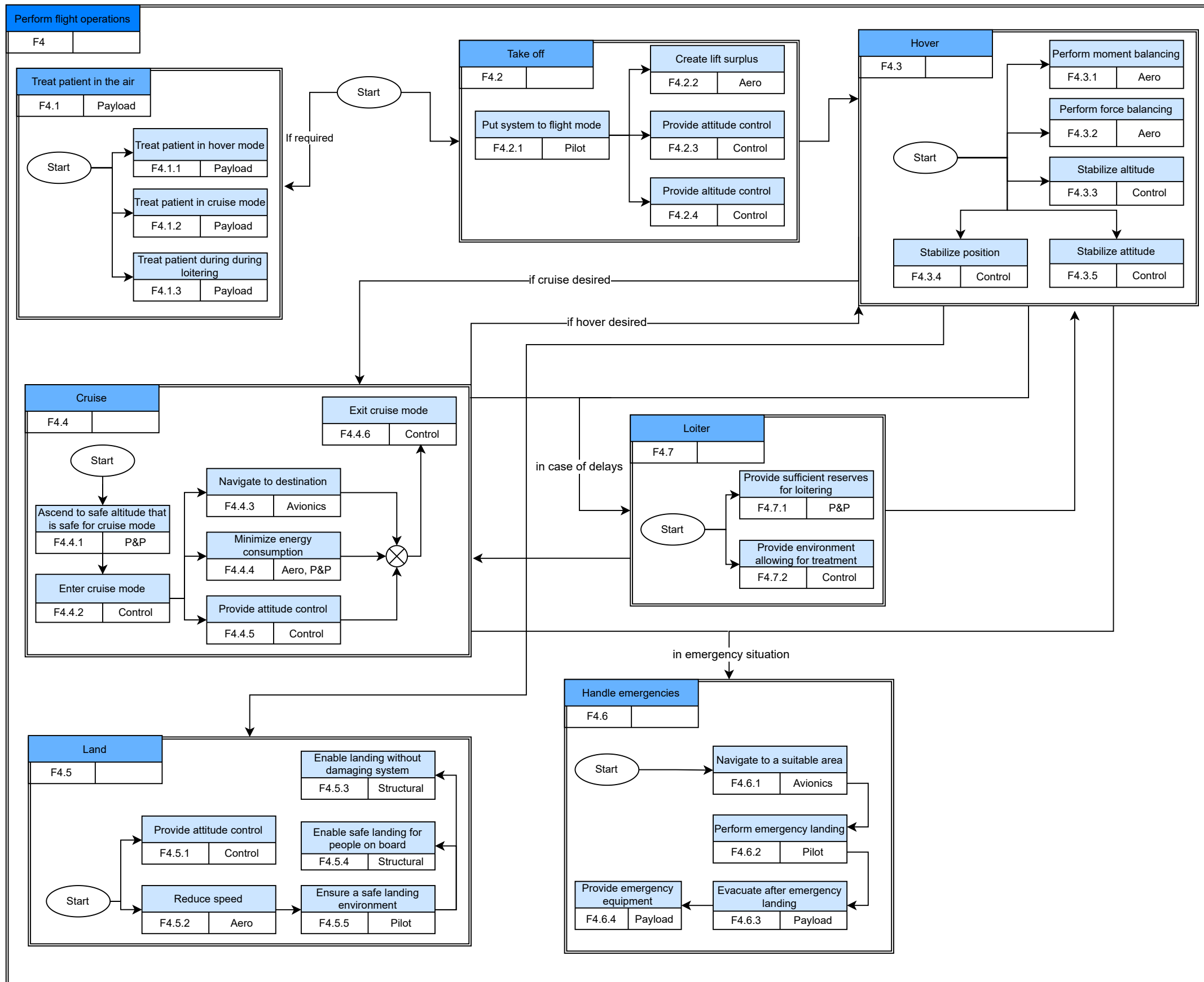


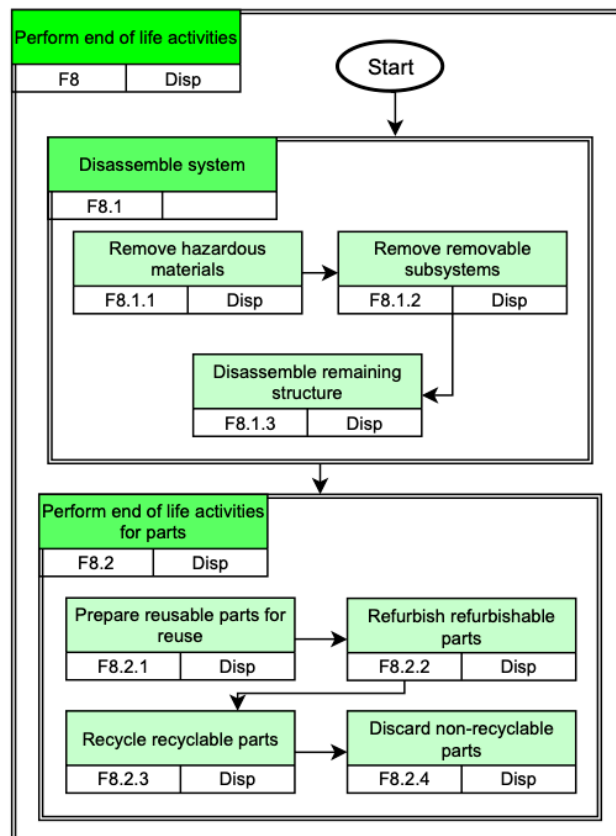
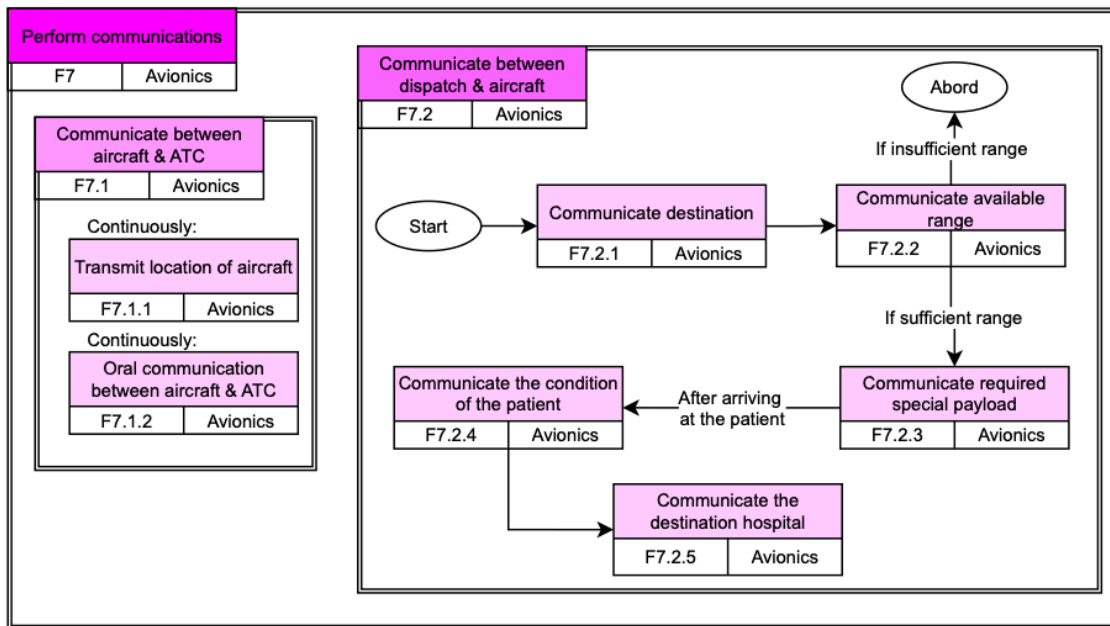
Legend



Systems abbreviations

- Aero - Aerodynamics
- P&P - Propulsion & Power
- MC - Maintenance crew
- Oper - Operations
- R&D - Research & Development
- Manu - Manufacturing team
- Disp - Disposal team





4

Sustainable Development Strategy

In this chapter, the sustainability part of the project will be explored. The United Nations Brundtland Commission defined sustainability as “meeting the needs of the present without compromising the ability of future generations to meet their own needs” in 1987 [13]. To ensure project sustainability, it is important to first establish the strategic goals that shall be achieved, which will be presented in Section 4.1. Afterwards, a plan can be made which explains how sustainability will be embedded in the different project phases, which can be found in Section 4.2. The systems sustainability performance will be discussed in Chapter 13.

4.1. Strategic Goals

The strategic goals are meant to make the system as scalable as possible. A common framework that can be used to quantify sustainability is the 3P framework, which is presented as the "Triple Bottom Line" by John Elkington[14]. It defines that sustainable development must consider profit, planet, and people. For the ResQProp system, this implies creating an affordable system, reducing greenhouse gases and noise emissions, and ensuring that the system does not create significant negative consequences for the people who are impacted by the system. Due to the system being part of the critical infrastructure of the countries, scaling it to partially replace ground ambulances and helicopters requires one further criterion: Minimizing strategic risks.

4.1.1. Profit

To ensure sustainable scalability and broad application, the system cost per mission must be similar to the cost per mission of a ground ambulance. Emergency helicopters are a bad comparison for acceptable cost since they are only deployed rarely and in very severe cases, which does not hold for the proposed eVTOL system. The profit part of the 3P framework will be assessed based on the mission cost and the maintainability of the vehicle.

4.1.2. Planet

Aerospace systems are generally very energy-intensive both during their production and during their operations. Reducing the climate impact (by reducing the greenhouse gas emissions) of the system can be done by using two approaches: reducing the amount of energy the system requires or ensuring that the energy that is being used is generated by using sustainable energy sources. Since the energy mix in the deployment area cannot be influenced by the team, the focus is put on reducing the energy that is used. To ensure that the system is scalable, it is required to minimize the climate impact of the entire project, including all life cycle stages, by minimizing greenhouse gas emissions.

The sustainability goal for the system are net negative life cycle greenhouse gas emissions. To achieve this, the eVTOL system must have lower greenhouse gas emissions for each mission than the ambulance and helicopter systems it replaces.

The most relevant greenhouse gases are carbon dioxide and methane. Carbon dioxide is produced during all production steps of the system, while methane is mainly emitted during the production of the battery. Furthermore, carbon dioxide is the most relevant greenhouse gas that is emitted during energy production. The different greenhouse gasses will be collectively measured in a CO_2 equivalent metric.

Viable end of life strategies are an important factor for the system impact on the planet. Certain modern materials such as composite structures are close to unrecyclable, especially due to their use of thermo set polymers. Therefore, their usage shall be minimized to increase the degree to which the system can be recycled.

4.1.3. People

To ensure a broad acceptance in the population it is necessary to reduce the noise of the system. This will allow it to not only operate during the day but also during the night. This is a relevant consideration since

the system will not only replace part of the existing helicopter fleet but also part of the ground ambulances, which causes it to be used very frequently.

But the 'people' part of the 3P framework should not only consider the people who are impacted by the operations of the system but also the ones who are impacted along its supply chain. Therefore, the goal is to minimize human rights violations and exploitative actions along the entire supply chain.

4.1.4. Strategic Vulnerabilities

Since the system will be part of emergency medical services, it is part of the critical infrastructure. Therefore, it is important to reduce the exposure to strategic risks such as supply chain risks, export restrictions on certain materials and technologies, and the energy availability risks. This ensures that the system will be operable and maintainable, independent of the political and economic environment.

To reduce the social impact and strategic vulnerabilities, the supply chain is limited to countries that are not affected by EU sanctions. An overview of the affected countries is given in the EU sanctions map [15]. It can be assumed that the countries with active EU sanctions pose potential strategic risks. Since it is difficult to get an insight into the intricate workings of global relations, this map allows at least to get a grasp of which countries might pose these risks.

4.2. Embedding Sustainability in Project Phases

Strategies to ensure that the sustainability requirements are met are implemented over the different stages of the project, from preliminary design to the product life cycle.

4.2.1. Sustainability during Preliminary Design

The most important part of the preliminary design stage is the tradeoff between the different concepts. Sustainability is not a direct criterion during this tradeoff. Instead, it is indirectly included in the peak power and takeoff weight requirements. An increase in peak power is indicative of an overall increase in operational energy usage, while an increase in MTOW requires an increase in raw material usage and thus emissions during the production of the system.

4.2.2. Sustainability during Detailed Design

During detailed design, sustainability will be taken into account during the considerations for the design of each subsystem. After the detailed design of the product is complete, the sustainability targets will be evaluated in Chapter 13 and it will be shown that the design offers a significant increase in sustainability over helicopters but is less sustainable than ground based ambulances.

4.2.3. Sustainability during Product Life Cycle

Sustainability measures, such as an end-of-life strategy, will be created during the different design stages. It will be ensured that these measures are followed in reality by providing continuous services for the product over its full life cycle. This includes supplying spare parts to the maintenance teams and providing an end-of-life service for the product that adheres to the end-of-life strategy.

These steps will lead to a design that will overall benefit the people and the environment over its life cycle. Even with reduced recyclability from the manufacturing processes, the climate and humanitarian impacts of the ResQProp will be positive and will pave the way for better and even more climate-friendly solutions in the years to come. In addition, by filling the gap between ambulances and helicopters, more lives will be saved more efficiently and will bring an overall leap forward for the emergency industry.

5

Concept Design

Once the mission and operations of the aircraft were finalized, an initial concept needed to be decided upon is to be further designed. In this chapter, an overview of the concepts for the design will be presented in Section 5.1. After which, the trade-off that was performed is presented, and the final chosen concept is outlined in Section 5.2.

5.1. Concepts for Design

In order to idealize on initial concepts, some top-level decisions were taken to narrow the design space. First, batteries are used as the system for energy storage. Secondly, it was decided that wings are needed to generate lift during cruise. These decisions were based on the outcome of a performance and mission analysis. They were due to safety, sustainability, and logistical concerns. Hydrogen, nuclear power plants, and internal combustion engines were not deemed adequate for the mission at hand. Therefore, the energy storage of choice is battery packs because they are safe to use around hospitals and can be recharged easily using existing architecture.

Furthermore, due to this decision, another top-level design decision could be taken: the eVTOL will use a wing for lift generation during cruise. Since batteries have a limited energy density and the fact that the design should minimize its climate impact, efficiency was deemed to be of utmost importance. Additionally, as powered lift during cruise requires significantly higher energy, a winged design was preferred.

Finally, by restricting the design space with these decisions, five concepts were analyzed in a trade-off procedure. These can be seen in Figure 5.1. In these figures, they are all presented in their take-off configuration.

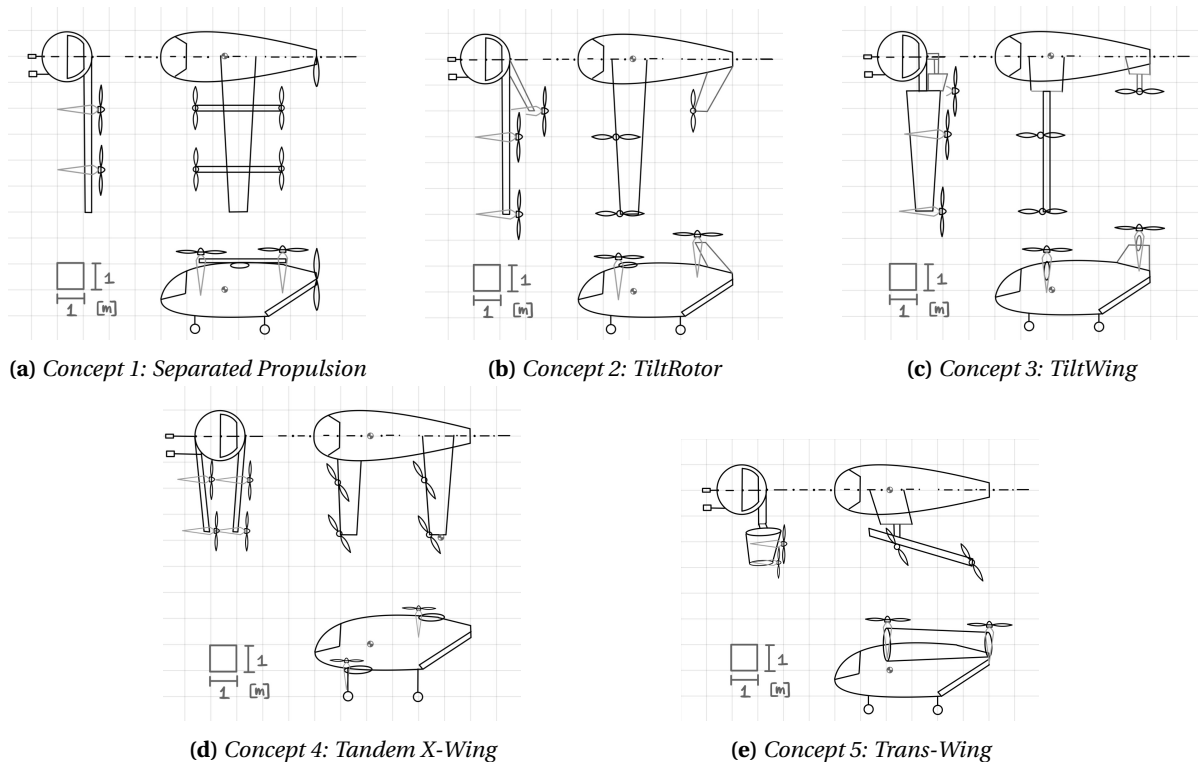


Figure 5.1: Overview of the Five Concepts

5.2. Concept Trade-Off

Once the concepts were created, a selection procedure was considered. The procedure revolved around the main lifting surface to be used, due to multiple configurations being viable. The trade-off logic was selected as follows:

1. Generate relevant and quantifiable criteria
2. Weigh each criterion according to its relative importance to the design
3. Grade each design on the selected criteria and find the best design option
4. Perform a sensitivity analysis to assess confidence of design decision

The criteria selected are of two types: qualitative and quantitative. Due to the novelty of the design and components used, some factors are not quantifiable since the technology has not been tested extensively yet. In order to account for these, engineering judgment and analysis were used. For the quantitative metrics, an extended analysis was performed where an iterative program calculated the performance metrics necessary for grading.

After giving each criterion a relative weight, the most optimum design could be selected, which in this case was concept 3, which includes a tilting wing mechanism. This is a configuration that trades mechanical complexity for more efficient flying. Although harder to control and tune, the energy necessary for completing a mission is minimized, reducing costs and increasing the sustainability of the design. A summary of the weights and scores given to each final design can be seen in Figure 5.2.

	Autoflight	Tilting Propellers	Tilting Wing	Double Wing	Trans Wing
Reliability (30%)	4	3	3	3	2
Maintainability (10%)	4	3	2	3	2
Controllability (20%)	5	4	3	5	3
Peak Power (20%)	1	3	5	2	2
Takeoff Weight (20%)	2	4	4	3	3
Total Score	3.2	3.4	3.5	3.2	2.4

Figure 5.2: Trade-Off Summary

6

Concept Sizing

The first step, once the concept has been decided, is to size the aircraft accordingly. The internal layout of the fuselage as well as its sizing will be presented in Section 6.1, from which the external configuration will then be shown in Section 6.2. Lastly, technical resource allocations will be described in Section 6.3.

Concept Sizing Symbols

X_{cg}	Center of gravity location	m	Mass	x	Centroid location
$A_{1/2}$	Disc area 1/2	$L_{1/2}$	Propeller arms	$X_{\text{longitudinal}}$	Offset of propellers
X_{tail}	Distance from tail to CG	ΔT_{tail}	Tail thrust difference	$\Delta T_{\text{rotorpair}}$	Rotor thrust difference
E	Energy	D_{rotor}	Diameter of the rotor	P	Power
η	Efficiency	FM	Figure of merit	v	Induced velocity
λ	Ratio	W	Weight	\dot{h}	Climb rate
V	speed	C_D	Drag coefficient	c	Cost
ρ	Air density	Q	Quantity	X_{nose}	Distance CG to nose

6.1. Internal Design

The internal layout of the aircraft relies heavily on the fuselage design, and the initial step in designing the fuselage is to understand the placement and sizing required for the payload necessary to complete the mission. The function of the fuselage is to protect the internal components from the external environment. From the mission objective and payload restrictions, the aircraft needs to be able to carry a pilot, two doctors, a patient, and the necessary medical equipment for emergency care of the patient. From these requirements, the floor plan as seen in Figure 6.1 is then created.

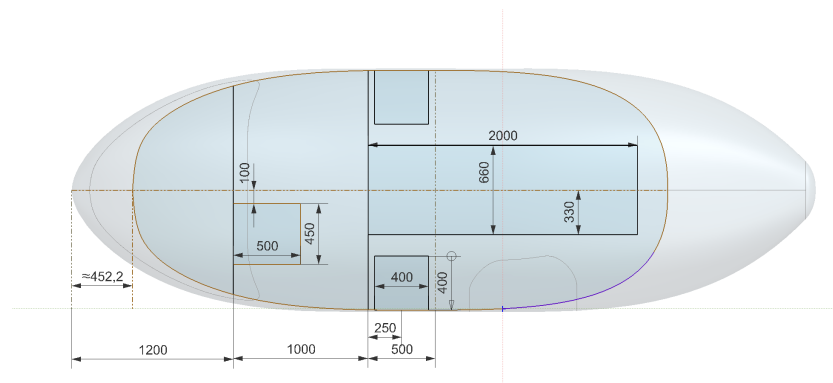


Figure 6.1: Floor plan for the fuselage

The pilot is offset from the center such that most of the equipment can have ample space next to the pilot, as we want our center of gravity quite far forward. This leads to a maximum width of the aircraft of 1.8 m, approximately, where the top of the patient and the two doctors are seated. Taking into consideration the wing attachment on the top of the fuselage and the space required for the batteries and landing gears underneath the floor, the cross-section as seen in Figure 6.2 is then derived.

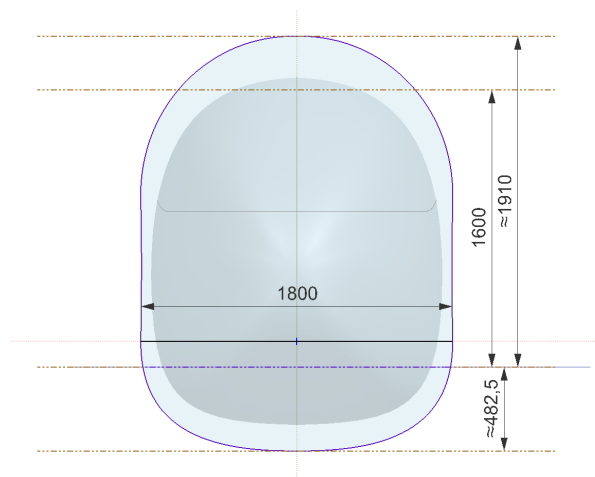


Figure 6.2: Cross-section of the fuselage as seen from the front

The cross-section differs along the span of the fuselage. Over the patient, the cabin height is the greatest, which is 1.6 m. This maximum height is maintained at 0.5 m from the patient tray location, as this was deemed the most critical location over which the doctor may need to intervene; therefore, a large height is required. In Figure 6.2, the maximum height shown is 1.9 m, but this also includes part of the hinge and the wingbox. The area around the legs and the feet of the patient was deemed a less critical location, where the doctor does not need a large space for access as injuries to these areas are seldom critical, therefore the fuselage design allowed for a lowering of the ceiling, which will later also give space for the tail attachment. The front of the fuselage was designed for only one seat for the pilot, offset from the center and placed on the left, and then the nose was rounded to give it an aerodynamic profile. Lastly, the tail cone is low enough to decrease the creation of vortices on the bottom, but with the thought in mind that a back door for patient roll-in is required. All these considerations lead to the side view of the cross-section as shown in Figure 6.3.

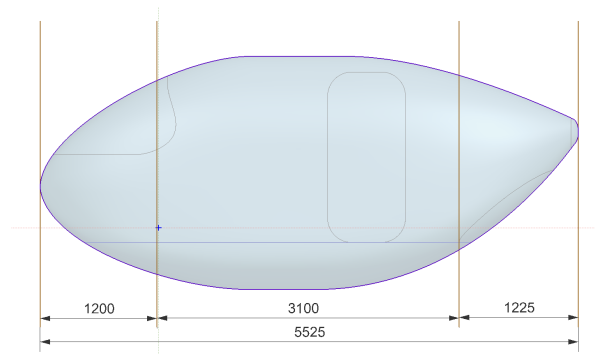


Figure 6.3: Cross-section of the fuselage as seen from the side

From Figure 6.3, the first section from the left is the nose cone, the middle section is the cabin compartment, and the right section is the tail cone. Once the fuselage shell is finalized, the different cutouts for human use are designed. The windshield is designed such that the pilot has as much visibility as possible; however, this can be increased. Two doors are placed on the fuselage. One on the side for normal entrance to the cabin for the pilot and the doctors, and one in the back. The one in the back is a two-panel hinged door, which opens to allow the sliding in of the patient tray. It is sized to also include space for the patient to be on top of the patient tray and still comfortably fit. Furthermore, the tray will slide in comfortably through this back door, onto tracks on the floor of the cabin, where it will lock in place during flight. More windows, to the sides and on the bottom, for the visibility of the pilot during crucial maneuvers, can be included in further iterations of its design. All these cutouts in the fuselage, as well as the final design, can be viewed in Figure 6.4.

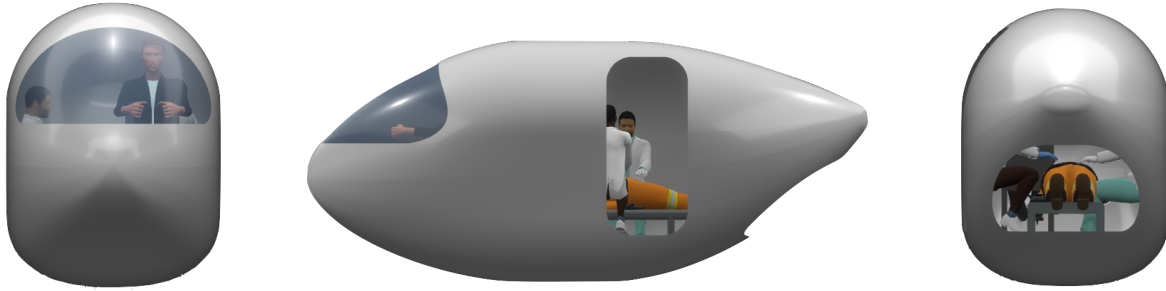


Figure 6.4: Windshield (on the right), side door (in the center), back door (on the left)

An overview of the final dimensions describing the fuselage is presented in Table 6.1.

Table 6.1: Defining dimensions for the fuselage design

Component	Value	Component	Value
Maximum length [m]	5.5	Cabin height [m]	1.6
Maximum height [m]	2.4	Underfloor height [m]	0.48
Maximum width [m]	1.8	Total volume [m ³]	14
Nosecone length [m]	1.2	Under the floor volume [m ³]	1.8
Tailcone length [m]	1.3	Over the floor volume [m ³]	12.2
Cabin length [m]	3.1	Cabin volume [m ³]	11.5

6.1.1. Center of gravity location

The next step, the fuselage design, is to locate the center of gravity. For stability and control purposes during both cruise and hover flight, the center of gravity of the fuselage is at the same location as the position of the hinge. Both the wing design and the hinge design will be explained in more detail in Section 7.1 and in Section 10.4. The hinge location is at 30% of the root chord, and the wing is placed at 1.7 m from the nose, leading to a hinge location and therefore the desired center of gravity of the fuselage of 2.13 m from the nose of the fuselage.

The center of gravity of the structural weight of the fuselage is calculated by looking at the fuselage skin, the windshield, the side door, the back door, and the floor. An overview of the materials used, the thicknesses of each component, and their respective masses is given in Table 6.2. Additionally, the doors and the floor are assigned structural reinforcements as well, and these are estimated to be 50% of the mass of the part for the doors, and 20% for the floor [16].

Table 6.2: Material, thickness, and mass of fuselage structure components

Component	Material	Density [kg/m ³]	Thickness [mm]	Mass [kg]	Reinforcements [kg]
Skin	Al6061-T6	2700	2	140	N/A
Side door	Al6061-T6	2700	4	16	8
Back door	Al6061-T6	2700	4	14	7
Floor	Al2024-T6	2780	3	50	10
Windshield	Glass	2500	4	30	N/A

Furthermore, the fuselage frame is estimated to weigh 150 kg and is made up of Al2024-T6, like the floor, as shown in Table 6.2. On the other hand, the skin of the fuselage, the side door, and the back door are assigned Al6061-T6, as it is slightly lighter, cheaper, and weaker, since these components are not load-bearing. A further explanation of the choice of material for the fuselage can be found in Subsection 10.1.2. All together, the fuselage structural center of gravity is then calculated and found to be at 2.63 m from the nose using the general formula:

$$x_{cg} = \frac{\sum m \cdot x}{\sum m} \quad (6.1)$$

Where m is the mass of the components, and x is their centroid location with respect to the nose of the aircraft. The structural center of gravity found is 0.50 m offset from the desired location, however, by adding

cabin furniture such as the seats for the pilot and doctors, the high-voltage batteries under the floor, low-voltage batteries in the front of the nose cone, cockpit instruments, the stretcher, and the medical equipment, the final center of gravity of the cabin is then calculated to be at 2.13 m from the nose of the aircraft. An overview of the components, masses, and their center of gravity with respect to the front of the aircraft is given in Table 6.3

Table 6.3: Integral components for fuselage center of gravity calculation

Component	Mass [kg]	Location [m]
HV Battery and AC	680	1.91
LV Battery	20	0.9
Pilot seat	12	1.45
Doctor seat	12	2.25
Cockpit instruments	20	0.45
Medical equipment	61	1.8
Stretcher	35	3.2

Next, the range for the center of gravity is determined. This is performed by first outlining different cases in which the occupants of the aircraft move around, causing the center of gravity to shift. For this, the pilot is always assumed to be sitting down at their seat and has their center of gravity at the same location; therefore, the only variables are the patient and the two doctors. The cases are described as:

- **Case 1:** both doctors are sitting down, the patient is lying down on the stretcher
- **Case 2:** both doctors are sitting down, there is no patient
- **Case 3:** both doctors are in the back of the aircraft, the patient is lying down on the stretcher
- **Case 4:** one of the doctors is next to the pilot, one is sitting down, the patient is lying down on the stretcher

The location of the center of gravity with respect to the nose of the aircraft for each of the passengers for the different cases can be seen in Table 6.4.

Table 6.4: Longitudinal center of gravity location with respect to the nose of the doctors

Person	Case 1 & 2 [m]	Case 3 [m]	Case 4 [m]
Doctor 1	2.25	3.7	1.45
Doctor 2	2.25	3.7	2.25

For the mass of a person, the average weight of a male in Germany is found to be 86 kg [17], and this value was rounded to 90 kg for a more conservative approach. As there will be a total of four passengers, and taking into consideration the stretcher and the medical equipment as part of the payload for the mission, the total payload mass comes out to 456 kg. A visualization of the center of gravity range variation can be seen in Figure 6.5.

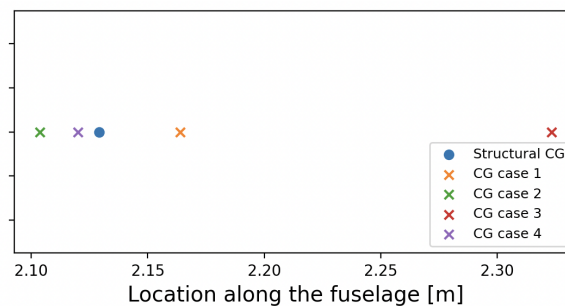


Figure 6.5: Center of gravity range variation along the length of the fuselage

As can be seen from Figure 6.5, the minimum center of gravity location is found at 2.10 m from the nose for case 2, the maximum at 2.32 m, resulting in a range of 0.22 m.

6.1.2. Fuselage Aerodynamics

In order to evaluate the performance of the fuselage and whether it is of an adequate silhouette in terms of aerodynamic properties, a computational fluid dynamics simulation was performed at zero angle of attack. The simulation is carried out using Star CCM+ from Siemens, in a turbulent regime, and at a cruise speed of 200 km/hr. An overview of the aerodynamic properties of the fuselage is presented in Table 6.5.

Table 6.5: *Aerodynamic properties of the fuselage*

Component	Value
Frontal Area [m ²]	3.72
Drag [N]	596
Cd [-]	0.09
Lift [N]	-612
Cl [-]	-0.09

As can be seen from the aerodynamic properties of the fuselage, it creates down force rather than lift; however, the amount is rather small compared to the maximum takeoff weight of the aircraft, only contributing 2%. The drag found is also found to be acceptable, considering the substantial height of the cross-section to the length of the fuselage, and the upward tilt of the tail cone. Therefore, from the conclusions presented in this section, the fuselage design and internal layout are finalized.

6.2. External Layout

Now that the fuselage has been defined, the configuration of the wing and the propellers can be designed around it. This also sets size constraints for the majority of the subsystems, making it a critical step in the design.

The most important constraints for the layout are compactness and redundancy. The former is demanded by MISS-FUNC-01, stating that the vehicle should fit in a 12 by 6 meter box in landing configuration. This ensures that the ambulance is always able to land on a street near the emergency. The redundancy requirement comes from the possibility that one engine fails. In this case, the aircraft should remain controllable, even during hover. Lastly, sufficient pitch control should be achieved.

6.2.1. Disc area and redundancy

Within these requirements, the disc area and wing lift over drag should be maximized. Disc area is important as it is directly related to hover power. Equation 6.10 shows the relation between the hover power and the disc area A [18]. Based on this, the ideal configuration would have two large rotors that cover the largest fraction of the allowed footprint. Unfortunately, such a design would be very unreliable as it would not be stable in the event of a single rotor failure, let alone controllable. Instead, multiple sets of rotors are used that would each be able to lift the vehicle independently. This way, if one rotor fails, the one it is paired to can be shut off, and the remaining pair can carry the vehicle without a resulting moment. To provide control, the turned-down propeller can provide small negative or positive thrust. This principle is commonly used by quadcopters.

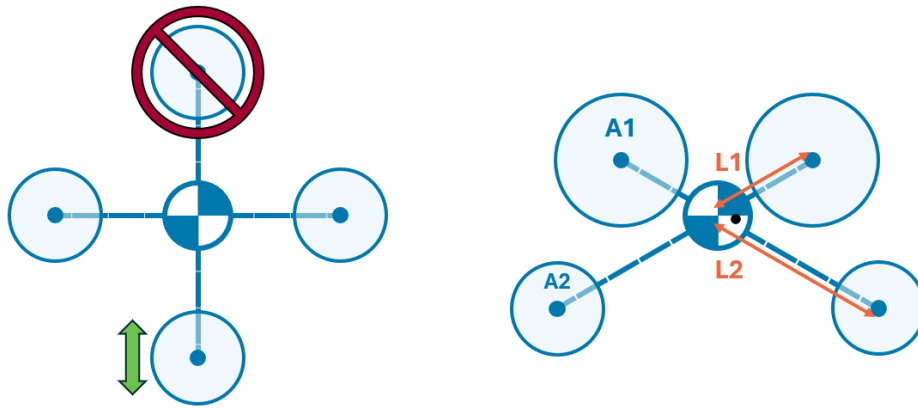


Figure 6.6: Quadcopter controllability in case of rotor failure (left) and area compensation to achieve redundancy for different arm lengths (right).

Figure 6.6 illustrates the scenario of a single rotor failure for a configuration with two propeller pairs. Next to it is a sketch of a layout containing different propeller arms $L1$ and $L2$. This increases the freedom in the design space, but to ensure the moment of both propellers around the center of gravity is similar, the inner propeller has to generate more thrust than the outer one. As it is most efficient for both propellers to have the same exhaust velocity and therefore disc loading, the areas $A1$ and $A2$ have to be scaled accordingly.

$$\frac{A1}{A2} = \frac{L2}{L1} = \left(\frac{\text{Diameter1}}{\text{Diameter2}} \right)^2 \quad (6.2)$$

Equation 6.2 can be used to sketch discs with correct proportions for any configuration with disc pairs connected by a line through the center of gravity. This leaves the number of pairs free to be chosen. The minimum amount for single rotor failure redundancy is 2 pairs, but more is also possible. Having 3 pairs, for instance, means that there are 2 pairs left to carry the vehicle in case of a rotor failure. Then each rotor only has to provide 150% of its nominal thrust as opposed to 200% for a quadcopter. The drawback of having more rotors is that they have to fit on the wing, and for a tiltwing, this generally results in a smaller combined area.

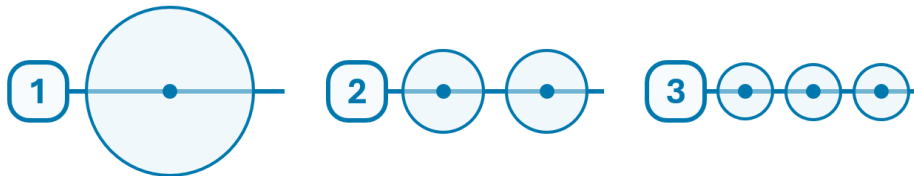


Figure 6.7: Disc area for 1, 2, and 3 rotors per wing.

Figure 6.7 illustrates how disc area decreases dramatically with the number of pairs. This has a large effect on hover efficiency and compensates for the larger motor weight. Furthermore, large thrust margins on the motors are also beneficial for control authority, which is why the least number of pairs that is still redundant is selected.

6.2.2. Pitch control

The design in the center of Figure 6.7 would be very efficient at flying vertically, but has no pitch control in horizontal flight. This could be solved by adding another thruster to the tail merely for pitch control. Unfortunately, this adds weight, creates drag during cruise flight, increases complexity, and introduces a new way of failure. Alternatively, the main rotor pairs could be spaced out over the longitudinal direction of the aircraft. As these rotors are designed to carry the entire weight of the aircraft, throttling them by a small amount can already create a large moment.

$$X_{\text{longitudinal}} = \frac{X_{\text{tail}} \cdot \Delta T_{\text{tail}}}{\Delta T_{\text{rotorpair}}} = \frac{4 \text{ [m]} \cdot 1000 \text{ [N]}}{\text{MTOW}} \approx 0.16 \text{ [m]} \quad (6.3)$$

Equation 6.3 assumes the rear rotors produce twice their nominal thrust and the front rotors generate no thrust at all to create a pitch moment. To demonstrate this an exemplary calculation is performed. For an estimated MTOW of 2600 kg, the front rotors would only have to be spaced 16 cm in front of the rear rotors to generate the same moment as a 1000 N ducted fan positioned at the end of a 4 m tail. The only drawback is that the wing has to accommodate this offset.

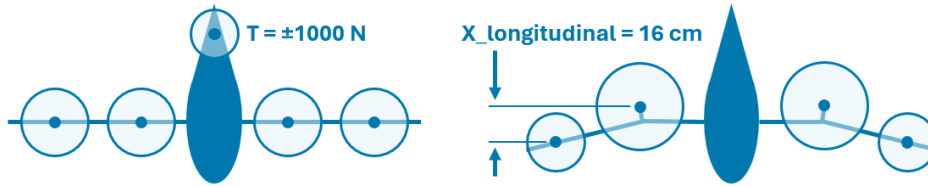


Figure 6.8: Equal amount of pitch control using a ducted fan (left) or main rotor spacing (right).

One way to solve this is to give part of the wing an anhedral, such that only two short pylons are needed to connect all four rotors to the wing. This is shown in Figure 6.8 and known as the gull design due to its resemblance to the wings of the seabird. According to [19], up to 20 degrees of anhedral on the outboard part of the wing might not perform worse than a straight wing. Furthermore, the bending moment is identical to a normal wing, as well; therefore, structurally, the wing only performs worse in terms of torsion and manufacturability. A more detailed trade-off has been performed in [20]. In this trade-off, the gull wing was also selected, so the next section will expand on this design.

6.2.3. Resulting External Layout

In the previous section, most of the parameters that were free to change have been selected. This section will try to design a layout that satisfies all of them whilst maximizing disc area. This is performed in a CAD program, as this allows geometries to be constrained in a specific way and can therefore be used to calculate the best geometry.

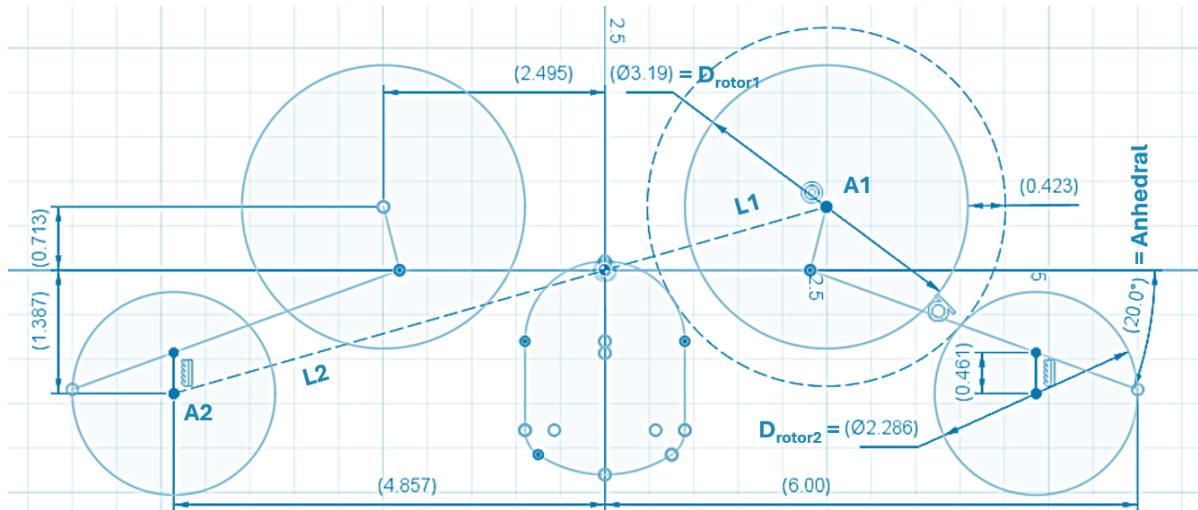


Figure 6.9: Front view of the wing and rotor configuration in horizontal flight mode

Figure 6.9 shows a simplified version of the final geometry that was found using this method. It was constructed by first drawing a front view of the fuselage and four large circles, indicating the rotors. The hinge location is in the center, and when the wing is tilted, this point will be in line with the center of gravity. That is why both rotor pairs are centered around this point (indicated by the diagonal dashed line). For the lower rotor to connect to the wing, it has to be placed farther outboard. This increases its distance to the cg and its relative diameter is sized according to Equation 6.2. Next, the $X_{\text{longitudinal}}$ distance is set to 2.1 m, as this is the least amount of spacing for which a tail duct is not needed. Lastly, the absolute diameter of the rotors has to be determined. This is constrained by setting the margin between the rotors and the fuselage

to about 20% of the rotor diameter. This is a value comparable to what existing designs like Joby and Archer Midnight feature.

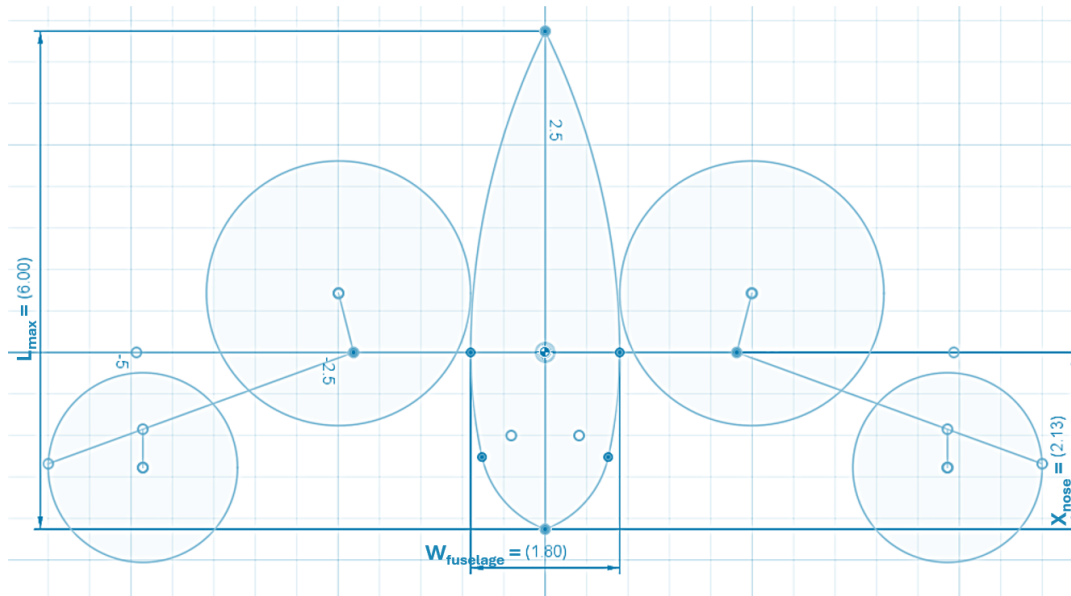


Figure 6.10: Top view of the wing and rotor configuration in vertical flight mode

Figure 6.10 shows the longitudinal placement of the wing on the fuselage. It is chosen such that the nose of the fuselage is in line with the most forward motors, thus maximizing the length of the fuselage in the limited space. This also yields a tail length value, which can be used by the aerodynamics department to size the tail surfaces.

Table 6.6: Summary of the parameters determined in this chapter.

Parameter	Value
Span [m]	12
Inner Span [m]	2.5
Anhedral [deg]	20
X_{nose} [m]	1.7
Propeller Margin [m]	0.42
Inner Rotor Diameter [m]	3.2
Outer Rotor Diameter [m]	2.3
Disc Area [m ²]	24
Longitudinal Hinge Position [m]	2.5

Table 6.6 contains the most important parameters from this section. Notice that a top view of the wing is not shown in any of these drawings because it is not tightly constrained. The aerodynamics department has the freedom to choose the best sweep and chord distributions, as long as the wing does not touch the ground in vertical flight mode.

6.3. Technical Resource Allocations

After coming up with the concept sizing, it is crucial to have the budgets for each technical resource, including schedule, volume, mass, power, and cost.

6.3.1. Time Budget

The first parameter to be budgeted is the time required to develop, manufacture, and maintain the eVTOL vehicle. These steps will be considered independently, the final result of this analysis providing the team with a time reference which will be used for contingency and technology management.

Development Stage

Given the scope of this project, the initial development stage has a set deadline of 10 weeks. This time will be used for the preliminary planning, market analysis, and design of this vehicle. This stage can be broken down into the following stages:

1. Project Planning(1 week)
2. Pre-Design(1 week)
3. Preliminary Design(3 weeks)
4. Detailed Design(5 weeks)

Manufacturing Stage

Following the design and checking the viability of the product, the manufacturing stage can begin. This stage will highly depend on the design chosen and the novelty of the technology chosen following the detailed design. In order to account for more in-depth design, manufacturing, and certification, a time budget of 2 years has been allocated for this.

Maintenance Stage

Finally, after the product has been produced and introduced into the market, it needs to be maintained, kept up to date with regulations, and improved for market competitiveness throughout time. As the succession of this model is uncertain given the newly opened and volatile eVTOL market, a minimum of 20 years of service is attributed. Given successful deployment and increased demand, this service time will be expanded in future stages.

6.3.2. Volume Budget

In order to better define the mass budget, the starting point is the necessary physical space for operation. This will dictate the need for structural elements and will provide a mass estimate for them.

The starting point for the volumetric budget is the space used in today's land vehicles for emergency operations. Thus, the ambulance chosen is the one currently used in the Netherlands, which is the Mercedes Sprinter Cargo [21]. Since the objective of the mission is to surpass the land ambulances in terms of performance, the interior volume of this vehicle is taken as the maximum volume needed.

Furthermore, to define a lower bound for this quantity, medical helicopters and similar eVTOL ambulances, such as ERC, are taken into account.

Table 6.7: *Volume Budget Table*

Quantity	Value [m ³]
Ground Ambulance [21]	15
ERC [22]	5.2
EC 145 [23]	6
Bell 412 [24]	6.2
Minimum Volume Required	6
Maximum Volume Required	15

6.3.3. Mass Budget

To iteratively estimate the mass budget, the analysis starts with an initial MTOW of 2500 kg. The mass of the aircraft is broken down into groups: payload, equipment, structure, propulsion, and power source. The weight for payload (456 kg) is calculated in Subsection 6.1.1; the weights for equipment (12% of MTOW) and structure (27%) are calculated as proportions of MTOW according to a research paper [25]. The mass of the propulsion is dependent on peak power use during takeoff and cruise; this is calculated through a statistical relation for motor weight and a scaling relation for propeller weight. The mass of the power storage is the product of battery energy density and total energy use per mission. These group weights are summed together to reach a new MTOW. If the assumptions for the weight ratios and other mission parameters are feasible, then the iterations should converge to an MTOW that makes the design possible. The whole mass estimation is done on a conservative basis to ensure the designed aircraft is able to fly and fulfill the requirements despite imperfect manufacturing and unaccounted design changes.

The detailed estimation method is presented below. The time in each flight phase is outlined in . The total energy per mission (two legs) follows Equation 6.4.

$$E_{\text{mission}} = 2(E_{\text{takeoff}} + E_{\text{transition1}} + E_{\text{climb}} + E_{\text{cruise}} + E_{\text{descent}} + E_{\text{transition2}} + E_{\text{hover}} + E_{\text{landing}}) \quad (6.4)$$

The energy for each flight phase is affected by the power. The discussion of the process for determining power from takeoff weight is deferred to Subsection 6.3.4.

With the energy density of the battery (the estimation assumes 275 Wh/kg), this leads to a battery mass with 80% degradation of capacity (SYS-PROP-11); it effectively reduces the battery energy density to 220 Wh/kg:

$$m_{\text{battery}} = 1.1 \frac{E_{\text{mission}} [J]}{0.80 \rho_{\text{energy}} [J/kg]} \quad (6.5)$$

The cell-to-pack factor 1.1 is introduced to account for the mass of the thermal system and the casing¹ [26].

A database for high-power electric motors with integrated inverters has been created. This leads to a linear relation between mass and peak power:

$$m_{\text{motor}} = 0.116 \cdot P_{\text{peak}} + 4.52 \quad (6.6)$$

In these relations, the power is in kW and the mass is in kg. The peak power is determined by the power required for a motor in one engine inoperative condition, where 200% of the motor thrust is required. The propeller mass is estimated by scaling the mass of the VoloConnect's propeller to the actual propeller diameter² [27]:

$$m_{\text{propeller}} = 4.35 \cdot D_{\text{rotor}} \quad (6.7)$$

Summing the masses up, the mass of the propulsion group can be obtained:

$$m_{\text{propulsion}} = \sum_i (m_{\text{motor}} + m_{\text{propeller}}) \quad (6.8)$$

The tilting wing mechanism with actuators is assumed to weigh 120 kg. The wing hinge mass is added to $m_{\text{structure}}$.

Finally, the new MTOW is calculated by,

$$m_{\text{MTOW}} = m_{\text{battery}} + m_{\text{equipment}} + (m_{\text{structure}} + m_{\text{wing hinge}}) + m_{\text{propulsion}} + m_{\text{payload}} \quad (6.9)$$

When the MTOW stops changing across iterations, the battery and propulsion system can supply sufficient power to perform the mission at their current mass estimate. Again, this estimate serves as an upper bound. The mass budget for some important elements is summarized in Table 6.9.

Table 6.8: Mass Estimation

Subsystem	Mass [kg]
Propulsion	315
Power Source	695
EOW	2140
MTOW	2600

6.3.4. Power Budget

This subsection discusses the power required for each flight stage at a given MTOW. The calculation is done for each propeller and or motor; the total power is the sum of individual powers. Hover power is the first one to be estimated, as it plays an important role in the power budget. Hover power is primarily induced power, calculated using momentum theory and corrected by the figure of merit:

$$P_{\text{induced}} = \frac{T^{\frac{3}{2}}}{\sqrt{2\rho S_{\text{disc}}}} \quad (6.10)$$

¹BYD Han 2023 has a cell-to-pack ratio of 90%. The lightweight aerospace materials and components should help achieve a similar number.

²An additional 2.5 kg is added and scaled to account for the variable pitch mechanism.

$$P_{\text{hover}} = \frac{P_{\text{induced}}}{FM} \quad (6.11)$$

Where T is the thrust required in hover (assumed equal to weight), S_{disc} is the disc area, and FM means figure of merit (equal to 0.8).

Takeoff power is modeled as an extension of hover power with an induced velocity correction:

$$v_{\text{ihv}} = \frac{P_{\text{induced}}}{T} \quad (6.12)$$

$$\lambda = \frac{V_{\text{climb}}}{v_{\text{ihv}}} \quad (6.13)$$

$$P_{\text{takeoff}} = P_{\text{hover}} \cdot \left(0.5\lambda + \sqrt{(0.5\lambda)^2 + 1} \right) \quad (6.14)$$

Furthermore, the power required during cruise flight has been estimated. The cruise power is determined by the thrust required to overcome aerodynamic drag, which is approximated using the aircraft's lift-to-drag ratio (L/D):

$$T_{\text{cruise}} = \frac{W}{(L/D)} \quad (6.15)$$

$$P_{\text{cruise}} = \frac{T_{\text{cruise}} \cdot V_{\text{cruise}}}{\eta_{\text{motor}} \cdot \eta_{\text{propeller}}} \quad (6.16)$$

Here, the lift-to-drag ratio, drag coefficients, and frontal surface areas are derived from a preliminary sizing of the fuselage and wing, complemented by initial simulation results. A L/D of 10.3 is estimated for the whole aircraft. The freestream velocity is taken from MIS-FUNC-06.

Climb power is calculated similarly to that of a propeller-driven aircraft during the climb phase, consisting of the power required to gain altitude and to overcome parasitic drag forces:

$$P_{\text{climb}} = \dot{h} \cdot W + \frac{1}{2} \rho V_{\text{air}}^3 (S_{\text{wing}} C_{D,\text{wing}} + S_{\text{fuselage}} C_{D,\text{fuselage}} + S_{\text{tail}} C_{D,\text{tail}} + S_{\text{strut}} C_{D,\text{strut}} + S_{\text{gear}} C_{D,\text{gear}}) \quad (6.17)$$

Here, the drag coefficients of each component are obtained either through aerodynamic simulation software (e.g., XFLR5) or from relevant literature sources.

The descent phase is assumed to consume zero power, as it is modeled as a gliding maneuver with the propulsion system turned off. Transition and landing phases are conservatively assumed to use the same power as in hovering.

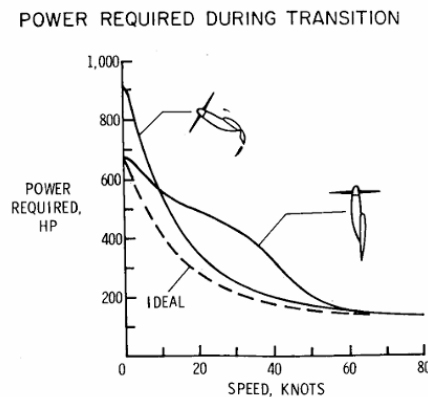


Figure 6.11: Hover Power vs. Transition Power [28]

As shown in Figure 6.11, the power required for the transition phase in a tiltwing configuration is consistently lower than that required for hovering. This supports the conservative assumption used in this analysis.

Furthermore, using the flight envelope defined in Figure 3.2, the total mission energy can be estimated by multiplying the power required in each flight segment by the duration of that segment.

The power budget for each phase of operation and total energy consumption is summarized in Table 6.9. The high takeoff power is due to high disc loading ($\approx 800 \text{ kg/m}^2$).

Table 6.9: Power Requirement and Total Mission Energy

Flight Phase	Power [kW]
Take-off	790
Transition 1	700
Climb	550
Cruise	180
Descent	0
Transition 2	700
Hover	700
Landing	700
Total Energy [kWh]	140

With a margin of 10%, the total energy should be around 155 kWh. This allows for some uncertainties existing since the design phase now is still conceptual and the MTOW might change as design goes on.

6.3.5. Cost Budget

Finally, to remain competitive in the market and comply with all defined requirements, the eVTOL must adhere to a cost budget. The cost model is primarily a function of mass and is divided into three main components: structure, powerplant, and others. The structure refers to the airframe. The powerplant consists of two parts: the battery and the engine. The others category includes manufacturing labor costs and remaining subsystems, such as avionics, air conditioning, and the flight control system. For the structural cost, the following equation is used [29]:

$$C_{\text{structure}} = 2600 \cdot m_{\text{airframe}}^{0.766} \cdot Q_{\text{airframe}}^{-0.218} \cdot \text{CEF} \quad (6.18)$$

Where Q_{airframe} refers to the quantity to be produced, and CEF is the cost escalation factor. CEF is used for contingency management, as it accounts for inflation. The powerplant cost is the sum of the battery and engine costs. The engine is priced at €500 per kilogram, while the battery is priced at €500 per kWh. [30] The “Other” category is more variable and case-dependent. Therefore, it is conservatively estimated as 1.5 times the sum of structural and powerplant costs to account for labor, integration, and minor subsystems.

Note that research, development, and tooling costs are excluded from the unit cost summary in Table 6.10. The margin applied is 10%, as the project remains in the conceptual design phase. At this stage, many design details are still evolving, and there are inherent uncertainties in cost drivers such as materials, system integration, and supplier pricing. A 10% margin provides a reasonable buffer to account for these unknowns while still guiding early-stage planning and trade studies.

Table 6.10: Unit Manufacturing Cost Summary (in 2025 EUR)

Cost Item	Amount (€)
Airframe	280,000
Engine	200,000
Battery	77,500
Total Cost	€557,500
Other (est. 1.5× structural + powerplant)	€169,500
Subtotal (before margin)	€727,000
Final Cost (with 10% Margin)	€800,000

7

Aerodynamics

The main aerodynamic characteristics of the design will be described in this chapter. This begins with a detailed wing design which will be optimized for aerodynamic purposes, presented in Section 7.1. Once the wing is designed, the tail will also be sized accordingly to the requirements, and this will be presented in Section 7.2, followed by the sizing of the control surfaces for both the wing and the tail in Section 7.3. Lastly, an overview of the specification will be given in Section 7.4.

Aerodynamics Symbols

S	Area	AR	Aspect ratio	Re	Reynolds number
W	Weight	N	Normal force	r	Radius
ρ	Air density	V	Velocity	l	length
μ	dynamic viscosity	C	Dimensionless Coefficient	b	span
C_l	Airfoil lift coefficient	C_L	Wing lift coefficient	α	Angle of attack
C_r	Root chord	C_t	Tip chord	Ω	Anhedral
MAC	Main aerodynamic chord	MGC	Main geometric chord	λ	Taper ratio
c	Chord	ϵ	Downwash angle	Λ	Sweep angle
d	Diameter	q	Dynamic pressure	L	lift
D	Drag	σ	Sidewash angle	β	Sideslip angle
δ_a	Aileron deflection	δ_r	Rudder deflection	p	Roll rate
q	Pitch rate	r	Yaw rate		

Subscripts

f	Fuselage	w	Wing	ac	Aerodynamic center
0	Zero angle of attack	α	Angle of attack	A-h	Aircraft without tail
p	Propeller	LE	Leading edge	TE	Trailing edge
h	Horizontal tail	v	Vertical tail	l	Starting point of the control surface
a	Aileron	r	Rudder	e	Elevator

*All values in SI units with conventional aircraft reference frame (x pointing towards nose, y pointing towards the right wing).

7.1. Wing Design and Optimization

In Chapter 6, the general shape of the wing has been determined. However, many parameters are still free to change. These include wing airfoil, twist, chord distribution, thickness, and sweep. These are tweaked carefully to make sure the wing fulfills its functions as much as possible. The most important functions of a wing are listed below:

Lift Generation In horizontal flight, the wing should be able to generate sufficient lift to cancel the weight of the aircraft.

Stall behavior Unlike other aircraft, an eVTOL does not have to land horizontally. This eliminates the need to fly at low velocities, and therefore the need for a high lift coefficient. Stall behavior should still be considered, as the aircraft can still stall in high load factor conditions at cruise speed. In such a scenario, the wing should stall gradually and remain controllable, which can be achieved by a gradual stall from the wing roots.

Drag Performance To extend the range of the aircraft, cruise drag should be as small as possible. It is composed of two parts; induced and profile drag. The latter can be reduced by selecting airfoils with a high

lift over drag ratio. Induced drag depends on the span and the shape of the lift distribution. Since the span is constrained, only the shape of the lift distribution can be made elliptical to improve performance.

Thickness The wing has to carry the loads of the produced lift and thrust of the engines, without becoming too heavy. Wing weight depends mostly on the thickness of the wing, which is why this is kept at a fixed value. This way the wing aerodynamics can be optimized, without compromising the structure.

To support all these functionalities, a broad range of airfoils is required. Stall behavior is influenced by the nose radius, while the lift-to-drag ratio is affected by the amount of camber. Additionally, a wide range of thickness-to-chord ratios must be available.

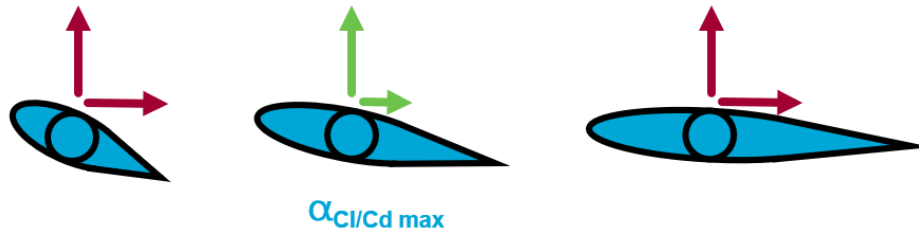


Figure 7.1: Airfoils with different thickness ratios providing the same amount of lift

Figure 7.1 illustrates how airfoils with different thickness ratios have to fly at different angles of attack to provide the same amount of lift, if thickness is fixed. For a certain thickness ratio, the airfoil achieves the largest lift over drag value, making it a better option. Because the thickness and required lift vary along the span of the wing, the optimal airfoil may also change along the wing. To accommodate this, the wing is split up into about 9 sections, for each of which the best option is calculated. To speed up this process, critical information about a large number of airfoils is stored in a database. These include the lift over drag ratio as a function of the angle of attack (approximated using a polynomial), the stall angle of attack, and the zero-lift angle of attack.

With this data, the following procedure can be carried out for each section:

1. Each airfoil in the database is scaled so that it is as thick as the wing should be at the selected section. This results in a different chord length for airfoils with a different thickness ratio.
2. From the elliptical lift distribution, the required lift at the selected section is calculated. Dividing this by the design dynamic pressure and the width of the section yields the chord- C_l product the section should generate.
3. Using the required chord- C_l product and the chord, the required lift coefficient for each airfoil is calculated.
4. The lift coefficient(C_l) is assumed to be achieved in the linear region of the C_l -alpha curve, and the slope of this curve is approximated by 2π . Combined with the zero-lift angle of attack this can be used to find the angle of attack each airfoil in the database would have to fly at to generate sufficient lift.
5. For this angle of attack, the lift over drag value of each airfoil can be found. Furthermore, the margin between the cruise and stall angle of attack can be determined.
6. Depending on the spanwise position of the airfoil, a certain amount of stall margin is desired. Closer to the root it should be less than near the wingtips. Based on this part of the airfoil can be excluded from the selection.
7. From the remaining airfoils, select the one with the best lift over drag.

With this method, the chord, twist, and airfoil type can be found for each point along the wingspan. However, this wing is finite and will create a downwash, impacting its own performance.

$$\alpha_{\text{induced}} = \frac{(c \cdot C_l)}{b \cdot \pi} \quad (7.1)$$

By the lifting line theory, the induced angle of attack is constant along the wing for an elliptical lift distribution and can be found using Equation 7.1. Adding this value to the previously found angles of attack yields the final cruise angle of attack for each section.

Table 7.1: Performance improvement before and after optimization

Specification	Before optimization	After optimization
$C_{L\text{Max}}$ [-]	1.7	2.1
L/D_{cruise} [-]	20	25
α_{cruise} [deg]	7.5	6.5
Oswald factor [-]	0.7	0.75
$C_{m\text{cruise}}$ [-]	0.07	0.12

7.2. Tail Sizing

The tail is sized for static stability during cruise. Although the aircraft has extra controllability by using differential thrust in all three axes due to the gull wing design, the aircraft is designed to be statically stable by using tail stabilizers.

In terms of tail configuration, it shall be designed and the tail surfaces should be placed in such a way that they have minimum interference with the fuselage, wing, and propellers. To achieve this, different configurations, including conventional tail, T-tail, V-tail, and H-tail are considered. By examining the front view of the aircraft, shown in Figure 6.9, the T-tail seems to have the least interference with the fuselage, propeller, and wing. This is an estimation as further performance needs to be examined by wind tunnel tests, which is out of the scope of the current design phase. Because of this, T-tail is chosen to be the tail configuration of the aircraft.

7.2.1. Horizontal Stabilizer

To achieve longitudinal stability, the longitudinal stability derivative $C_{m\alpha}$ has to be negative. The tail size follows the equation below [31].

$$\frac{S_h}{S} = \frac{\bar{x}_{cg} - \bar{x}_{ac} + SM}{\frac{C_{L\alpha h}}{C_{L\alpha A-h}} \left(1 - \frac{d\varepsilon}{d\alpha}\right) \frac{l_h}{\bar{c}} \left(\frac{V_h}{V}\right)^2} \quad (7.3)$$

where the $S.M.$ is set to be 0.025 in this case. The aerodynamic center of the aircraft is assumed to follow the following formula (Equation 7.4).

$$\left(\frac{x_{ac}}{\bar{c}}\right)_{wf} = \left(\frac{x_{ac}}{\bar{c}}\right)_w - \frac{1.8 b_f h_f l_{fn}}{C_{L\alpha A-h} S \bar{c}} + \frac{0.273 b_f c_g (b - b_f)}{(1 + \lambda) \bar{c}^2 (b + 2.15 b_f)} \tan \Lambda_{1/4} \quad (7.4)$$

where the aerodynamic center of the wing, $\left(\frac{x_{ac}}{\bar{c}}\right)_w$ is assumed to be the quarter chord point, and the effect of motor nacelles is neglected for simplicity because of the time constraint given for the project. The lift curve of the horizontal tail and fuselage is calculated by using the DATCOM method given by Equation 7.5 and Equation 7.6.

$$C_{L\alpha h} = \frac{2\pi A_h}{2 + \sqrt{4 + \left(\frac{A_h \beta}{\eta}\right)^2 \left(1 + \frac{\tan^2 \Lambda_{0.5C_h}}{\beta^2}\right)}} \quad (7.5)$$

$$C_{L\alpha A-h} = C_{L\alpha w} \left(1 + 2.15 \frac{b_f}{b}\right) \frac{S_{net}}{S} + \frac{\pi}{2} \frac{b_f^2}{S} \quad (7.6)$$

The aircraft also needs to be able to stay trimmed during cruise, so the controllability needs to be considered as well. The controllability curve is given by Equation 7.7.

$$\frac{S_h}{S} = \frac{\bar{x}_{cg} + \frac{C_{mac}}{C_{L\alpha A-h}} - \bar{x}_{ac}}{\frac{C_{Lh}}{C_{L\alpha A-h}} \frac{l_h}{\bar{c}} \left(\frac{V_h}{V}\right)^2} \quad (7.7)$$

where

$$C_{mac} = C_{mac_w} + C_{mac_{fus}} \quad (7.8)$$

and

$$C_{mac} = C_{m_{0\text{airfoil}}} \left(\frac{A \cos^2 \Lambda}{A + 2 \cos \Lambda}\right) \quad (7.9)$$

$$C_{m_{ac_{fus}}} = -1.8 \left(1 - \frac{2.5b_f}{l_f}\right) \frac{\pi b_f h_f l_f}{4S\bar{c}} \frac{C_{L_0}}{C_{L_{\alpha_{A-h}}}} \quad (7.10)$$

Combining Equation 7.3 and Equation 7.7, the scissor plot for the horizontal stabilizer is plotted as Figure 7.4. The two red dashed lines marked the most forward and backwards center of gravity positions. The center of gravity position with the corresponding tail ratio needs to stay in the green area to reach static stability and controllability. It can be seen that the minimum horizontal tail size is about 28% of the wing size to achieve both longitudinal stability and controllability.

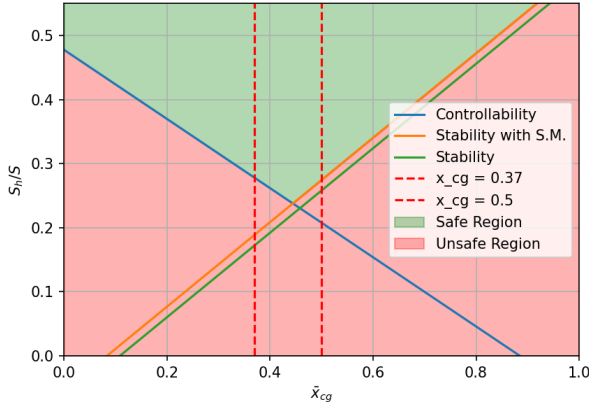


Figure 7.4: Longitudinal stability and controllability (scissor plot)

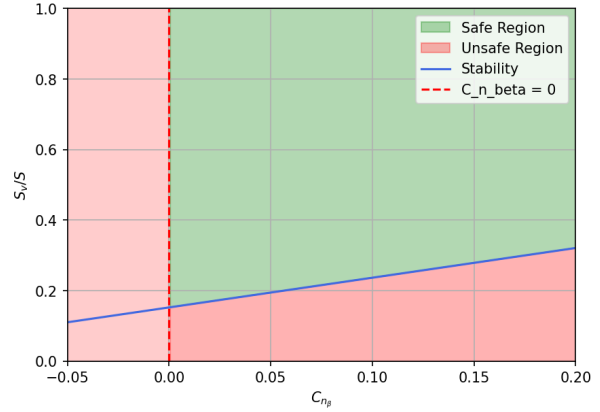


Figure 7.5: Directional stability

7.2.2. Vertical Stabilizer

Analogy to longitudinal stability, the static directional stability is determined by C_{n_β} . In directional stability analysis, the gravity of the aircraft does not play a role, so the curve can be plotted simply against C_{n_β} itself. The $C_{n_{\beta_{A-h}}}$ of the fuselage is estimated by the DATCOM method as well:

$$C_{n_{\beta_{A-h}}} = C_{n_{\beta_f}} + C_{n_{\beta_p}} \quad (7.11)$$

where

$$C_{n_{\beta_f}} = \left(0.3 \frac{l_{cg}}{l_f} + 0.75 \frac{h_{f_{max}}}{l_f} - 0.105\right) \frac{S_f l_f}{S b} \left(\frac{h_{f1}}{h_{f2}}\right)^{\frac{1}{2}} \left(\frac{b_{f2}}{b_{f1}}\right)^{\frac{1}{3}} \quad (7.12)$$

$$C_{n_{\beta_p}} = -0.053 B_p \Sigma \left(\frac{l_p d_p^2}{S b}\right) \quad (7.13)$$

Note that f_1 and f_2 in the equation refer to the value at 1/4 of the fuselage from the nose and 3/4 of the fuselage from the nose. Then, the total directional stability can be expressed by Equation 7.14 and is plotted as Figure 7.5. It can be seen from the plot that the minimum vertical tail size is about 22% of the wing size.

$$\frac{S_v}{S} = \frac{C_{n_\beta} - C_{n_{\beta_{A-h}}}}{C_{Y_{\beta_v}} \frac{l_v}{b} \left(1 - \frac{d\sigma}{d\beta}\right) \left(\frac{V_v}{V}\right)^2} \quad (7.14)$$

7.2.3. Dynamic stability

After sizing both the horizontal and vertical tails, the dynamic stability analysis can be carried out by using XFLR5 [32]. For cruise condition ($V = 55.6 [m/s]$), the eigenvalues corresponding to each mode are plotted in Figure 7.6 and Figure 7.7. It can be seen from the figure that all modes are dynamically stable (real part of the eigen modes is negative), except for the spiral mode, while the spiral is often unstable for most of the aircraft [33]. Note for this part, the effect of the shape of the fuselage is neglected (the fuselage is modeled as a point mass at the hinge), and usually, the fuselage is destabilizing.

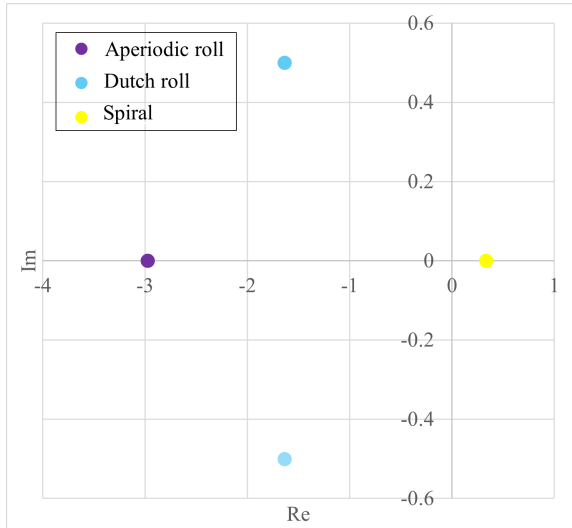


Figure 7.6: Lateral modes

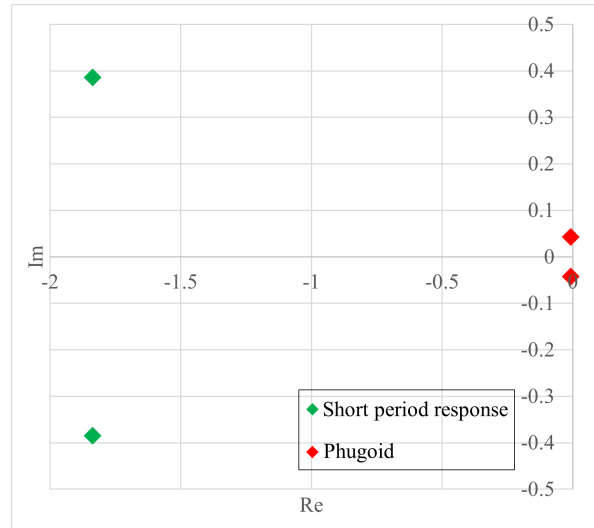


Figure 7.7: Longitudinal modes

7.3. Control Surfaces Sizing

For control surfaces sizing, a roll, pitch and yaw rate requirement is set. For eVTOLs, there is no certification requirement on the maneuverability of the vehicle. However, it is always desired to achieve a certain level of maneuverability. As the to-be-designed aircraft is able to hover and have extra controllability due to the gull-wing design, the control surfaces sizing is simplified to straight and steady flight. In this case, the full linearized symmetrical flight EoM for aircraft flight dynamics reduces to the following [34]:

$$C_{m_q} \frac{q\bar{c}}{V} + C_{m_{\delta_e}} = 0 \quad (7.15)$$

Similarly, for asymmetrical flight

$$\begin{bmatrix} C_{l_p} & C_{l_r} \\ C_{n_p} & C_{n_r} \end{bmatrix} \begin{bmatrix} \frac{pb}{2V} \\ \frac{rb}{2V} \end{bmatrix} + \begin{bmatrix} C_{l_{\delta_a}} & C_{l_{\delta_r}} \\ C_{n_{\delta_a}} & C_{n_{\delta_r}} \end{bmatrix} \begin{bmatrix} \delta_a \\ \delta_r \end{bmatrix} = 0 \quad (7.16)$$

The stability derivative is estimated by

$$C_{l_p} = -\frac{(c_{l_a} + c_{d_0})C_r b(1 + 3\lambda)}{24S} \quad (7.17)$$

This considers only the contribution of the wing, while there is a lack of literature on estimating other dynamic stability derivatives, which are usually obtained from wind tunnel tests, flight tests or CFD. For this project, a very rough estimation of these stability derivatives is carried out. As the damping frequency varies linearly with respect to mass squared, the fuselage mainly contributes to C_{n_r} and C_{m_q} , these two dynamic stability derivative are linearly scratched with respect to the fuselage-wing mass ratio. This is a very rough estimation for preliminary design, and the calculation has to be updated if a wind tunnel test or CFD simulation is carried out in the future design process.

The roll rate, pitch rate and yaw rate requirements are all set to 30 degrees per second since there is no clear certification on eVTOLs. The maximum deflection angle of the aileron and elevator is set to 30 degrees, and the maximum deflection angle for the rudder is set to 15 degrees. The control surfaces start from the 3/4 chord point.

7.4. Specifications

The final wing and tail design specification is listed in Table 7.2, Table 7.3 and Table 7.4. An illustration of the wing, tail, and control surface position is shown in Figure 7.8 and Figure 7.9.

Table 7.2: Wing Planform Specification

Parameter [Unit]	Value
S_{wing} [m^2]	11.27
$b_{wing, net}$ [m]	10.2
$b_{wing, gross}$ [m]	12.0
MGC [m]	0.93
MAC [m]	1.09
AR [-]	13.12
λ [-]	0.46
Λ_{LE} [deg]	1
$C_{r, wing}$ [m]	1.4
$C_{t, wing}$ [m]	0.644
Ω [deg]	15
b_{1a} [m]	4.86
S_a [m^2]	0.19

Table 7.3: Horizontal Stabilizer Specification

Parameter [Unit]	Value
S_h [m^2]	3.47
b_h [m]	4.14
MGC _h [m]	0.84
MAC _h [m]	0.89
AR _h [-]	4.95
λ_h [-]	0.4
Λ_{LE} [deg]	15.48
$C_{r, h}$ [m]	1.2
Airfoil [-]	NACA0012
Ω [deg]	0
b_{1e} [m]	0
S_e [m^2]	0.43

Table 7.4: Vertical Stabilizer Specification

Parameter [Unit]	Value
S_v [m^2]	2.5
b_v [m]	3.34
MGC _v [m]	1.49
MAC _v [m]	1.51
AR _v [-]	4.47
λ_v [-]	0.67
Λ_{LE} [deg]	15.02
$C_{r, v}$ [m]	1.794
Airfoil [-]	NACA0012
Ω [deg]	0
$l_{v, LE}$ [m]	3.6
$C_{t, v}$ [m]	1.2
Λ_{TE} [deg]	0
b_{1r} [m]	0.33
S_r [m^2]	0.47

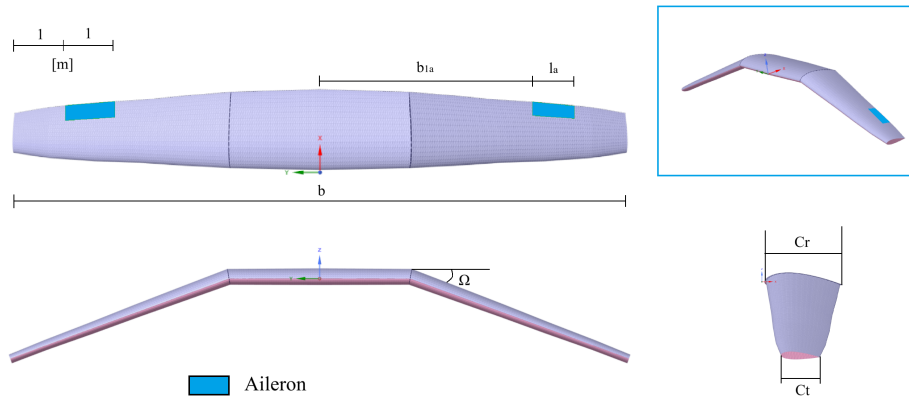


Figure 7.8: Final wing platform design

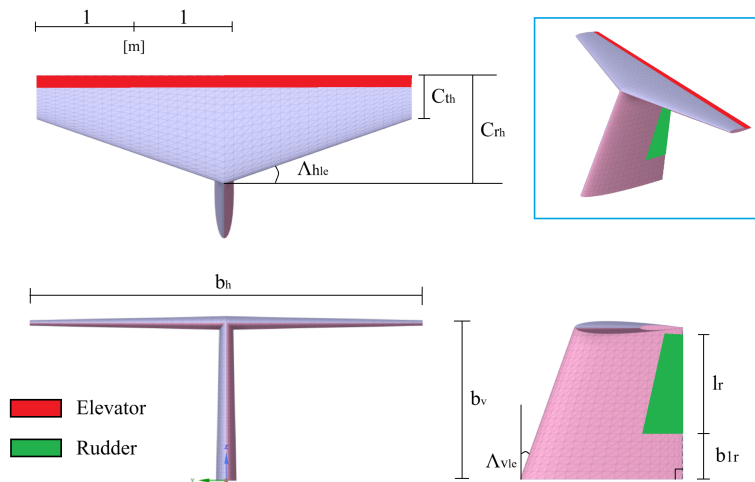


Figure 7.9: Final tail design

7.5. Sensitivity analysis

A sensitivity analysis is carried out for the wing platform design and tail design for the main inputs. Since there are too many inputs for the design, only the inputs that changes during the iterative design process are included in this section. Sensitivity analysis on rudder and elevator sizing is not carried out since the dynamic stability derivatives are rough estimations. For vertical and horizontal tail sizing, it can be seen from Table 7.7 and Section 7.6 that wing area does not have a significant impact on the size of the tail. However, this is based on the fact that in the sensitivity analysis, it is assumed the lift provided by the wing stays the same, while the only variable in this case is the wing area. Tail efficiency, that is, the local airspeed ratio between the main wing and the tail, has a significant impact on the size of the tail, thus, the exact value need to be refined in further design to get a more accurate output.

Table 7.5: Sensitivity analysis on horizontal tail sizing

Parameter	Low Value	High Value	S_h Range	Change (%)
Wing area (S_w) [m^2]	9	13.5	3.33 → 3.38	1.5%
Tail efficiency (V_h/V) [m/s]	0.64	0.96	4.84 → 2.14	-55.8%
Cg range (\bar{x}_{cg}) [-]	0.104	0.156	3.04 → 3.15	3.6%

Table 7.6: Sensitivity analysis on vertical tail sizing

Parameter	Low Value	High Value	S_v Range	Change (%)
Wing area (S_w) [m^2]	9	13.5	2.43 → 2.56	5.56%
Tail efficiency (V_v/V) [m/s]	0.8	1.2	3.95 → 1.81	-54.3%

Table 7.7: Sensitivity analysis on aileron sizing

Parameter	Low Value	High Value	S_a Range	Change (%)
Wing span (b) [m]	9.6	14.4	0.095 → 0.22	132%
Cruise speed (V_c) [m/s]	44	66	0.20 → 0.13	-35 %
Roll requirement (deg^{-1}) [-]	24	36	0.12 → 0.19	58.3%

Propulsion and Power

In this chapter, the propulsion and powertrain system design will be discussed. Starting from the thrust, the geometry of the propellers will be determined, further yielding the power requirements (Section 8.5). From the power needs, the motors will be selected, as well as the electronics to complete their functions in Section 8.3. Finally, Section 8.4 will illustrate the battery cell choices and configurations, accompanied by the battery management system and air conditioning system.

Powertrain Symbols

DC	Direct Current	AC	Alternating Current	I	Current
V	Voltage	E	Energy	C	Capacity
Γ	Circulation	r	Radial distance from center	V'	Induced Velocity
R_{hub}	Hub Radius	R_{tip}	Tip Radius	V_∞	Freestream Velocity
N_b	Number of blades	J	Advance Ratio	Ω	Rotational speed in $\frac{rad}{s}$
ρ	Air density	W	Total Velocity	c	Chord distribution
T	Thrust	C_L	Lift Coefficient	C_D	Drag Coefficient

8.1. Required Power and Energy

As mentioned earlier in Chapter 6, the conservative estimate for maximum takeoff weight is 2600 kg. In order to size the powertrain, two parameters need to be estimated accurately first: energy and power figures.

In order to have an overview of the performance metrics that the system needs to accommodate, a power envelope for one leg of the mission has been created, as can be seen in Figure 8.1. Here, the graph shows the takeoff and landing phases, with the horizontal line representing the cruise phase at constant velocity. It can be observed that during cruise, the large propellers use less power than the small ones due to the simulator not optimizing the thrust distribution to the engines, which can be improved in further iterations of the design.

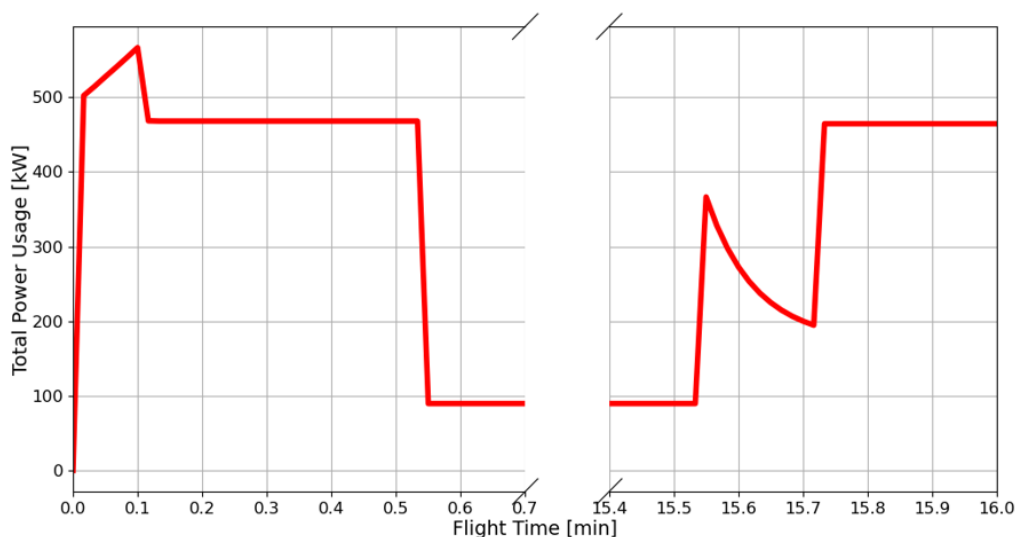


Figure 8.1: Power envelope for one-way segment of round-trip mission

This envelope follows the procedure used to design the propeller geometry, as will be explained further in Section 8.5; this is more accurate than the power estimation in Subsection 6.3.4. Here, the takeoff, cruise, and landing phases were modeled, and the transitioning phases were replaced with further pure vertical movement. This was done due to the complex nature of the transitioning maneuver. To account for the energy loss, it was assumed that the vertical takeoff and landing use more energy due to the lifting surface not providing lift. This way, the total energy was considered to be a worst-case scenario, where the transitioning required power is the same as the one used in takeoff. From Figure 8.1, the total energy used for the complete mission is around 124 kWh, and the maximum power used by all engines is 550 kW, which occurs during takeoff.

8.2. List of Components

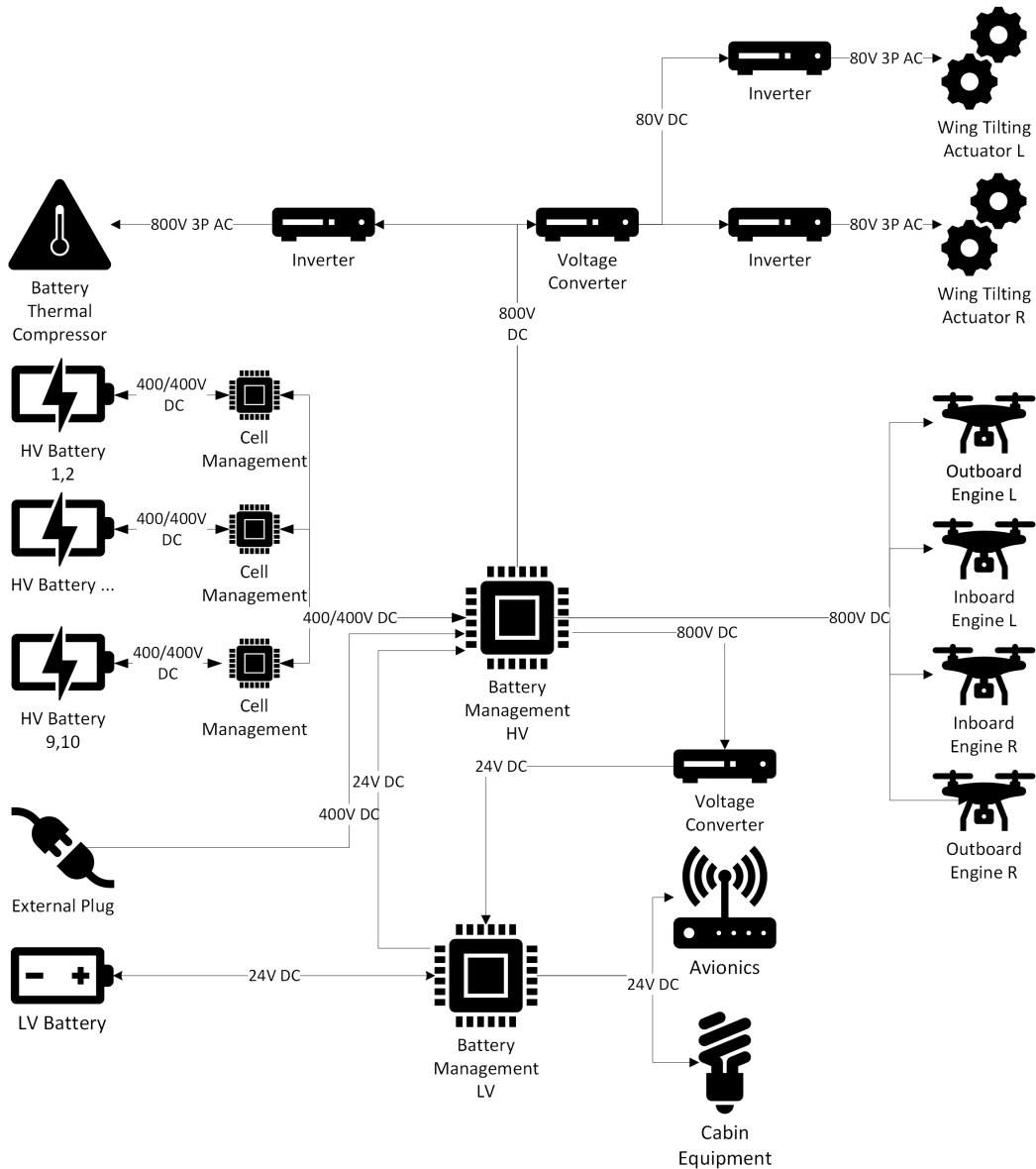


Figure 8.2: Electrical diagram for powertrain system.

Figure 8.2 shows the connections between different electrical components in the powertrain system. It features an 800V high-voltage system and a 24V low-voltage system. The HV battery management device shown in the middle delivers 800V DC to the four propulsion motors. The four DC-AC inverters (not shown) are either integrated or placed adjacent to the motor. The 800V DC also gets converted into 800V 3-phase AC for the thermal control compressor in the top left. Top right, a voltage converter steps down the 800V DC

to 80V DC, which then gets inverted into 80V 3-phase AC for the hinge actuators for the tilting wing. Lower voltage is used for the hinge actuator due to the low back voltage (EMF) at low rotation speed. The HV battery management also charges the LV system through a step-down converter from 800V to 24V DC. The 24V battery also requires a simple battery management device. It supplies 24V DC to cabin equipment such as lighting, avionics, which include control panels and control surface actuators, and the HV battery management device for digital logic and communication. Lastly, the HV battery pack contains ten 400V modules, of which each can be charged at 400V DC. The details are explained in later sections of this chapter. The low-voltage system has little influence on the design and is not investigated.

Table 8.1: *Component Specifications for the HV Electric System*

Component	Qty	Unit Mass (kg)	Cruise Power (kW)	Takeoff Power (kW)
Inboard motor with inverter	2	50.0	50	174
Outboard motor with inverter	2	35.0	30	103
Hinge motor	2	11.0	0	15
Thermal control (Cabin)	1	-	9	9
Thermal control (Battery)	1	50.0	4	4
Battery cells	1100	0.526	-	-
Battery and cell management	60	0.2	-	-
Converter 800V–24V	1	2.0	-	-
Converter 800V–80V	2	4.5	-	-
Inverter for hinge motor	2	5.0	-	-
HV cable (m)	39	1.1	-	-
Bus bar for cells	10	1.0	-	-
Total	-	906	173	597

Table 8.1 indicates the mass and power of each HV component. The masses are obtained from available commercial products. The cabin thermal control uses the same system as that of the battery, so the mass is not counted twice. The power is estimated through the calculations in Section 8.1 and Subsection 8.4.8.

8.3. Propulsion Motors

The maximum power demand occurs during the takeoff phase. Given the power requirements, the inboard and outboard propellers exhibit significantly different demands; thus, two types of motors are selected. When considering the motors to be used, the design criterion is based on the worst-case scenario, namely, one engine inoperative. In the case of a single failure, Section 6.2 explains that only one inboard engine and one outboard engine can be in use, as the third engine has to be shut off to maintain moment equilibrium. To be able to hover with only two operative motors, each motor should be capable of producing 2 times the normal thrust. This sets the maximum required power values for the propulsion motors.

Table 8.2: *Peak power usage for inboard and outboard propellers*

Propeller Type	Peak Power [kW]
Inboard Propeller	368
Outboard Propeller	193

The motor chosen for the inboard propellers is the HPDM-350 (Figure 8.3) from H3X Technologies, capable of delivering 350 kW continuous power. It integrates an inverter and has a total mass of only 50 kg. Although the peak power requirement slightly exceeds 350 kW, this is acceptable, as the continuous power rating typically corresponds to around 70% of the peak capability of the motor (for durations less than 30 s)[35].



Figure 8.3: HDPM-350 [36]

The outboard propellers require less power; hence, the Evolito D1700 2x3 motor (shown in Figure 8.4) is selected. It can provide 250 kW of continuous power with a mass of 30 kg. However, it is not equipped with an integrated inverter. To address this, the HPDI-190 inverter from H3X is selected (see Figure 8.5). This inverter is lightweight (2.2 kg) while offering high power density.



Figure 8.4: Evolito D1700 [37]



Figure 8.5: HDPI-190 [38]

Regarding the maximum torque, the same design logic applies. Table 8.3 justifies the motor selection based on the peak torque requirements and capabilities. Both motors provide a comfortable margin over the required values, ensuring robustness under transient loading and accommodating degradation over time.

Table 8.3: Torque Requirements for Inboard and Outboard Motors

Motor Type	Peak Torque Required [kNm]	Peak Torque Provided [kNm]
Inboard Motor	1.20	1.24
Outboard Motor	0.55	1.50

The motor thermal control is another important problem to be considered. Both motors have their individual cooling mechanisms, utilizing liquid cooling. Meanwhile, as the motors are exposed to airflow due to the tiltwing configuration, air cooling also contributes to thermal control. This combined effect further helps avoid potential issues caused by overheating.

8.4. High Voltage Batteries

Cruise Current [A]	Takeoff Current [A]	Normal Voltage [V]	Battery Capacity [kWh]	C-rate [1/h]
216	746	800	155	3.9

Table 8.4: HV battery parameters.

The high-voltage battery matters in the design, as it is selected as the sole power source for the eVTOL. This section begins with considerations of voltage and discharge rate, followed by the selection of battery cells and their configuration. The battery management system (BMS) and the air conditioning system are then presented to conclude this section. The key parameters of the battery are summarized in Table 8.4.

8.4.1. Battery Capacity

Battery capacity indicates the amount of energy that can be stored and extracted from a battery. Measured in kWh, it is simply the product of power multiplied by time. In Section 8.1, it has been calculated that a

designed mission needs at most 124 kWh of energy. Since the battery capacity degrades as the battery cycle increases, the battery capacity is required to be 155 kWh, given 20% capacity degradation.

8.4.2. Voltage Requirement

The battery design starts from the desired voltage. The motors specify a broad operating range of 400–900 V. Upon investigating several relatively mature eVTOL systems, such as Archer's, it is observed that most utilize an 800 V architecture [39]. The rationale primarily lies in efficiency; higher voltage allows for lower current, thereby reducing resistive (I^2R) losses during power transmission. Based on this reasoning, 800 V is selected as the battery pack voltage.

8.4.3. Discharge Rate

At takeoff, where the power consumption is the highest, 634 A of current needs to be supplied to the electric motors. This sets a minimum discharge rate for the HV battery, which is defined by C-rate. C-rate measures the number of hours it takes to completely charge or discharge the battery. While little charging time is preferred to increase the turnover rate, a high C-rate is associated with low battery cycles, so the choice should be made on a minimum basis. With the battery capacity in Table 8.4, the required C-rate can be obtained from Equation 8.1, where we can see that the high battery capacity allows for a reasonable C-rate.

$$\text{C-rate [h}^{-1}] = \frac{I_{\max} \cdot V_{\text{nom}}}{E_{\text{Battery [Wh]}}} = 3.9 \quad (8.1)$$

8.4.4. Battery Energy Density

Battery energy density, usually measured in Wh/kg, represents the amount of energy that can be stored per unit weight. Due to its influence on the MTOW, it is a critical measure that affects the cost and feasibility of the design.

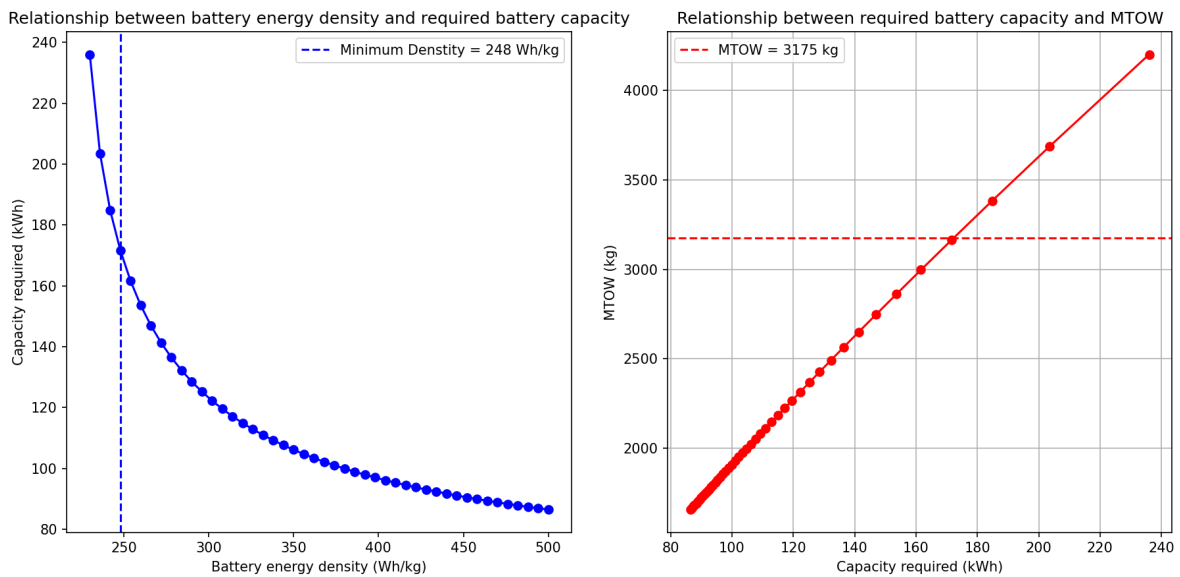


Figure 8.6: Relationships between battery energy density, required battery capacity, and MTOW. The red dashed line indicates the maximum MTOW according to MIS-CERT-06. The blue dashed line indicates the required minimum battery density to meet the MTOW requirement.

Figure 8.6 uses the iterative estimation tool for MTOW and energy usage explained in Subsection 6.3.3 to illustrate the relationship between battery energy density, required battery capacity, and maximum takeoff weight. It is clear from the right plot that the MTOW increases linearly with the battery capacity. Also, the required battery capacity falls off exponentially with increasing battery energy density. So, to attain a lower MTOW, the battery energy density needs to be maximized. Given the limit of 3175 kg for certification, the battery energy density needs to be at least 248 Wh/kg to meet the requirement. The iterative MTOW estimation uses 275 Wh/kg.

8.4.5. Battery Cell Choice

Various rechargeable battery technologies are available for the design as summarized in Table 8.5. The Li-ion options are further considered for their commercial readiness. The distinction between NMC (nickel manganese cobalt) and LFP (iron phosphate) batteries is the cathode material. Solid-state battery uses solid electrolyte, while the generic Li-ion uses liquid electrolyte; semi-solid state has both liquid and solid electrolytes.

Battery Type	Density (Wh/kg)	Cycle Life	Safety	Maturity Level
Li-ion (NMC)	240–280	1000–3000	Safety	Mature
Semi-Solid State (NMC)	300–350	1000–1500	Safe	Early commercial
Li-ion (LFP)	150–205	2500+	Very Safe	Mature
Solid-State Lithium (Condensed)	500	N/A	Safe	Pre-commercial
Lithium-Sulfur (Li-S)	450	700+	N/A	In development

Table 8.5: Comparison of different battery technologies in June, 2025.

Considering the high discharge rate requirement and the need for high energy density to reduce overall system weight, semi-solid state battery technology emerges as a promising candidate. Upon further investigation, the company Grepow offers multiple battery series that meet the design constraints. The 5C High Energy Density Semi-Solid State (NMC) series (see Figure 8.7) is evaluated.



Figure 8.7: Grepow 5C High Energy Density Semi-Solid State Battery [40]

The main concerns are mass, capacity, and thickness, which together determine the volume and integration feasibility. The battery pack is intended to be placed beneath the cabin floor, where space is limited. The reason for underfloor allocation is based on three considerations. First, placing the battery pack under the floor lowers the center of gravity, contributing to improved stability. Second, due to the tiltwing configuration, it is challenging to place nearly half of the overall weight elsewhere without affecting the aerodynamic balance. Finally, it is safer to place the battery pack under the passengers than above them due to its large inertia.

As shown in Figure 8.8, battery mass increases almost linearly with capacity. This supports the selection of higher-capacity cells to minimize the number of individual units required. In Figure 8.9, the scatter is more noticeable. Cells that exhibit a low thickness-to-capacity slope (closer to the origin) are preferred. These considerations ultimately narrow the choice down to GRPA1C0200. With 288.4 Wh/kg (greater than 275 Wh/kg); it promises an MTOW that fulfills the requirement.

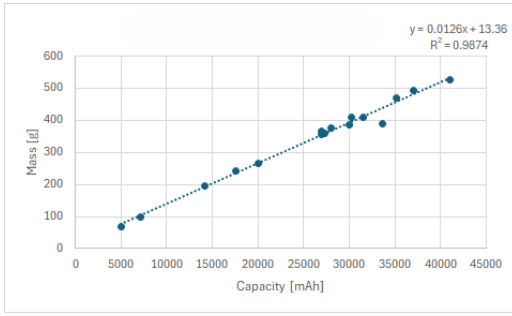


Figure 8.8: Battery capacity vs. mass

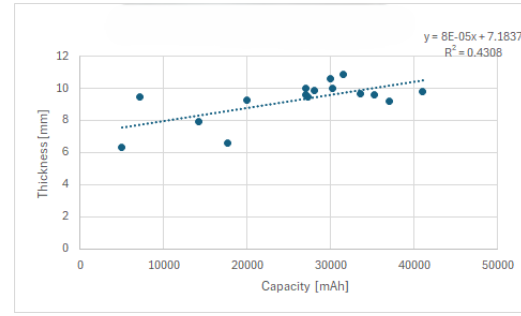


Figure 8.9: Battery capacity vs. thickness

Lastly, given the 5C discharge rate, this battery degrades to 80% of its initial capacity only after 1100 cycles, allowing the HV battery to last at least 0.6 years before replacement for 5 missions per day.

8.4.6. Battery Configuration

The battery configuration begins with the voltage needed. Putting the cells in series increases the voltage; this leads to Equation 8.2.

$$n_{\text{series}} = \frac{V_{\text{desired}}}{V_{\text{cell}}} = \frac{800 \text{ [V]}}{3.7 \text{ [V]}} \approx 220 \quad (8.2)$$

Then, looking into the current output derived from cell energy and capacity, the parallel series can be determined by Equation 8.3.

$$n_{\text{parallel}} = \frac{E_{\text{need}}}{V_{\text{desired}} \cdot C_{\text{cell}}} = \frac{1.55 \text{ [kWh]}}{800 \text{ [V]} \cdot 41 \text{ [Ah]}} \approx 5 \quad (8.3)$$

Taking into account the limited volume available beneath the cabin floor, the battery packs are segmented into 10 separate modules to allow for greater flexibility in orientation. As a result, each module consisting of 110 cells in series would give a nominal voltage of 400V; the desired 800V can be reached by connecting two modules in series. Each battery module (configured as 110s 5p) measures 1.1 m × 0.15 m × 0.2 m, with a 1-centimeter clearance on both sides between the casing and the battery cells. This deliberate spacing facilitates thermal expansion and enhances heat dissipation, thereby improving the overall safety and performance of the battery system. The electrical connection between individual cells is established via a busbar, which is a metal sheet. This design choice is inspired by the battery pack architecture from Tesla, which employs busbars to reduce both weight and cost[41]. Additionally, for efficient maintenance and replacement of batteries, a cutout in the fuselage floor shall be created.



Figure 8.10: Tesla Busbar[41]

8.4.7. Battery Management System

A battery management system is crucial for this high-power powertrain system, where safety and efficiency are paramount. First, it monitors the state of charge and the health of the battery pack. Second, it regulates the current and voltage during charging and discharging for protection. Third, it actively balances cell voltages to ensure the best performance. Additionally, it talks to the charger to prevent overcharging and to the thermal control for battery conditioning. The battery management system for a module typically contains one or more Battery Management Units (BMU), multiple Cell Monitoring Units (CMU), and some Battery Junction Boxes (BJB). The CMUs are used to monitor and balance the cells, and the BJBs limit the total voltage and current.

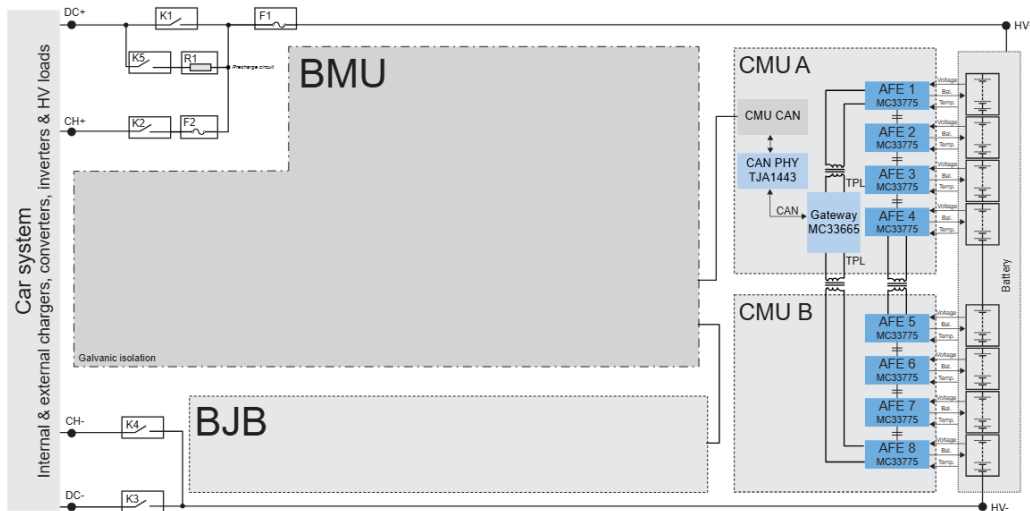


Figure 8.11: 400V battery management system design from NXP [42]

Figure 8.12 shows the configuration for a 400V battery module. In this design, each battery module contains one BMU, which is connected to two CMUs through a daisy chain. Each CMU regulates 55 cells.

8.4.8. Thermal Control

The efficiency, capacity, and lifespan of the battery are severely impacted by the temperature [43]; hence, thermal control is a vital consideration. The thermal control of the battery is shared with the cabin and follows the same design as a home split system air conditioner. In summer, the power is supplied to a common compressor, and the heat of the battery is removed through a twisted coolant pipe. For heating, aside from the heat pump, a resistive heater can be added to accelerate the rate of heating and maintain the temperature in more extreme weather.

The power consumption of the cabin thermal control uses an electric vehicle as a reference, which typically requires 3-4 kW to heat up a 2.8-4.5 m³ cabin in winter [44]. With a usable cabin volume of 11.5 m³, the power consumption of the heating of the aircraft heating unit is estimated to be 9 kW by scaling the volume, three times that of an EV.

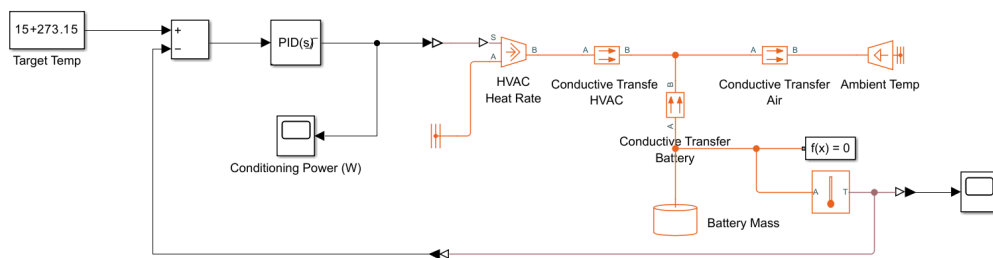


Figure 8.12: Simscape Simulation for Battery Conditioning

To estimate the power consumption for battery conditioning, a Simscape simulation is created with Newton's law of cooling. Requirement MIS-FUNC-18 demands the system to be able to operate between -20 and 40 °C. Since the desired operating temperature for the battery is around 15 to 25 °C, 1.3 kW of heat transfer rate is required to maintain 25 °C in 40 °C of ambient temperature, and 2.9 kW of heat transfer rate is required to maintain 15 °C in -20 °C outside temperature. As usual, the limiting case is heating. If a heat pump is used with a typical coefficient of performance of 2 at -20 °C, then the power required from the compressor is 1.5 kW, and if a resistive heater is used, then the power (2.9 kW) is simply the heat transfer rate with a small loss. In total, 9 + 4 kW is estimated for the conditioning of the cabin and the battery. Note that these numbers are

for the power required to maintain the relative difference and should not be used to size the compressor or the heater, which require more power to change the temperature than to maintain it.

8.4.9. Charging Device

As mentioned in Subsection 8.4.6, each one of the ten battery modules has a nominal voltage of 400 V. To supply 800 V of system voltage, two modules can be paired up in series. In Section 3.1, the eVTOL is designed to be compatible with the existing 400 V EV charging infrastructure. This means the batteries need to be in parallel while charging. A battery configuration switch (BCS) shown in Figure 8.13 can be used to switch between 400 V (charging) and 800 V (discharging).

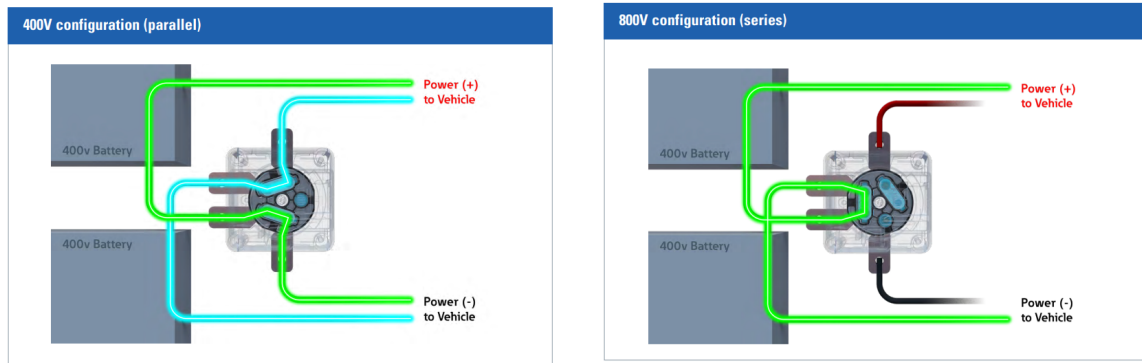


Figure 8.13: Working Principle of Battery Configuration Switch (BCS) from Eaton [45]

A potential issue occurs when the batteries have different voltages while in parallel charging. To solve this, cell balancing needs to be performed before charging. A typical fast charger from Fastned (fast charging network operator in Europe) delivers 300 kW. With a dual charger, the optimal charging time for the 155 kWh battery can be as low as 31 minutes (supported by the 5C cells), meeting requirement SYS-OPER-01.

8.5. Propeller Design

After performing a mass estimation and a configuration trade-off, the thrust requirements were estimated and distributed to the four propellers. The design philosophy was decided upon as follows: firstly, a tool for designing propellers and estimating their performance was created. Next, a parameter sweep was conducted in order to select the most efficient geometry, and afterwards, a power envelope was created in order to design the rest of the propulsion system.

8.5.1. Circulation Distribution Design Method

To design the propeller, multiple methods have been considered, many of which proved inaccurate due to assuming a light blade loading ($\leq 200 \frac{N}{m^2}$). This assumption entails that W and W_1 can be considered perpendicular, which is not the case in heavily loaded propellers. These velocities can be seen in Figure 8.14[46].

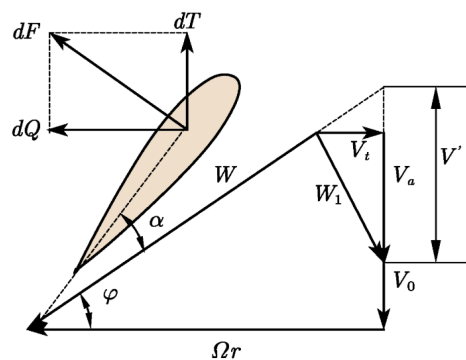


Figure 8.14: Propeller Velocity Triangles

Due to the selected geometry and takeoff mass, the blade loading to be achieved to maximize efficiency is $800 \frac{N}{m^2}$, which is constant at all propellers. Due to this assumption, many propeller design tools are not feasible for design, so the method used is the circulation distribution method [47]. According to vortex theory, the optimal circulation distribution considering finite blades can be defined as seen in Equation 8.4.

$$\Gamma(r, V') = (\Gamma_\infty(r, V') + \Gamma_\infty \left(\frac{R_{\text{hub}}^2}{r}, V' \right) - \Gamma_\infty(R_{\text{hub}}, V')) \cdot F \quad (8.4)$$

Where R_{hub} is the radius of the propeller hub, and Γ_∞ is the optimum circulation of an infinite span blade, which is defined as seen in Equation 8.5 and Equation 8.6.

$$\Gamma_\infty(r, V') = \frac{V_\infty V'}{n_s N_b} \cdot \frac{x^2}{1 + x^2} \quad (8.5)$$

$$x = \frac{2\pi n_s r}{V_\infty} \quad (8.6)$$

Where n_s is the rotational velocity in revolutions per second, and x is the reciprocal of the local advance ratio. Additionally, Prandtl's correction factor was used, which is shown in Equation 8.7 and Equation 8.8.

$$F = \frac{2}{\pi} \arccos(e^{-f}) \quad (8.7)$$

$$f = \frac{N_b}{2} \frac{R_{\text{tip}} - r}{R_{\text{tip}}} \frac{\sqrt{1 + J^2}}{J} \quad (8.8)$$

Where J is the advance ratio. Finally, to connect the circulation distribution with the thrust requirements of the vehicle, Equation 8.9 was used.

$$T = \int_{R_{\text{hub}}}^{R_{\text{tip}}} \rho \Gamma(r, V') \left(\Omega r - \frac{N_b \Gamma(r, V')}{4\pi r} \right) dr \quad (8.9)$$

Finally, after solving for V' and the circulation distribution from the thrust, the propeller geometry can be created. From geometry:

$$\phi = \arctan \frac{V_\infty V'}{\Omega r} \quad (8.10)$$

$$\theta = \phi + \alpha \quad (8.11)$$

Here, θ is the blade twist angle, which is computed using the inflow angle ϕ and α , which is the angle at which the lift over drag is maximum for the present airfoil. Furthermore, the chord distribution along the blade can be obtained using the Kutta-Joukowski theorem as seen in Equation 8.12.

$$dL = \rho \Gamma(r) W dr = \frac{1}{2} \rho W^2 C_L \cdot c \cdot dr \quad (8.12)$$

Due to not assuming that W_1 is perpendicular to W (which is the case for highly loaded propellers), this method provided a reliable geometry generator for propellers. Multiple models were simulated due to the nature of the flight profile: the propellers need to perform efficiently in both takeoff and cruise conditions, which is not ideal. Models designed for takeoff will perform poorly in cruise conditions and vice versa. This meant that the propeller geometry to be used needs to balance these flight conditions to achieve the best overall efficiency. To tackle this design challenge, a flight envelope simulator was created.

8.5.2. Propeller Parameter Sweep and Final Geometry

To switch the flight regime for each propeller geometry created, the used power was modeled as the sum of the induced thrust power and profile drag power, which can be computed using Equation 8.13 and Equation 8.14.

$$P_{\text{induced}} = T \cdot (V_\infty + V') \quad (8.13)$$

$$P_{\text{profile}} = \int_{R_{\text{hub}}}^{R_{\text{tip}}} \frac{N_b}{2} \rho c \cdot C_D \cdot W dr \quad (8.14)$$

Finally, the main driving factor of the geometry was lowering the battery mass, which made the total energy expended by the propellers the main characteristic to take into account. The results of the parameter sweep can be seen in Figure 8.15.

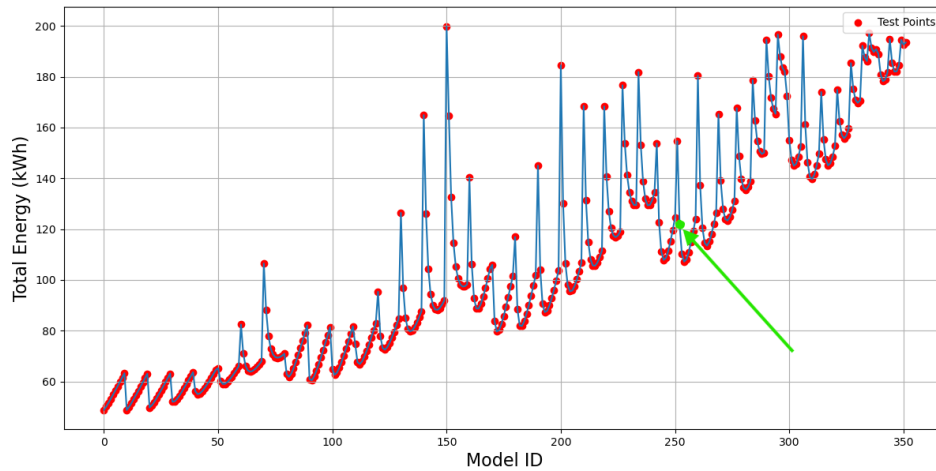


Figure 8.15: Propeller Parameter Sweep Results

Here, to avoid geometry overfitting to the simulation and to account for different flight profiles, a design which uses a similar energy during a mission compared to real eVTOLs was chosen[48], which yielded a total energy consumption of ≈ 124 [kWh]. The chosen geometry can be seen in Figure 8.15 with a green indicator. The final geometry parameters can be seen in Figure 8.16, and in Table 8.6. Also, a performance diagram is presented in Figure 8.17.

Table 8.6: Propeller Final Parameters

Parameter	Value
Inbound Diameter [m]	3.19
Outbound Diameter [m]	2.286
Number of Blades [-]	5
Material Used [-]	CFRP
Hub Diameter Radius [m/m]	15%
Airfoil Used [-]	S1223
Total Energy Used [kWh]	124

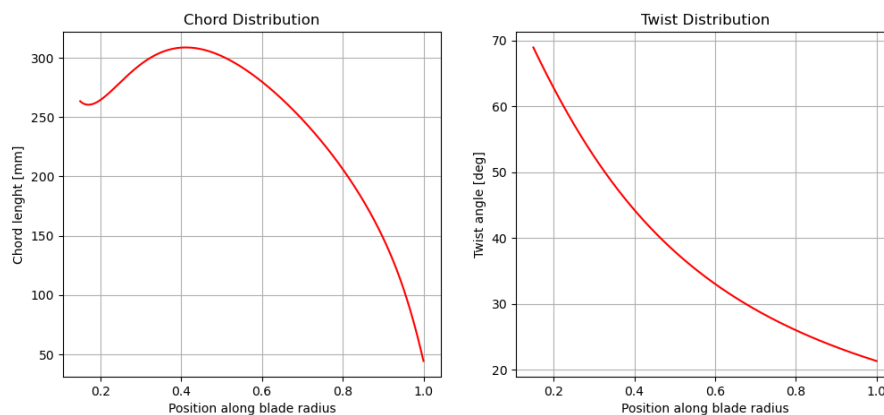


Figure 8.16: Propeller Chord and Twist Distributions

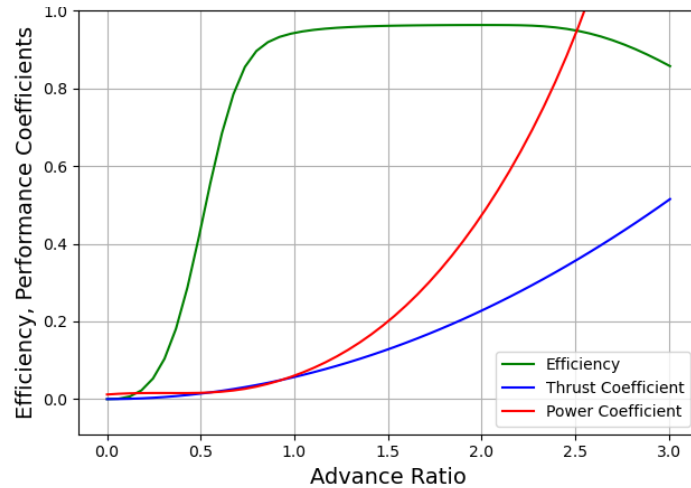


Figure 8.17: Propeller Performance Diagram

8.5.3. Additional Considerations

Due to the complexity of creating an optimal propeller for the flight envelope, multiple assumptions and considerations were taken into account. For completeness, these are presented below.

- Variable Pitch System:** Because of the flight envelope, a variable pitch system was considered to achieve maximum efficiency during all flight phases by modifying the pitch angle dynamically. Additionally, this aids in the control characteristics, as will be further explained in Subsection 9.1.5. The downsides are increased weight, which does not make a difference given the increases in propulsive efficiency, and an increase in reliability due to extra parts being necessary.
- Constant Airfoil Used:** Due to the extended design space, a constant airfoil was used, as mentioned in Table 8.6. This can be improved in further iterations of the design, as most models used in eVTOLs use multiple airfoils along the blades in order to maximise efficiency and thrust produced in different flight conditions. The current airfoil is chosen due to its high camber, which is crucial for takeoff conditions. The stall angle of attack is on the lower side; however, this is compensated for by the variable pitch system.
- Material Used:** The material chosen for the propeller blades and hub is CFRP. For this component, stiffness and being lightweight are crucial for performance. Due to displacements and moments of inertia driving propeller performance, carbon fiber composites become the most suitable option. The mass estimation of the blades, hubs, and variable pitch systems was taken from propeller manufacturers [49].
- Clearance and Interaction:** Due to aerodynamic interactions, clearance between propellers and between propellers and the fuselage plays an essential role in performance and noise. In this design, the clearance considered is 20% of the propeller diameter, which is enough to keep interaction losses under 2% [50]. However, it is recommended that in future iterations to analyze these interactions using CFD.
- Noise:** Due to the highly loaded conditions during takeoff, most noise estimation techniques fail due to using Blade Element Momentum Theory, which relies on the lightly loaded assumption discussed before. The takeoff noise requirements can be validated in further iterations by testing or using more advanced techniques, such as RANS simulations. In order to prevent transonic flow at the blade tips, the engine's rotational speed is limited such that the Mach number at the tips never exceeds 0.7. This is to prevent drag divergence and the extra noise associated with it. The noise signature during cruise conditions was estimated at ≈ 47 dB. This can be further improved by optimizing the control and design of the propellers for noise. The results of simulating the inboard propeller in XROTOR can be seen below, in Figure 8.18, considering a flight altitude of 300m.

$M_\infty = 0.162$ $V/\Omega R = 0.600$
 $M_{tip} = 0.314$ $C_p = 0.221$
 Altitude = 300 m Climb angle = 0°

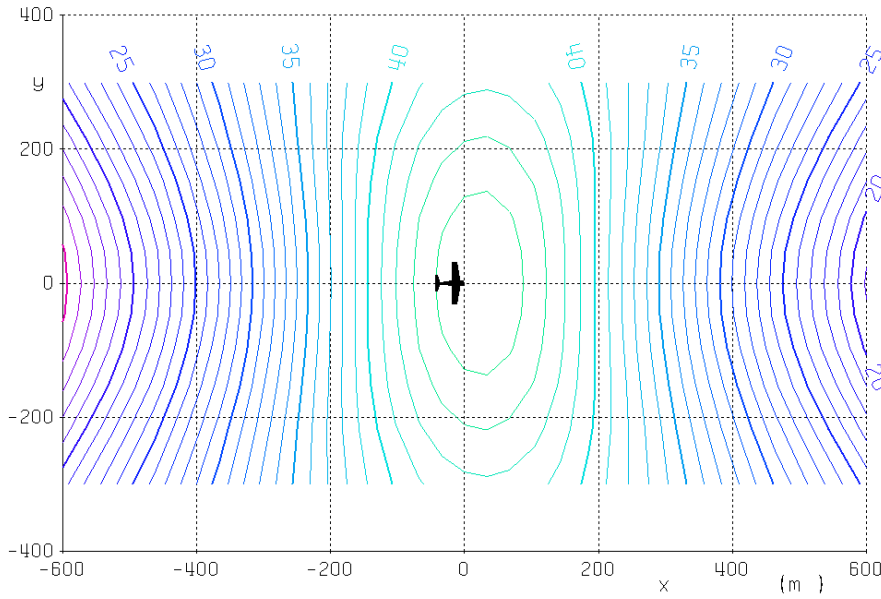


Figure 8.18: *Inboard Propeller Noise Footprint*

- Sensitivity Study:** Finally, a sensitivity study was conducted to assess the robustness of the inputs. In Figure 8.19, the results of this study can be seen. A change of 10% was applied to each of the inputs, and the change in final energy used during the mission was compared to the initial result. The only input that was changed more significantly was the number of blades. As can be seen, the only metrics that produce more than 10% variation of the result are the nominal thrust and the number of blades. Due to this, the effect of these inputs should be assessed further in future iterations of the design.

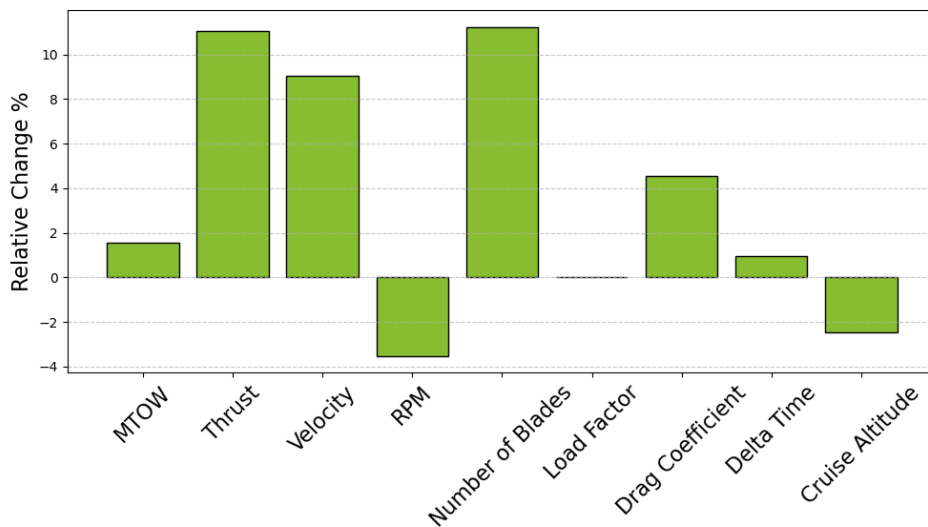


Figure 8.19: *Propeller Sensitivity Study*

Control and Avionics

During the conceptual design stage of the project, controllability was not the main focus of the different concepts. Instead, a focus was put on the performance with the assumption that further actuators, such as a ducted fan, might be added if they are required for control. Evaluating the performance of the system during the different flight phases and in different conditions is a challenging issue due to its dynamics varying over the flight and it operating in highly nonlinear regions. It has been determined that the most critical flight phases and maneuvers are gust rejection during hover and transitioning between the different flight phases. In this chapter, the structure of the model will be presented and the required simulations conducted. Furthermore, potential failure modes and the avionics structure will be explored.

Control and Avionics Symbols

κ	Wing angle	b	In body frame	e	In earth frame
w	In wing frame	m	Vehicle mass	F	Force
M	Moment	ρ	Density	v	Velocity
S	Area	α	Angle of attack	C_{wing}	Wing force coefficients
K_{wing}	Wing moment coefficients	B	Reference length matrix	T_y^w	Rotation matrix (y-axis)
T_{be}	Transform: earth to body	T_i	Individual propeller thrust	A_{disc}	Total disc area
r	Position vector	$C_{L\alpha}$	3D lift slope	$C_{l\alpha}$	2D lift slope
AR	Aspect ratio	Q/T	Torque/thrust ratio	C_p	Power coefficient
C_T	Thrust coefficient	D	Propeller diameter	Ω_i	Propeller direction
T	Vector of motor thrusts	w	Propulsion wrench	J	Jacobian
j_i	Wrench derivative w.r.t. T_i				

Creating the dynamic model of the system requires several assumptions which drastically simplify the process. Without making these assumptions, the modeling process would have been significantly more complicated and time consuming to a point where it would have been unfeasible. The assumptions and their identifiers are presented in Table 9.1.

Table 9.1: List of control-related assumptions

Identifier	Assumption
ASM-CTL-01	The critical flight maneuvers are in the longitudinal symmetry plane of the aircraft.
ASM-CTL-02	The inertia matrix only contains its diagonal components (I_{xx} , I_{yy} , I_{zz}) with the off-diagonal terms being 0 and the inertia of the wing is neglected.
ASM-CTL-03	The rotor wake induces an approximately uniform flow over the wing.
ASM-CTL-04	Incompressible and inviscid flow is assumed over the entire flight envelope.
ASM-CTL-05	The fuselage can be approximated as an ellipsoid with a length/diameter ratio of 2.
ASM-CTL-06	The aerodynamic forces on the fuselage can be approximated as the drag due to the velocity components (X_b , Y_b , Z_b).
ASM-CTL-07	The center of pressure of the fuselage has an approximately constant location.
ASM-CTL-08	The horizontal stabilizer can be approximated as an elliptical lift distribution.
ASM-CTL-09	Interference on the horizontal stabilizer that is caused by the propulsion system or the wing can be neglected.

Identifier	Assumption
ASM-CTL-10	The only significant forces and moments that the horizontal stabilizer generates are its lift force and its moment due to the force offset.
ASM-CTL-11	The effect of the elevator can be approximated as a fully movable horizontal stabilizer.
ASM-CTL-12	The power and thrust coefficients of the propellers are approximately constant over the flight profile.
ASM-CTL-13	Due to the variable pitch mechanism, the achieved thrust and torque values of the propellers can be approximated as a first order lowpass filter with a time constant of 0.1 s.
ASM-CTL-14	The elevator lift behavior due to its actuator dynamics can be approximated as a first order lowpass filter with a time constant of 0.1 s.
ASM-CTL-15	The hinge behavior due to its actuator dynamics can be approximated as a first order lowpass filter with a time constant of 0.5 s.

9.1. Aircraft Model

At the core of the Aircraft model is the Simulink 6 DOF Euler angles block which takes the body forces and moments as inputs and outputs position, velocity, and attitude information. Forces and moments are only applied in the longitudinal symmetry plane which turns the model into a 3 DOF model. This is done since according to **ASM-CTL-01** the critical maneuver is in this symmetry plane. Furthermore, expanding the model to 6 DOF comes with a lot of added complexity but only limited added value as both gust rejection and transition are mostly influenced by pitch control.

There are three main components of the forces and moments acting on the aircraft: gravity, aerodynamics, and the propulsion system.

9.1.1. Reference Frames

Three different reference frames are defined to simplify the calculation of the different forces and moments.

- **E-frame:** the E-frame is the vehicle-carried normal Earth reference frame, where X_e is positive in north direction, Y_e in east direction and Z_e is positive perpendicular to earth's surface pointing down
- **B-frame:** the B-frame is the body frame of the vehicle. The same b-frame as commonly used for conventional aircraft Figure 9.1 is used for the eVTOL. The force and moment inputs of the 6 DOF block are applied in the B-frame.
- **W-frame:** the W-frame is the wing reference frame. It is defined such that the thrust vectors of the engines are aligned with X_w and that $Y_w = Y_b$ Figure 9.2. Therefore, in horizontal flight where the thrust is aligned with the X_b axis, the B-frame and W-frame will be identical.

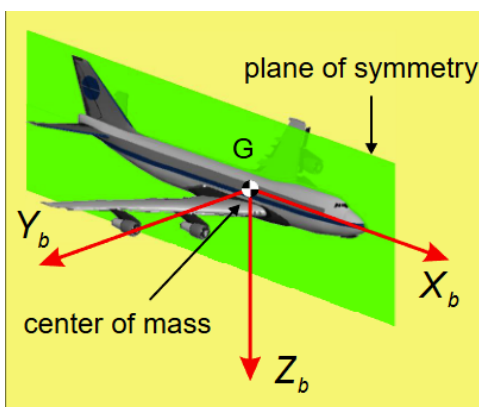


Figure 9.1: B-frame definition[51]

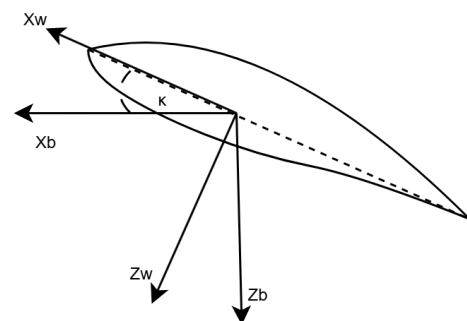


Figure 9.2: W-frame definition

9.1.2. Gravity and Inertia

The inertia of the aircraft has been approximated with the sum of the wing inertia and the fuselage inertia. The wing is approximated as a flat plate and while the fuselage inertia is approximately attained from CAD. To further simplify the model, **ASM-CTL-02** is made which specifies that only the diagonal components of the inertia matrix (I_{xx} , I_{yy} , I_{zz}) are used while the off-diagonal terms are assumed to be 0.

Gravity is modeled as a constant force in the positive Z_E direction, which is transformed to and applied in the B-frame using \mathbb{T}_{be} which is a rotation matrix containing the Euler angles of the vehicle.

$$\mathbf{F}_{\text{grav}}^{\text{B}} = \mathbb{T}_{BE} \begin{bmatrix} 0 \\ 0 \\ 9.81 \end{bmatrix} m \quad (9.1)$$

9.1.3. Aerodynamic Model

The aerodynamics model is split up into multiple components: wing aerodynamics, fuselage aerodynamics, and tail aerodynamics.

Wing Aerodynamics

The aerodynamics underlie one essential assumption: **ASM-CTL-03** states that the wake that is generated by the rotors generates a flow over the wing that is close to uniform. This assumption might not be completely accurate, but it significantly simplifies the modeling process of the wing aerodynamics. It causes the wing to never operate at an angle of attack where it is at risk of stall. Thus, the traditional Buckingham- π -theorem base approach [52] can be used where the Forces and moments depend on the free-stream velocity and a set of coefficients.

$$\mathbf{F}_{\text{wing}}^{\text{W}} = \frac{1}{2} \rho |\mathbf{v}_{\text{eff}}|^2 S \mathbb{T}_y^w (\alpha + pi) \mathbf{C}_{\text{wing}}(\alpha, \beta, M, Re) \quad \mathbf{M}_{\text{wing}}^{\text{W}} = \frac{1}{2} \rho |\mathbf{v}_{\text{eff}}|^2 S B \mathbf{K}_{\text{wing}}(\alpha, \beta, M, Re) \quad (9.2)$$

$$B = \begin{bmatrix} b & 0 & 0 \\ 0 & c & 0 \\ 0 & 0 & b \end{bmatrix} \quad (9.4)$$

Here, \mathbf{C}_{wing} is a vector of force coefficients and \mathbf{K}_{wing} is a vector of moment coefficients. According to **ASM-CTL-04**, it is assumed that the flow is incompressible and inviscid and thus that \mathbf{C}_{wing} and \mathbf{K}_{wing} are only dependent on the angle of attack. Furthermore, only the forces and moments in the longitudinal symmetry plane are considered. Therefore:

$$\mathbf{C}_{\text{wing}} = \begin{bmatrix} C_D \\ C_L \\ 0 \end{bmatrix} \quad (9.5)$$

$$\mathbf{K}_{\text{wing}} = \begin{bmatrix} 0 \\ C_m \\ 0 \end{bmatrix} \quad (9.6)$$

$$B = \begin{bmatrix} 0 & 0 & 0 \\ 0 & c & 0 \\ 0 & 0 & 0 \end{bmatrix} \quad (9.7)$$

The lift and drag coefficients are represented in the wing reference frame by transforming them with $\mathbb{T}_y^W(\alpha + \pi)$ as shown in Equation 9.2. In the aerodynamic model for the wings, $\mathbf{v}_{\text{eff}} = \mathbf{v}_{\infty} + \mathbf{v}_{\text{ind}}$ is the effective velocity that replaces the free stream velocity. It is the sum of the free stream velocity and the velocity that is induced over the wing. This effective velocity is also used to calculate the angle of attack that is used to read the aerodynamic coefficients from the lookup tables that have been generated in XFLR5.

The propeller induced velocity is calculated by using a simplified momentum theory based approach [53] and is mainly driven by the thrust of the propellers, T_i . $v_{x,\infty}^W$, the x-component of the free stream velocity in the W-frame, is artificially limited to set negative values to 0 since the momentum theory based approach will not yield accurate results in reverse thrust.

$$\mathbf{v}_{\text{ind}}^{\text{W}} = \sqrt{\frac{2 \sum T_i}{\rho A_{\text{disc}}} + (v_{x,\infty}^W)^2} \begin{bmatrix} 1 \\ 0 \\ 0 \end{bmatrix} \quad (9.8)$$

The aerodynamic forces and moments in the wing reference frame are transformed to the body reference frame by applying $\mathbb{T}_{BW} = \mathbb{T}_y^W(-\kappa)$.

The couple moments that the wing generates around the center of gravity are calculated in the B-frame. Finally, the total moment in the B-frame is calculated.

$$\mathbf{M}_{\text{wing,couple}}^{\text{B}} = \left(\mathbf{r}_{\text{wing}}^{\text{B}} - \mathbf{r}_{\text{cg}}^{\text{B}} \right) \times \mathbf{F}_{\text{wing}}^{\text{B}} \quad (9.9) \quad \mathbf{M}_{\text{wing,total}}^{\text{B}} = \mathbf{M}_{\text{wing,couple}}^{\text{B}} + \mathbf{M}_{\text{wing}}^{\text{B}} \quad (9.10)$$

Fuselage Aerodynamics

The fuselage is modeled by approximating it as an ellipsoid with a length/diameter ratio of 2, as stated by **ASM-CTL-05**. Thus, the drag coefficient is approximately 0.3 in X_B direction and 0.5 in the other directions[54]. As stated by **ASM-CTL-06**, it is assumed that the aerodynamic forces on the body can be approximated as the drag due to the velocity components in X_B , Y_B and Z_B . The dynamic pressure is calculated for the different velocity components while keeping the sign of the velocity. Aerodynamic forces are approximated by calculating each drag component by multiplying the dynamic pressure with the projection area (S_x , S_y , S_z) from the specified direction and its drag coefficient.

$$q_i^{\text{B}} = \frac{1}{2} \rho v_i^{\text{B}} |v_i^{\text{B}}| \quad (9.11) \quad \mathbf{F}_{\text{fus}}^{\text{B}} = \begin{bmatrix} q_x S_x & q_y S_y & q_z S_z \end{bmatrix}^{\text{B}} \begin{bmatrix} 0.3 \\ 0.5 \\ 0.5 \end{bmatrix} \quad (9.12)$$

According to **ASM-CTL-07**, it is assumed that the location of the center of pressure of the fuselage is approximately constant. Thus, aerodynamic moment of the fuselage is calculated by calculating the couple moment around the center of gravity.

$$\mathbf{M}_{\text{fus,total}}^{\text{B}} = \left(\mathbf{r}_{\text{cop,fus}}^{\text{B}} - \mathbf{r}_{\text{cg}}^{\text{B}} \right) \times \mathbf{F}_{\text{fus}}^{\text{B}} \quad (9.13)$$

Empennage Aerodynamics

Since only forces and moments in the longitudinal plane of symmetry are considered, any vertical contributions of the tail are neglected. The horizontal tail is approximated as a symmetrical and thin airfoil with $C_{L_\alpha} = 2\pi$. The C_{L_α} of the 3-dimensional tail is approximated by using Prandtl's lifting line theory[55], which approximates the horizontal tail with an elliptical lift distribution, as stated in **ASM-CTL-08**.

$$C_{L_\alpha} = \frac{C_{l_\alpha}}{1 + \frac{C_{l_\alpha}}{\pi AR}} \quad (9.14)$$

Any interference from the propellers are neglected as stated in **ASM-CTL-09** and only the lift and its moment due to its lift offset are considered as stated in **ASM-CTL-010**.

The effect of the elevator is approximated by simply changing the angle of attack of the full horizontal stabilizer as would be the case for a fully movable stabilizer, as stated in **ASM-CTL-11**.

9.1.4. Propulsion Model

The propulsion system is modeled by applying the forces and moments that the individual propellers supply to the aircraft. The motor torque and motor force are related by the torque to thrust ratio [56] as shown in Equation 9.15. According to **ASM-CTL-12**, it is assumed that C_P and C_T are constant during the flight. In reality, this ratio is not constant during flight as C_P and C_T depend on the inlet velocity and the pitch angle of the propeller.

$$\frac{Q}{T} = \left(\frac{C_P}{C_T} \right) \left(\frac{D}{2\pi} \right) \quad (9.15)$$

where T_i is the scalar thrust values for the individual motors are the input of the propulsion model. The combined motor forces and torques are calculated in the W-frame. Ω_i represents the direction of the torque that is caused by each rotor.

$$\mathbf{F}_{\text{prop}}^{\text{W}} = \sum_{i=1}^4 \begin{bmatrix} T_i \\ 0 \\ 0 \end{bmatrix} \quad (9.16) \quad \mathbf{Q}_{\text{prop}}^{\text{W}} = \sum_{i=1}^4 \frac{Q}{T} \begin{bmatrix} 0 \\ 0 \\ \Omega_i T_i \end{bmatrix} \quad (9.17)$$

The forces and torques are converted to the B-frame by applying $\mathbb{T}_{BW} = \mathbb{T}_y^{\text{W}}(-\kappa)$. Finally, the couple moment of each motor and the total moment of the propulsion system are calculated in the B-frame using

the center of gravity and motor locations¹.

$$\mathbf{M}_{\text{prop,couple}}^{\text{B}} = \sum_{i=1}^4 \left(\mathbf{r}_{\text{prop},i}^{\text{B}}(\kappa) - \mathbf{r}_{\text{cg}}^{\text{B}} \right) \times \mathbf{F}_{\text{prop},i}^{\text{B}} \quad (9.18)$$

$$\mathbf{M}_{\text{prop,total}}^{\text{B}} = \mathbf{Q}_{\text{prop}}^{\text{B}} + \mathbf{M}_{\text{prop,couple}}^{\text{B}} \quad (9.19)$$

9.1.5. Actuator Model

The actuators are modeled dynamically to approximate their response behavior and limitations as shown in Figure 9.3.

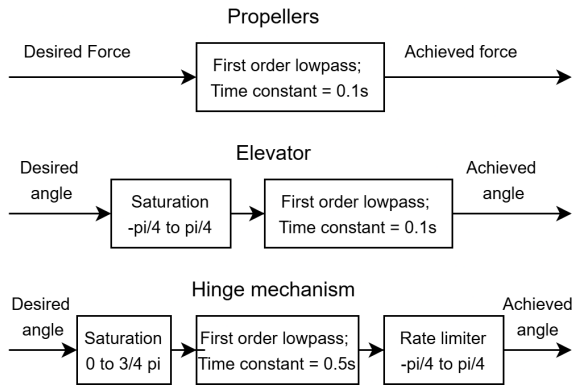


Figure 9.3: Actuator model

- **Propellers:** Controlling thrust through varying the propeller angular velocity would cause very high torque spikes and a challenging control problem due to their inertia. This is one reason why variable pitch propellers will be used. Therefore, according to **ASM-CTL-13** a time constant of 0.1 s can be assumed.
- **Elevators:** Elevator actuators are generally very fast. Therefore, according to **ASM-CTL-14** a time constant of 0.1 s can be assumed.
- **Hinge:** Due to the inertia of the hinge mechanism, a time constant of 0.5 s is assumed as defined in **ASM-CTL-15**. The rate limiter and saturation define the hinge limitations as specified in Section 10.4.

9.2. Motor Mixer

The motor mixer uses the thrust and torque of the individual propellers to achieve the required body forces and moments that are needed in hover control. For traditional quadcopters, this is done by mapping the individual thrust settings to the body forces and moments in a motor mixing matrix[57]. It relates a vector of the individual motor thrusts, $\mathbf{T} \in \mathbb{R}^4$, to the wrench ($\mathbf{w} \in \mathbb{R}^4$) of the propulsive system. The wrench of the propulsive system is defined as a vector containing the total thrust, $\sum_{i=1}^4 T_i \in \mathbb{R}$ and the body moments: $\mathbf{w} = \left[\sum_{i=1}^4 T_i \quad M_x^B \quad M_y^B \quad M_z^B \right]^T$. As the moment arms around the center of gravity change when the wing is tilting, this matrix varies depending on the wing angle. To simplify generating this matrix, the system is linearized at each time step and assembled in a Jacobian matrix, $J \in \mathbb{R}^{4 \times 4}$. If this matrix is inverted, it represents the motor mixing matrix.

$$\mathbf{j}_i = \frac{\mathbf{w}(T_i + \delta) - \mathbf{w}(T_i)}{\delta} \quad (9.20)$$

$$J = \begin{bmatrix} \mathbf{j}_1 & \mathbf{j}_2 & \mathbf{j}_3 & \mathbf{j}_4 \end{bmatrix} \quad (9.21)$$

$$\mathbf{T} = J^{-1} \mathbf{w} \quad (9.22)$$

9.3. Hover Control

Hover control is achieved through multiple nested PID controllers as shown in Figure 9.4. A velocity controller (blue area) is responsible for generating the desired force vector. The aerodynamic and gravity forces are fed forward and the resulting vector is input into the thrust alignment subsystem. It generates the required attitude of wing to align its thrust axis ($-Z_B$ axis) with the desired force vector. Furthermore it calculates the magnitude of the desired force vector to generate the required total thrust, which is sent to the motor mixer.

A special consideration in the control of the tilting aircraft is that compared to a quadcopter it has an additional actuator, namely the hinge which controls the wing angle. Therefore, there are two methods of achieving the required pitch attitude of the wing: the aircraft can be pitched as a whole or the wing angle can be changed. Due to passenger comfort, it is generally preferred to change the angle of the wing over changing the attitude of the vehicle. Therefore, the desired pitch angle is directly transformed to a desired wing angle

¹The moments arms of the motors depend on and are changed according to the wing angle. This is achieved by relating the motor position to the hinge position in the W-frame, converting that vector to the B-frame and adding it to the hinge position in the B-frame.

(red area) and the wing angle that is attained after the actuator dynamics and limitations (gray area) is subtracted from the desired pitch angle. This leaves the pitch control to only compensate for the wing pitch angle that can not be achieved by adapting the wing angle due to its actuator dynamics and limitations.

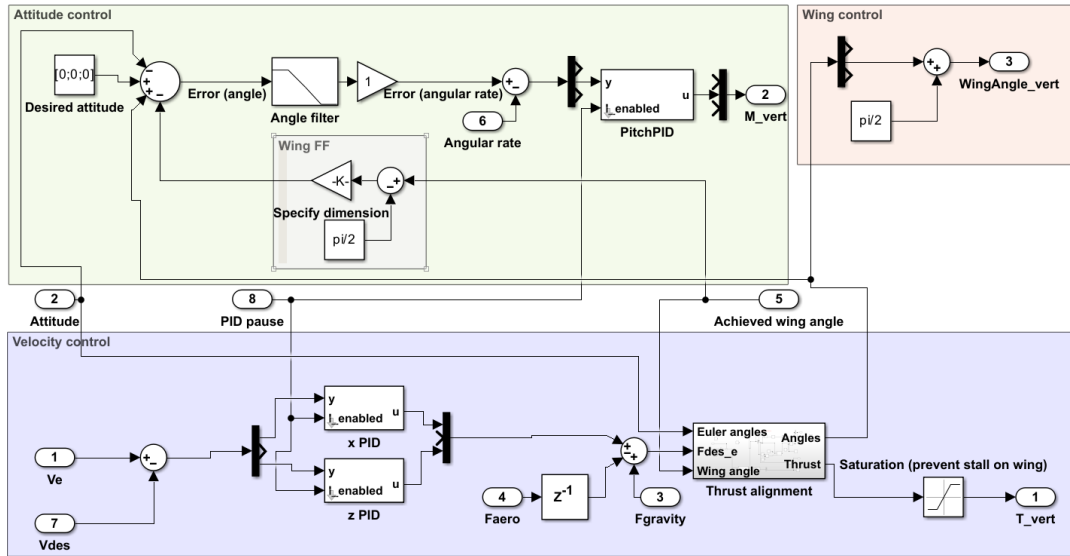


Figure 9.4: Hover control system

This control allocation strategy enables the wing angle to smoothly change with increasing velocity as shown in Section 9.5. It can be seen as a simple implementation of dynamic control allocation, where the high frequency and low frequency components of a desired output (pitch angle) are divided between different actuators as presented by Ola Härkegård [58].

The remaining attitude is passed to a nested angle and angular rate controller (green area), which is commonly used in existing quadcopter controllers[59]. This is done since it provides much better stability compared to directly relating the error in the angle to desired body moments. The "Angle filter" is added to remove the high frequency components from the angle error and thus drastically reduce the peak load on the propulsion system as discussed in Section 9.6. It has to be bridged during horizontal-vertical transition as discussed in Subsection 9.5.2. The function of the PID pause lines will be explained in Section 9.5. Noted that the hover controller is stable up to an approximate velocity of 40 m/s.

9.4. Cruise Control

During cruise, the control surfaces become operational and the wing is locked at $\kappa = 0$. This requires slightly different control logic and differently tuned controllers compared to hover control as shown in Figure 9.5. Again, a velocity controller (blue area) determines the required thrust and aircraft attitude.

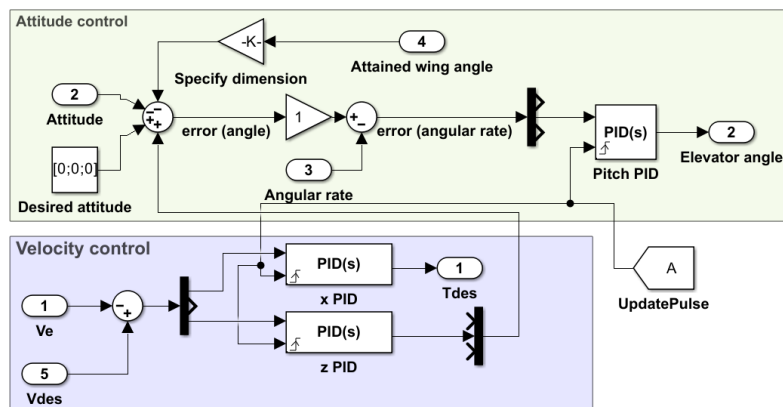


Figure 9.5: Cruise control system

To reduce actuator wear, the wing angle will be constant during cruise flight. Therefore, there is only a feed-forward of the current wing angle which is only relevant during transition as described in Section 9.5. The pitch attitude is controlled via the elevator rather than the propulsion system. Without an elevator, the aircraft becomes uncontrollable but only adding a small elevator provides enough control to make the pitch authority of the propulsion system negligible. Note that the cruise controller is stable down to a velocity of approximately 25 m/s.

9.5. Transition

Transition is the flight phase which is the most challenging to control. The main drawback of using separate controllers for hover and cruise control is that at certain points during the flight, the aircraft has to switch the flight controllers. Since the hover controller becomes unstable above 40 m/s and the cruise controller becomes unstable below 25 m/s, there is a window of 15 m/s where the control logic can be switched safely. The controllers are configured to transition from horizontal flight to cruise when above 35 m/s and to transition back when below 32 m/s. This hysteresis logic is used to prevent rapid oscillations between the controllers. In future iterations of the controller, the hysteresis band can be increased to prevent gusts from causing controller switches.

9.5.1. Hover to Cruise Transition

Transition from hover to cruise is drastically simplified by the dynamic control allocation part of the hover controller tilting the wing forward as the aircraft accelerates. This causes the wing to already be below an angle of 10° and thus to only have a small angle left to transition to completely horizontal, which is shown in Figure 9.7d. At the point of transition the controller outputs from the hover controller are instantaneously disabled and the outputs from the cruise controller are enabled. At the same time, a pulse is sent via the "UpdatePulse" block in the cruise control system which resets its PID controllers. This removes any integral values that accumulate during hover flight and thus prevents them from destabilizing the control system. Furthermore, the "PID pause" signal in the hover control system is switched to 0, freezing the integrators in its PID controllers to preserve their state during cruise. This transition control allows the reference velocity to be ramped over the transition velocity without causing instabilities as shown in Figure 9.6.

9.5.2. Cruise to hover transition

Transition from cruise flight back to hover flight is significantly more difficult compared to transitioning from hover to cruise. The cruise controller always sets the wing to an angle of $\kappa = 0$, even during decelerating. However, the hover controller tilts the wing far back during decelerating to create an excess force component in $-Xb$ direction. Therefore, the gap between the desired wing angle of the different control systems is significantly larger compared to transitioning from hover to cruise. Switching controllers while the gap in the wing angles is too high causes the control system to become unstable. This causes simply ramping over the transition velocity to be unsafe.

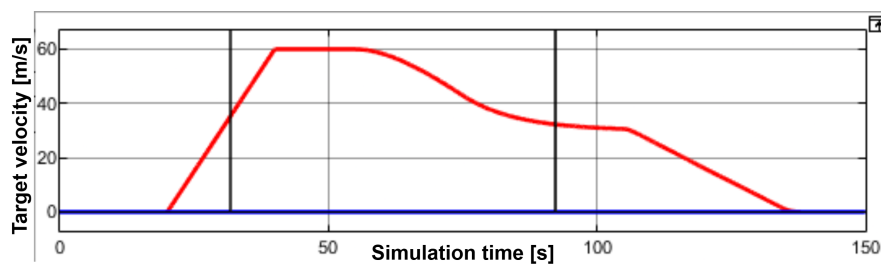


Figure 9.6: Target velocity; Red = \dot{X}_E ; Blue = \dot{Z}_E ;

A solution to that issue is to stop decelerating and reach approximately a steady state before switching the controllers, as shown in Figure 9.6. If the hover velocity controller does not try to slow down the aircraft at the switching time, it produces a wing angle that is close to horizontal, as shown in Figure 9.7d, and enables a safe transition.

Furthermore, it is required to not use the "Angle filter" which is shown in Figure 9.4 since it causes the transition from cruise to hover to become unstable. This can be done by simply 'bridging' it during this transition.

9.5.3. Transition Results

The results from the transition simulation in Figure 9.7 show that it is possible to take off vertically, accelerate and transition to cruise, and to slow down and transition back to hover. All of this can be achieved without significant coupling between horizontal and vertical velocity as can be seen in Figure 9.7a and Figure 9.7b. This is beneficial for operations as it gives the operators the freedom to choose an optimal flightpath with the only limitation being the approximate steady state when transitioning back to hover.

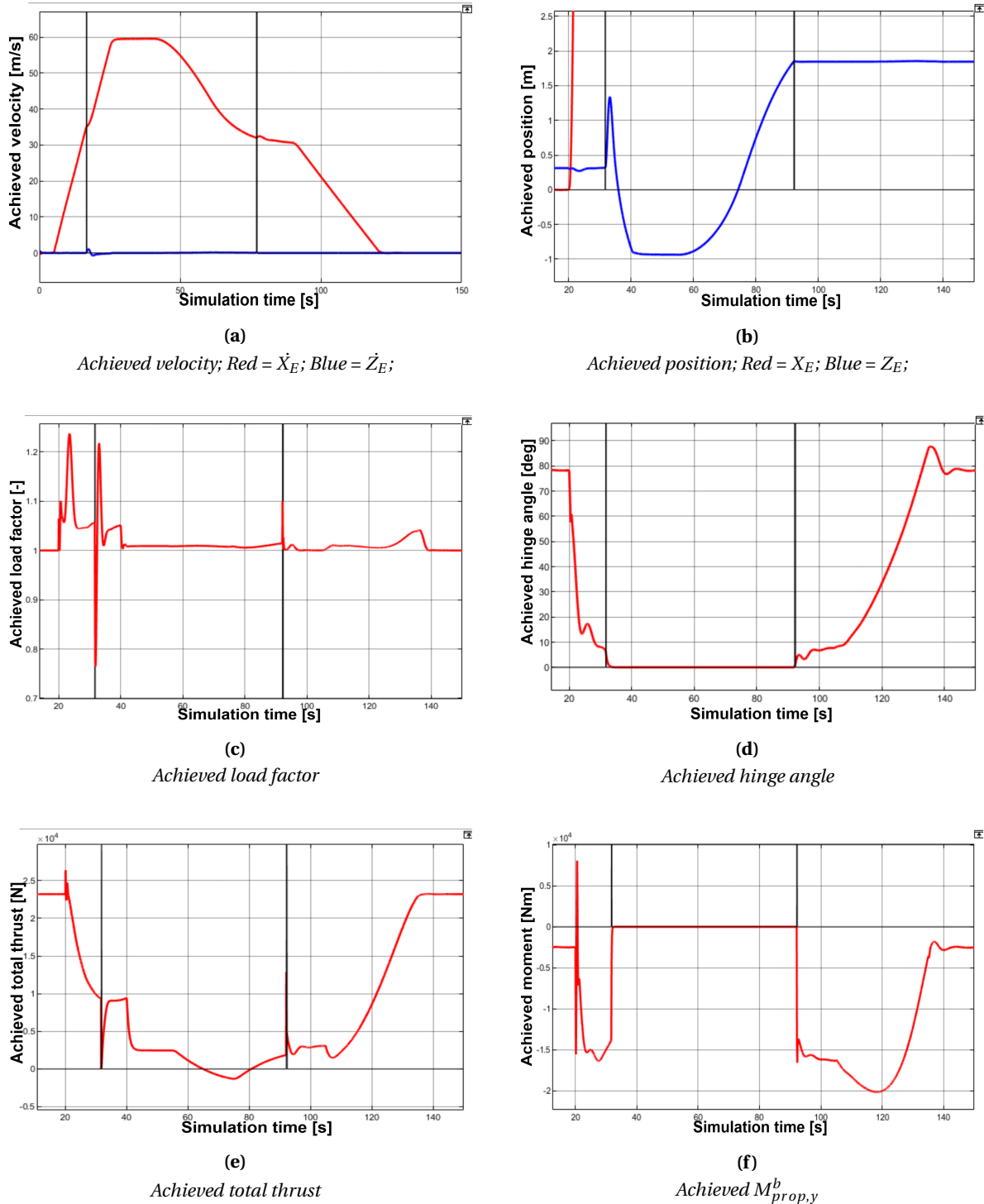


Figure 9.7: Transition performance metrics over the flight profile; Black vertical lines indicate switching of controllers

Furthermore, the maximum moment that the propulsion system delivers during the transition is below 21 kNm (Figure 9.7f), which is well within the capabilities of the propulsion system. The required thrust over the flight profile barely exceeds the required thrust during hovering and only turns slightly negative (Figure 9.7e) which is achievable due to the use of variable pitch propellers. The load factor stays between 0.75 and 1.25 over the entire flight profile. This range of load factors is justifiable since they are not sustained for a long time and within what can be expected on a conventional airliner.

9.6. Gust Rejection

A fast and effective gust rejection is an important property of the hover control system. The ResQProp will be landing in confined spaces such as on roads. According to requirement **SYS-CTRL-07**, the aircraft shall be able to reject an instantaneous horizontal gust of 9.144 m/s within 3 m.

Due to the significant wing surface area that is exposed to the gust while hovering, a gust along the X_B axis is the critical case. The gust response of the system can be analyzed with the existing 3 DOF model since it lays within the X_B-Z_B plane by implementing a step input of 9.144 m/s after the system has initially stabilized (20 seconds).

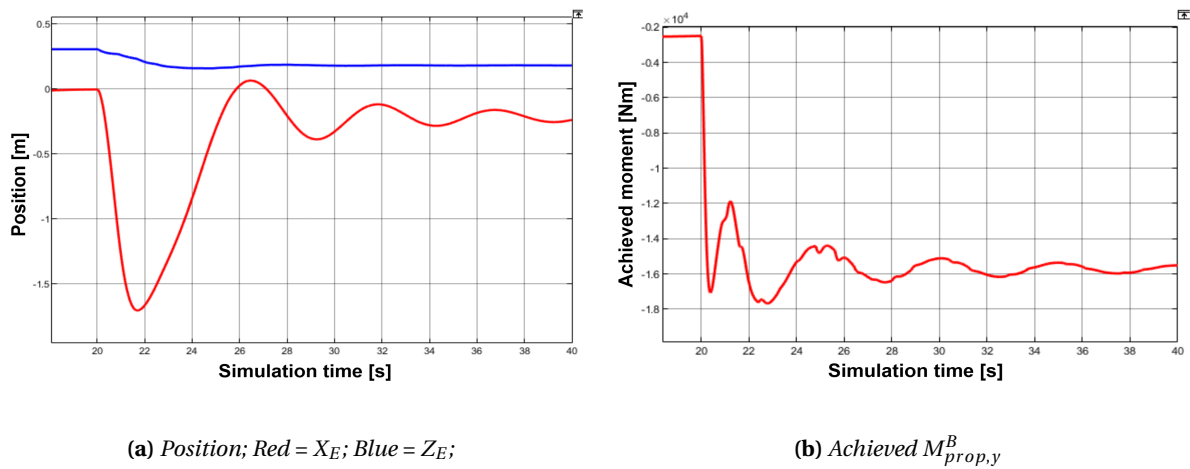


Figure 9.8: Front gust rejection simulation results

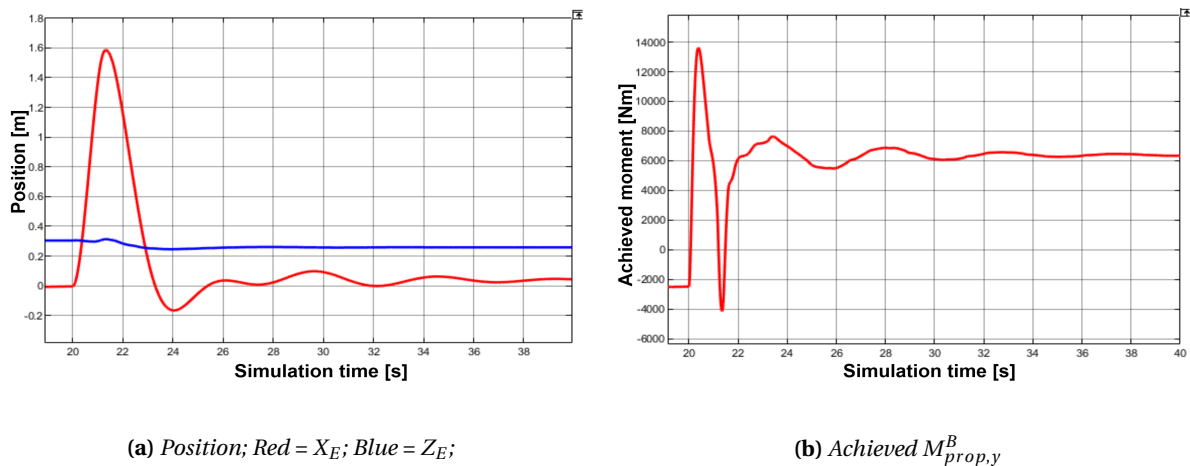


Figure 9.9: Rear gust rejection simulation results

As shown in Figure 9.8a and Figure 9.3, the X_E position of the aircraft stays within ± 2 m during both of the maneuvers, which fulfills requirement **SYS-CTRL-07**. Furthermore, the aircraft does not lose any altitude

² but rather ascends slightly during the maneuver, which means that the gust rejection is also safe at a very low altitude such as during landing.

9.7. Controller Robustness

Controller robustness against phase disturbances is commonly quantified by its phase margin. Since the concept of the phase margin is only defined for linear time-invariant (LTI) systems, it is beneficial to find an alternative measure to quantify it. Therefore, the transition and gust rejection simulations are repeated and the actuator time constants increased until the system becomes unstable or the system fails to meet the requirements. This is done while keeping the other time constants constant. During gust rejection, this is only done for the hinge and propulsion system time constants since the elevator is inoperative in that flight condition but for transition, the elevator time constant is also varied. The results are given in Table 9.2. The Actuators time constants should ideally still remain well below the values given since the closer they are, the more oscillatory the responses become.

Table 9.2: Results from controller robustness analysis; Acceptable time constants in [s]

Actuator\Maneuver	Front gust rejection	Rear gust rejection	Transition
Hinge	1.2	2.3	2.6
Propulsion system	0.3	0.4	0.3
Elevator	irrelevant	irrelevant	0.5

9.8. Critical View on the Model

As shown in Table 15.1, the sensitivity analysis of certain model parameters verified that highly uncertain parameters such as the actuator time constants or the exact transition profile only have a limited influence on the moments that are required from the propulsion system. The only critical aspect of the flight profile is that the transition between the different flight controllers takes place during approximately stationary flight with a constant velocity.

No real validation of the model could be performed since there is no real flight data available for a similar configuration. Therefore, a potential validation strategy involves building a scaled mode and demonstrating that it performs as described by the model.

The model relies on a broad range of assumptions, including an approximately uniform flow being induced over the wing by the propulsion system (**ASM-CTL-03**). This assumption is not very realistic but significantly simplifies the analysis and allows for the generation of approximate moment requirements that can be used to size certain subsystems and act as a first way to check whether the system is feasible.

The model has been mainly used to generate requirements for other subsystems. Therefore, it is working with preliminary center of gravity and wing locations. These do not heavily influence the results of the model but may cause slight inaccuracies.

9.9. Future considerations

If the design of the system shall continue in the future, it is highly recommended to perform certain actions to increase model confidence.

- **Adapt model to newest design:** Adapting the model to the newest design, including a revised inertia estimation would increase the accuracy of its results.
- **Empennage and elevator model:** The empennage and elevator model has been simulated very rudimentary since it is not very significant for the most critical flight conditions (gust and transition). The cruise part of the flight shall be analyzed more accurately, a more refined empennage and elevator model could be beneficial.
- **Wing aerodynamics:** Modeling the aerodynamics of the wing under the influence of the propeller wake a challenging issue. One approach to make it more accurate could be by modeling the sections behind the different propeller separately and to apply only the propeller induced velocity to the section that is directly behind the propeller. A sketch for such a model is shown in Figure 9.10.

²The Z_E axis points downwards as specified in Subsection 9.1.1.

- **Fuselage aerodynamics:** In its current state, the fuselage aerodynamics are modeled quite rudimentary to limit the amount of computation time that might be required to get a more accurate model. To ensure highly accurate aerodynamics also at very high angles, it might be beneficial to adopt methods that are not Buckingham- π -theorem based and thus remain accurate independent of the flow direction. One potential approach is adopting phi-theory[52].
- **Create 3D model:** Adapting the model to a 3 dimensions (6 DOF) might offer additional insight into the system performance such as during side gusts but requires a significant amount of computational power to generate suitable aerodynamic coefficients in three dimensions. This also includes adding a rudder model.
- **Create validation model:** A small unmanned model of the system could be created to validate that the model is an accurate representation of the system.

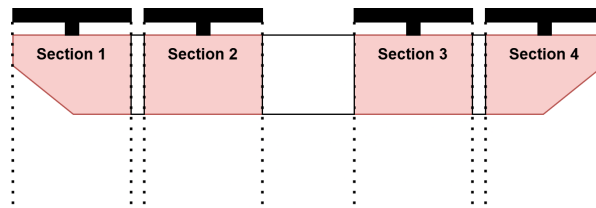


Figure 9.10: Proposed new wing model

9.10. Failure

Several failure modes have to be considered to be established. These include single engine failure, failure of the hinge, and failure of the control surfaces.

9.10.1. Single Engine Failure

The engines are sized to be capable of providing twice the required thrust in hover. Due to the aerodynamic torque of the motors, the aircraft will no longer be controllable purely by using the propulsion system. Instead, pitch and roll control will be provided by the propulsion system, with yaw control being provided by the ailerons.

Due to the design of the disc area in Subsection 6.2.1, single engine failure in cruise is not critical since the diagonally opposing engine to the one that failed can be completely disabled without inducing any pitch or yaw moments. The roll moment that is created can simply be counteracted by using the ailerons. The aircraft can then be landed horizontally with the small propellers probably breaking off.

9.10.2. Hinge Failure

If the hinge gets stuck during hovering, landing is trivial. If it gets stuck during cruise, the aircraft can be landed horizontally as described in Subsection 9.10.1. If the hinge gets stuck at an angle between hover and cruise, a horizontal landing can still be completed since the wing will not stall due to the induced velocity caused by the propellers and since the engine thrust will be at least partially angled upwards.

9.10.3. Control Surface Failure

Aileron A failure of one of the ailerons can be compensated with the other aileron moving independently. In case the aileron gets stuck at its maximum or minimum value, this will lead to a complete loss of the roll authority that is provided by the ailerons. In this case, using differential thrust and aerodynamic torque of the propulsion system can be used to offer some degree of roll authority.

Elevator A failure of the elevator can be considered as critical since only a single elevator is used in the aircraft design and since it offers significantly more control authority than differential thrust. A potential fix is using split elevators that are actuated independently. In case half of the elevator fails, this would allow the other half to still provide pitch authority at the cost of roll coupling. This roll coupling can be counteracted via the ailerons.

Rudder Failure of the rudder can be counteracted by using differential thrust since in cruise the moment arms around the yaw axis are significantly larger than around the pitch axis.

9.11. Avionics

The avionics system consists of a few key parts: sensors, communication devices, pilot panel, actuators, voting devices, and flight computers. The sensors and pilot panel send measurements and pilot inputs through data buses to the flight computers. The computers then send display information to the pilot panel and commands to the actuators, while talking to the communication equipment.

Figure 9.11 illustrates the complete flow of sensor, control, and communication data in the avionics system. The architecture includes three flight computers that receive inputs from distributed sensor modules through three CAN buses (125 kB/s), including GPS, radars, position encoders, air data computers³, IMUs, and magnetic heading devices. Each flight computer processes the data independently and transmits it via RS-422 (1250 kB/s) to data voting modules, which ensure redundancy and consensus in control decisions. The ADS-B transponder and COM/NAV radios are integrated into the avionics system for certification purposes, using a dedicated data bus known as ARINC 429 (12.5 kB/s), which is widely adopted in civil aviation for its reliability and unidirectional data transmission.

In particular, each sensor CAN bus has multiple transmitting devices. A priority list thus needs to be created for the CAN bus to avoid packet loss of important data because of multiple sensors trying to use the bus simultaneously. The IMUs are critical to the fly-by-wire system and therefore receive the highest priority. Special consideration needs to be taken to make sure the high update rate (500 - 1000 Hz) does not block the transmission of less prioritized data.

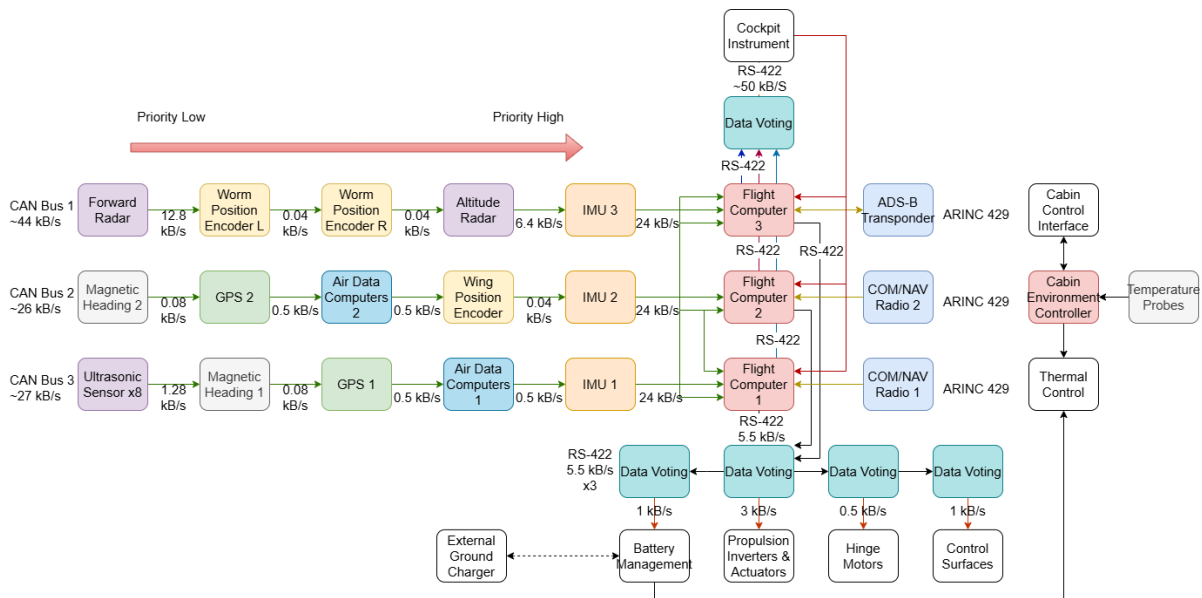


Figure 9.11: Data connections between avionics components with data rates in kilobyte per second

The avionics layout for the aircraft has to provide a significant amount of redundancy since flying the aircraft without a flight by wire or autopilot system will be very challenging. The proposed avionics layout in Figure 9.11 offers triple redundancy for all critical systems and a data voting system that allows the system to detect faulty sensors or flight computers. The data voting allows the flight control system to function when one out of three computers fails. The probability of catastrophic failure follows a binomial distribution (p is the failure probability):

$$P(\text{catastrophe}) = 1 - \binom{3}{2} p^1 (1-p)^2 - \binom{3}{3} p^0 (1-p)^3 \quad (9.23)$$

The chance of a catastrophic failure cannot exceed $1e-9$ per hour per requirement MIS-CERT-04. For a single computer, it is impossible to achieve this probability; however, the failure rate for a single computer can be increased to $1.83e-5$ per hour since due to the triple redundancy, one single flight computer failing does not lead to system failure. This can be achieved with a commercial x86 computer.

³For digitization of pitot-static data

Structures and Materials

In this chapter, the structures surrounding the ability of the wing will be designed. In Section 10.1, a material selection will be presented for the wingbox and the fuselage. A load analysis on the wing will then be performed in Section 10.2, followed by the wingbox design in Section 10.3. Then, the design for the hinge mechanism used to rotate the wing will be presented in Section 10.4. Lastly, the landing gear design will be described in Section 10.5.

Structures and Materials Symbols

γ	Correlation factor	A	Area	$M_{1,2}$	Material Index
η	Plasticity reduction factor	A_m	Enclosed area	M	Bending moment
μ	Poisson's ratio	b	Sheet width	N	Normal force
ω	Angular velocity	b'	Stiffener pitch	P	Power
σ	Normal stress	C	Buckling coefficient	q	Shear flow
τ	Shear stress	C_R	Relative cost	r	Radius
ρ	Density	E	Elastic modulus	T	Torque
GR	Gear ratio	F	Force	t	Thickness
		F_b	Breaking force	V	Shear force
		I_{xx}	Moment of inertia	W_{wing}	Wing weight
		l	Length of the beam	Y	Lewis Factor
		l_{cg}	Longitudinal distance from CG	$2w_e$	Effective sheet width

10.1. Material Selection

This section will explain the process behind choosing the material for the wingbox and fuselage. The focus lies on the material selection for the wingbox as this is the main load-bearing structure of the eVTOL, which can be optimized for low weight and low cost.

10.1.1. Wingbox Material Selection

The process of selecting the optimal material for the wingbox starts with defining what the material candidates are for this structural application, and with that, eliminating the other options. Within the aerospace industry, it is conventional to use metals, such as aluminium alloys, magnesium alloys, and steels [60]. In addition, composites are widely used within the sector nowadays. It needs to be determined what the optimal material is for this application, choosing between metals and composites. Material selection is determined by its function, the objectives, and its constraints, provided by Table 10.1 [61].

Table 10.1: Function, objectives, and constraints of the wingbox

Function	Wingbox
Objectives	<ul style="list-style-type: none"> • Minimize weight • Minimize cost
Constraints	<ul style="list-style-type: none"> • Stiffness: must not deflect too much under the design loads • Strength: must not fail under the design loads

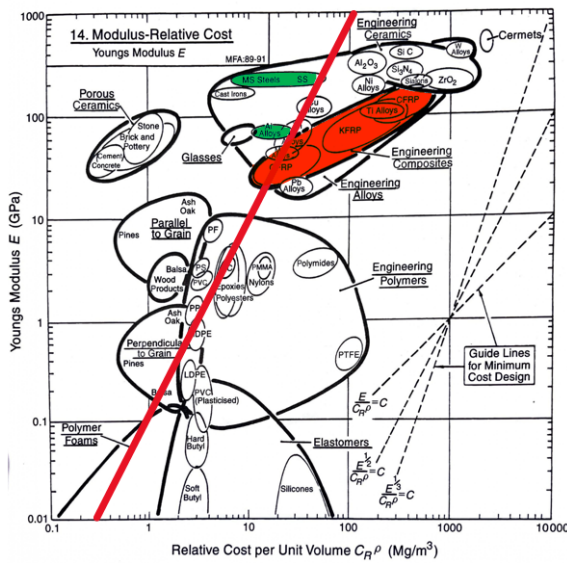
Following from Table 10.1, the material indices that characterize the required performance of the material

used for a wingbox can be defined. Two functions represent the performance that needs to be optimized. First, the material should have a high stiffness for a beam application, while being low in cost and lightweight. Secondly, the material should have a high strength for a beam application, while again being low in cost and lightweight. Respectively, these are represented by (10.1) and (10.2) [61].

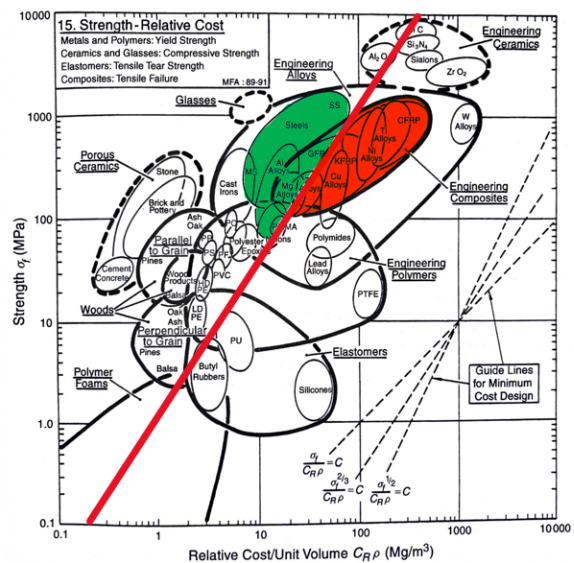
$$M_1 = \frac{E^{\frac{1}{2}}}{C_R \rho} \quad (10.1)$$

$$M_2 = \frac{\sigma_f^{\frac{2}{3}}}{C_R \rho} \quad (10.2)$$

These material indices are implemented in two material selection charts evaluating the material performance using the index. Figure 10.1 shows the two material selection charts; in this chart, the respective index is drawn tangent to the aluminium alloys area in red. The two charts indicate that steel and aluminium alloys have similar performance for these two material indices. Magnesium alloys perform worse regarding the Young's modulus against the relative cost. Additionally, composites are also less suitable for this application, which eliminates them from consideration in the material selection for the wingbox. This reasoning is illustrated through the use of green and red colors in the charts, which show steels and aluminium alloys in green and composites in red.



(a) Material selection chart for Young's modulus against relative cost



(b) Material selection chart for strength against relative cost

Figure 10.1: Material selection charts with the respective material index presented by the red line, the high performing materials in green and the underperforming materials in red. [61]

With this analysis, it comes out that aluminium alloys and steel are the prime candidates for this application. In the industry, it is conventional to use aluminium over steel [60], for multiple reasons. First, aluminium has better manufacturability than steel, as the wingbox is designed as a conical tube, it is beneficial to have this better manufacturability property [61]. Also, aluminium is better resistant to the environment than steel [61]. Lastly, if weight is prioritized over cost, aluminium is beneficial over steel. The strength-to-weight ratio is dependent on the geometry and optimizing it for a beam under loading, a similar case to the wingbox, shows that it is lower for aluminium [61]. Following all these findings, an aluminium alloy is most optimal for the wingbox design.

In the aerospace industry, two high-strength aluminium alloys are commonly used for aircraft structures. These aluminium alloys are Al2024 and Al7050 [62]. From literature, it is found that Al2024 performs better in terms of corrosion resistance and workability [62]. Both of these properties are of key importance for the wingbox. Durability is an important criterion to result in a sustainable design and to reduce maintenance costs. The workability is important as the wingbox is designed to be a conical tube, as explained in Section 10.3, which requires good workability. Another key benefit of the Al2024 alloy is its medium to high strength-to-weight performance, which results in a desirable thickness for the wingbox design where buckling is not dominant. This is explained in more detail in Subsection 10.3.2.

In addition to choosing the sub-class of the aluminium alloy, the heat treatment for the material needs to

be chosen, as it strongly affects its properties. From a material database, it can be found what the optimal heat treatment is for this application. The material database indicates that the T6 heat treatment is beneficial because it provides the alloy with a high strength-to-weight ratio, while maintaining good workability and corrosion resistance [63]. The key properties of this material are given in Table 10.2 [63]. In addition to using this material for the wingbox, the decision is made to use it for the complete wing due to its versatility in applications, with its beneficial properties in strength-to-weight ratio, corrosion resistance, and workability. Using a single alloy simplifies manufacturing and maintenance while ensuring consistent performance across all components. So, Al2024-T6 is used for the wing skin, the wingbox, ribs, and stringers.

Table 10.2: *Properties of Al2024-T6*

Composition	Al-Cu-Mg (1–2.5% Cu)
Density (kg/m³)	2780
Tensile yield strength (MPa)	345
Shear stress (MPa)	283
Young's modulus (GPa)	72.4

10.1.2. Fuselage Material Selection

The material selection for the fuselage is less detailed compared to the wingbox; however, the objectives remain similar to those for the wingbox: minimize weight and cost, and it must not fail under the design loads. For the fuselage, two components are considered: the fuselage frame and the fuselage skin. For the frame, the focus is shifted to aluminium, as it is inherently cheaper than composites, will outperform steel in corrosion resistance, lowering maintenance costs, is lighter, and easier to manufacture. Therefore, the material selected for the fuselage frame is Al2024-T6 for the same reasoning as for the wingbox.

For the fuselage skin, more properties are available as were described in Section 6.1, therefore a deeper analysis of the material choice can be performed. The metrics for this analysis are the same as for the fuselage frame, to be as light and cheap as possible. Material strength was not considered to be as important as this component is low load-bearing. A list of materials most commonly used for aviation fuselage skins, along with their properties, is presented in Table 10.3 [16].

Table 10.3: *Alternative Fuselage Material Densities and Costs*

Material	Density [kg/m³]	Cost [€/kg]
Al2024-T6	2780	13.76
Al6061-T6	2700	11.18
AISI 4130	7850	1.677
CFRP	1600	204.68
GFRP	2100	20.64
AZ31B	1770	31.648

From Table 10.3, the first two are aluminium alloys, AISI 4130 is a steel alloy, CFRP and GFRP are reinforced polymers, and AZ31B is a magnesium alloy. In Figure 10.2, the mass fraction to the MTOW is plotted against the total cost of the fuselage for each of the materials, respecting the configuration that was described in more detail in Section 6.1.

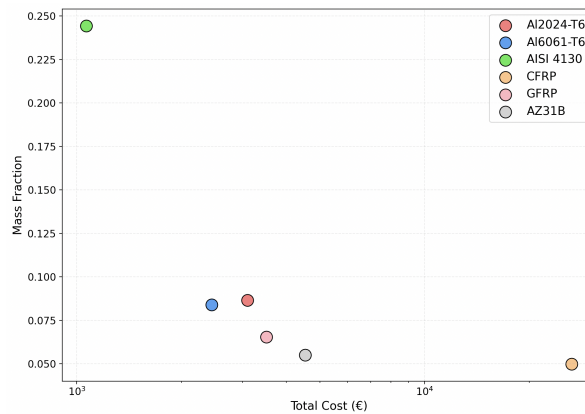


Figure 10.2: Mass Fraction vs Total Cost of Fuselage for Different Materials

In Figure 10.2, the material in the bottom left corner is the most desirable for the set metrics. As can be seen, this is Al6061-T6, and therefore the final choice for the fuselage skin material. From Table 10.3, it can be noted that the two aluminium alloys considered vary very little in both density and cost, although Al6061-T6 performs better against these metrics. Furthermore, although steel is 7 times cheaper compared to Al6061-T6, it is also 35% heavier in terms of its mass fraction. On the other hand, the carbon fibre reinforced polymers are 40% of the weight, but are 18 times more expensive than Al6061-T6, also strengthening the choice for the aluminium alloy. The glass fibre reinforced polymers, although not as expensive as the CFRP, are also lighter, but are more expensive. Lastly, the magnesium alloy performs nearly as well as the CFRP in terms of density; however, it is also still 3 times as expensive as the Al6061-T6. Overall, it is clear that when looking at cost and weight, for this non-load-bearing component of the eVTOL, Al6061-T6 is the better choice.

10.2. Load Analysis

The loads on the wing during normal operation and the failure modes, such as an engine failure, need to be defined before the wingbox design process can start. All the different loading cases are analyzed to ensure the wingbox can withstand the different loading cases it could experience within its lifespan. These load cases will result in a load on the wing visualization, which functions as the starting point for the generation of the internal loading diagrams.

10.2.1. External Loads

An important characteristic of a VTOL is its ability to transition from vertical flight to horizontal flight. The ambulance eVTOL does this by rotating its wing, where in vertical flight the propellers are pointing upwards and in horizontal flight they point forwards. The wingbox is rotating inside the fuselage, and the engines are fixed on the wingbox. Therefore, the orientation of the thrust to the wingbox is not changing between the two flight modes. In horizontal flight, the wing is generating lift and drag, in contrast to vertical flight, where it is assumed not to generate any aerodynamic forces. For the lift force in horizontal flight, different cases are considered, which follow from the flight envelope given by Figure 11.2. This shows that the load factors to be evaluated are 1, 2.5, and -1. Additionally, there is a difference between the thrust levels during vertical and horizontal flight. The combination of the different load cases is shown by Figure 10.3.

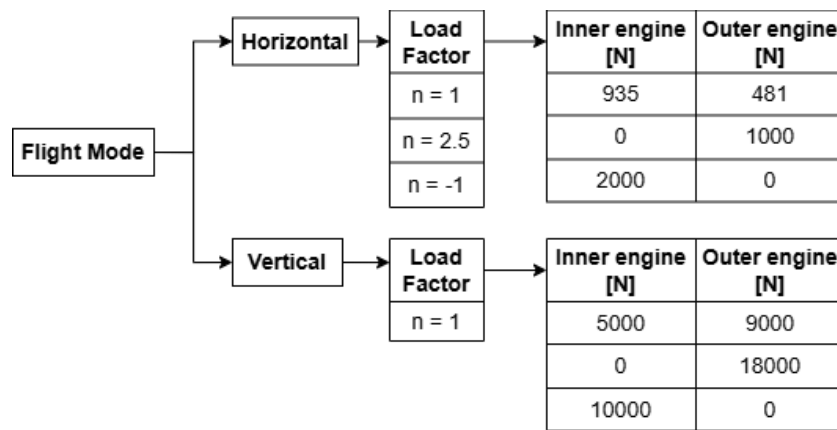


Figure 10.3: Tree diagram showing the combination of different loading cases considered to be experienced by the wingbox.

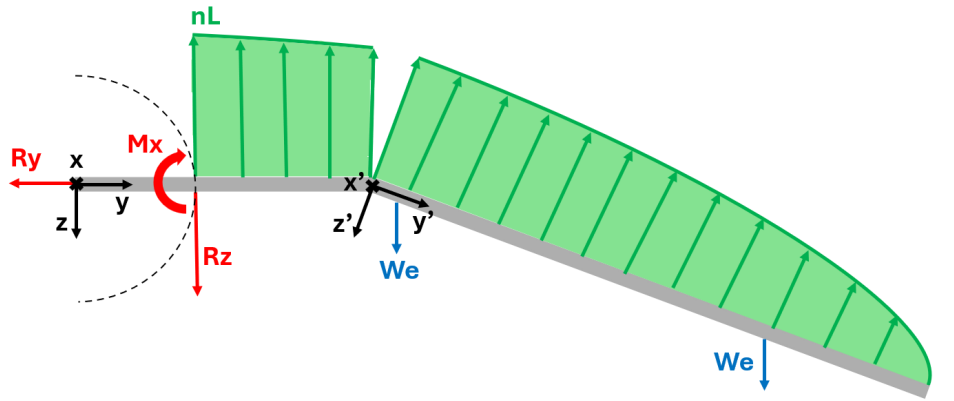
In addition to the aerodynamic loads and the thrust loads explained above, some other forces are acting on the wingbox. These are the weight of the motors, structural self-weight, and the aerodynamic moment. Some key assumptions are made regarding all the loads and the boundary conditions, provided by Table 10.4.

Table 10.4: Structural assumptions regarding the load analysis

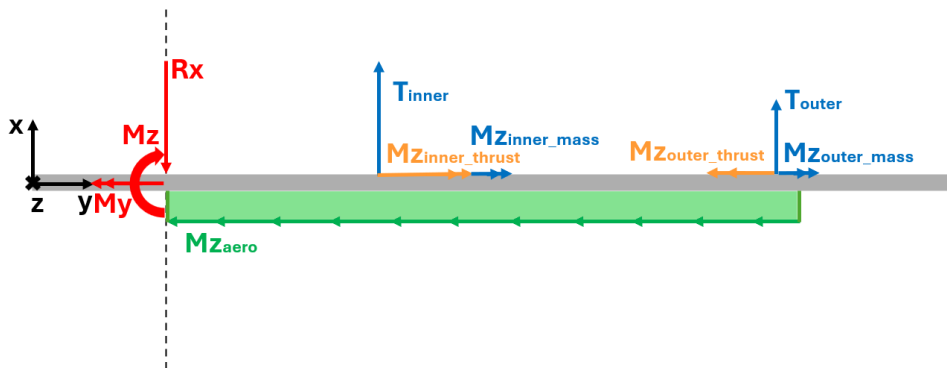
Identifier	Assumption
ASM-STRU-01	The aerodynamic loads on the wing in vertical flight are neglected.
ASM-STRU-02	Only the nose-up moment generated on the wingbox by the aerodynamic forces is implemented from the wing root onwards, and until the center of pressure moves behind the central line of the wingbox.
ASM-STRU-03	The aerodynamic moment is modelled as a constant distribution along the wingspan.
ASM-STRU-04	The self-weight of the wing is neglected.
ASM-STRU-05	The lift distribution computed using XFRL5 represents the actual lift distribution on the wing.
ASM-STRU-06	The loads resulting from drag are neglected in both flight modes.
ASM-STRU-07	All the degrees of freedom are constrained at the fuselage-wing interface, except for the normal force.
ASM-STRU-08	In between the fuselage walls, no lift force will act on the wingbox structure.

The assumptions are valid within the scope of this wingbox design. ASM-STRU-01 can be neglected as it is small in comparison with the generated aerodynamic loads in horizontal flight. Additionally, the shear force generated by the engine thrust in vertical flight is much larger and drives the sizing in the wingbox design. ASM-STRU-02 is conservative, as only the aerodynamic moment that is acting in the same direction as the torque generated by the thrust levels is incorporated. ASM-STRU-04 is justified as the loading diagrams are used to design the wingbox and the wing, and the weight of the wing is uncertain at this point. Preferably, a conservative approach is taken by not adding the weight. In case the load factor is -1, this assumption is non-conservative, but the shear force will always remain lower than the shear force experienced when the load factor is 2.5 as the wingbox weight is much smaller. Concluding, this assumption makes the wingbox sizing slightly more conservative, which is found to be beneficial over including an uncertain wing self-weight at this stage. ASM-STRU-07 comes from the hinge design in which the wingbox will act as the rotating axis within bearings. This means that the normal force in contrary to all the other loads, is not transferred to the fuselage structure. The normal force will act in the opposite direction on the left wing; ultimately, the wingbox will be in tension inside the fuselage.

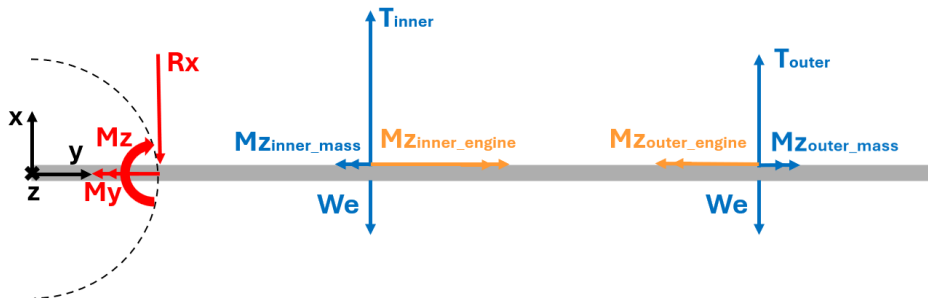
Concluding from this analysis, all the loads are combined and visualized by Figure 10.4.



(a) Loading diagram for horizontal configuration, spectating from the rear



(b) Loading diagram for horizontal configuration, spectating from the top



(c) Loading diagram for vertical configuration, spectating from the rear

Figure 10.4: The loading diagrams of the wing in horizontal flight and vertical flight, showing the reference systems, all the considered external loadings, and the respective internal constraining loadings.

10.2.2. Internal Loading Diagrams

All the defined loads given above are combined, and the internal shear forces, normal force, and moments are analyzed. It is desired to find the loads acting perpendicular and parallel to the plane of the wingbox cross-section. Following from this, it is reasoned that the reference frame used for the internal load analysis should rotate around the x-axis after the kink to ensure the y-axis stays aligned with the wingbox, this is visualized in Figure 10.4. From now on, the axis system of the initial horizontal part of the wingbox is called the initial reference frame, and the axis system after the kink is the rotated reference frame.

The rotation of the reference frame affects the composition of the internal loads from the aerodynamic forces, engine weight, and engine torque. Firstly, the aerodynamic forces act perpendicular to the wing; thus, after the kink, the aerodynamic forces act at an angle to the initial reference frame. Ultimately, these aerodynamic forces after the kink generate a normal load on the initial horizontal part of the wingbox. Secondly, the weight of the engines mounted on the angled part of the wing is decomposed into a perpendicular and

parallel force to the wingbox. This generates a normal force in the wingbox in the rotated reference frame. Thirdly, the torque generated by the engines mounted to the wingbox will be much higher in the horizontal part of the wingbox, thus in between the fuselage and the kink, as the offset perpendicular to the wingbox to the outside thrust force is much larger.

In addition to rotating the reference frame around the kink, it is also rotated with the wingbox if it changes from horizontal to vertical flight. The y-axis will remain parallel with the wingbox. Thus, the reference frame is fixed onto the wingbox.

All of the external loads are visualized in Figure 10.4 and the internal loading diagrams are provided by Figure 10.5 for the horizontal flight mode and Figure 10.6 for the vertical flight mode. Referring to the reference frames, the initial reference frame is used from the origin to the bend at 2.241 meters. After this point, the rotated reference frame is applied until the wing tip.

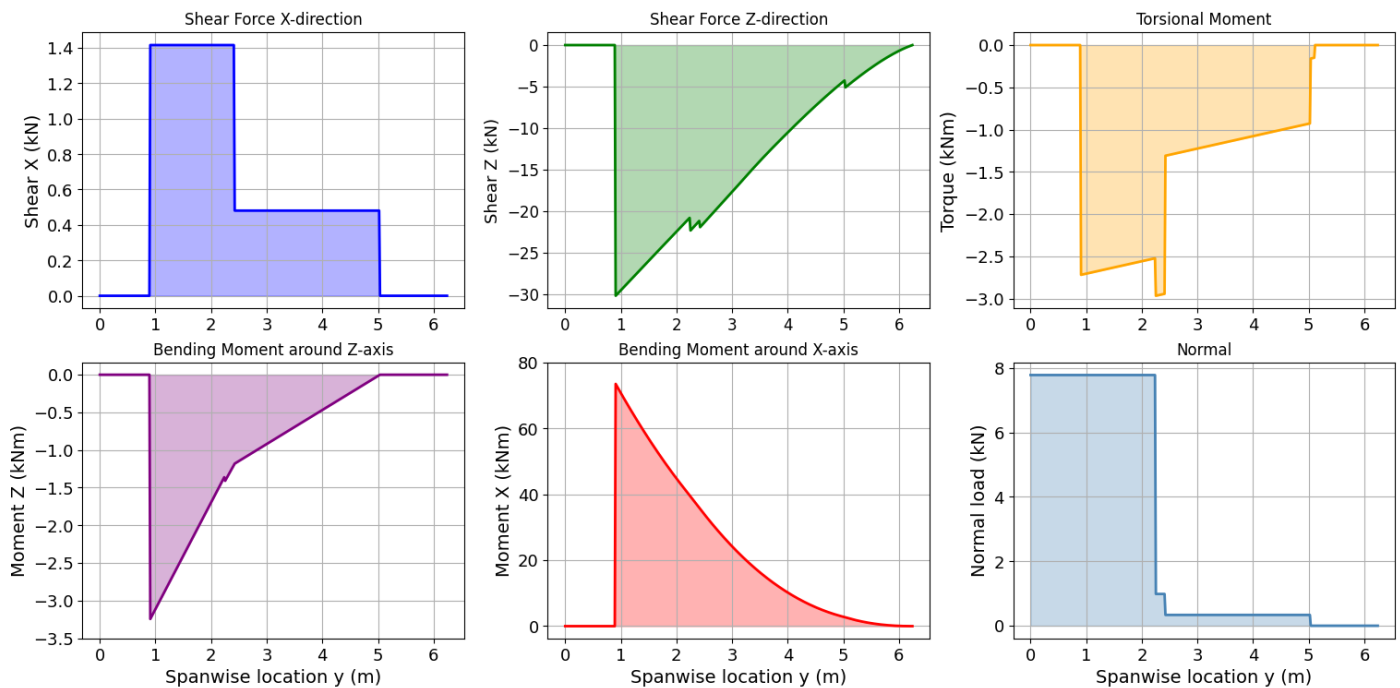


Figure 10.5: Internal loading diagrams of the wingbox in horizontal flight with a load factor of 2.5 and all engines operational

Key points in horizontal flight with a loading factor of 2.5 are highlighted. First, the highest loads are induced on the wingbox by the lift force, which generates a high internal shear force in the z-direction and a high internal moment around the x-axis. The normal force diagram shows that the rotated lift after the kink generates a significant normal force in the horizontal part of the wingbox. The weight of the engines is taken higher than the actual weight of the engines in the final design. This conservative estimate, in combination with the engine thrusts, results in a negative torsional moment. The reduced thrust levels during horizontal flight lead to a smaller bending moment around the z-axis when compared to the vertical flight internal load diagrams.

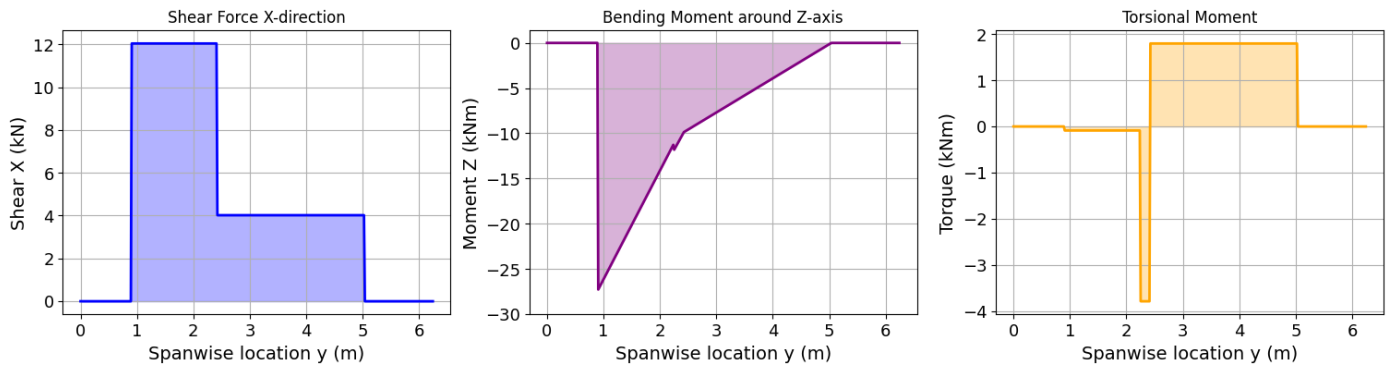


Figure 10.6: Internal loading diagrams of the wingbox in vertical flight where lift is neglected and both engines are operational.

In vertical flight, shown by Figure 10.6, there is no internal load in the z-direction as the lift force is neglected. This assumption also results in neglecting the normal load and the bending moment around the x-axis. The shear force in the x-direction, and resulting from this, the high internal bending moment around z, is generated by the high thrust levels in vertical flight. These high thrust levels generate a large torque between the two engines. The two engines are configured on the wing such that they generate almost similar torques in opposite directions, visualized by the almost zero torque between the wing root and the first engine. The inner engine is located just to the outside of the kink in the wing; this generates a high but thin negative torsional peak in the internal loading diagram between the kink and the inner engine.

10.3. Wingbox Design

Once all the loads that the wing will be subjected to are known, the wingbox design can be started. First step in the design is general sizing of the structural elements, then structural analysis for various failure modes, and lastly optimization to ensure that the final weight stays as low as possible.

10.3.1. General Sizing

Designing a wingbox for a tiltwing aircraft is associated with many challenges. Mainly, the structure has to carry loads in all directions, so the optimal shape of the cross section varies from that of other conventional aircraft. The transition phase between vertical and horizontal flight is of concern in this case. For that reason, instead of the wingbox consisting of two spars and skin, a cylindrical element was used. It was decided that it would be the most efficient option for the diverse loading conditions. Additionally, because of the large anhedral and the engines being offset from the wing, torsion was quite a limiting problem in the case of one engine inoperative emergency. A circular closed section, once again, proved to be the most efficient shape for resisting torsional loads. In the end it was decided that the wingbox would be made out of a cylinder located at the thickest point of the airfoil, which is at around 30% of the chord length, and stiffened skin plates spanning from 30% to 75% of the chord length to leave room for control surfaces near the trailing edge of the wing. The actual geometry can be seen in Figure 10.7a.

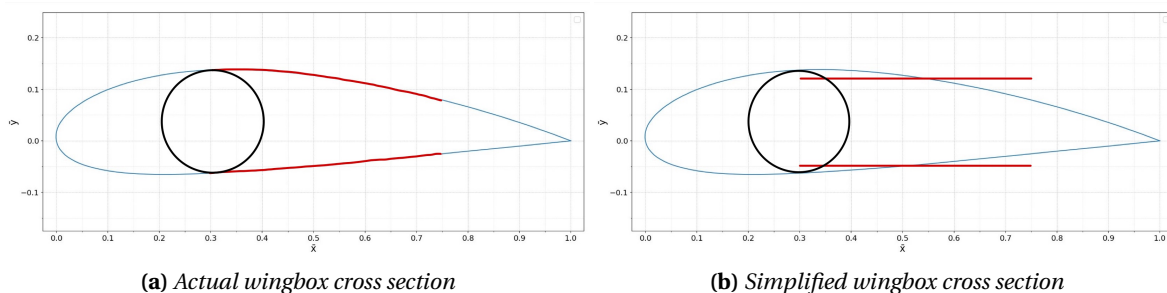


Figure 10.7: Wingbox geometry

For the sake of simplifying calculations, the skin was approximated as flat plates. In reality, it would be curved to take on the shape of the airfoil. This is a conservative assumption as the curvature would increase

its moment of inertia and resist bending more efficiently, thus it adds a safety margin to the design. The simplified model geometry that was analyzed in the design process can be seen in Figure 10.7b. Some additional assumptions that aim to simplify the calculations while considering various failure modes are listed in Table 10.5.

Table 10.5: *Structural assumptions regarding structural analysis of the wingbox*

Identifier	Assumption
ASM-STRU-09	Thin-walled structure. Thickness is much smaller than other representative dimensions throughout the span of the wing so this is a valid assumption that can serve to simplify calculations.
ASM-STRU-10	It is assumed that only the conical element carries any shear flow due to shear loads and torsion. This provides a safety margin for the design of this element, as it is analyzed to withstand higher loads than it will in reality.
ASM-STRU-11	Skin plates are approximated to be flat plates. In reality they will take on the shape of the airfoil. This assumption provides conservative results as the curvature will increase the moment of inertia of the plates, meaning that they will be able to carry greater stresses than analyzed.
ASM-STRU-12	Cross section is assumed to be symmetrical with respect to the x-axis. Chosen airfoils do not have a large camber so this assumption is valid and neglects the effect of product of inertia of the cross section.
ASM-STRU-13	The stringers are assumed to be point areas and their centroids coincide with the top and bottom skin plates. This is a conservative assumption as it neglects the moment of inertia of individual stringers and only considers their Steiner term and in reality the stringers will be placed further away from the center since the skin plates are curved.
ASM-STRU-14	Skin plates are assumed to only carry axial stresses due to lift induced bending. Since the circular closed section is meant to carry shear flows this is a valid assumption at this stage of the design.
ASM-STRU-15	For skin buckling it is assumed that the plates have all of their edges simply supported. In reality the connection points might provide more support so this is a conservative assumption that underestimates the buckling performance of skin plates.

Some constraints regarding the design of the wingbox were set by aerodynamics and flight performance. They were incorporated and added to the list of design choices set before optimizing the shape of the structural elements throughout the wingspan. They are as follows:

- The maximum thickness of the airfoil at the root is 0.27 m.
- The wing thickness is constant throughout the fuselage and it starts to taper after the fuselage. The taper ratio is set to 0.5.
- The diameter of the part is equal to the thickest part of the airfoil and is decreasing linearly throughout the span according to the taper ratio, forming a truncated cone shape.
- The thickness of the conical part is piecewise constant and is decreasing along the wingspan.
- The ribs are placed at the locations along the span where the thickness of the cone changes.
- The number of stringers on top and bottom skin plates is the same and changes per interval between two ribs.
- Skin thickness is constant at 1 mm for the entire wing.
- Safety factor of 1.5 is used in all the stress calculations. This is a standard value for aerospace structures.

The decisions to implement the taper ratio as well as to decrease the thickness of the main load-carrying element are taken to reduce the weight of the structure and avoid over-designing the parts that are not as heavily loaded as the root. In order to find the optimal values for the number of stringers, thickness of the conical part at each interval, and the lengths of each interval, various failure modes are considered, namely yielding and buckling under combined loading for the conical element, and buckling of stiffened panels for the skin.

10.3.2. Structural Analysis of the Conical Element

The conical element has to carry shear, torsional, bending, and axial loads as determined in Section 10.2. The first failure mode that is analyzed for that part is yielding under combined loading. It is considered to fail when plastic deformation occurs. For that, the maximum von Mises equivalent stress [64] is computed at each point of the span for the given loading conditions. The criterion that needs to be satisfied states that the equivalent stress has to be lower than the yield strength, σ_{yield} , of the material used, as can be seen in (10.3), where τ is the shear stress and σ is the normal stress.

$$\sigma_{yield} \geq \sqrt{3\tau^2 + \sigma^2} \quad (10.3)$$

Shear flow, q , and normal stresses are obtained using (10.4) and (10.5) for a symmetric cross section [64]. The maximum value for each is found for the cross section at a given spanwise position.

$$q = -\frac{V_z}{I_{xx}} \int_0^s t z ds - \frac{V_x}{I_{zz}} \int_0^s t x ds + q_{s0} \quad (10.4)$$

$$\sigma_y = \frac{M_x I_{zz} z + M_z I_{xx} x}{I_{xx} I_{zz}} \quad (10.5)$$

Here, V_x and V_z are shear force acting on the wingbox, and M_x and M_z are the bending moments. I_{zz} and I_{xx} are the moments of inertia of the cross section, and t is its thickness.

Additionally, shear flow due to torsion and normal stress due to axial loads, which are constant throughout the cross section, are found using (10.6) and (10.7) [64], where A_m is the enclosed area and A is the cross-sectional area at a given spanwise position. All of the computed stresses are then superimposed to find the maximum magnitude of stresses acting on the cross section at a given spanwise location. With that, an iterative process can be used to find the minimum thickness of the conical section for each location required to sustain experienced loads.

$$q = \frac{T}{2A_m} \quad (10.6) \quad \sigma = \frac{N}{A} \quad (10.7)$$

Another failure mode that is considered for the conical element is the buckling under combined loading - bending and torsion. In order to analyze this structure, it is divided into shorter parts at the points where ribs are placed along the wingspan. Then, their geometry is approximated as circular cylindrical shells with uniform thickness to allow for the use of empirical formulas for shear buckling of isotropic thin-walled cylinders [65]. At taken intervals, the change in the diameter is considered small enough that the analysis remains valid. To ensure that a sufficient safety margin is maintained, critical buckling stress was found at each interval and set as a constraint for the design to meet. Critical stress, σ_{cr} , for cylinders in bending is given by (10.8), where the correlation factor, γ can be computed using (10.9) [65].

$$\frac{\sigma_{cr}}{\eta} = \frac{\gamma E}{\sqrt{3(1-\mu^2)}} \cdot \frac{t}{r} \quad (10.8)$$

$$\gamma = 1.0 - 0.731 \cdot (1 - e^{-\phi}) \quad \text{where} \quad \phi = \frac{1}{16} \sqrt{\frac{r}{t}} \quad (10.9)$$

For buckling due to torsion, relation (10.10) [65] is used to find the critical shear stress. It is dependent on the length of the element, l , which makes longer beams more susceptible to buckling, and radius r .

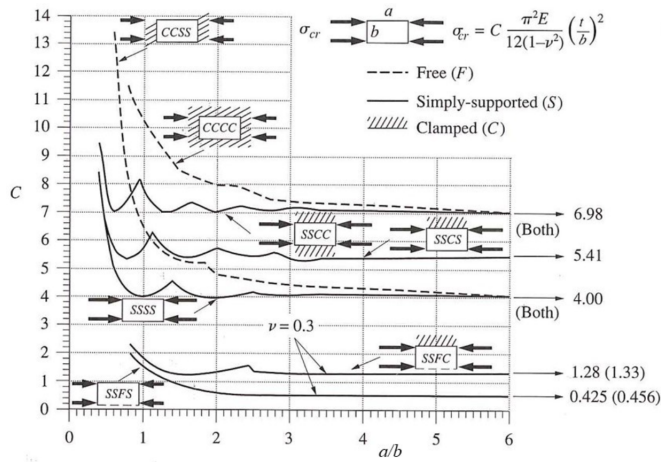
$$\tau_{cr} = \frac{0.747 \gamma^{3/4} E}{\left(\frac{r}{l}\right)^{5/4} \left(\frac{l}{r}\right)^{1/2}} \quad (10.10)$$

Lastly, for cases considering combined loading, the interaction equation is shown in (10.11) [65]. It defines the region in which the structure doesn't fail due to buckling when subjected to stresses caused by different types of loading. The sum of the ratios of experienced normal and shear stresses to their critical values for a given geometry cannot exceed 1.

$$R_b + R_t^2 = \frac{\sigma}{\sigma_{cr}} + \left(\frac{\tau}{\tau_{cr}}\right)^2 = 1 \quad (10.11)$$

10.3.3. Structural Analysis of Stiffened Skin Panels

The skin of the wingbox gives it the shape of the airfoil, which is what allows for the production of lift in cruise. It takes up a big fraction of the weight of the wing and is a load-carrying element. It is assumed that skin carries only axial loads caused by lift. Since the thickness of skin is not very large, it is taken to be 1 mm across the span, it is susceptible to thin plate buckling. Without any reinforcement, its critical stress can be found using (10.12) [66], where the value of buckling coefficient C depends on the aspect ratio of the analyzed plate and its boundary conditions. For this case, the edges are assumed to be simply supported on all sides (SSSS) and a higher aspect ratio is taken to find the asymptotic value of 4.0, as can be seen in Figure 10.8. For the plates with the width b as found for the considered wingbox, the critical stress is well below the expected stress that the plates will have to sustain in regular operating conditions. For that reason, the plates have to be stiffened using stringers. The stringers chosen for this design are 25x25x3 mm L-stringers. Their crippling stress can be computed using (10.13) and (10.14) [64]. The buckling coefficient C can once again be found using Figure 10.8, where for both elements of an L-stringer, three sides are free and one is simply supported (SSFS), which gives the value of 0.425.



$$\sigma_{cr} = C \frac{\pi^2 E}{12(1-\mu^2)} \left(\frac{t}{b}\right)^2 \quad (10.12)$$

$$\sigma_{cc} = \frac{\sum \sigma_{cc}^{(i)} A_i}{\sum A_i} \quad (10.13)$$

$$\frac{\sigma_{cc}^{(i)}}{\sigma_{yield}} = \alpha \left[\frac{C}{\sigma_{yield}} \frac{\pi^2 E}{12(1-\mu^2)} \left(\frac{t}{b}\right)^2 \right]^{1-n} \quad (10.14)$$

Figure 10.8: Buckling coefficient [66]

Then, the effective sheet width can be calculated using (10.15). It is the width of the skin capable of carrying the same stress as the stiffener and depends on the crippling stress of used stringers found in the previous steps. Here, the buckling coefficient depends on the ratio of stringer pitch to thickness of the plate. For the values of b/t over 110, it takes on the value of 6.98. With the effective sheet width $2w_e$ and stiffener pitch b' known, the new width of the skin not supported by the stiffeners can be found as $b' - 2w_e$ and the buckling stress of the panel, $(\sigma_{cc})_{panel}$, can be calculated using (10.16).

$$2w_e = t \sqrt{\frac{C\pi^2}{12(1-\mu^2)}} \sqrt{\frac{E}{(\sigma_{cc})_{stiffener}}} \quad (10.15)$$

$$(\sigma_{cc})_{panel} = \frac{\sum \sigma_{cc}^{(i)} A_i}{\sum A_i} \quad (10.16)$$

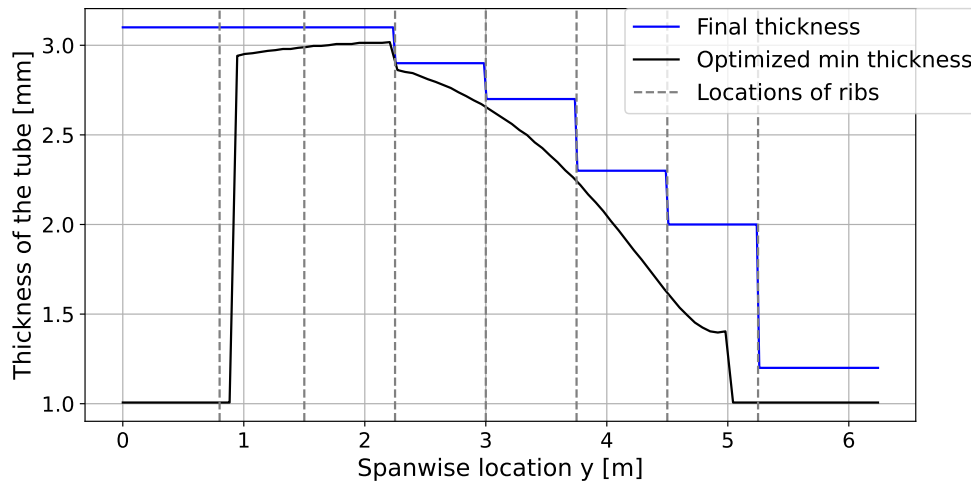
10.3.4. Final Wingbox Design

Once all the constraints are set, the design can be optimized to minimize the weight. The variables that have to be optimized are the thickness of the conical element and the number of stringers at each interval. The final design parameters can be found in Table 10.6. The decided thickness distribution compared to the ideal thickness distribution of the conical element is visualized in Figure 10.9.

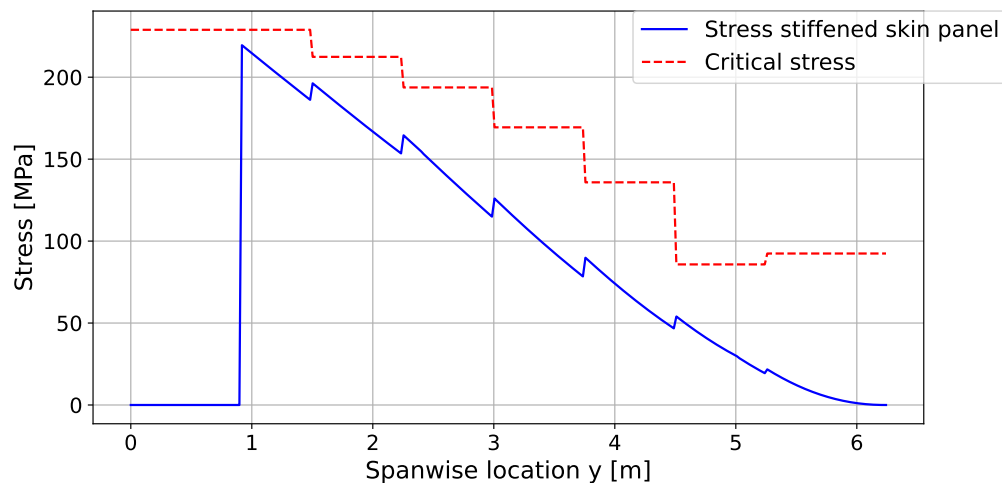
Table 10.6: Final wingbox geometry along the half span

Distance from root [m]	0–1.5	1.5–2.25	2.25–3.0	3.0–3.75	3.75–4.5	4.5–5.25	5.25–6.24
Cone thickness [mm]	3.1	3.1	2.9	2.7	2.3	2.0	1.2
Number of stringers	12	10	8	6	4	2	2

Skin thickness = 1 mm, Taper ratio = 0.5, Max diameter at root = 0.27 m, Cone mass \approx 65 kg

**Figure 10.9:** Cone thickness at each interval compared to optimal thickness distribution for all the load cases

The stiffened skin panels can also withstand expected loads for the geometry described in Table 10.6, as can be seen in Figure 10.10. The critical stress was taken as the lowest calculated stress for each interval, which occurs at the widest part of the panel where the stiffener pitch is the largest, and set as a constraint for the entire length of the panel.

**Figure 10.10:** Critical buckling stress for stiffened skin panels along the half span

10.3.5. Sensitivity Analysis on the Wingbox Design

The current wingbox design is based on the thrust loads defined by the powertrain department and the aerodynamic loads defined by the aerodynamics department. At this phase of the design process, it is still highly

iterative, and these load characteristics could change. Therefore, it is valuable to understand how a change in the loads would affect the wingbox design and consequently the weight increase. This is visualized by Figure 10.11, which shows the change in optimized wingbox weight to a change in loads. For this analysis, all the loads are multiplied by the scaling factor.

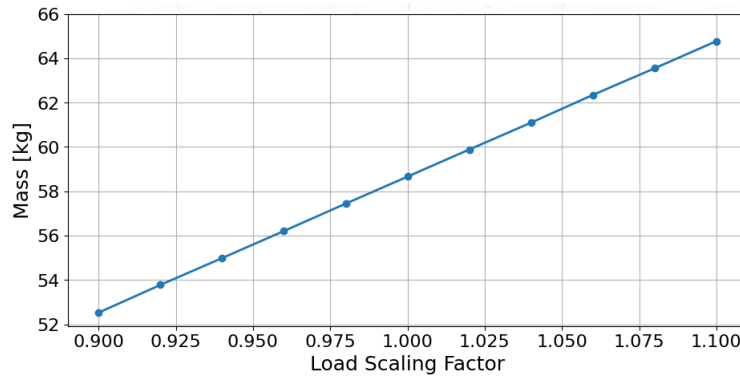


Figure 10.11: Sensitivity analysis on the change in wingbox weight with a change in wing loading.

This analysis shows that the optimized wingbox weight changes proportionally with the change in combined loading. It should be noted that this is the optimized wingbox weight, which is not checked for buckling. Therefore, in reality, the weight is expected to decrease less for a load decrease than is shown in the figure. The linear relationship shown in the figure makes sense, as it is derived from a simplified model by not considering buckling, and in addition, the material has isotropic properties. However, it still gives a valuable insight into the effect of the changing wingbox weight on the total MTOW, which is very small. The total MTOW is 2470 kg, and a change in the MTOW if the loads on the wing increase or decrease by 10% equals $\pm 0.25\%$.

10.4. Hinge Design

Due to the required rotation of the wing, a hinge needed to be designed. The process for this design is presented in this section. In order to design the hinge, the torque requirement will be calculated in Subsection 10.4.1. Next, a choice for the hinge mechanism will be explained in Subsection 10.4.2, and lastly, the motor requirements to drive the hinge mechanism will be explained in Subsection 10.4.3, as well as a final motor selection.

10.4.1. Torque Requirement

The first consideration for the hinge is the torque it needs to sustain during rotation. This includes: propulsive, aerodynamic, and gravitational torque, which will be superimposed to design for the maximum case. Inertial torque is neglected as the wingbox is assumed to be rotating at a constant velocity. The propulsive torque is found to be 21 kNm (Chapter 9). Aerodynamic torque is calculated using Equation 10.17.

$$T_{\text{aero}} = c_m \frac{1}{2} \rho V^2 S c \quad (10.17)$$

Where $c_m = -0.491$, $\rho = 1.225 \text{ kg/m}^3$, $S = 11.3 \text{ m}^2$, and $c = 1.4 \text{ m}$. V was considered to be the relative speed between the largest transition speed the aircraft will be flying at, 35 m/s, and the rotational speed of the wingbox. The rotational was found to be negligible compared to the transition speed, and therefore, 35 m/s is used. These result in an aerodynamic torque equal to 5.8 kNm in magnitude. The next consideration is the gravitational torque, which can be calculated using Equation 10.18.

$$T_{\text{gravitational}} = W_{\text{wing}} + r_{\text{arm}} \quad (10.18)$$

The mass of the wing is taken as 190 kg, and $r_{\text{arm}} = |c_{\text{hinge}} - c_{\text{cg}}|$. Where c_{hinge} is the location of the center of the hinge along the root chord, which is 0.4326 m from the leading edge of the wing. c_{cg} as mentioned in Chapter 7 is at 0.584 m from the leading edge of the wing. This leads to a r_{arm} of 0.15 m, which leads to a gravitational torque value of 0.28 kNm. An overview of all the torque contributions for the hinge design is presented in Table 10.7.

Table 10.7: Torque considerations for the hinge

Component	Torque [kNm]
Propulsion	21.00
Aerodynamic	5.80
Gravitational	0.28
Total	27.1 \approx 30

10.4.2. Hinge Mechanism Design

Due to the circular cross-section of the wingbox, a gear mechanism was selected. The overlap with the fuselage is 1.8 m, which provides ample space for multiple gears, which decreases the forces forced on the point of contact between the gear and the wingbox, making it less likely to fail. Therefore, the hinge is designed for two gears, equally spaced from the symmetry axis of the fuselage, each with a requirement of 15 kNm of torque capacity.

A helical gear attached to the wingbox and a worm to drive the rotation are selected for this purpose. The helical gear will provide higher torsional performance [67], and more teeth will be in contact with the worm, therefore ensuring a smoother transition between engagement and disengagement of the teeth during rotation. A preferable quality since the wing needs to be able to rotate to within a degree of accuracy. The worm will offer more precise control capabilities, as well as the ability to back-lock.

The gear is designed from the wingbox. As found in Section 10.3, the wingbox diameter is 27 cm. For the heavy-duty mechanical transmission that the hinge needs to provide, and aiming for a smaller-sized gear tooth, a module of 6 is chosen [68]. The variables used to size the helical gear are presented in Table 10.8 [68].

Table 10.8: Tooth characteristics

Component	Value	Unit
Module	6	-
Circular Pitch	18.98	mm
Teeth	48	-
Pitch Diameter	290	mm
Tooth height	13.64	mm
Gear height	23.64	mm
Helical angle	20	$^{\circ}$ [69]

The next step is to consider how wide the gear needs to be to be able to sustain the torque requirement. To calculate this, the Lewis Factor Equation is used, which first calculates the tangential load on the teeth with [70] using Equation 10.19.

$$W_t = \sigma \cdot w_{\text{face}} \cdot m \cdot Y \quad (10.19)$$

Where σ is the tensile strength of the material used for the gear, w_{face} is the width of the gear, m is the module, and Y is the Lewis factor, which is dependent on the number of teeth of the gear, and is equivalent to 0.4 for this gear [70]. For the tensile strength, a material needs to be assigned, and steel was found to be the most commonly used for gears, specifically S55C, which is most often used for machine structural purposes [71]. This offers a tensile strength of 650 MPa and a density of 7.85 g/cm³. To increase the surface strength of the teeth, hardening through heat-treatment is advisable, as well as polishing the tooth surface to reduce the friction between them during rotation [71]. From the tangential load, the torsional strength that the tooth can handle can then be calculated. This is done using the following:

$$T_{\text{gear}} = W_t \cdot R_{\text{pitch}} \quad (10.20)$$

Where R_{pitch} is the radial pitch of the gear, which is 145 mm. Working backwards from the torsional strength that the gear is supposed to withstand, 15 kNm, a tooth face of 80 mm is found. Furthermore, the hinge is required to provide 135 $^{\circ}$ of rotation, and therefore to save on weight, the gear is trimmed to size, and

then flanges are extruded to provide space to bolt the gear to the wingbox. A representation of the helical gear is presented in Figure 10.12.

From the helical gear, the worm is designed. The diameter of the shaft is found by: $d_{\text{worm}} = w_{\text{face}} - h_{\text{tooth}} \cdot 2 = 52.73 \text{ mm}$. The same tooth profile is used on the worm and threaded with a pitch of 60.29 mm, leading to three threads along the worm, which is also the contact space with the helical gear. The length of the worm is taken as twice this, at 121 mm. The worm shaft extrudes 150 mm on each side, such that attachments on each side can be placed to connect the worm to the top fairing of the wing on top. The worm design is shown in Figure 10.13.

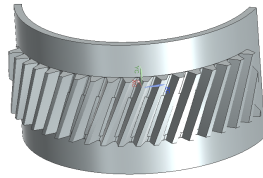


Figure 10.12: *Helical gear on the wingbox*



Figure 10.13: *Worm design*

Once meshed together, and including attachments both from the worm to the wing fairing, as well as bearing connections between the wingbox itself and the wing fairing, the final assembly looks as presented in Figure 10.14.

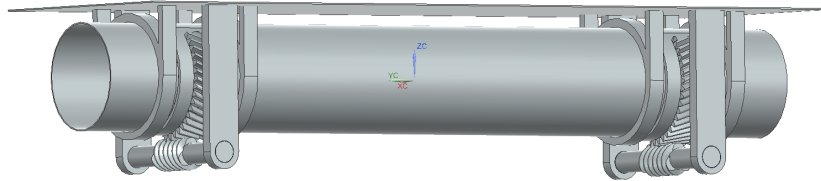


Figure 10.14: *Hinge assembly*

The gears are also designed such that the helical angles are opposite to each other, to achieve a more symmetrical load distribution. Furthermore, for the support of both the wingbox and the worm shafts to the top skin, needle bearings will be used. This is to reduce the friction between the components and reduce wear on the parts. The hinge mechanism will also be shuttered off from the rest of the aircraft, to protect the hinge from outside debris that may interfere with the mechanics of the gears, and a lubrication mechanism could be introduced in the finalized detailed design.

As previously mentioned, the gears are going to be made out of steel, S55C. Measured in the CAD environment, after assigning a material density of 7.85 g/cm^3 , the weight for a singular helical gear is 6.01 kg, and the weight for a singular worm is 8.44 kg, for a total weight of 29 kg.

10.4.3. Motor Requirements

The last consideration for the hinge mechanism is the motor that drives the process. The first step requires the calculation of the gear ratio between the helical gear and the worm, which is calculated using:

$$\text{GR} = \frac{\text{teeth}}{\text{threads}} = \frac{48}{3} = 16 \quad (10.21)$$

From controls (Chapter 9), there is a requirement to be able to rotate the wingbox by 45° in one second. This is 0.79 rad/s for the helical gear and 12.57 rad/s for the worm. The motor will therefore need to provide 120 RPM. Then, the power requirement is calculated using:

$$P_{\text{motor}} = T \cdot \omega_{\text{helical}} = 15 \cdot 0.79 = 11.64 \text{ [kW]} \quad (10.22)$$

Including an efficiency ratio of 0.9, this leads to a power requirement for the motor equal to 12.94 kW. Lastly, the torque requirement is calculated using:

$$T_{\text{motor}} = \frac{P_{\text{motor,req}}}{\omega_{\text{worm}}} = \frac{12.94}{12.57} = 1.03 \text{ [kNm]} \quad (10.23)$$

These three requirements are then used to find an off-the-shelf motor that can be used such that each motor can drive one of the gears. A suitable motor is the SIMOTICS T-1FW6 built-in torque motor with water cooling, manufactured by Siemens [72]. This motor provides a maximum torque of 174 Nm, a maximum speed of 840 RPM, 15 kW of power, a 159 mm diameter, and weighs 19.2 kg. A gearbox of ratio 7:1 is used to reduce the motor and fit the requirements.

The final weight for the whole mechanism, not including the attachments to the wing fairings, including two helical gears, two worms, and two motors, is 67 kg. This value does not include the weight of the gearboxes required for each gear. Further design considerations would be to analyze probable failure modes of the mechanism that would be catastrophic during flight. One of which could be that the motor fails or grinds to a halt unexpectedly, leaving the wing unable to rotate any further. In this case, a manual clutch mechanism could be designed to decouple the failed motor. Furthermore, a sophisticated locking mechanism should be designed such that it is not all reliant on the back-locking mechanism of the worm.

10.5. Landing Gear

Any landing or ground operation of the eVTOL requires some load absorption and stability against tipping over, for which the landing gear has to be designed. The landing gear design consists of several parts: landing gear type selection, placement, and sizing, which will be further discussed in the following subsections.

10.5.1. Landing Gear Type Selection

Firstly, possible options for a landing gear are: wheels, skids, retractable, or non-retractable landing gear. The main pros and cons of each option considered are summarized in Table 10.9.

Table 10.9: Landing gear option evaluation

Landing gear type	Pros	Cons
Skids	Can absorb high loads	Troublesome horizontal landing
Retractable landing gear	Low drag	Additional mechanism required, additional weight and volume, lower reliability
Non-retractable landing gear	Low weight, high reliability	High drag

To evaluate the better option, the function and requirements for this component of the assembly need to be understood. The main functions of the landing gear are: load absorption in landing, ensuring stability and controllability of the vehicle during ground operations, and ensuring horizontal landing possibility. Subsequently, the requirements are: minimized drag in horizontal flight, minimized weight increase, and high reliability. Due to the wing being close to the ground in the horizontal flight condition, it has been decided that the eVTOL will use its capability of landing in horizontal mode only if the hinge gets stuck. This, however, implies a potential sacrifice of lower propellers due to the potential impact on the ground. For selecting type optimum choice two main factors are possibility of horizontal landing and available space needed for the landing gear below the floor as the battery is located there. The retractable landing gear is the one occupying the most space below the floor and, based on the CAD model, does not fit, this leads to exclusion of this type of landing gear. Also, the skids will be discarded due to troublesome landing possibility. This means the landing gear will be non-retractable. The drag coefficient increase ΔC_{DS} can be assumed to be around 0.5 [73]. However, the reference area for a landing gear is the frontal area of the tire. As will be explained in the next subsections, the diameter of the wheel is 27cm, and the width is 20 cm. Therefore, the drag and reference area for 3 landing gears is 0.081 m^2 . This is equal to 13% of the wing drag.

10.5.2. Landing Gear Placement

To successfully place the landing gear, the first step is its configuration selection. It was decided to use a nose wheel configuration.

During landing gear placement, several things are considered: the distance from the cg, the required length of the landing gear, and lateral spacing. In terms of longitudinal placement, consideration of whether landing gears further from the center of gravity are preferable. For the nose gear, increased distance to the cg is beneficial to reduce the forces experienced, yet is disadvantageous in reduction of controllability during horizontal landing. As explained before, it has been decided to land on a runway only during emergency cases; therefore, the controllability in such cases is deemed to be a less relevant problem. Next to that, due to the tilted nose of the fuselage, the nose landing gear closer to the front would result in lower ground clearance, which in turn causes the doors to be located closer to the ground, which makes the operations easier.

Similarly, for rear landing gear, further distance to the center of gravity is preferable as the load reduction and lowered ground clearance are preferable over problems like tail strike, which are not imposed on the aircraft due to the design choice of not performing horizontal take-offs. The limiting factor, however, is the door location, as it is not preferable to locate the landing gear next to the door. Additionally, the lateral placement of the rear landing gears has to be considered. Since non-retractable landing gear is chosen, the fuselage storage room is not limiting for the length of the landing gear struts, and therefore, more laterally spaced out landing gears are beneficial to avoid turnover angle issues. The downside, however, is the weight, drag, and structural complexity of such a choice. Considering these factors, the optimum landing gear placement is determined as seen in Equation 10.24.

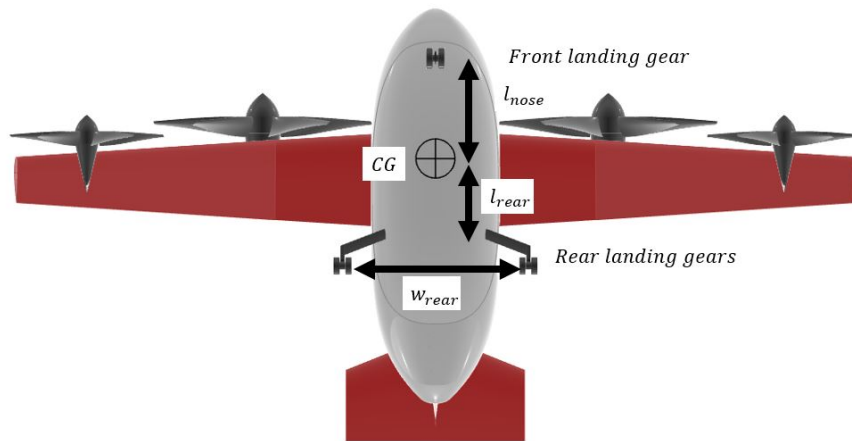


Figure 10.15: eVTOL ambulance seen from below, indicating landing gear and centre of gravity

In this configuration, the force on the gears can be calculated as shown in Equation 10.24.

$$\begin{cases} l_{nose} \cdot F_{nose} - 2 \cdot l_{rear} \cdot F_{rear} = 0 \\ F_{nose} + 2 \cdot F_{rear} = MTOW \end{cases} \quad (10.24)$$

In Equation 10.24 l_{nose} is the longitudinal distance between the cg and the nose landing gear, l_{rear} is the distance between the rear landing gear and cog, F_{nose} , F_{rear} are the exerted force on the nose or rear landing gear respectively. Assuming MTOW of 26 kN and both l_{nose} and l_{rear} being 1.5 m, the resultant forces are $F_{nose} = 17$ kN and $F_{rear} = 8.5$ kN. This does, however, cause to turnover being a potential problem, yet, since the horizontal landing is treated as an emergency case, it has been assumed to be acceptable.

10.5.3. Landing Gear Sizing

Based on the calculations shown before, the nose landing gear experiences much higher loads than the rear landing gear. Therefore, to distribute the load more equally, it has been decided to have 2 wheels at the front and one wheel per strut at the rear. This way, the maximum load a wheel would experience would be 8.5 kN, which would be experienced by one of the front wheels. For simplicity, it will be assumed that all the wheels are the same and will be sized based on the largest load. Besides the force experienced, it is important to determine the tire pressure to properly size the wheel. Since the aircraft is meant to land in different locations, including wet, boggy grass. As shown in Figure 10.17 [74] the tire maximum pressure is 210-310 kPa; for the selection, 310 kPa will be chosen as vertical landing is likely to be less demanding on the tires than a horizontal one. As shown in the Figure 10.16. For an inflation pressure of 3.1 kg/m³ (310 kPa) and a static load of 850 kg (8.5 kN), a reasonable fit is 7.00-5 tire.

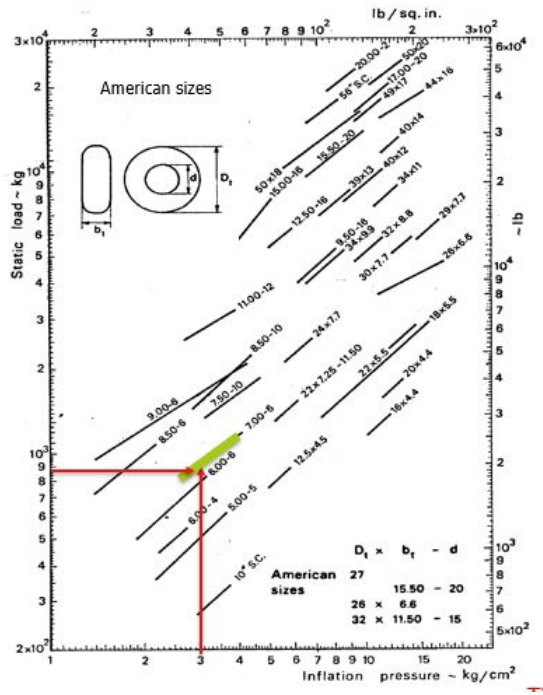


Figure 10.16: Landing gear sizing [75]

Description of Surface	Maximum Allowable p (kPa)	Tire Pressure p (psi)
Soft, loose desert sand	170-240	25-35
Wet, boggy grass	210-310	30-45
Hard desert sand	280-410	40-60
Hard grass	310-410	45-60

Figure 10.17: Landing gear tire pressure indication [74]

This means the minimum tire outer diameter is 18 cm (7 inches), and the width is 13 cm (5 inches). However, these seem to be low; thus, a safety factor of 1.5 will be applied, resulting in a finalized tire diameter of 27 cm and a width of 20 cm.

10.5.4. Additional notes

Besides sizing for regular vertical landings, the eVTOL shall be able to land on a slope of up to 14° as shown in the MIS-SERV-03 requirement, which requires a braking force as shown in Figure 10.18. This case assumed static equilibrium with the propellers not exerting any force upwards. As explained before, the wing is able to rotate up to 135° and it is then possible to reach the wing tilt angle such that the propellers and their produced thrust is pointing directly upwards and thus would produce sufficient thrust for takeoff and landing. Therefore, no thrust produced is the limiting case.

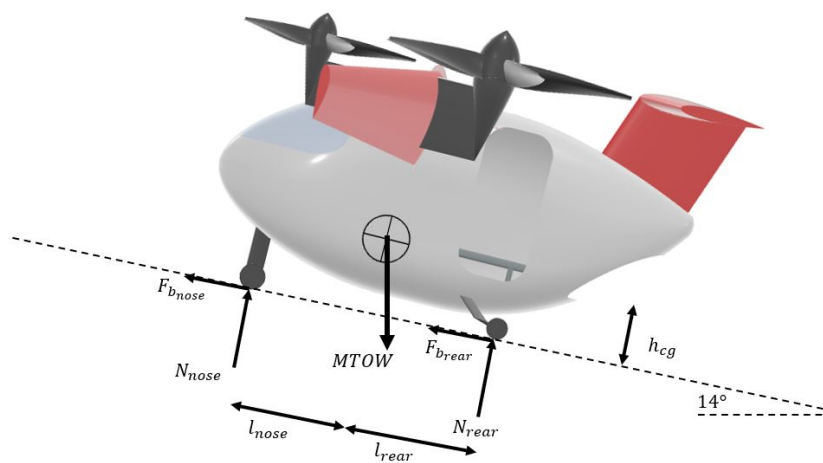


Figure 10.18: Free Body Diagram of an eVTOL landing on 14° slope

In Figure 10.18 $F_{b_{nose}}$ and $F_{b_{rear}}$ represent the required breaking force, N_{nose} and N_{rear} represent the normal force experienced by tires, h_{cg} represent the CG height. From the diagram shown in Figure 10.18, and ensuring moment and force equilibrium, the required breaking force can be calculated. However, this is an indeterminate system, which would require further information not available at this stage. Takeoff and landing possibilities on such slopes are determined by the performance of the propulsive and control systems, which were proven to be sufficient in Chapter 9.

10.6. Crash Structure

One of potential emergency loads of the aircraft is a vertical impact after falling after a potential thrust loss in vertical flight. For such cases a crash structure shall be made which would comply with following requirements: SYS-STRU-11, SYS-STRU-12, SYS-STRU-13, SYS-STRU-14. The crash structure would serve 2 purposes: saving people from a direct impact and protecting the batteries from causing a chain reaction that could result in fire or explosion due to battery location below the floor. Additionally, as stated in SYS-PROP-10, any fire from escaping the battery storage system. This likely results in 2 crash structures- one for cabin, designed to absorb loads of the vertical impact, and another one for the batteries, designed to contain batteries and prevent load path going to batteries, which should also be fire retardant. Further design of these structures would be one of the most important next steps as the space below the floor is limited and therefore might affect the rest of the design.

11

Final Design

After the aforementioned design steps have been taken, an overview of the configuration is presented in this chapter. This encompasses the results of the detailed design phase, where every component comes together. Firstly, an overview accompanied by visualizations and engineering drawings will be presented in Section 11.1. Afterwards, the mass and power budget can be seen in Section 11.2. A performance analysis of the final design will be carried out in Section 11.3. Finally, a computational fluid dynamics simulation will be presented in Subsection 11.4.1.

11.1. Final Design Overview

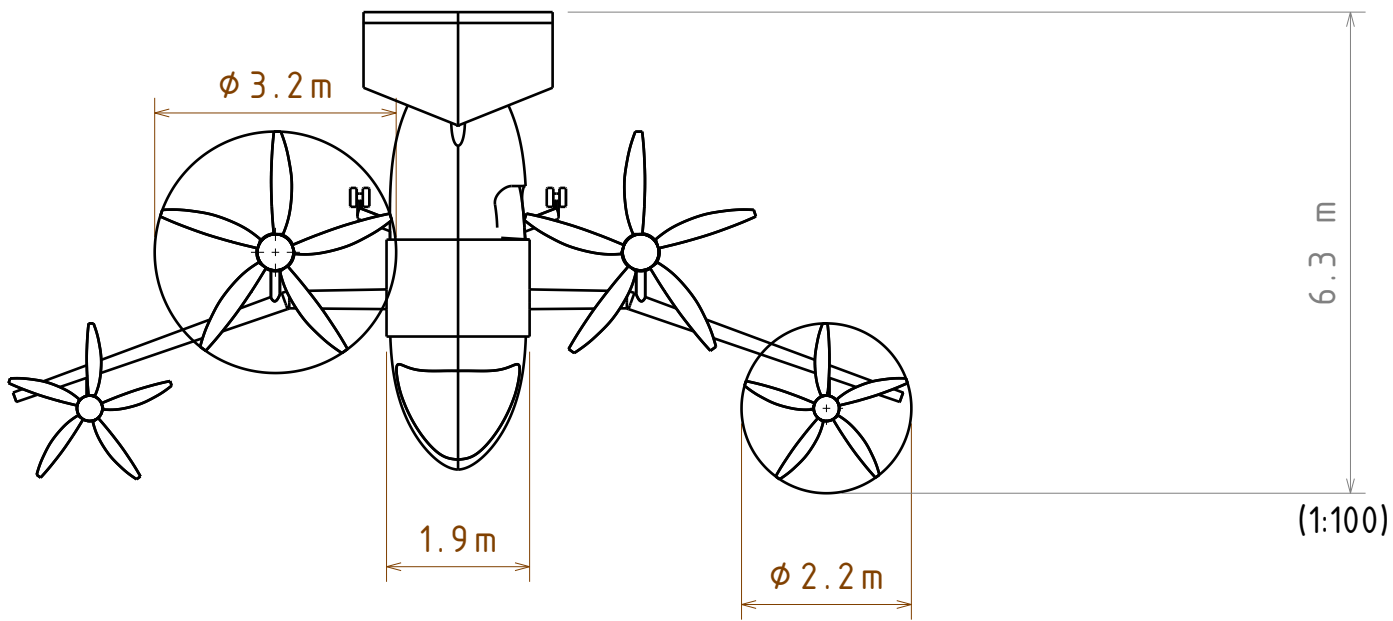
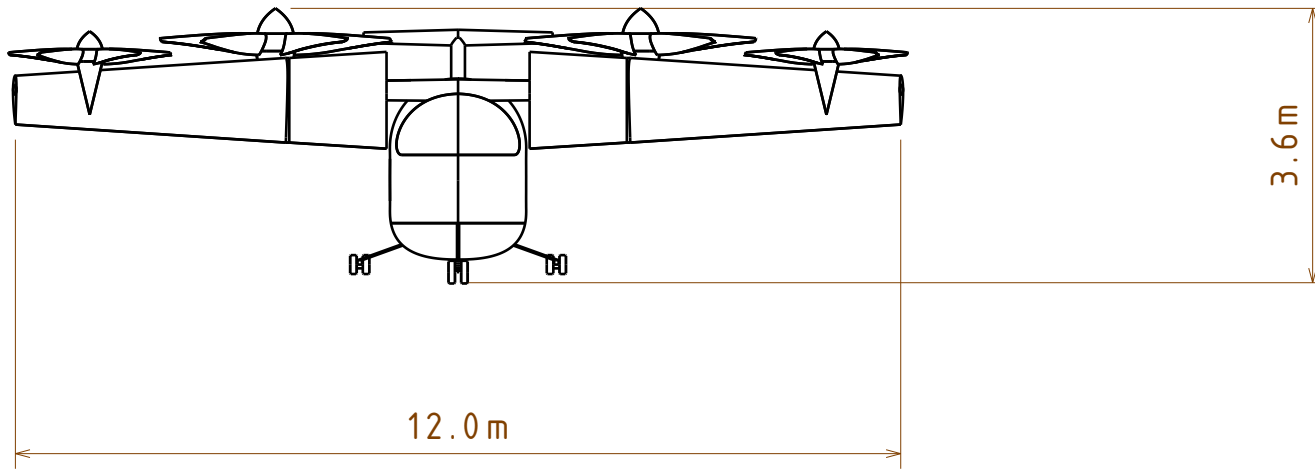
A 3D render of the vehicle can be seen in Figure 11.1. Here, the cruise configuration is shown in an isometric view. Additionally, the main design decision and takeaways are mentioned here. The chosen configuration is a tiltwing, which increases power efficiency and usage by minimizing the propeller blockage by the wing when compared to lift and cruise or tiltrotor designs. This makes the design more sustainable and environmentally friendly; however, it adds complexity and reduces stability and controllability. The powertrain was designed to sustain increased power surges and instabilities, also aiding in control. and this was done by choosing an adequate power point and discharge rate for the engines and energy storage. The main lifting surface presents a kink where an anhedral angle is applied, providing control and stability during takeoff. The fuselage features two doors for the patient and operators, and accommodates all necessary equipment for the mission at hand. Engineering drawings of the final design can be seen in Section 11.2 and Section 11.2.

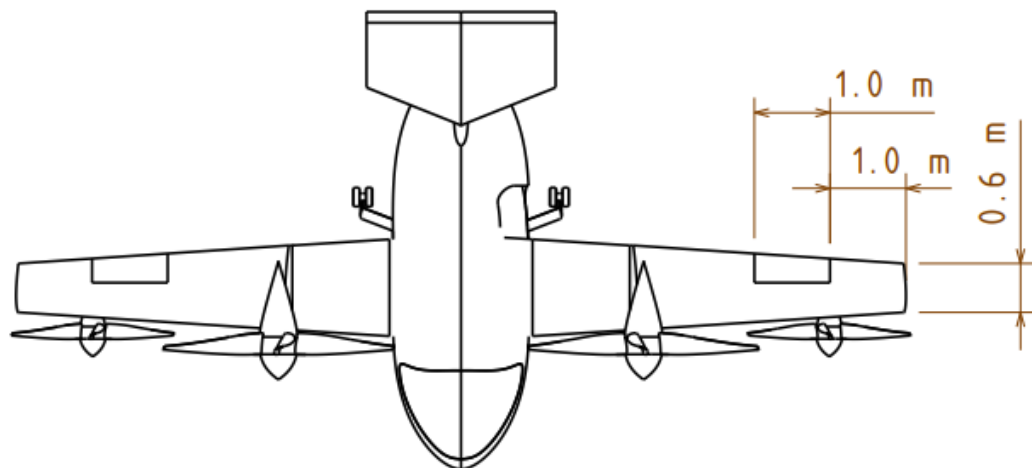
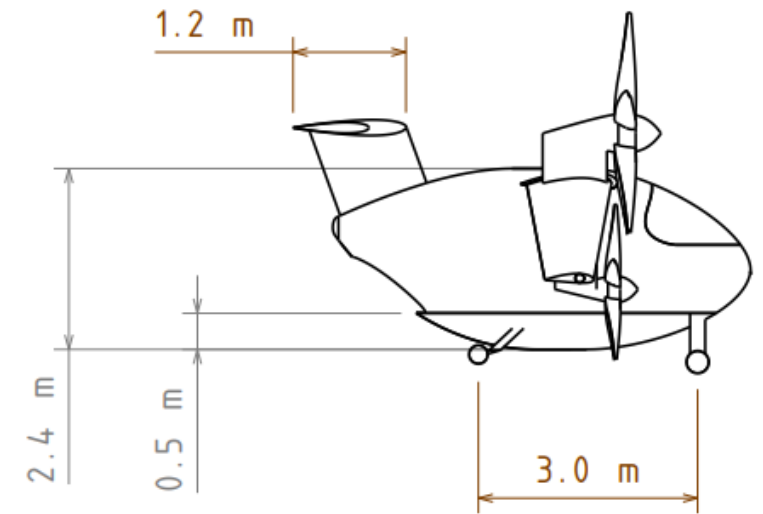
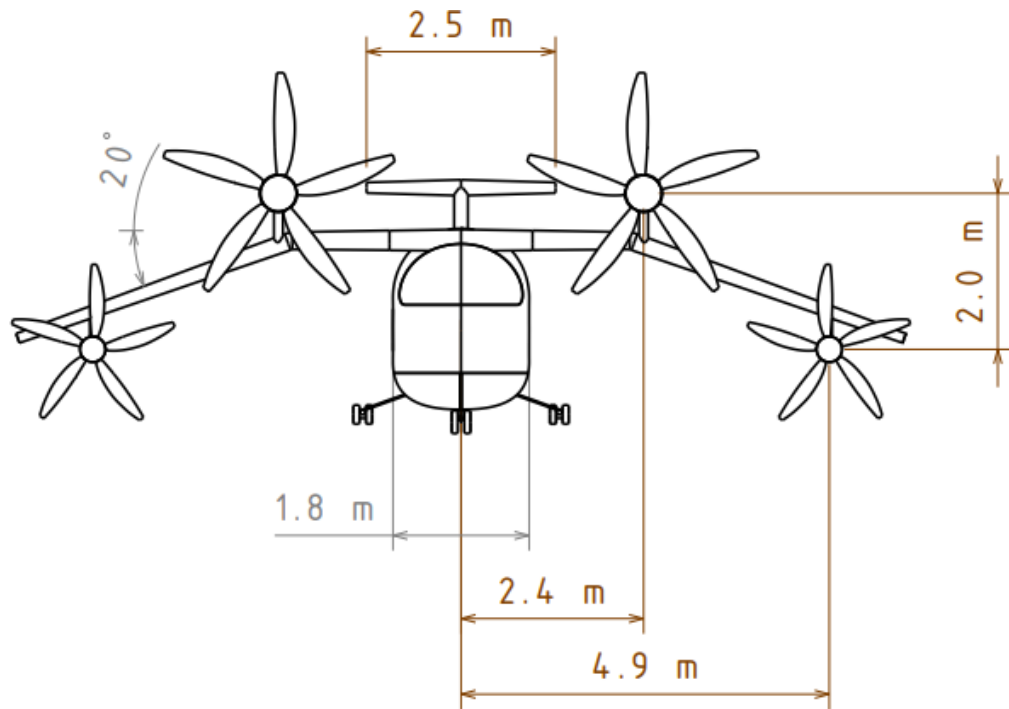


Figure 11.1: *Isometric Rendered View*

11.2. Mass and Power Breakdown

Table 11.1 summarizes the mass and power values of individual components. The purpose is to verify that the designed aircraft will be able to take off, which happens when the total takeoff weight (2472 kg) is less than the designed takeoff weight (2600 kg). As can be seen, the aircraft is over-designed and can achieve better performance at a higher monetary cost. Another iteration of the design can be done to optimize the takeoff weight based on the mass breakdown. However, the design is feasible and acceptable for a proof-of-concept prototype.





(1:100)

Table 11.1: Component breakdown of aircraft mass and power consumption

Component	Mass (kg)	% of Total Weight	HV Power (kW)	LV Power (W)	Remark
Fuselage	525	21			
Fuselage skin	140				2mm Alu
Fuselage frame	150				
Fuselage side door	24				4mm alu+50% additional
Fuselage back door	21				4mm alu+50% additional
Fuselage windshield	30				5mm glass
Fuselage floor	60				4mm alu+20% additional
Landing Gear	100				
Wing & Tail	335	14			
Wing skin	87				1mm alu
Wing box	100				
Wing hinge structure	40				
Wing hinge actuator	48		30		
Wing control surfaces	6				
Wing control surface actuators	2			520	
Engine mounting struts	10				All four struts
Tail skin	13				
Tail structure	15				
Tail control surfaces	3				
Tail actuators	12			1150	
Propulsion & Power	1048	42			
Variable pitch propellers	100				
Motors	170		550		
Cables	45				Copper cable
Converters and inverters	21				
Battery management system	12			50	
HV battery (with casing)	630				
LV battery	20				
Thermal System	50		13		
Cabin and Furnishing	85	3			
Cockpit instruments	20			300	
Seats	36				3x GT3 Seats (997) in carbon fiber
Fuselage furnishing	29			100	From PZL M15 Belphegor
Avionics & Sensors	23	1			
IMU	1			11	
GPS/GNSS Receiver	2			29	
Flight Computer	2			48	
Navigation lights	0.3			12	
Communication system	0.6			10	
Pitot-static system	4				
Air data computers	2			14	For digitalization of pitot-static data
External cameras	0.2			10	
Forward/altitude radar	0.6			30	
Wing position encoder	0.3			2	
Magnetic heading sensor	1			9	
Wiring	10				
Payload	456	18			
Passengers	360				4 passengers
Medical Instruments	96			0	Internal battery
Takeoff Weight with Payload	2472	100	597	2295	
Iteratively estimated MTOW	2600				

11.3. Performance Analysis

In order to quantify the market competitiveness and robustness of the design, overall flight performance parameters are evaluated. These come in the form of a V-n diagram and computing several performance metrics, namely the maximum velocity, climb performance, and maximum range.

11.3.1. V-n Diagram

The flight envelope is a useful tool to determine where the limits are for the aircraft, both structurally and in terms of controllability. In order to create the velocity and load diagram, multiple velocity parameters need to be calculated.

The load factors n_{\max} and n_{\min} are selected to be within the values for conventional aircraft [76], as the VTOL will not be subject to harsh maneuvers requiring larger load factors. $C_{L_{\max}}$ is taken from data which combines both the wing and the tail of the aircraft, more of which is described in Chapter 7.

From the parameters discussed in previous chapters, the stall speed, V_S , of the aircraft can then be calculated using standard atmospheric conditions at the flight altitude of 300 m. Stall speed is calculated when the load factor $n=1$, therefore the lift produced is equal to the weight, which is taken as the maximum takeoff weight. The stall speed is found as follows:

$$V_S = \sqrt{\frac{2 \cdot W}{\rho C_{L_{\max}} S}} = 44.23 \text{ [m/s]} \quad (11.1)$$

The maneuvering speed, V_A , is the maximum speed at which the aircraft can still control the aircraft fully while experiencing the full load factor. This can be calculated from the stall speed and the maximum load factor. This is found to be as follows:

$$V_A = V_S \cdot \sqrt{n_{\max}} = 44.23 \cdot \sqrt{2.5} = 69.94 \text{ [m/s]} \quad (11.2)$$

Next, the dive speed, V_D , is required. Beyond this speed, any aerodynamic load or gust may cause structural failure. Therefore, it is an essential parameter to calculate, and it is computed using an empirical formula acquired from EASA [77]. The design dive speed is a direct relationship with the cruise speed, as follows:

$$V_D = 1.4 \cdot V_C = 1.4 \cdot 56 = 77.78 \text{ [m/s]} \quad (11.3)$$

Lastly, the negative stall speed is also calculated. This is the minimum speed at which the aircraft stalls under the minimum load factor. The relationship with stall speed is given as:

$$V_{\text{neg}} = V_S \sqrt{|n_{\min}|} = 44.23 \cdot \sqrt{|-1|} = 44.23 \text{ [m/s]} \quad (11.4)$$

Combining the stall speed, maneuvering speed, cruise speed, and dive speed, along with the maximum and minimum load factors, leads to the creation of the flight envelope. This is presented in Figure 11.2

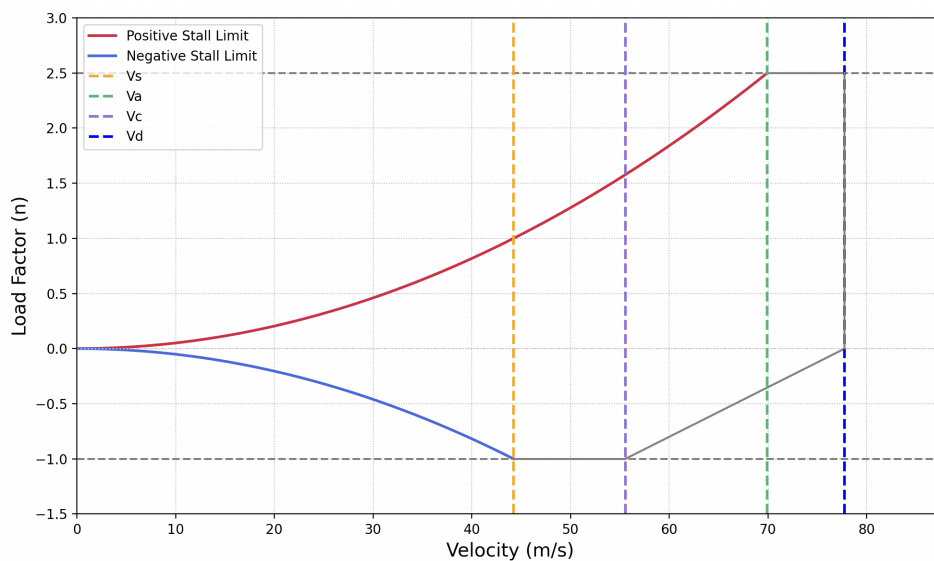


Figure 11.2: V-n diagram

From Figure 11.2, and the values computed previously, it can be seen that the maneuvering speed is higher than the cruise speed. This is to be expected as the cruise speed is relatively slow compared to the cruising speeds of conventional aircraft. However, this also means that the aircraft can have the full range of controllability at the designed cruise speed, which is advantageous to the design.

11.3.2. Flight Performance Metrics

In order to check that requirements are met and to remain market competitive, the performance metrics are quantified in this section. The most important parameters that will be considered are the velocity, climb performance, and range, which are discussed below. It is to be noted that the results found here differ significantly from the V-n diagram presented below. This is due to the fact that the formulas used are empirical and do not apply perfectly to eVTOLs because of their novelty as vehicles. A more in-depth analysis that considers both results is recommended in future iterations of the design.

Maximum Velocity

The maximum velocity the eVTOL can achieve is an essential metric due to the urgent nature of the mission. An overview of the velocity envelope can be seen in Figure 11.3.

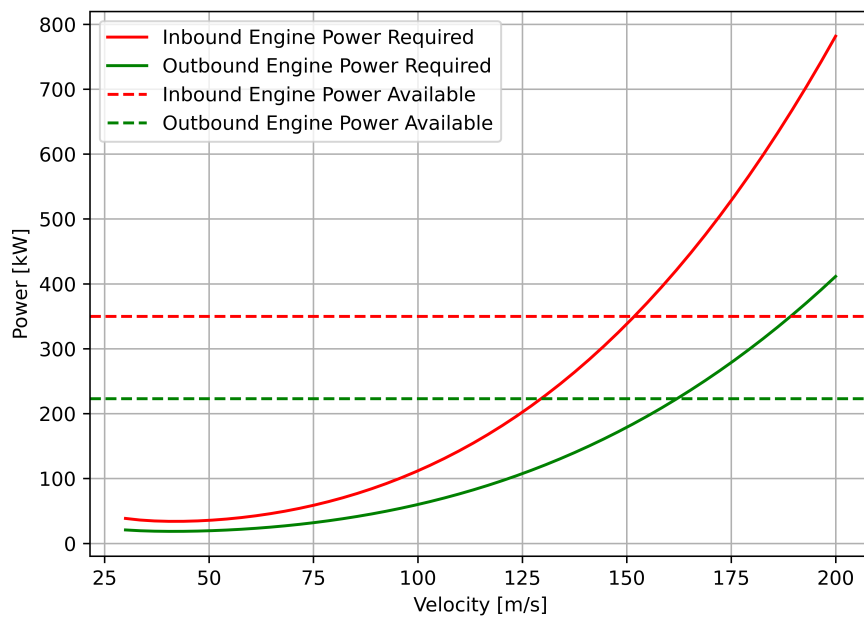


Figure 11.3: Velocity Power Diagram

From the figure, the maximum velocity is $\approx 150\text{m/s}$. This could be increased further by using the extra power available to the inbound engines after the outbound ones are set at full throttle. A tradeoff between used energy and time to reach the patient is thus possible due to having a margin significantly larger than the cruise speed. Furthermore, missions which require less range but are more time-critical can be performed significantly faster

Maximum Rate of Climb and Climb Gradient

The climb performance of the vehicle becomes very relevant in missions that require taking off and climbing in non-ideal terrains and regions. Since cruising is much more energy efficient than vertical flight, a high climb performance can improve the performance of the vehicle in many scenarios, especially in mountainous regions around Bavaria. The formulas and results for the maximum rate of climb and climb gradient are shown below:

$$\text{RoC} = \frac{P_a - P_r}{W} = v_{\infty} \sin(\theta) = 30.5 \frac{\text{m}}{\text{s}} \quad (11.5)$$

$$\text{Gradient} = \frac{T - D}{W} \cdot 100\% = \tan(\theta) = 55\% \quad (11.6)$$

Where θ is the climb angle. The climbing performance of the vehicle is very high, which is expected. Due to having powerful engines designed to perform in vertical flight conditions, a lot of available power is not used during cruise.

Maximum Range

Finally, finding the maximum range the vehicle can reach is essential in order to plan emergency missions around it. The absolute maximum was found by considering a single take-off and landing and finding the maximum range at an interval of cruise velocities, results of which can be seen below, in Figure 11.4:

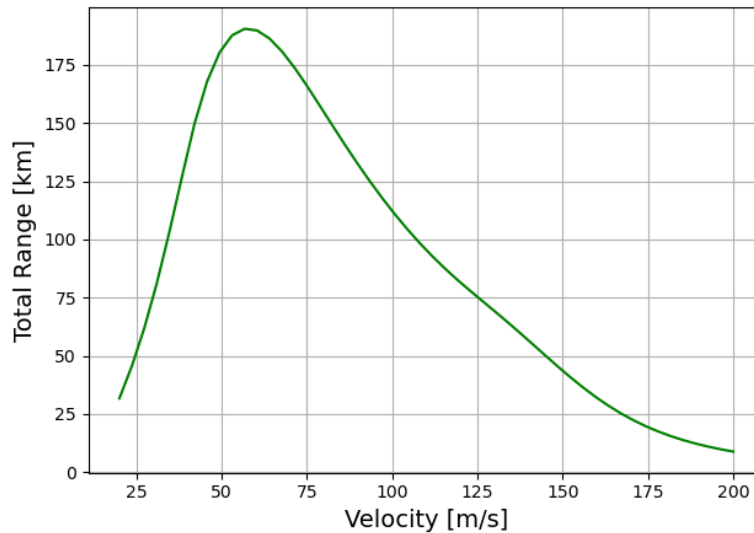


Figure 11.4: Range Diagram

As can be seen, the nominal cruise speed is very close to the optimum due to the vehicle being heavily optimized for this value, which proves the techniques used in this process yield a desirable result. In the case of a single takeoff and landing, the maximum range is $\approx 185\text{ km}$. This metric can be very useful when dispatching the emergency vehicle to an off-design location or when other vehicles are not available. Having a backup plan for off-design missions is essential for emergency missions by making more missions possible and, in turn, getting to the patient more quickly.

11.4. Computational Fluid Dynamics

11.4.1. Simulation setup

A whole aircraft CFD simulation was carried out at the end of the project to analyze the performance of the aircraft and to verify the simplified calculation process in the previous chapters. The CFD software used for this project is ANSYS Fluent [78] and is carried out on the DelftBlue supercomputer[79]. The simulation contains 4 million polyhedral cells, 5 cell zones, and the SST k-omega turbulence model was used. A rotational reference frame is applied in the vicinity of the propellers to simulate the rotating propeller, according to the rotational speed of the propeller calculated in the previous chapters. Boundary conditions for inlet, outlet, and side are velocity inlet, pressure outlet, and symmetry, respectively. Four sets of simulations were done with four different angles of attack ($0^\circ, 3^\circ, 6^\circ, 9^\circ$). Each simulation was run until the lift and drag forces stabilized and the target residual was met. It was observed that the higher the angle of attack, the more iterations were needed to stabilize the force calculation. A mesh-independent test was carried out on a simplified mesh of 2 million polyhedral cells, and a force difference of 10% – 15% was found. It was also found that the cruise lift ($L = W \approx 25000\text{ [N]}$) is reached when $AoA = 9^\circ$. However, the drag force obtained from the CFD is higher than expected, as 6000 [N] of drag force is obtained at cruise conditions. Note that the boundary layer is not fully resolved, it can be seen from Figure 11.5b. A maximum y^+ value of 280 is obtained on the surface of the fuselage.

11.4.2. Improvements from CFD

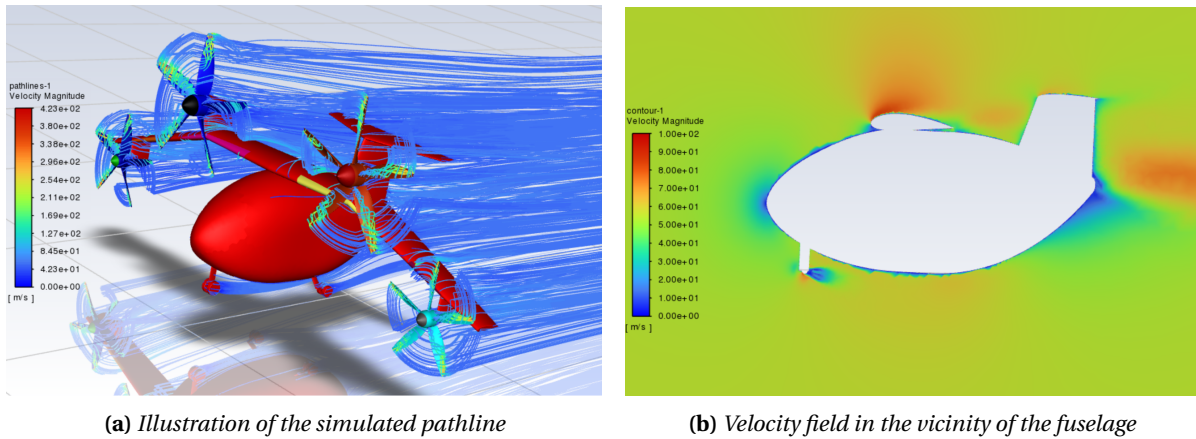


Figure 11.5

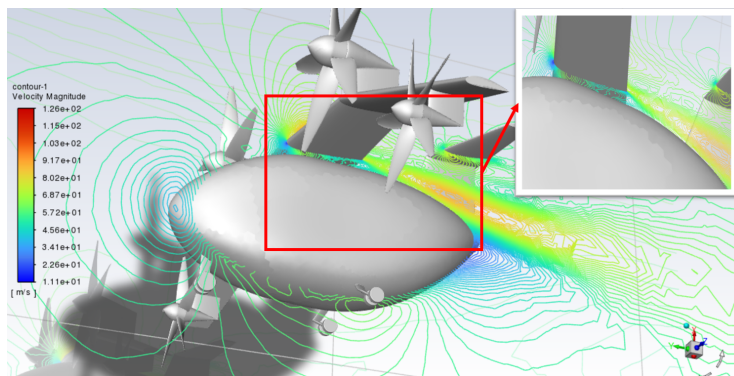


Figure 11.6: Velocity contour of the aircraft

The first observation from the CFD result is that fairings needed to be added to fill the narrow gap between the fuselage and the wing. From Figure 11.6, it can be seen that the gap between the fuselage and the wing generates extra vortices, which will potentially increase drag. Other solutions to this are to lower the wing or change the radius of curvature of the upper part of the fuselage.

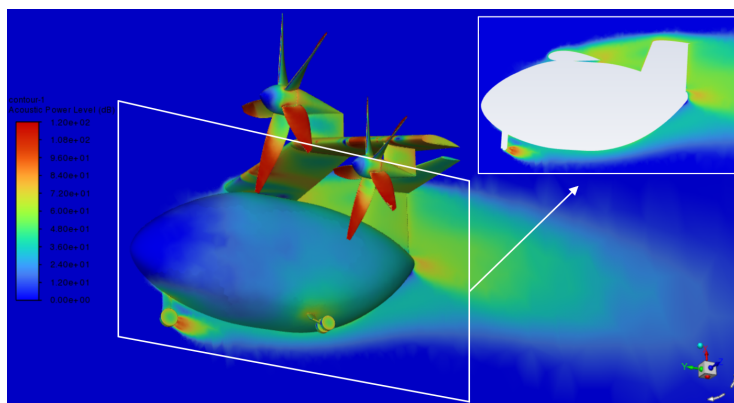


Figure 11.7: Noise emission from Broadband spectrum model of the aircraft

spectrum model is plotted as Figure 11.7. It can be seen that besides of the propeller, the landing gear also has a significant contribution to the noise emission. In future design, a retractable landing gear will be preferred in terms of the noise requirement.

However, the CFD simulation has not been fully verified and optimized, and thus the results used for flight performance analysis and aeroacoustics will be assumed to be indications for the further steps of the design, not verification of the design.

Acoustic performance was also analyzed using CFD. Ffowcs Williams and Hawkins acoustic Model was used. It was found that 300 meters away from the aircraft, the SPL is around 75dB at the side of the aircraft and around 65dB at the bottom of the aircraft. Note that the sound pressure level is just an indication and is underestimated since the time step for the transient simulation is 0.0005 [s], which makes the highest resolvable frequency to be 2000[Hz]. To further analyses the source of the noise, the noise emission pattern using the broadband

Risk Management

In this chapter, two approaches to risk assessment will be presented. First, a reliability, availability, maintainability, and safety (RAMS) assessment will be performed and will be presented in Section 12.1. This is followed by a list of risks for both the subsystems as well as the system as a whole, along with mitigation and contingencies, as will be presented in Table 12.2.

12.1. RAMS

RAMS analysis is a crucial process in systems engineering and project management. It involves examining the long-term operational characteristics of a system and analyzing their effect on the life of the aircraft.

12.1.1. Reliability

Reliability is the measure of how failure-free a system is during a predefined operational time, for which the main representative number is the failure rate (FR), and the other is the mean time between failures (MTBF). For this section, the FR will be analyzed using a top-down method, examining the system failure as a whole. In order to do this, three indices are presented. The technological age index (IA), is based on the years in which the design took place [80]. For the eVTOL described in this report, this amounts to the lower range of values. Next, the complexity index (IC) is considered; this describes the complexity of the aircraft, which for VTOLs is considered very high [80]. Lastly, the role index (IR), which defines the importance of the role of the aircraft, for which the eVTOL falls under the category of civil aircraft. An overview of the index values is given in Table 12.1 [80].

Table 12.1: *Indices used for quantifying reliability*

Index	Value
Age index (IA)	0.6
Complexity index (IC)	1.6
Role index (IR)	1.0

The failure rate of any aircraft is dependent on the maximum empty weight (MEW). Heavier MEW relates to more complexity, larger structural loads, which translates to more potential for failure. This is taken as the estimated MTOW of 2600 kg, excluding the payload, which, as previously mentioned, amounted to 456 kg. The MEW resulted in 2144 kg. The failure rate can therefore be calculated using Equation 12.1.

$$\lambda = \left(\frac{\lambda}{\text{MEW}} \right)_{\text{MCA}} \cdot \text{IR} \cdot \text{IC} \cdot \text{IA} \cdot \text{MEW} \quad (12.1)$$

Where $\left(\frac{\lambda}{\text{MEW}} \right)_{\text{MCA}}$ is equal to 1.8, as found from empirical statistics. Using the values in Table 12.1, the failure rate can therefore be calculated and found to be equal to 3.7, which is found to be an acceptable value.

12.1.2. Maintainability

Maintainability is the measure of the complexity needed for system repairs or maintenance, which is driven by standardization, accessibility, and modularization [81]. An estimation can be made to quantify the maintainability expressed in maintenance man-hours (MMH) per flight hour (FH) [81]. This takes into account two new indices, which are the maintenance role index (IRM) and the design to maintain coefficient (CDTM) [80]. The first is based on the role of the eVTOL, which is assumed to be for civil purposes [80]. The second is based on the level at which maintainability was considered during the design process until now [80]. This

was considered to be at a low to medium level, as maintainability was a factor in the tradeoff process. However, at this stage of the design, it is not given close attention. The values corresponding to these indices are presented in Table 12.2 [80].

Table 12.2: *Indices used for quantifying maintainability*

Index	Value
Maintenance role index (IRM)	1.5
Design to maintain coefficient (CDTM)	1.5

In addition to these two indices, the maintainability depends on IA, IC, and MEW, which are explained in Subsection 12.1.1. The relation between all these parameters is given by Equation 12.2.

$$\frac{\text{MMH}}{\text{FH}} = \frac{1}{6} \cdot \text{IRM} \cdot \text{CDTM} \cdot \text{IC} \cdot \text{IA} \cdot \text{MEW}^{0.25} \quad (12.2)$$

The maintainability is calculated using this equation and is found to be equal to 0.44 maintenance man-hours per flight hour. In the industry, typical values for small VTOL aircraft range between 0.5 and 1 MMH/FH [82]. Comparing the result of the eVTOL ambulance with this result shows it is estimated to require slightly less maintenance than typical small eVTOLs.

12.1.3. Availability

Availability is determined by reliability and maintainability, measuring the duration during which the vehicle is available and not out of service. At this stage of the design, it is decided to quantify the inherent availability. This value indicates the availability considering only the downtime due to maintenance after failure [81]. So, preventive maintenance or delays within logistics or supply are neglected [81]. The inherent availability informs on the system's ability to remain available, based only on its reliability and maintainability characteristics, and is calculated using Equation 12.3 [81]. In this formula, the mean time between failures (MTBF) is the inverse of the failure rate. And the mean time to repair (MTTR) is given by the maintenance hours per flight hour (MMH/FH) divided by the number of mechanics.

$$A_i = \frac{\text{MTBF}}{\text{MTBF} + \text{MTTR}} \quad (12.3)$$

The intrinsic availability is dependent on the number of mechanics as illustrated by Figure 12.1.

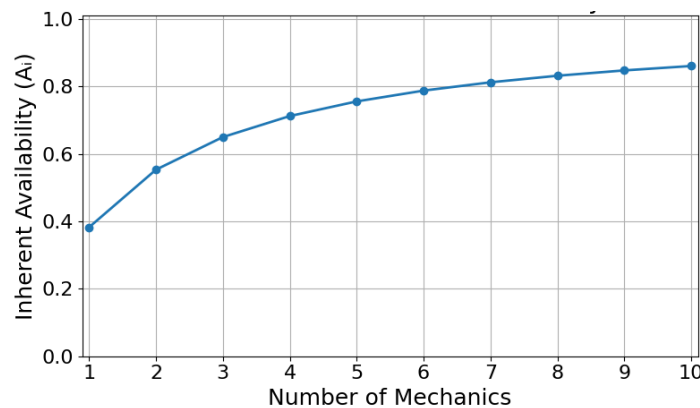


Figure 12.1: *The relation between the intrinsic availability and the number of mechanics*

If only one mechanic is available to perform maintenance, the intrinsic availability equals 0.38, meaning an availability of 38%. With five mechanics, an availability of 76% is reached, and eventually it converges to an availability of 100% with increasing the number of mechanics.

12.1.4. Safety

The safety of the system is a fundamental aspect to consider as it concerns the state to which the risk level of the design is acceptable, and must not be exceeded. One way of quantitatively measuring the safety of a system is through a dependency on the reliability failure rate as previously calculated. Similarly, using a safety role index (RL), which equates to $10e-6$ for civilian-type aircraft, the safety failure rate is calculated using Equation 12.4 [80].

$$\lambda_s = \frac{\lambda}{\text{RL}} = 3.7 \cdot 10^{(-6)} \quad (12.4)$$

A full technical risk assessment for the systems of the VTOL will be presented in Table 12.2. More general risks that may affect the long-term operations of the VTOL are also considered. For this, two cases are considered: in-flight failure and ground failure.

In-flight failure: Engine failure is a large safety concern, where faults in the motors or the propellers cause a loss of thrust and therefore a loss in lift; however, the VTOL is designed for single-engine failure to account for this concern. Secondly, transition failure, due to hinge mechanism failure, is also a large concern, considering that the VTOL is designed for vertical landing and takeoff; however, due to the winged design, this allows for emergency landings on runways. Another safety concern would be loss of communications with airspace officials, which may be due to electrical short circuits, damaged antennas, or bad weather. Similarly, avionics failure is considered, where the aircraft suffers from control and stability issues, and this could become a catastrophic safety concern.

Ground failure: The main concern for ground operations is the vicinity of the aircraft to its environment. The VTOL will be landing on busy streets or slopes with natural elements, and a safety concern is that the environment does not damage the aircraft. Furthermore, there will be a danger of people or other living beings near the wings and propellers of the aircraft, which should be avoided. Ground handling incidents, of moving the eVTOL with tow trucks for maintenance purposes, can also cause damage to the eVTOL. Lastly, landing gear failure is another concern for safety, as there could be catastrophic failure structurally or in the tires upon landing that would cause the whole aircraft to crash into the ground, and considering that the batteries are stored in the underside of the aircraft, this could cause large safety issues.

12.2. Technical Risks

The first step of risk management is to identify the risks. The risks are discovered through brainstorming and by considering possible failures for each of the subsystems, as well as analyzing incidents involving past, similar aircraft. They are divided into operational and developmental risks - so things that can occur during the operational lifetime of the aircraft and those that can pose threats during the design and manufacturing phases. In the next stage, the concept-specific risks regarding the tiltwing design were compiled. Each risk is assigned a unique identifier according to the following convention: RI-XXX-YY, where RI stands for risk, XXX refers to the responsible subsystem or developmental stage, and YY is the number of the risk. The abbreviations used are: PPL (propulsion), CTL (control), STR (structures), AERO (aerodynamics), OPS (operations), DEV (developmental), TW (tiltwing).

After identifying the risks and their impacts, the probability of their occurrence and their effect is evaluated on a numerical scale. For probability, the scale varies from 1 to 5, corresponding to "Rare" and "Very likely", respectively. Similarly, the values for the effect range from 1 to 4 and corresponding to "Negligible" (few consequences), "Marginal" (minor incident), "Critical" (serious incident with significant reduction in safety margins), and "Catastrophic" (destroyed vehicle and possible injury/death). The results of this investigation are compiled on Section 12.2,

Once the risks were identified, mitigation strategies could be set up, actions preventing the risk from occurring, and contingency strategies, ensuring that if the risk does occur, its effect is minimized. The most crucial risks were the ones with a probability and effect above 2. Still, the strategies were provided for each risk, which were then evaluated one more time on the numerical scales and assigned new, post-mitigation values. Additionally, a team member responsible for mitigating each risk was defined and included in the tables. The results can also be found on Section 12.2.

To aid visualization of the threats, risk maps are created. On them, it can be seen that the most dangerous risks are moved out of the "red zone" of high risk by decreasing the probability of their occurrence or the effect they would have on the system and the mission. As a result, all of the risks fall within the moderate and low risk areas, which are deemed acceptable. It can be observed that for some of the risks, their place on the map did not change after the mitigation. This is due to a few reasons. Firstly, some risks are inherent and cannot be mitigated in any meaningful way. Additionally, a 1-5 scale would require a larger change in probability

and effect change than possible through the mitigation and contingency strategies provided. Hence, even though some actions are taken, their effect might not be visible on the coarse classification scale. The maps can be seen in Table 12.3 and Table 12.4, where the risks were shortened using only the first 1 or 2 letters of the middle part of the identifier and their number (e.g. RI-AERO-04 → A4, RI-TW-01 → TW1).

Risk ID	Event	Impacts	Pre-mitigation		Mitigation	Contingency	Post-mitigation		Team member
Propulsion									
RI-PPL-03	Engine or motor experiences overheating during flight	Potential fire hazard	3	2	Use cooling system	Find the nearest landing site to land and turn the engine off to cool it down	1	4	Powertrain engineer
RI-PPL-04	Battery failure	Complete loss of thrust	2	4	Operate within the operating limits and implement frequent maintenance to inspect battery health, have the battery be split into multiple units to ensure redundancy	Switch off the defected battery and make use of the remaining units	1	3	Powertrain engineer
RI-PPL-05	Propeller detachment or blade failure	Loss of thrust, risk of debris penetration	3	4	Operate within operating limits and implement frequent maintenance. Locate propellers such that they cannot hit the pilot.	Shut down damaged propeller and create a differential between the remaining rotors for stability	1	3	Propulsion engineer
RI-PPL-06	Unexpected thrust oscillation or surge	Flight instability and potential structural damage	4	1	Introduce power management system	Allow the autopilot to stabilize the aircraft through controls	2	1	Powertrain engineer
RI-PPL-07	Mounting failure	Motor detachment, loss of thrust, potential structural damage	2	4	Perform vibration analysis and load analysis; operate within operating limits	Shut down affected component to prevent further damage, attempt emergency landing as soon as possible	1	3	Propulsion engineer
RI-PPL-08	Propeller overspeed	Risk of structural damage	3	2	Set V_{ne} , use constant speed propeller	Design for a propeller structure that offers certain overspeed tolerance	2	1	Propulsion engineer
RI-PPL-09	Battery fire	Structural failure and potential casualties due to high temperature	2	4	Fire protection, using flame retardant material	Introduce fire suppression system	1	3	Powertrain engineer
RI-PPL-10	Too low battery temperature	Battery efficiency drops significantly, potential risk of battery failure	2	4	Battery heating system if operates in cold area or avoid to operate in cold area	Abort mission, land as soon as possible if mission starts	1	2	Powertrain engineer
RI-PPL-11	Bus bar corrosion	Bus bar breaks, short circuit	2	4	Cover the bus bar with anti-corrosion material, frequent inspection	Replace corroded bus bar	1	2	Powertrain engineer
RI-PPL-12	Energy management system failure	Runaway control of energy system, motor or avionics overheat	2	4	Switch to back up energy management system	Replace or repair the faulty energy management system	1	1	Powertrain engineer
RI-PPL-13	Pitch variable mechanism fail	Unable to control the propeller pitch	2	3	Frequent and adequate maintenance	Decrease the thrust on the inoperative propeller, shut down the propeller if necessary	1	2	Powertrain engineer
Control									

RI-CTL-01	Power outage	Loss of flight computer and avionics	2	4	Introduce power management system	Switch to backup electricity source, and land as soon as possible	1	3	Powertrain engineer
RI-CTL-02	Control system crash	Loss of flight computer or manual flight control	2	4	Backup flight computer	Turn to manual control	1	2	Avionics engineer
RI-CTL-03	Control cable failure	Runaway control	2	2	Perform frequent maintenance checks	Make sure the remaining control surfaces can keep the aircraft stable	1	1	Control engineer
RI-CTL-05	Instability caused by shifting of C.G.	Loss of control	3	3	Establish the C.G. range where the aircraft remains stable, operate within these limits, have sensors to alarm the pilot before the aircraft becomes unstable	Move the equipment inside the cabin to shift the C.G.	2	2	Control engineer
RI-CTL-06	Controller diverges	Loss of control	1	2	Increase the robustness of the controller	Switch to manual control, fly in horizontal mode if possible	1	3	Control engineer
RI-CTL-07	Control surfaces stucked	Loss of control	1	3	Frequent inspection, adequate maintenance	Use differential thrust or thrust vectoring to counter the effect of stucked control surfaces	1	2	Control engineer
Structure and materials									
RI-STR-03	Failure of mechanical fasteners	Increased loads on remaining fasteners	4	2	Implement safety factors to allow slightly higher loads than expected without failure	Implement a fail-safe design	2	1	Structures engineer
RI-STR-04	Corrosion of integral structural elements	Lower critical loads than expected	3	4	Use anti-corrosion coatings; maintenance checks	Modular design that allows for easy replacement of an affected part	2	2	Materials engineer
RI-STR-05	Material defects	Lower critical loads than expected	3	2	NDT methods, avoid manufacturing methods that can introduce unwanted material defects	Land as soon as possible. Remove affected batches and replace parts from validated batches afterwards.	2	1	Materials engineer
RI-STR-07	Premature failure due to fatigue	Component failure before expected service life	2	4	Frequent inspection, NDT methods. Ensure redundancy in the design.	Land as soon as possible. Remove affected batches and replace parts from validated batches afterwards.	1	2	Structures engineer
RI-STR-08	Hinge fail during transition	Fail to transit between vertical mode and horizontal mode	1	4	Frequent inspection, ensure maintenance is adequate.	Emergency landing.	1	3	Structure engineer
RI-STR-09	Hinge wearing	Helical gear slips during flight, wing rotates unexpectedly	3	4	Frequent inspection, apply lubricant	Emergency landing, replace helical gear, review design	1	3	Structure engineer
Aerodynamics									
RI-AERO-04	Interference between rotors and motors	Reduced overall performance	3	3	Simulation techniques for validating configurations	Reevaluate the design, improve flow method	2	2	CFD engineer

RI-AERO-05	Stall during fixed-wing transition	Risk of uncontrollable descent	2	2	Thorough flight dynamics and performance analysis, cockpit warnings before entering the stall	Take manual control of the aircraft and move out of stall	2	1	Aerodynamics and control engineer
RI-AERO-06	Aircraft climbs to high altitude causing lack of lift	Risk of stalling in horizontal flight	1	3	Set operational ceiling, check terrain enroute before flight	Descent to the safe altitude is possible	1	1	Aerodynamics engineer
Operation									
RI-OPS-01	Patient is too heavy	Inability to take off	2	3	Find alternative mode of transportation or treat on location	Wait for the alternative mode of transport while keeping the patient stabilized	1	2	Mission engineer
RI-OPS-02	Patient is scared of flying	Delayed arrival, potential distraction to crew	4	1	Design for patient safety and comfort	Sedate the patient	2	1	Mission engineer
RI-OPS-03	Patient unfit for air transport	Alternative transport required	3	4	Find alternative mode of transportation or treat on location	Wait for the alternative mode of transport while keeping the patient stabilized	2	3	Mission engineer
RI-OPS-04	Unavailable medical personnel	Mission delay	2	4	Assign multiple medics/ doctors to each VTOL	Deploy replacement doctors/ medics	1	2	Mission engineer
RI-OPS-05	Pilot unavailable	Mission delay	2	4	Assign pilots to each VTOL	Find replacement pilot	1	2	Mission engineer
RI-OPS-06	Excessive wind conditions	Alternative transport required	2	4	Design for different wind conditions.	Find alternative way of transporting the patient	1	4	Mission engineer
RI-OPS-07	Congested airspace before take off	Mission delay	2	3	Delay take off until it can be performed safely	Fly at lower altitudes with authorization	2	2	Mission engineer
RI-OPS-08	Bird strike	Subsystem damage and reduced performance	2	3	Monitor bird activity in the areas along the flight path. Perform validation on bird strike cases.	Implement safety protocols, land if necessary.	2	2	Flight performance engineer
RI-OPS-09	Landing site destroyed by environment (e.g floods)	Diversion required	2	4	Since emergencies can occur anywhere, there is no real way to mitigate this risk	Search for the closest alternate safe spots for landing	2	3	Mission engineer
RI-OPS-10	Landing site at hospital unavailable	Diversion required	3	4	Communicate with the hospital before arrival	Search for other safe spots for landing and keep a list of alternate hospitals in the area	1	2	Mission engineer
RI-OPS-11	Fire onboard	Threat to crew and aircraft	2	3	Maximize fire retardancy in the design, include manual ways to stop the fire onboard.	Deploy onboard fire extinguishing system	1	2	Flight performance engineer
RI-OPS-12	Power grid unavailable	Charging system delay	1	3	Backup charging deposits	Use emergency power system / generator	1	1	Flight performance engineer

RI-OPS-13	Navigation system failure	Increased reliance on pilot skill	1	3	Include alternative ways in the design	Use backup (analog) navigation system	1	2	Flight performance engineer
Tilt wing									
RI-TW-01	Wings getting stuck in take-off configuration	Horizontal flight not possible	1	3	Perform frequent inspection to ensure that the mechanism performs as expected	Attempt vertical landing	1	3	Flight performance engineer
RI-TW-02	Wings getting stuck in cruise configuration	Vertical landing not possible	1	3	Perform frequent inspection to ensure that the mechanism performs as expected	Attempt horizontal landing	1	3	Flight performance engineer
RI-TW-03	Flow separation when the wing is positioned at certain angles of attack	Instability during transition between hover and cruise	2	3	At this stage of the design process it is deemed to early to establish how to mitigate this risk	Adjust the design or flight angle range.	2	3	Aerodynamics engineer
RI-TW-04	Propeller whirl flutter	Possible structural failure of the propeller, mounting, or the wing	1	3	Perform aerodynamic analysis to establish flight envelope and operate within the limits	Reduce the speed to below whirl flutter speed	1	2	Propulsion engineer
RI-TW-07	De-icing mechanism on the wing fails	Loss of lift, mass increase, possible ice fragments going into propellers	1	3	Use back up de-icing mechanism.	Back up de-icing mechanism	1	2	Structures engineer
RI-TW-08	Failure of HVAC	Performing medical operations in the aircraft becomes impossible, crew discomfort	2	2	Use back up ventilation system.	Back up ventilation system	1	2	Flight performance engineer
RI-TW-09	Aeroelastic flutter of the wing	Flexing of the wing and reduced aerodynamic performance	2	2	Perform aeroelastic analysis to establish flight envelope and operate within the limits	Reduce the speed to below flutter speed	1	2	Aerodynamics engineer
RI-TW-10	Aeroelastic flutter of the tailplane	Flexing of the tailplane and reduced aerodynamic performance	2	2	Perform aeroelastic analysis to establish flight envelope and operate within the limits	Reduce the speed to below flutter speed	1	2	Aerodynamics engineer
RI-TW-11	Single motor failure	Decreased thrust, unbalanced torque	2	2	Introduce power management system and perform frequent maintenance	Use control surfaces to compensate for unbalanced thrust	2	2	Propulsion engineer
RI-TW-12	Multiple motor failure on the same wing	Significant thrust loss and unbalanced torque,	1	3	Introduce power management system and perform frequent maintenance	Attempt horizontal landing	1	3	Propulsion engineer
RI-TW-13	Multiple motor failure on different wings	Significant thrust loss and unbalanced torque	1	3	Introduce power management system and perform frequent maintenance	Attempt horizontal landing	1	3	Propulsion engineer

Development									
RI-DEV-01	Poor controllability	Delays due to the need to adjust the design	2	2	Controllability analysis	Reevaluate the controls, fix them	1	1	Control engineer
RI-DEV-02	Underestimating the weight of the aircraft in the initial stages of the design	Delays due to the need to redesign of multiple subsystems	3	1	Implementing safety factors	Reevaluate the design accounting for the changes in the weight of the aircraft	2	1	Structures engineer
RI-DEV-03	Insufficient safety factors	Potential structural failure when facing extreme conditions	2	2	Refer to industry standard for what numerical values are typically used	Reevaluate the design using updated safety factors	1	1	Structures engineer
RI-DEV-04	Wrong use of software tools	Unreliable software outputs	3	1	Using correct tools for each analysis type, verifying results with hand calculations	Re-do the analysis using validated tools	1	1	Structures engineer
RI-DEV-05	Wrong data obtained from CFD simulation	Incorrect control model	2	2	Multiple validation techniques	Obtain aerodynamics characteristic from wind tunnel test	1	1	CFD engineer
RI-DEV-06	Wrong data obtained from calculations	Incorrect aerodynamic properties	2	2	Perform verification of the used tools	Obtain calculation result through a different method	1	1	Aerodynamics engineer
RI-DEV-07	Required manufacturing tolerances being too high	Parts not possible to manufacture and delays due to redesign	3	2	Design for parts that do not require exact alignment and allow adjustability	Simplify the interfaces between parts	2	1	Manufacturing engineer

Table 12.3: Risk map before mitigation

Severity / Likelihood	Rare	Unlikely	Moderate	Likely	Very Likely
Catastrophic	S8	P4, P7, P9, C1, C2, S7, O4, O5, O6, O9, P10, P11, P12	P5, S4, O3, O10, S9		
Critical	O12, O13, TW1, TW2, TW4, TW5, TW6, TW7, TW12, TW13, C7, A6	O1, O7, O8, O11, TW3, P13	P3, C5, A4		
Marginal	C6	C3, A5, D1, D3, D5, D6, TW8, TW9, TW10, TW11	P8, S5, D7	S3	
Negligible			D2, D4	P6, O2	

Table 12.4: Risk map after mitigation

Severity / Likelihood	Rare	Unlikely	Moderate	Likely	Very Likely
Catastrophic	O6	P3, P4, P5, P7, P9, C1, O5, TW1, TW2, TW6, TW12, TW13, C6, S8, S9	O3, O9, S4, TW3		
Critical					
Marginal	C2, S7, O1, O4, O10, O11, O13, TW4, TW5, TW7, TW8, TW9, TW10, P10, P11, P13, C7	C5, A4, O7, O8, TW11			
Negligible	C3, O12, D1, D3, D4, D5, D6, P12, A6	P6, P8, S3, S5, A5, O2, D2, D7			

Sustainability Assessment

As discussed in Chapter 4, the sustainability goals are evaluated after the detailed design stage is complete. This will be done in this chapter. The sustainability of the eVTOL system will be assessed by comparing it to the performance of German ambulances and EC135 helicopter systems.

13.1. Greenhouse Gas Emissions

The greenhouse gas emissions of the vehicle have been estimated, taking the product lifespan of 20 years with 5 missions daily and assuming that creating the structure of the eVTOL and helicopter creates similar CO₂ emissions per kg of structure as during the production of cars. Finally, the emissions that are due to the generation of electricity are assumed to be 0.321 kg/kWh [83].

Since the battery of the eVTOL system is degraded after 1100 missions, a battery refurbishment process is required to repair the battery cathode material and restore it close to its original performance. Existing processes [84] offer such repair capabilities with only very limited greenhouse gas emissions of 8.2 kg CO₂-eq/kg cathode repaired. The final emissions breakdown is given in Table 13.1, and a time series of the cumulated emissions is shown in Figure 13.1.

Table 13.1: Greenhouse gas emissions breakdown for the eVTOL, ambulance, and helicopter systems

	eVTOL	Ambulance	Helicopter
Production emissions [ton CO ₂ eq]	40	13	5.4
Operational lifetime emissions [ton CO ₂ eq]	1850	1650	12700
Total lifetime emissions [ton CO ₂ eq]	1890	1663	12705.4
Total emissions per mission [kg CO ₂ eq]	52	46	348

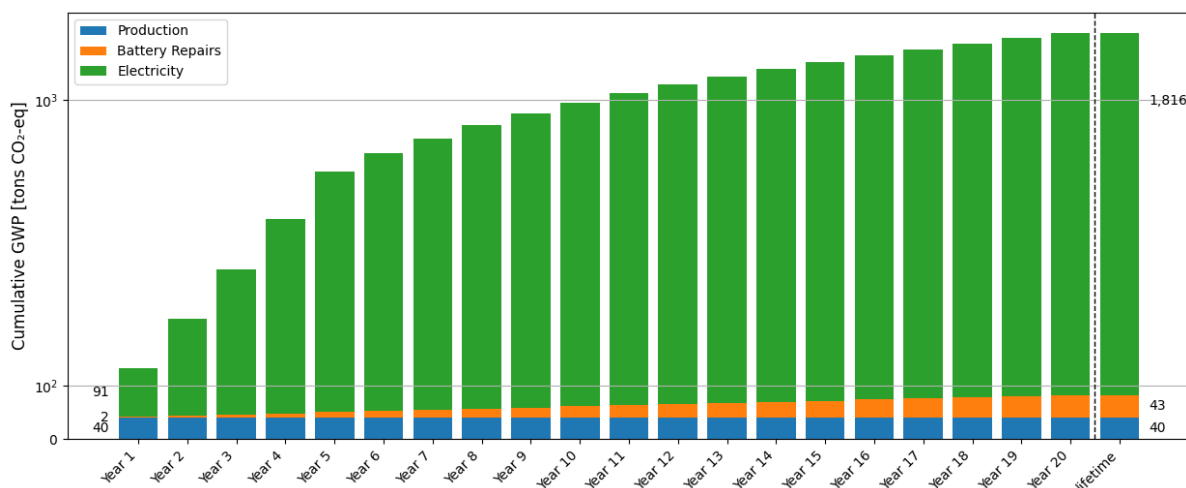


Figure 13.1: Life cycle analysis of greenhouse gas emissions

13.2. Strategic Goals Assessment

The strategic goals are meant to make the system as scalable as possible. These steps aim to lead to a design that will overall benefit the people and the environment over its life cycle. Its implementation helps gain the approval and support of the public.

Recyclability

The weight fraction of components that are easily recyclable or reusable is approximately 80%. This includes all aluminum and steel components that are used in the structure, as well as the seats, batteries, and motors. According to the European Union, this number falls in line with the 80% weight-wise recyclability of cars [85] and helicopters [86]¹. Therefore, the ResQProp system will have a recyclability that is comparable to its alternatives.

Noise

While at cruise, the eVTOL system will emit approximately 47 dB of ground noise as shown in Section 8.5. This is in the range of a modern vehicle driving slowly [87] and thus quieter than an ambulance. The main noise issue of the eVTOL system is the high noise level that is generated during takeoff and landing due to the high disc loading and proximity to the ground. Even though the noise during takeoff is significantly higher than during cruise, it will still emit less noise than a helicopter since the tips of its propellers will not be traveling at supersonic speeds, and it does not require any turbines. The issue with the high takeoff and landing noise is that the eVTOLs will be stationed at hospitals, which are frequently located in densely populated areas and thus create a significant disturbance for people living in proximity to the hospitals. The scores for noise are given qualitatively in Table 13.2.

Social Impact

The social impact that is created by the production of the system is very similar for the ambulance and helicopter systems since they use comparable materials. Due to the global supply chains, they do not receive a qualitative score of 5 but of 4. This is also true for the eVTOL system, but the use of NMC811 batteries leads to a very large amount of cobalt being used in the production. Cobalt mining is often done in very poor conditions and is described as "modern day slavery" [88]. This causes the qualitative social impact score of the eVTOL to be reduced to 3.

Cost per Mission

The cost per mission of the eVTOL is measured by its direct operational cost (DOC). As shown in Table 14.8, the DOC for the eVTOL is 908 EUR per flight. The cost for an ambulance ride in Germany is 520 EUR [89]. The use of an emergency helicopter costs 60 EUR/flight minute[90]. If an EC135 travels at 250 km/h, the trip will take 24 minutes, costing 1440 EUR.

Maintainability

Maintainability between the vehicles is compared by using the approximate maintenance cost divided by the kilometers traveled to achieve a fair comparison between the different vehicles. The high maintenance costs of the eVTOL are mainly caused by the required battery replacement, and the high maintenance costs of the helicopter are caused by its high mechanical complexity.

13.3. Strategic Risks

The operational strategic risks of the ambulance and the helicopters mainly arise due to the uncertainty in the delivery of fossil fuels in the form of gasoline and kerosene. These are issues that the eVTOL ambulance does not face since it is not dependent on fossil fuels. Its strategic risks are caused by the uncertainty in the supply of battery components. Since it is assumed that the batteries will not be replaced every 1100 missions but merely repaired and refurbished, this risk is only relevant during the production of additional eVTOLs and not during their deployment. Thus, the transition to eVTOLs lowers the operational risk of emergency medical services significantly.

The supply chain risks in the production of new eVTOLs are similar to the supply chain risks of ambulances and helicopters, since the production of all of these complicated systems is highly globalized. Therefore, both ambulances and helicopters receive a qualitative score of 3, and the eVTOL a qualitative score of 4.

¹This number is for commercial aircraft but can be assumed to be close to the value for helicopters

13.4. Sustainability Spider Map

The results of the sustainability assessment are collected in Table 13.2 and Figure 13.2. They show that the eVTOL system performs worse or as well as the ground-based ambulance in every category except for its benefits to strategic risks. It also performs better or as good as the helicopter in all measures except for its social impact.

Table 13.2: Sustainability results

	eVTOL	Ambulance	Helicopter
CO2 equivalent per mission [kg]	52	45	348
Recyclability (%)	80	80	80
Noise (qualitative score)	3	4	2
Social impact (qualitative score)	3	4	4
Cost per mission [EUR]	910	520	1440
Maintainability (approximate) [EUR/km]	0.21	0.13	0.24
Strategic risk (qualitative score)	4	3	3

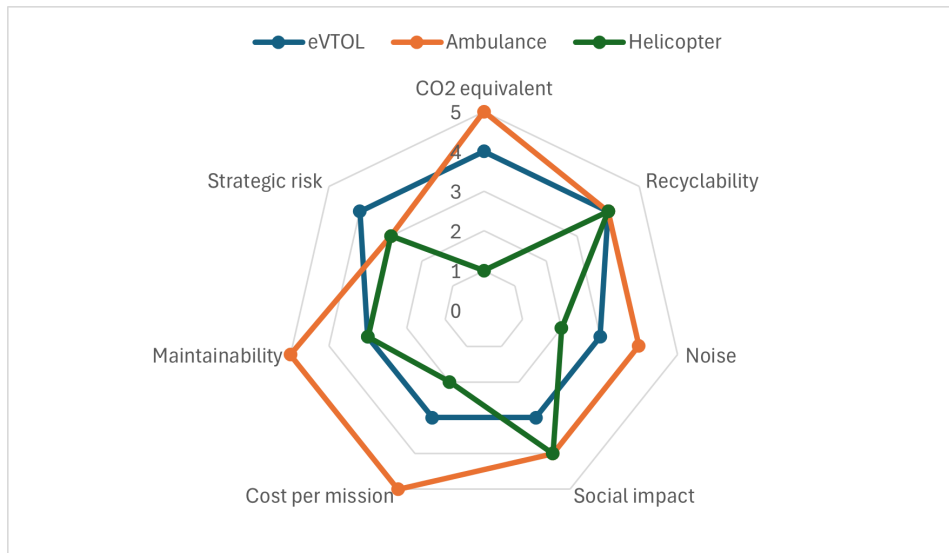


Figure 13.2: Spider chart assessing sustainability

14

Cost Breakdown

In this chapter, a detailed cost breakdown of the ResQProp is presented to provide a commercial perspective. The analysis encompasses expenses across various development phases Section 14.1 as well as subsystem-level costs. Beyond the capital expenditures, the direct operational costs Section 14.2 are also evaluated to highlight the competitive advantage of ResQProp compared to medical helicopters.

Symbols

Q	Total production units	Q_M	Qualification model quantity
Q_{Proto}	Number of prototypes	W	Airframe weight [kg]
V_H	Cruise speed [km/h]	P_{sm}	Max small propeller power [kW]
P_{bm}	Max big propeller power [kW]	D_{sp}	Small propeller diameter [m]
D_{bp}	Big propeller diameter [m]	C_E	Energy cost per flight [EUR]
C_{airframe}	Airframe depreciation per flight [EUR]	ROI	Return on investment
F_{EXP}	Experience factor	QDF	Quantity Discount Factor

Subscripts

eng	Engineering	tool	Tooling
mfg	Manufacturing	dev	Development
ft	Flight Test	qc	Quality Control
mat	Materials	em	Electric motor
bat	Battery	av	Avionics
lg	Landing gear	csprop	Propellers

14.1. eVTOL Development and Procurement Cost

The model employed in this section is based on a modified DAPCA IV cost model, adapted specifically for hydrogen-electric eVTOL aircraft [91]. The primary inputs include weight, cruising speed, power need, and selected geometric parameters as shown in Table 14.1. In addition to the eVTOL-specific parameters, the production plan also plays a significant role in the cost estimation. A total of 150 units are planned for production over a five-year period, based on the presence of approximately 60 hospitals in the Bavaria region. Each hospital is expected to be equipped with 2 to 3 eVTOLs to ensure adequate reachability and coverage.

Table 14.1: Cost model inputs and production quantities

Item	Value	Notes
Production Units (Q) [units]	150	Amount to be produced within 5 years
Qualification Model (Q_M) [units]	1	
Prototype Quantity (Q_{Proto}) [units]	2	
Engine Configuration [-]	2 + 2	Two small + two big
Airframe Weight (W) [kg]	902	= 1990 lbs
Cruise Speed (V_H) [km/h]	200	= 108 KTAS
Max Small Propeller Power (P_{sm}) [kW]	250	= 335 hp
Max Big Propeller Power (P_{bm}) [kW]	350	= 469 hp
Small Propeller Diameter (D_{sp}) [m]	2.26	= 7.40 ft
Big Propeller Diameter (D_{bp}) [m]	3.21	= 10.52 ft

Apart from the production quantities in planning, there are some factors to be applied to gain a more accurate estimation, especially for the certification phase. These factors are listed below in Table 14.2. The reason for the certification factors being less than one is due to the original model being used for military aircraft cost estimation, which always follows a stricter certification process. Table 14.3 indicates the hourly rate for different departments. The general cost of each phase is shown in Table 14.4.

Table 14.2: Certification factors

Factor	Value
$F_{cert,eng}$	0.67
$F_{cert,mfg}$	0.75
$F_{cert,dev}$	0.50
$F_{cert,ft}$	0.50
$F_{cert,qc}$	0.50
$F_{cert,mat}$	0.75

Table 14.3: Hourly rates (2019 EUR)

Role	Rate (€)
R_{eng}	80
R_{tool}	53
R_{mfg}	46

Table 14.4: RDT&E and production costs

Cost Item	Cost (EUR)
C_{eng}	5,600,000
C_{tool}	85,000
C_{mfg}	34,000,000
C_{dev}	190,000
C_{ft}	42,000
C_{qc}	2,210,000
C_{mat}	3,000,000

To clarify, the development cost C_{dev} is the cost for development support such as logistics. However, there are some missing costs in the cost model; thus, several component costs are listed below, including electric motors, battery packs, and propellers. Note that the landing gear is set to be negative because the design is non-retractable, which has lower complexity and requires fewer manufacturing hours.

Table 14.5: Component costs (in 2019 EUR)

Component	Cost (€)	Notes
C_{em}	244,000	Electric Motor
C_{pms}	25,000	Power Management System
C_{bat}	100,000	Battery Pack
C_{csprop}	96,000	Propellers
C_{av}	130,000	Avionics
C_{lg}	-6,500	Landing gear (cost reduction)

Table 14.6: *Estimated eVTOL subsystem costs (in 2019 EUR)*

Subsystem	Estimated Cost (€)
Propulsion System	390,000
Energy Storage (Battery)	136,500
Avionics and Flight Control	150,000
Airframe Structure	287,000
Total Estimated Cost	965,000

From these components, a rough cost summary of each subsystem is presented in Table 14.6. In Table 14.7, the total cost for the technical phase—such as engineering—is adjusted using a Quantity Discount Factor (QDF). This factor accounts for the increase in worker productivity as experience accumulates during production. The QDF is defined as shown in Equation 14.1.

$$\text{QDF} = F_{\text{EXP}}^{1.44 \cdot \ln(Q)} \quad (14.1)$$

where F_{EXP} is the experience factor, set to 0.90 in this case, and Q is the quantity produced. This yields a QDF value of 4.30. In addition to the QDF, the inflation rate is incorporated to provide a more accurate estimate of the total program cost. A 5% margin is then applied to account for potential unmodeled costs, given the novelty of eVTOL technology and the limited availability of relevant statistical data. Instead of the 10% margin in the cost budget, now all the components are known.

Table 14.7: *Total program cost (EUR)*

Description	Value	Unit / Notes
Total Cost	1,570,350	2019 EUR
Total Cost (With Inflation)	1,805,250	2025 EUR
Final Cost (With 5% Margin)	≈ 1.9 million	2025 EUR

14.2. eVTOL Direct Operational Costs

Table 14.8: *Direct operational cost breakdown (in 2019 EUR)*

Item	Cost (EUR)
C_{airframe}	27
C_E	56
C_{crew}	235
C_{maint}	18
C_{batD}	89
C_{ins}	348
Total DOC (2019 EUR)	773
Total DOC (2025 EUR)	908

This section focuses on the operational cost per flight, which is crucial for the operators. Note that the direct operational costs will be discussed here; the indirect operational costs are more related to the service provision costs, which are out of the scope.

There are two types of direct costs presented in Table 14.8. The first is variable costs, which include electricity, crew, and maintenance—these are highly correlated with economic activity. The second is fixed costs, such as battery and airframe depreciation, which remain relatively constant over time. Finally, the final operational cost is around 910 EUR in 2025.

14.3. Return on Investment

Before discussing profitability or return on investment (ROI), a retail price for the eVTOL must be established. However, most eVTOLs are not yet commercially available, as they have not been certified for airworthiness. Therefore, comparisons are made using prices of existing medical helicopters, which are mature and certified

products. Additionally, the government budget allocated for hospital infrastructure in Bavaria over the next decade is considered.

Table 14.9: Unit prices of new medical helicopters[92]

Helicopter Model	Unit Price (2025 EUR)
Bell 407GX _i	3.1 million
Airbus H125	3.3 million
AgustaWestland AW119 Koala	3.5 million
Airbus H130	4 million

As shown in Table 14.9, there is a range of prices among helicopter models[92], primarily due to differences in capacity, range, and mission flexibility. According to a recent report [93], the German federal government plans to invest approximately 50 billion EUR from 2026 to 2035 in hospital transformation. This indicates robust public financial support for health-related innovations. Taking these factors into account, the final retail price of the proposed eVTOL is set at 2.5 million (2025 EUR). Based on this price point and the cost estimation, the return on investment is calculated using Equation 14.2.

$$\text{ROI} = \frac{\text{Net Profit}}{\text{Investment}} = 31.6\% \quad (14.2)$$

After rounding up, the ROI is approximately 32%, indicating a highly favorable financial outcome for the eVTOL investment.

14.4. Sensitivity Analysis

Sensitivity analysis is performed to show the relationships between inputs and outputs. In this case, airframe weight, cruise speed, and production units are chosen to help assess the robustness of the cost model and understand the impact of uncertainty in input parameters on the final result, which is the final cost of the program.

Table 14.10: Sensitivity analysis of total cost

Parameter	Low Value	High Value	Total Cost Range (2025 EUR)	Change (%)
Production Quantity (Q)	100	200	2,050,000 → 1,790,000	-12.8%
Airframe Weight (W) [lb]	1,000	3,000	1,360,000 → 2,370,000	+74.4%
Cruise Speed (V_{cruise}) [KATS]	50	150	1,420,000 → 2,190,000	+54.3%

As shown in Table 14.10, increasing the number of eVTOLs produced over five years leads to a reduction in the unit cost, due to economies of scale. In contrast, higher airframe weight and cruise speed result in increased costs, as heavier or faster aircraft require more robust structures and higher energy demands. Notably, the cost model is highly sensitive to changes in airframe weight and cruise speed, with variations exceeding 50%. This significant sensitivity can be attributed to the relatively large differences in the input values tested.

Verification and Validation

This chapter presents the verification and validation procedures applied throughout the design and development of the ResQProp eVTOL ambulance. The goal of these procedures is to ensure that the tools developed, models implemented, and design decisions made are both technically sound and aligned with stakeholder requirements. Firstly, the tools and models used are considered in Section 15.1, followed by the compliance matrix of the design in Section 15.2. Furthermore, the requirements verification is explained in Section 15.3. Finally, a discussion about V&V for the whole design is presented in Section 15.4.

15.1. Tools and Models for V&V

In order to ensure that all tools used and created by the team give realistic results, verification and validation procedures need to be followed. Since multiple tools were used with different objectives, each tool will be discussed in the following, organized by department.

Powertrain

For power and energy calculations, a propeller generating tool was created. The verification procedures used were unit testing, checking the outputs, and testing edge cases to assess the robustness of the tool. Furthermore, the tool is validated by comparing results with a real design and by conducting a sensitivity study.

Firstly, the results of the implementation used were compared to an existing propeller geometry, namely the APC Thin Electric 10x7. The nominal operating conditions were used as input, and the output is compared with the real geometry in Figure 15.1.

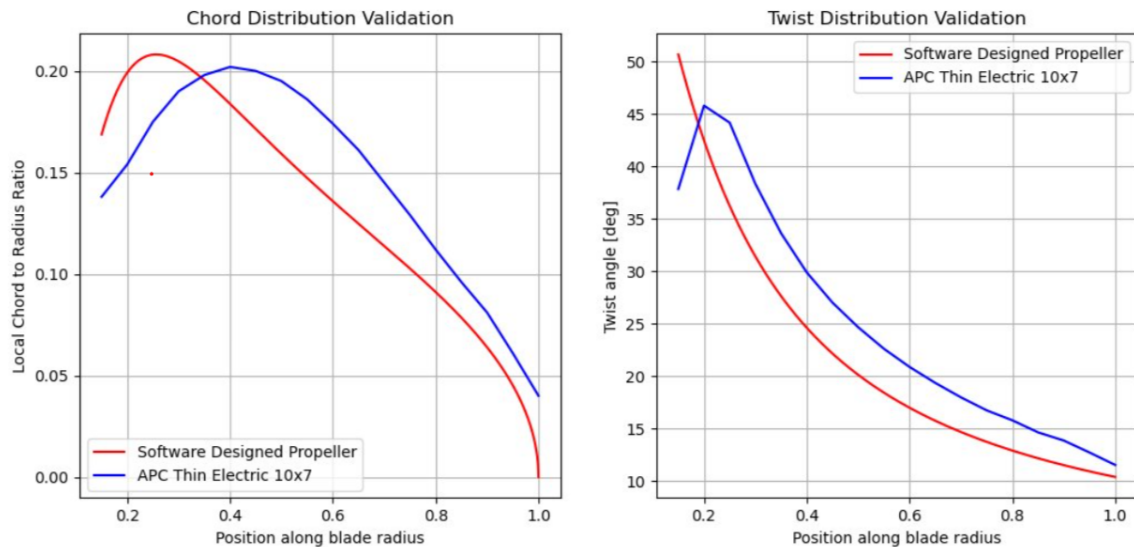


Figure 15.1: *Propeller Geometry Validation*

It can be observed that the simulated and the real geometries share multiple features, like the decreasing twist angle and the kink in the chord close to the hub. What this entails is that the simulation captures real design features of propellers. The features are not identical, which is expected given that the real designs went through physical iteration and testing for improvement.

Furthermore, in order to also validate the propeller performance metrics, the energy and power figures have been compared to existing and produced eVTOLs, such as the Joby S4. What was found is that the battery capacity is consistent with the presented eVTOL ambulance; however, takeoff power is overestimated.

This happens due to the propeller design not implementing the newest technology available and not being iterated upon using flight tests. The actual figures can be seen in Table 15.1.

Table 15.1: *Powertrain validation figures*

Model	Battery Capacity [kWh]	Peak Power [kW]
Joby S4	150	236 [30]
ResQProp	155	507

Aerodynamics

For the preliminary design of the wing, a Python program was used to optimize the geometry and obtain a rough estimate of lift and drag. These values were then verified by comparing them with an analysis of the same geometry using XFLR5. The error was found to be within acceptable bounds, as described in Section 7.1.

Python scripts were also used for tail sizing and control surface sizing. For tail sizing, the tail aims to provide both static and dynamic stability. An analysis of the lifting surfaces was done, neglecting the effect of the fuselage. Further verification and validation could involve full CFD analysis, wind tunnel test, and actual flight test.

Mass and Power Estimation

Mass and power for the designed aircraft were estimated using an iterative Python script. To verify whether this method makes sense, the model was tested on a comparable existing design. Design characteristics of the Joby S4 aircraft from [30] and [94] were used to estimate its MTOW and cruise power.

Input Parameter	Joby S4	Output parameter	Joby S4	Model Estimation
Payload Mass [kg]	500	MTOW [kg]	2400	2480
Range [km]	242	Cruise Power [kW]	180	200
Cruise Speed [km/hr]	322	Hover Power [kW]	911	778
Disc Area [m ²]	63			
Lift over Drag	12.6			
Pack-level Battery Density [Wh/kg]	235			
Rotor Figure of Merit	0.73			

Table 15.2: *Model output compared to actual performance for the Joby S4 aircraft.*

Table 15.2 shows a small discrepancy in power and mass values, but considering the high sensitivity of weight to parameters such as range and battery energy density, the magnitude of these errors is deemed acceptable.

Control

During the creation of the simulation, unit tests were conducted on each subsystem by creating sample inputs and comparing them to the outputs they generated. The outputs were checked for correct dimensions, correct signs, and a correct order of magnitude.

A sensitivity analysis has been conducted by varying the most uncertain inputs, namely the vehicle mass, the velocity profile for the transition, and the time constants for the hinge and the propulsion system. The inputs have been varied by 10% and the outputs have been compared to their original value. The outputs that were considered are the peak absolute value of the pitching moment that the propulsion system has to create during a front gust, a rear gust, and the transition. The elevator data is not considered in the sensitivity analysis since it only becomes relevant during cruise, and the moment that the propulsive system provides in this flight stage is close to 0.

The percentage change in the outputs at a 10% increase ¹ are shown in Table 15.3. The peak moment in transition, when changing the velocity at which the transition from cruise to hover takes place, is unstable. This is due to this transition velocity being dependent on the chosen flight profile, since transition requires

¹The switching velocity from cruise to hover has been decreased by 10% instead

an approximately stable flight condition, which is not given when just switching this velocity without altering the velocity profile.

Table 15.3: *Sensitivity analysis for different control maneuvers. All changes in %*

Input	Peak moment front gust	Peak moment rear gust	Peak moment transition
Switching velocity hover to cruise	Not applicable	Not applicable	0
Switching velocity cruise to hover	Not applicable	Not applicable	unstable
Hinge time constant	0.905	0.147	0.0992
Propulsion time constant	0.0565	0.441	0
Ramp up velocity	Not applicable	Not applicable	0
Ramp down velocity	Not applicable	Not applicable	0.496
Mass (+ inertia)	1.02	2.939	0.595

Structures

Multiple tools were made in Python and used to understand the loads on the wing, design the wingbox, and check for buckling. The first two are the most fundamental, thus a tool generating internal load diagrams from the external geometry and the external forces, and a tool that uses these internal loads to calculate the stresses within the wingbox geometry. These two tools are then used in an optimization code, which converges to the required thickness for the wingbox at many points along the wingspan for a given diameter at that location to optimize for minimal weight.

The loads.py file is particularly important to be verified precisely, as it is the starting point of the complete structural design of the wingbox. For verification of this file, unit tests are performed, and the internal load diagrams generated by the code are compared to those produced by a third-party tool called "Ftool". For this comparison, the combined loads on the wingbox are modelled and compared, and the result between the two internal load diagrams from the code and Ftool is the same, ultimately verifying the loads.py code.

The stress_calculations.py file uses the results from loads.py and inserts the geometry of the wingbox at many points along the wingspan to calculate the internal shear and normal stresses at every section. This file is checked using unit tests for every function, which compare the result for a simplified case given by the code to the result using hand calculations. For every function, the same result is reached, again verifying this file.

Lastly, the optimization code is verified by visually inspecting the convergence of the combined stress to the given stress bound. This shows that the highest combined stress converges to the yield stress and follows this bound parallel or stays below it along the complete wingspan.

At this stage of the design, the tools can not be validated yet, but this is an important step in future phases of the project. The loads on the wing should be validated to check how close they are to reality. This starts with getting better lift estimates using CFD models or wind tunnel testing and comparing these to the acquired lift distribution using XFLR5. The internal stresses are validated by comparing them to data acquired from real-world strain-gauge tests on the wingbox. These tests show the strain in the wingbox under different internal loads, ranging from torsional, shear, and moment loads. These strain measurements can then be used to calculate the corresponding internal stresses. Finally, the performance of the complete wingbox design should be validated with actual load tests.

Cost Breakdown

As previously mentioned, there is limited publicly available data on the cost breakdown of eVTOLs, which restricts the scope and robustness of validation. Given these constraints, Lilium serves as the primary reference for comparative analysis.

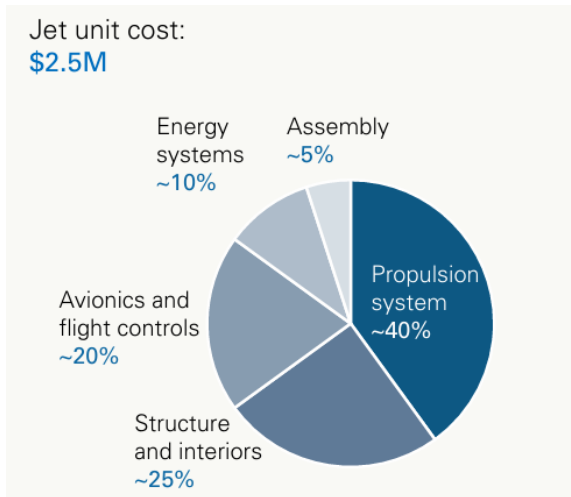


Figure 15.2: Cost breakdown of Lilium Jet[95]

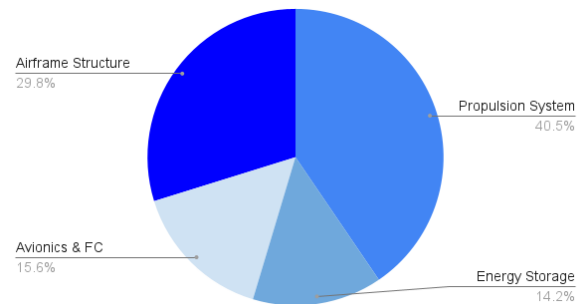


Figure 15.3: Cost breakdown of ResQProp

The primary difference between the two distributions lies in the Avionics and Flight Control segment. This difference can be attributed to Lilium's design focus on longer-range, intercity operations, which inherently require more advanced communication, navigation, and flight control systems. Apart from this variation, the overall cost allocation shows general alignment, supporting the validity of the current model. The Airframe Structure costs more because of the innovative wing design and the manufacturing complexity, while the battery consumes less capital because it is not customized. Note that no assembly cost is considered in the cost breakdown pie chart for ResQProp.

15.2. Compliance matrix

In this section, the compliance matrix is presented, which shows whether the current design complies with the stakeholder requirements.

Table 15.4: Stakeholder requirement compliance matrix

Requirement ID	Requirement	Check	Value	Verification
REQ-STK-01	The mass of the payload shall be no less than 400 kg.	✓	456 kg	Analysis. Final design weight estimation results presented in Chapter 11. (Analysis)
REQ-STK-02	The indicative maximum footprint on the ground shall not exceed a diameter of 12 m.	✓	6.3x12 m	Demonstration. CAD model pictures in Chapter 11.(Demonstration)
REQ-STK-03	The aircraft shall respond to an emergency in 50km radius in 15 minutes from its base.	✓	60 km radius reached in 15 min	Analysis. Design according to Figure 3.2. (Analysis)
REQ-STK-04	The new vehicle shall respect European noise emissions over urban areas..	-	-	Not verified. Aeroacoustic CFD simulations of the full vehicle shall be performed. (Analysis)
REQ-STK-05	The cabin noise level shall not exceed 60 dB.	-	-	Not verified. Aeroacoustic CFD simulations of the full vehicle shall be performed. (Analysis)
REQ-STK-06	The vehicle shall have electric power autonomy for 100 km operation radius with take-off and landing at 2 sites, plus a reasonable reserve.	✓	120 km range with 3 TOLs	Design according to Figure 3.2
REQ-STK-07	The vehicle shall be able to operate at 5m distance from people and 3m from any object.	-	-	Not verified. Downwash analysis shall be performed (Analysis)
REQ-STK-08	The aircraft shall be able to fly in windy conditions, up to 8 Beaufort, also in case of rain or snow.	✓	Takeoff/landing at 20 m/s wind, cruise less limiting	Analysed using Simulink model. Gust rejection (limiting case) presented in Section 9.6 (Analysis)
REQ-STK-09	The vehicle shall be able to land and take-off at unprepared and uneven sites. .	✓	-	Landing gear pressure selected accordingly, presented in Subsection 10.5.3 (Demonstration)
REQ-STK-10	The propulsive system shall offer redundancies in case of failure of any main component.	✓	-	Use of 2 pairs of counter rotating propellers, shown in Section 6.2 which can be used as explained in Section 6.2.(Analysis, Demonstration)

REQ-STK-11	The vehicle shall be able to transport the patient safely to a hospital.	✓	Maximum load factor during normal operations 1.2g	Verified using Simulink transition model, shown in Section 9.5 (Analysis)
REQ-STK-12	The main structure shall have a lifetime equal or longer than a helicopter ambulance.	-	-	Not verified. Lifetime estimation shall be produced, including fatigue testing. (Test)
REQ-STK-13	If battery-electric propulsion is chosen, then the battery should be easily replaceable.	✓	-	Batteries located below the floor and are accessible as shown in Section 6.1 and Section 8.4(Demonstration)
REQ-STK-14	The main structure shall be recyclable.	✓	80 % recyclable	Usage of recyclable materials (metals) explained in Section 13.2.(Demonstration)
REQ-STK-15	The cost of the vehicle shall not exceed 2M Euros.	✓	1.9 M Euros	Cost breakdown estimations, presented in Section 13.2(Analysis)
REQ-STK-16	The cost of operation, including distributed hubs and vehicles, shall not exceed 1000 Euro/flight.	✓	908 Euros	Cost estimation presented in Section 14.2(Analysis)
REQ-STK-17	The aircraft shall comply with EASA regulations.	×	-	Not verified. Noise simulations shall be performed.(Analysis)
REQ-STK-18	The aircraft shall be able to fly in mountainous regions.	✓	Maximum altitude 3000m	As presented in Section 8.5, propellers can provide sufficient thrust at least up to 3000m.(Analysis)
REQ-STK-19	The aircraft shall be designed to allow efficient and straightforward maintenance operations.	✓	-	Explained in Section 12.1(Demonstration)
REQ-STK-20	The aircraft shall be able to fly during day-time and night-time.	-	-	Not verified. Aeroacoustic CFD simulations shall be produced to determine whether maximum noise at take off does not exceed limiting noise requirement. (Analysis)
REQ-STK-21	The aircraft shall be capable of rapid deployment to respond to emergencies.	✓	Deployable within 2 minutes	Designed to operate based on Figure 3.1 (Analysis)

15.3. Requirement Verification and Validation

The next project steps can be taken once full clarity of the current status of the design is achieved. The best way to do so is by performing requirement verification and validation. In Table 15.5, a summary of already verified or not yet verified requirements, as shown using ✓ or - respectively in the Result column. A × in the Result column shows that the requirement has not been met. In the column Value, the current value estimate is presented, in the last two columns, verification and validation methods are shown.

Table 15.5: *Mission and systems requirement compliance matrix*

Requirement ID	Type	Requirement	Result	Value	Verification method	Validation method
MIS-SERV-01	Mission	The aircraft shall have a range of at least 120 km with 2 landings.	✓	120 km, 2 landings	Analysis	Test
MIS-SERV-02	Mission	The aircraft shall have a cruise speed of at least 200 km/h.	✓	200 km/h	Analysis	Test
MIS-SERV-03	Mission	The aircraft shall be able to land on a slope of 14 deg.	-	-	Analysis	Test
MIS-SERV-04	Mission	The aircraft shall be able to climb vertically at 5.0 m/s.	✓		Analysis	Test
MIS-SERV-05	Mission	The aircraft shall be able to fly at an altitude ranging from 0 to 1500 m.	✓	3000 m	Analysis	Test
MIS-SERV-06	Mission	The aircraft shall be able to operate in wind up to 62 km/h.	✓	25 m/s	Analysis	Test
MIS-SERV-07	Mission	The aircraft shall be able to operate in rain and snow conditions.	✓	-	Analysis	Test
MIS-SERV-08	Mission	The aircraft shall be able to follow the IFR (Instrument Flight Rule).	-	-	Analysis	Test
MIS-FUNC-01	Mission	The projection of the landing configuration shall cover no more than a 6 x 12 m rectangle.	x	6.3 x 12 m	Demonstration	Demonstration
MIS-FUNC-02	Mission	The aircraft shall carry at least two medical workers and one patient.	✓	2 medical workers, 1 patient, 1 pilot	Analysis	Test
MIS-FUNC-03	Mission	The aircraft shall carry functioning medical equipment onboard weighing up to 100 kg.	✓	96 kg	Analysis	Inspection

Continued on next page

Requirement ID	Type	Requirement	Result	Value	Verification method	Validation method
MIS-FUNC-04	Mission	The aircraft shall constrain pilot input to avoid a crash.	✓	Fly-by-wire	Test	Test
MIS-FUNC-05	Mission	The pilot shall have full control over the aircraft until reaching constraints.	✓	Fly-by-wire	Test	TEst
MIS-FUNC-06	Mission	The doctors and patients shall be transported comfortably.	-	-	Analysis	Demonstration
MIS-FUNC-07	Mission	The maximum noise in the cabin shall be 60 dB.	-	-	Analysis	Test
MIS-FUNC-08	Mission	The energy storage shall last 1000 missions before replacement.	✓	1100 missions	Analysis	Test
MIS-FUNC-09	Mission	The aircraft shall have less than 50% of the carbon life cycle footprint of medical helicopters.	✓	15%		
MIS-FUNC-10	Mission	The aircraft shall be recyclable for at least 50%.	✓	80%	Analysis	Inspection
MIS-FUNC-11	Mission	The energy storage shall be easily replaceable.	✓	-	Demonstration	Demonstration
MIS-FUNC-12	Mission	The critical systems shall allow for easy visual inspection.	✓	-	Demonstration	Demonstration
MIS-FUNC-13	Mission	The maximum perceived external noise on the ground shall be 50 dB for a cruising aircraft.	-	-	Analysis	Test
MIS-FUNC-14	Mission	The maximum perceived external noise from 100 m shall be 70 dB for an aircraft taking off.	-	-	Analysis	Test
MIS-FUNC-15	Mission	The aircraft shall require a maximum of 60 minutes for refuelling/recharging for the next flight.	✓	31 minutes	Analysis	Test
MIS-FUNC-16	Mission	The aircraft shall provide a stable structural behavior during normal operating conditions.	✓	Max load factor 1.2 g	Analysis	Test
MIS-FUNC-17	Mission	The aircraft shall have a lifetime of 20 years.	✓	30 years	Analysis	Analysis

Continued on next page

Requirement ID	Type	Requirement	Result	Value	Verification method	Validation method
MIS-FUNC-18	Mission	The aircraft shall function between -20 and +40 degrees Celsius.	✓	-20 to +40 ° C	Analysis	Test
MIS-CERT-01	Mission	The energy storage casing shall withstand regulatory ultimate inertia factors and loads.	-	-	Analysis	Test
MIS-CERT-02	Mission	The medical workers shall survive in a crash during normal operation.	-	-	Analysis	Test
MIS-CERT-03	Mission	The aircraft shall fulfill all EASA compliance requirements for VTOL.	✓	-	Analysis	Inspection
MIS-CERT-04	Mission	The aircraft shall have a catastrophic failure rate of 1e-9 per flight hour at most.	-	-	Analysis	Analysis
MIS-CERT-05	Mission	The safety critical systems shall have redundancy (Single failure criteria).	✓	-	Demonstration	Test
MIS-CERT-06	Mission	The aircraft's MTOW shall be less than 3175kg.	✓	2600 kg	Analysis	Inspection
MIS-CERT-07	Mission	The aircraft's roll, pitch and yaw rates shall be able to attain at least 10 deg/sec during hover.	✓	10 deg/s	Analysis	Test
MIS-CERT-08	Mission	The aircraft's roll rate shall be able to reach at least 20 deg/sec during cruise.	✓	20 deg/s	Analysis	Test
MIS-CERT-09	Mission	The aircraft's pitch rate shall be able to reach at least 10 deg/sec during cruise.	✓	30 deg/s	Analysis	Test
MIS-CERT-10	Mission	The aircraft shall be able to sustain a 2G turn.	✓	2.5 g	Analysis	Test
MIS-COST-01	Mission	The whole aircraft shall cost less than 2 million euros.	✓	1.9 M€	Analysis	Inspection
MIS-COST-02	Mission	The cost of a 100 km mission shall not exceed 1000 euros excluding labor.	✓	910€	Analysis	Inspection

Continued on next page

Requirement ID	Type	Requirement	Result	Value	Verification method	Validation method
MIS-COST-03	Mission	The aircraft shall require less training to fly than a helicopter.	-	-	Analysis	Analysis
SYS-OPER-01	Operations	The energy storage system shall be energized from 20% to 100% within 45 min.	✓	31 min	Analysis	Inspection
SYS-OPER-02	Operations	The energy storage system shall be compatible with conventional energy supply system (EV charger, liquid natural gas).	✓	400 V EV Charger	Demonstration	Demonstration
SYS-OPER-03	Operations	The cabin design shall allow the entry and exit of a medical stretcher without effort.	✓	-	Demonstration	Demonstration
SYS-OPER-04	Operations	The medical stretcher shall be secured inside the cabin with easy mechanical locks.	✓	-	Demonstration	Demonstration
SYS-OPER-05	Operations	The cabin shall allow for two medical workers to be safely located beside the stretcher.	✓	-	Demonstration	Demonstration
SYS-OPER-06	Operations	The cabin shall host an inventory for the medical equipment within the reach of medical workers.	✓	-	Demonstration	Demonstration
SYS-OPER-07	Operations	The cabin door shall be closed by the staff inside the cabin in 10 s.	-	-	Demonstration	Demonstration
SYS-OPER-08	Operations	The cabin shall have a climate control system to provide 22 degrees Celsius.	✓	-	Analysis	Test
SYS-OPER-09	Operations	Access to the cabin door(s) shall be unobstructed by aircraft components with a width clearance of 3 m.	-	-	Demonstration	Demonstration
SYS-OPER-10	Operations	The cabin shall have illumination for medical operation onboard.	✓	-	Demonstration	Demonstration
SYS-OPER-11	Operations	The normal operation of the aircraft shall not induce more than +1.5 g on the passengers.	✓	Max load factor 1.2 g	Analysis	Test

Continued on next page

Requirement ID	Type	Requirement	Result	Value	Verification method	Validation method
SYS-OPER-12	Operations	The operational empty weight with power storage shall not exceed 2775 kg.	✓	2600 kg	Analysis	Inspection
SYS-STRU-01	Structures	The structure of the aircraft shall provide connection interfaces to other systems.	✓	-	Analysis	Demonstration
SYS-STRU-02	Structures	The cabin shall have a volume of at least 11 m ³ .	✓	14 m ³	Inspection	Inspection
SYS-STRU-03	Structures	The projection of the cabin on the ground shall not exceed 6 x 12 m.	×	6.3x12m	Inspection	Inspection
SYS-STRU-04	Structures	The structure shall provide a barrier to protect the cabin interior from the outside environment.	✓	-	Demonstration	Demonstration
SYS-STRU-05	Structures	The main structure shall be able to hold the weight of the payload of at least 400 kg.	✓	465 kg	Analysis	Test
SYS-STRU-06	Structures	The effects of fatigue in the system shall not be critical throughout its lifespan.	-	-	Analysis	Test
SYS-STRU-07	Structures	The main structure shall ensure that no location on the aircraft structure retains moisture for more than 6 hours under typical operating environmental conditions.	✓	-	Analysis	Test
SYS-STRU-08	Structures	The cabin structure shall not deflect more than 0.02 m under all operating conditions	-	-	Analysis	Test
SYS-STRU-09	Structures	The lifting structure shall not deflect more than 5% of the wingspan under all operating conditions.	-	-	Analysis	Test
SYS-STRU-10	Structures	The landing system shall not deflect more than 0.06 m under vertical landing conditions.	-	-	Analysis	Test

Continued on next page

Requirement ID	Type	Requirement	Result	Value	Verification method	Validation method
SYS-STRU-11	Structures	The shock absorption of the landing system shall not damage the main structure during landing under normal operating conditions.	-	-	Analysis	Test
SYS-STRU-12	Structures	The structure for the battery shall not deform when dropped from a height of 15.2 m.	-	-	Analysis	Test
SYS-STRU-13	Structures	The structure shall protect the cabin interior in case of a crash with loads up to 15 g.	-	-	Analysis	Test
SYS-STRU-14	Structures	The body and structure shall not fracture during expected worst-case conditions.	-	-	Analysis	Test
SYS-STRU-15	Structures	The structural system shall not exceed a cost of 300000 euros.	-	-	Analysis	Inspection
SYS-STRU-16	Structures	The cabin structure shall reduce the acoustic noise perceived in the cabin to 60 dB.	-	-	Analysis	Test
SYS-STRU-17	Structures	The structure shall be able to be manufactured within the EU with common equipment in the aviation industry.	-	-	Inspection	Demonstration
SYS-STRU-19	Structures	The structure shall have a cockpit windshield opening allowing for 70 ° lateral FOV and 60 ° vertical FOV.	✓	60 ° vertical, 70 ° lateral	Demonstration	Demonstration
SYS-STRU-20	Structures	The landing system shall be capable of holding the aircraft statically stable on a slope up until 14 deg.	-	-	Analysis	Test
SYS-STRU-21	Structures	The main structure shall hold its structural integrity up until a load factor of 2 g.	✓	2.5 g	Analysis	Test

Continued on next page

Requirement ID	Type	Requirement	Result	Value	Verification method	Validation method
SYS-STRU-22	Structures	The eigenfrequency of the aircraft structure shall be at least 1.5 of the highest induced vibration frequency.	-	-	Analysis	Test
SYS-AERO-01	Aerodynamics	The upward force in cruise shall be at least 1.3 times the weight at 2000 m barometric altitude.	-	-	Analysis	Test
SYS-AERO-03	Aerodynamics	The L/D of the aircraft in cruise shall be at least 14.	x	10.3	Analysis	Test
SYS-AERO-05	Aerodynamics	The speed never to be exceeded shall be at least 1.2 times the maximum cruise speed.	-	-	Analysis	Test
SYS-AERO-06	Aerodynamics	The diameter of the propeller shall be less than 6 m.	✓	Max diameter 3.2m	Demonstration	Demonstration
SYS-AERO-07	Aerodynamics	All propeller installed on the aircraft shall not produce more than 70 dB of noise perceived from 100 m away during takeoff.	-	-	Analysis	Test
SYS-AERO-08	Aerodynamics	The propellers shall be positioned such that a safe walkable area around the aircraft is created.	✓	-	Demonstration	Demonstration
SYS-AERO-09	Aerodynamics	The propellers shall be counter-rotating pairs.	✓	-	Demonstration	Demonstration
SYS-AERO-10	Aerodynamics	The control surfaces shall provide maneuvering agility during cruise.	✓	-	Analysis	Test
SYS-CTRL-01	Control	The control system shall take inputs from the pilot to control the propulsion system and the control surfaces.	✓	-	Demonstration	Demonstration
SYS-CTRL-02	Control	The control system shall allow the pilot to maneuver the aircraft with 6 degrees of freedom during take-off and landing.	✓	-	Demonstration	Demonstration

Continued on next page

Requirement ID	Type	Requirement	Result	Value	Verification method	Validation method
SYS-CTRL-03	Control	The control system shall allow the pilot to climb, descend, and change the flight direction of the aircraft during cruise.	✓	-	Analysis	Test
SYS-CTRL-04	Control	The control system shall have flight envelope protection.	✓	-	Inspection	Inspection
SYS-CTRL-05	Control	The control system shall have autopilot.	-	-	Demonstration	Demonstration
SYS-CTRL-06	Control	The manual control of the aircraft shall require less training time than driving.	-	-	Test	Test
SYS-CTRL-07	Control	The control system shall reject instantaneous gust disturbances up to 9.144 m/s without being displaced more than 3m	✓	1.71m	Analysis	Test
SYS-CTRL-08	Control	The control system shall not induce oscillation at the mechanical resonance frequency of the aircraft.	-	-	Analysis	Test
SYS-CTRL-09	Control	The avionics system shall have triple redundancy for flight critical sensors.	✓	-	Analysis	Test
SYS-CTRL-10	Control	The avionics system shall have triple redundancy for flight computers.	✓	-	Analysis	Test
SYS-CTRL-11	Control	The avionics system shall broadcast the aircraft's flight data.	✓	-	Analysis	Test
SYS-CTRL-12	Control	The avionics system shall support radio communication up to 120 km.	✓	-	Analysis	Test
SYS-CTRL-13	Control	The avionics system shall have sensors providing necessary and reliable flight data to the control system.	-	-	Analysis	Demonstration

Continued on next page

Requirement ID	Type	Requirement	Result	Value	Verification method	Validation method
SYS-CTRL-14	Control	The avionics system shall provide location data with 20 m of accuracy.	✓	-	Analysis	Test
SYS-CTRL-15	Control	The avionics system shall contain collision detection.	✓	-	Analysis	Test
SYS-CTRL-16	Control	The avionics system shall contain a traffic collision avoidance system.	✓	-	Analysis	Test
SYS-PROP-01	Propulsion	The propulsion system shall provide thrust during take-off to reach a climb rate of 5 m/s.	✓	30 m/s	Analysis	Test
SYS-PROP-02	Propulsion	The propulsion system shall provide thrust during cruise to reach a cruise speed of 200 km/h.	✓	-	Analysis	Test
SYS-PROP-03	Propulsion	The propulsion system shall use environmentally friendly power source.	✓	-	Inspection	Inspection
SYS-PROP-04	Propulsion	The propulsion system shall provide enough agility to reject instantaneous gust disturbances up to 9.14 m/s without being displaced more than 3m.	✓	1.7 m	Analysis	Test
SYS-PROP-05	Propulsion	The powertrain system shall contain a power management system.	✓	-	Demonstration	Demonstration
SYS-PROP-07	Propulsion	The high voltage part of the powertrain system shall be shielded from the passengers.	✓	-	Demonstration	Demonstration
SYS-PROP-08	Propulsion	The powertrain system shall not cause interference with sensitive medical equipment or avionic equipment.	✓	-	Analysis	Test
SYS-PROP-09	Propulsion	The powertrain system shall survive a lightning strike.	-	-	Analysis	Test
SYS-PROP-10	Propulsion	Any fire in the powertrain system shall be contained.	✓	-	Demonstration	Demonstration

Continued on next page

Requirement ID	Type	Requirement	Result	Value	Verification method	Validation method
SYS-PROP-11	Propulsion	The power storage component shall have a lifespan of 1000 cycles at 80% depth of discharge before degrading to 80% of its initial capacity.	✓	1100	Analysis	Test
SYS-PROP-12	Propulsion	The power storage component shall be replaceable with common equipment.	✓	-	Inspection	Inspection
SYS-PROP-13	Propulsion	The power storage component shall not deform or rupture in a crash defined by EASA regulations.	-	-	Analysis	Test
SYS-PROP-14	Propulsion	90% of the replaced power storage shall be recyclable.	-	-	Analysis	Demonstration
SYS-PROP-15	Propulsion	The power storage and management components shall function between an external temperature of -20 and +40 degrees Celsius.	✓	-	Analysis	Test
SYS-PROP-16	Propulsion	The aircraft should be able to maintain its altitude with 75% engine power.	✓	50%	Analysis	Test

15.4. Verification and Validation of the Design

Verification of the design will be performed by proving that the requirements are fulfilled. Verification will be conducted on two levels: on system level and on subsystem level. During the detailed design process, the system requirements will be broken down into subsystem requirements. The subsystems will be verified by ensuring that all of the subsystem requirements are met. After the subsystem requirements have been verified, it has to be shown that the subsystems perform together as expected by verifying the system requirements. Below each table, the verification and validation methods for some critical requirements are explained. The procedures, required facilities, and expected costs² are discussed.

SYS-STRU-13 and SYS-STRU-14 The crash test is critical for the eVTOL which is going to carry human. Safety is the important consideration in these requirements. The crash test can be conducted at the Landing and Impact Research facility at NASA's Langley Research Center as they successfully performed crash test for a full-scale mockup eVTOL aircraft cabin in 2022. Using the overhead mass to represent other structures such as wing, hanging the cabin with four crash test dummies on board, and release it with the possible angle the eVTOL when there is a loss in propulsion system. Collect the data from the dummies and change the angles or the dummy placements for different scenarios. [96]

SYS-OPER-08 To verify this, a test can be conducted for climate control of the cabin enclosure mock-up. The temperatures across the cabin space are monitored, with the climate control system trying to heat up/cool down the cabin from an external temperature between -20 °C and +40 °C. The validation involves a full aircraft subjected to the same environment. The cost would mostly come from the use of a warehouse with temperature control that can accommodate the full aircraft. The exact number would range between

²These costs exclude labor and insurance.

1000 euros and 10000 euros depending on the whether such a warehouse is needed. If the testing can be conducted on a cold day or a hot day during the validation process, then the warehouse cost is not needed.

SYS-CTRL-15 This requirement can be verified by a flight test. For collision avoidance during hovering, the test could be made by placing artificial obstacles of various sizes and shapes around the takeoff and landing area. The collision avoidance performance of the aircraft can be observed and investigated. For cruise, the test could require the aircraft to fly over a mountain range or an unpopulated tall structure such as a radio tower. The validation can be done by demonstrating several flights in real and unstructured environments. Due to the level of safety and preparation required, these tests and demonstrations would be costly. The cost for the testing would be in the order of 500000 euros (equivalent to 500 flight operations).

Project Production and Development

The detailed the start of detailed design of the eVTOL ambulance has been started, documented, and checked against the requirements set. This section will expand on the phases that follow this initial detailed design phase to be able to realize the project and get the ResQProp ambulance on the market. First, the next steps in the project are presented in Section 16.1. This is followed by an in-depth production plan in the manufacturing, assembly, and integration of the subsystems of the eVTOL, as will be presented in Section 16.2.

16.1. Project Design and Development Logic

As the first phase after the design phase, as described in this report, the detailed designs will need to be finalized. Each department will further work out all the subsystems to the minute detail to realistically get the eVTOL up in the air. Once all the subsystems are designed in more detail, system integration will need to occur and be further optimized until it converges to a finalized version of the design.

A prototype can then be manufactured. This prototype will function as a vital validation system in the realization of the eVTOL, and it will bring systems engineering into practice as it will physically integrate all the systems. Various testing at defined facilities will be performed on this prototype to validate the design, among others including its structural integrity, the electronics, and its aerodynamic behavior. From this validation process, the design can therefore be improved and optimized.

Once the design of the eVTOL is finalized, the extensive certification process will be able to start. After the design is certified by the appropriate authorities, the manufacturing facilities can be scouted out. Furthermore, distinct manufacturing capacities need to be ensured in order to be able to meet the market demand for the ambulance eVTOL. For this, two steps will need to be taken: the market will need to be analyzed, and potential customers will be reached out to in order to get early investments and gain an understanding of the market needs.

Once this is established, the mass production will be sized such that the eVTOL can enter the market according to the required capabilities from the market analysis. At this point, the first eVTOLs will be able to come into the operations realm, and therefore will need to be equipped accordingly. One life of operations will take around 20 years, after which, its life will be sustainably ended. All of these phases following this initial detailed design are illustrated in Figure 16.2.2 and preliminarily planned out in Figure 16.2.2.

16.2. Production Plan

After the design phase, for the project to become a reality, it has to be manufactured and assembled. The following subsections explain the proposed manufacturing plan for crucial aircraft components, as well as assembly plan that describes how different parts will be joined together and all the systems will be integrated into the final product.

16.2.1. Manufacturing Plan

Production of an aircraft starts with the manufacturing of individual parts. Those range from ribs in the wingbox to full fuselage panels. Each part requires a different manufacturing process. Those depend on the size, complexity, and material of the parts.

Wingbox and Fuselage Parts

All parts of the wingbox, as well as the outer structure of the fuselage, are made out of Aluminum 2024. It provides good workability, so a number of processes can be used in its production.

- Skin: Thin metal sheet processes are considered for shaping the aircraft skin. Stretch forming is the most common process for double curved shells and is used in the aerospace industry for forming aircraft skins [97].

- **Stringers:** For chosen L-stringers with a thickness of 3 mm, rubber forming would be the most suitable process. It requires only one product-specific die and can be used for mass production.
- **Conical elements:** Thin metal sheets can be formed into conical shapes using rolling [98]. For that, the first step is to cut out an unfolded component from an aluminum sheet of the desired thickness. Then, the component can be put through a rolling machine that bends it into the desired shape. Lastly, the edges are welded to create a continuous joint. For Al2024, welding can be a challenging process, but it is possible using friction stir welding [99]. Rolling is a very versatile process that can accommodate changes in the design. It is ideal for this design as the wingbox requires multiple elements defined by different radii of curvature. The rolling machine allows for size changes and can be adjusted for each component.
- **Ribs:** Ribs are another structure made out of thin sheet metal with flanged edges and often cutouts in the middle. For cutting the component, abrasive water jet cutting is recommended as it doesn't apply heat that would alter the properties of the material. Then, rubber forming can again be used to form curved flanges or stiffening beads. [97]

Propellers

Propeller blades are chosen to be made out of carbon fiber (CFRP). The most optimal process to achieve the desired shape is lay-up. First, mould has to be made out of different materials to give carbon fiber layers the correct shape. The mould can be reused for further manufacturing of the blades. Then, pieces cut out of prepreg sheets are placed into the mould. Since wet reinforcement is recommended, the product taken out of the mould has to be placed in a vacuum bag to make sure that all the excess air gets removed and there are no voids between the layers. Lastly, the blades need to go through the curing process in the oven. Since carbon fiber is significantly more difficult to recycle than aluminum, it is crucial to make sure as little waste is produced as possible. For cutting out pieces from prepreg sheets, the placement of patterns should be optimized. This can be done using CNC nesting. [97]

16.2.2. Assembly Plan

The assembly of the aircraft concerns more organizational side of the operation. The sequence in which the parts are produced and joined together affects the efficiency of the process and the rate at which new vehicles can be delivered. The work packages making up one subassembly should take approximately the same amount of time for their completion to ensure that the assembly line can continue with no delays [97]. The proposed approach can be seen in Figure 16.1. First, the work is divided into smaller assemblies, such as the wingbox, main, and front fuselage assemblies. They consist of joining the structural elements. In the next stage, aircraft systems and control surfaces are integrated into the product. At that stage, the fuselage can be sealed, surface protection can be applied, and doors and windows can be fitted. Then, some assemblies are joined together, creating integrated wing and fuselage assemblies. Entering the final phase, the wing and fuselage can be joined, and one of the last steps is adding the engines to the assembly, along with the cabin equipment and software uploads. Lastly, necessary system tests are performed to make sure everything is well integrated and the final product can be painted as ordered by the customer. Sufficient quality control should be performed throughout the entire assembly line to ensure that it is up to standard and the final product has no defects.

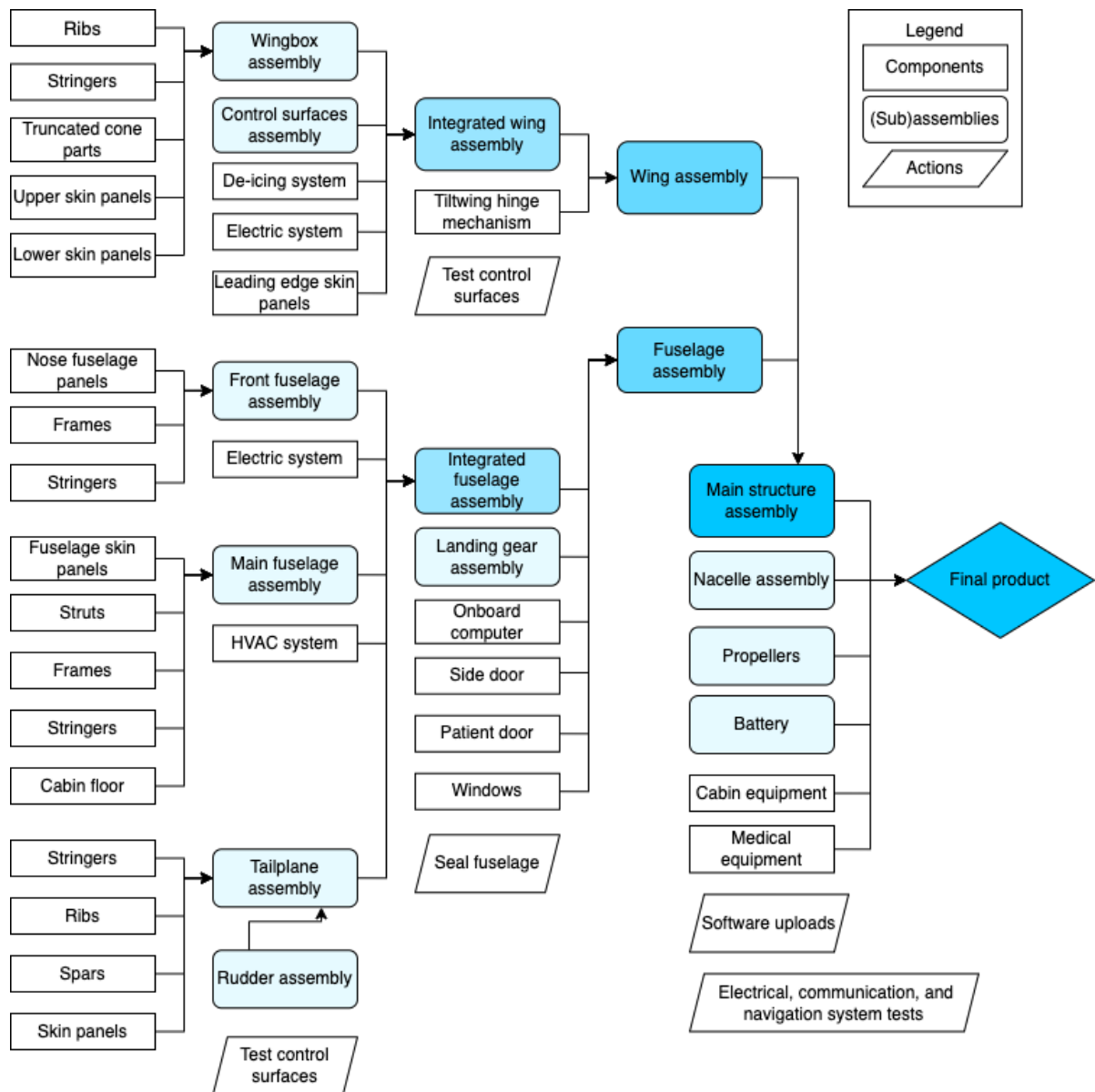
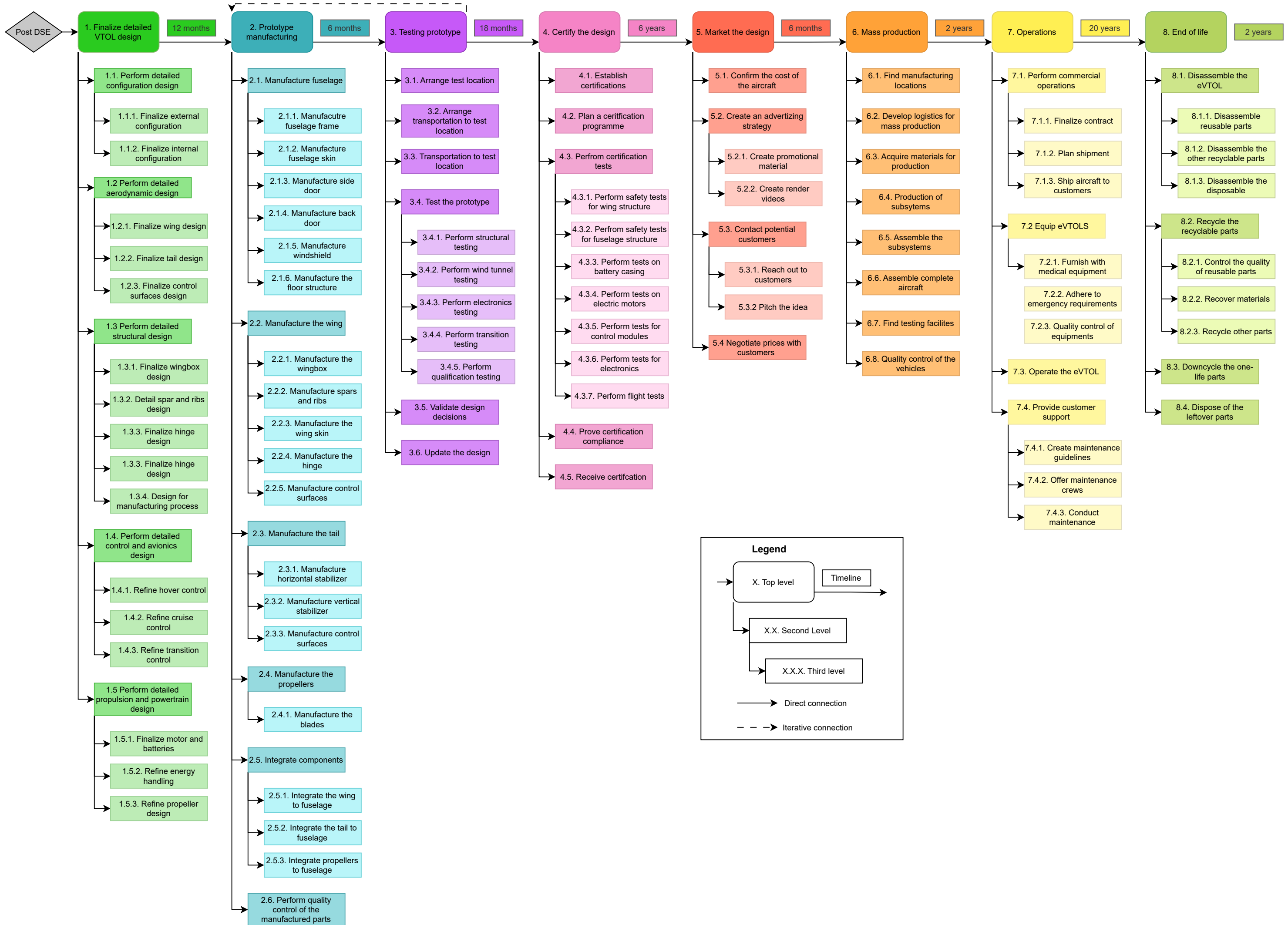


Figure 16.1: Assembly plan



Conclusion

The ResQProp eVTOL ambulance concept addresses a critical gap in emergency medical services by offering a fast, sustainable, and cost-effective alternative to traditional ambulances and helicopters, particularly for rural regions in Central Europe. Through a rigorous design process informed by stakeholder requirements, market analysis, and detailed technical tradeoffs, the final tiltwing configuration was shown to be capable of meeting mission demands with a cruise speed of 200 km/h and a 100 km round-trip range. The latest iteration of the design can be seen in Figure 17.1.

Key innovations such as efficient aerodynamics, electric propulsion, and robust systems design enable rapid response times and simplified operations, while a simple infrastructure strategy ensures compatibility with existing hospital layouts and charging necessities. In terms of sustainability, ResQProp achieves significant reductions in greenhouse gas emissions and noise compared to helicopter alternatives, while offering mission costs competitive with ground ambulances. Additionally, ResQProp improves patient care by transporting patients to the appropriate medical facility, as opposed to helicopters, which only bring a paramedic on scene.

By integrating engineering, operational, economic, and environmental considerations, the ResQProp design demonstrates that eVTOL ambulances are not only technically feasible but also socially and financially scalable. With further development and validation, the system has the potential to revolutionize emergency medical services, improve patient outcomes, and pave the way for a broader adoption of urban air mobility solutions in healthcare.

The most impactful recommendations are related to mission and engineering design, and are the next step in certifying the vehicle. The mission and infrastructure considerations could be further expanded upon by considering less prepared regions in Europe, such as eastern and Nordic mountainous regions, and the Iberian Peninsula.

The vehicle should be further analyzed with more advanced engineering tools available. For example, the aerodynamic and propulsive characteristics should be further optimized and validated using CFD and wind tunnel tests. Furthermore, the structure can be optimized using advanced Finite Element Method solvers to decrease structural mass. A crash structure around the energy storage system must also be considered to certify the vehicle and improve safety in further design steps.



Figure 17.1: *ResQProp in cruise configuration*

Bibliography

- [1] “How many people live 15 minutes away from a hospital? - Products Eurostat News - Eurostat,” , n.d.. URL <https://ec.europa.eu/eurostat/web/products-eurostat-news/-/ddn-20221010-1>.
- [2] Jánošíková, , Jankovič, P, Kvet, M., and Zajacová, E, “Coverage versus response time objectives in ambulance location,” *International Journal of Health Geographics*, Vol. 20, No. 1, 2021, pp. 1–16. doi:10.1186/S12942-021-00285-X;TYPE=ARTICLE;KWRD=EMERGENCY, URL <https://ij-healthgeographics.biomedcentral.com/articles/10.1186/s12942-021-00285-x>.
- [3] “Population on 1 January by broad age group, sex and NUTS 3 region,” , n.d. URL https://ec.europa.eu/eurostat/databrowser/view/demo_r_pjanaggr3__custom_16426352/default/table?lang=en.
- [4] “Germany Ambulance Services Market Size & Outlook,” , 2024. URL <https://www.grandviewresearch.com/horizon/outlook/ambulance-services-market/germany>.
- [5] “How far can an Air Ambulance Helicopter fly?” , n.d.. URL https://www.medical-air-service.com/blog/how-far-can-an-air-ambulance-helicopter-fly_7625.html.
- [6] “Erlang (unit) - Wikipedia,” , n.d. URL https://en.wikipedia.org/wiki/Erlang_%28unit%29?utm_source=chatgpt.com.
- [7] “Annual mission statistics of DRF Luftrettung,” , n.d. URL <https://www.drf-luftrettung.de/en/mediacenter/newsberichte/drf-luftrettung-fordert-verbesserungen-in-der-luftrettung-0>.
- [8] Paoli, A., Pascolini, M., Cipolotti, G., and Spagna, A., “Is Helicopter Really Faster Than Ambulance? The Padua Helicopter Emergency Medical Services Station Experience,” *Air Medical Journal*, Vol. 39, No. 5, 2020, pp. 399–403. doi:10.1016/J.AMJ.2020.05.012, URL <https://www.sciencedirect.com/science/article/pii/S1067991X2030119X>.
- [9] “The fleet | Midlands Air Ambulance Charity,” , n.d. URL <https://www.midlandsairambulance.com/missions/our-fleet/>.
- [10] “Archer successfully completes multiple battery pack drop tests - Green Car Congress,” , n.d. URL <https://www.greencarcongress.com/2024/03/20240329-archer.html>.
- [11] “eVTOL Operational Costs And Profit: “Does Anyone Have a Clue... Yet?” - eVTOL Insights,” , n.d. URL <https://evtolinsights.com/2022/11/evtol-operational-costs-and-profit-does-anyone-have-a-clue-yet/>.
- [12] “Tariefbeschikking regionale ambulancevoorzieningen 2023 - TB/REG-23628-01 - Nederlandse Zorgautoriteit,” , n.d. URL https://puc.overheid.nl/nza/doc/PUC_625934_22/2/.
- [13] “Connect: UNESCO/UNEP environmental education newsletter, vol. XIII, no. 2 - UNESCO Digital Library,” , n.d. URL <https://unesdoc.unesco.org/ark:/48223/pf0000153582>.
- [14] Elkington, J., “Enter the Triple Bottom Line,” n.d.
- [15] “EU Sanctions Map,” , n.d. URL <https://www.sanctionsmap.eu/#/main?search=%7B%22value%22:%22%22,%22searchType%22:%7B%22id%22:2,%22title%22:%22From%20FSD%22%7D%7D>.
- [16] Kurinjimalar Ramu, Ramachandran Manickam, Vimala Saravanan, and Sathiyaraj Chinnasamy, “Assessment on Selection of Appropriate Materials for Fuselage of an Aircraft,” *Aeronautical and Aerospace Engineering*, Vol. 1, No. 1, 2023, pp. 28–36. doi:10.46632/aae/1/1/4.
- [17] “Height, weight and body mass index of the male population,” , 3 2023.
- [18] “Resources | Aerodynamics for Students,” , n.d. URL https://aerodynamics4students.com/aircraft-performance/rotor_momentum_analysis.php.

- [19] "(PDF) Investigating the Spanwise Camber Controversy," , n.d. URL https://www.researchgate.net/publication/321157063_Investigating_the_Spanwise_Camber_Controversy.
- [20] Balster, Coman, Chen, Hendriks, Liu, Moghari, Pieters, Vasilevskis, Wang, and Wiczorowska, "DSE Group 28 - eVTOL Ambulance, Midterm report," , 2025.
- [21] Mercedes-Benz, "Mercedes-Benz Sprinter Brochure," , 2018. URL https://www.auto-brochures.com/makes/Mercedes_Benz/Sprinter/Mercedes%20Benz_US%20Metris-Sprinter_2018-2.pdf.
- [22] ERC System, "We solve the time-cost dilemma of air transportation," , 2025. URL <https://www.erc-system.com>.
- [23] Wikipedia, "Eurocopter EC145," , 2025. URL https://en.wikipedia.org/wiki/Eurocopter_EC145#:~:text=The%20EC145%20features%20a%20larger%20cabin%20space%20than,ft%29%20to%206.0%20m%20%28210%20cu%20ft%29.
- [24] Bell Textron Inc., "SUBARU BELL 412EPX," , 2025. URL <https://www.bellflight.com/products/bell-412>.
- [25] Duffy, M. J., Wakayama, S., Hupp, R., Lacy, R., and Stauffer, M., "A study in reducing the cost of vertical flight with electric propulsion," *17th AIAA Aviation Technology, Integration, and Operations Conference, 2017*, 2017. doi:10.2514/6.2017-3442.
- [26] Nigel, "Cell to Pack Mass Ratio," , n.d. URL <https://www.batterydesign.net/cell-to-pack-mass-ratio/>.
- [27] "Flight performance estimation of a wing + propeller + multirotor-type eVTOL aircraft," , n.d. URL <https://flyingcarevtol.com/news/info/1239.html>.
- [28] Robert H. Kirby, "AERODYNAMIC CH MAC TEFUSTICS OF PROPE LLER-DRIVEN VTOL AIRCRAFT," Tech. rep., 3 1961. URL <https://ntrs.nasa.gov/api/citations/20040047148/downloads/20040047148.pdf>.
- [29] Daniele Carugo, "Politecnico di Torino Corso di Laurea Magistrale in Ingegneria Aerospaziale Development and production costs estimation methodology for eVTOL," Tech. rep., 4 2024.
- [30] Jha, A., Prabhakar, N., Karbowski, D., and German, B., "Urban Air Mobility: A preliminary case study for Chicago and Atlanta," *2022 IEEE Transportation Electrification Conference & Expo (ITEC)*, IEEE, 2022, pp. 300–306. doi:10.1109/ITEC53557.2022.9814052.
- [31] Oliviero, F., "AE3211-I Systems Engineering and Aerospace Design, Aircraft Part," *TU Delft*, 2025.
- [32] Deperrois, A., "XFLR5," , 2024. URL <https://www.xflr5.tech/xflr5.htm>.
- [33] How, J., "Aircraft Lateral Dynamics," , 2003. URL https://ocw.mit.edu/courses/16-61-aerospace-dynamics-spring-2003/1f0a14b69fb824f3892ddb008b037b80_lecture18.pdf.
- [34] Alexander, i. V., "AE3212-I Aerospace Flight Dynamics, Aircraft Part," , 2025.
- [35] CAT, "ELECTRIC POWER RATINGS GUIDE GENERATOR SETS," Tech. rep., 2017.
- [36] H3X Technologies, "H3X Product hpdm-350," , 2025. URL <https://www.h3x.tech/products/hpdm-350>.
- [37] Evolito, "Axial Flux Electric Motors: A Revolutionary Approach," , 2025. URL <https://evolito.aero/axial-flux-motors/>.
- [38] H3X Technologies, "H3X Product HPDI-190," , 2025. URL <https://www.h3x.tech/products/hpdi-190>.
- [39] Aviation International News, "Archer Details Motor and Battery Design for the Midnight eVTOL Air Taxi," , 11 2022. URL <https://www.ainonline.com/news-article/2022-11-18/archer-details-motor-and-battery-design-midnight-evtol-air-taxi>.

- [40] Grepow, "5C High Energy Density Semi-Solid State Battery," , 2025. URL <https://www.grepow.com/nmc811-battery/5c-semi-solid-state-high-energy-density-battery.html>.
- [41] Nigel, "2022 Tesla Model Y 4680," , 12 2022. URL <https://www.batterydesign.net/2022-tesla-model-y-4680/>.
- [42] NXP, "HVBMS Cell Monitoring Unit (CMU)," , 2025.
- [43] Rolls Battery Support, "How Does Temperature Impact Battery Efficiency and Lifespan?" , 9 2023. URL [https://support.rollsbattery.com/en/support/solutions/articles/208147-how-does-temperature-impact-battery-efficiency-and-lifespan-#:~:text=Temperatures%20below%20the%20nominal%2025%C2%BAC%20\(77%C2%BAF\)%20reduce,life.%20Major%20problems%20occur%20at%20temperature%20extremes.](https://support.rollsbattery.com/en/support/solutions/articles/208147-how-does-temperature-impact-battery-efficiency-and-lifespan-#:~:text=Temperatures%20below%20the%20nominal%2025%C2%BAC%20(77%C2%BAF)%20reduce,life.%20Major%20problems%20occur%20at%20temperature%20extremes.)
- [44] Joe Finnerty, "The most common things that drain your electric car battery," , 5 2023. URL <https://www.gridserve.com/what-common-things-drain-your-electric-car-battery-and-by-how-much-#:~:text=Climate%20control&text=Whether%20that%27s%20keeping%20you%20cool,per%20hour%20to%20run%20heaters.>
- [45] Eaton, "Battery configuration switch," , 2025. URL <https://www.eaton.com/us/en-us/catalog/emobility/battery-configuration-switch.html>.
- [46] Adkins, C. N., and Liebeckt, R. H., "Design of optimum propellers," *https://doi.org/10.2514/3.23779*, Vol. 10, No. 5, 2012, pp. 676–682. doi:10.2514/3.23779, URL <https://arc.aiaa.org/doi/10.2514/3.23779>.
- [47] Shi, S., Huo, J., Liu, Z., and Zou, A., "Rapid Design Method of Heavy-Loaded Propeller for Distributed Electric Propulsion Aircraft," *Energies*, Vol. 17, No. 4, 2024, p. 786. doi:10.3390/en17040786.
- [48] Luminary Cloud, "Fine Tuning Joby Aviation's Air Taxi," , 2024. URL <https://www.luminarycloud.com/case-studies/joby/>.
- [49] AXALP, "Propeller Systems for Electric Propulsion," , 2025.
- [50] de Vries, R., van Arnhem, N., Sinnige, T., Vos, R., and Veldhuis, L. L., "Aerodynamic interaction between propellers of a distributed-propulsion system in forward flight," *Aerospace Science and Technology*, Vol. 118, 2021, p. 107009. doi:10.1016/j.ast.2021.107009.
- [51] "AE3212_I_8_Frames_and_Transformations - AE3212-I Aerospace Flight Dynamics & Simulation, including Flight Test (2024/25 Q3)," , n.d. URL <https://brightspace.tudelft.nl/d21/1e/content/684928/viewContent/3902579/View>.
- [52] Ribeiro Lustosa, L., Defaÿ, F., Moschetta, J.-M., Ribeiro, L., and Lustosa, L. R., "Global Singularity-Free Aerodynamic Model for Algorithmic Flight Control of Tail Sitters," *Journal of Guidance, Control, and Dynamics*, Vol. 42, No. 2, 2019. doi:10.2514/1.G003374, URL <https://oatao.univ-toulouse.fr/21708https://doi.org/10.2514/1.G003374>.
- [53] "Propeller Thrust," , n.d. URL <https://www.grc.nasa.gov/www/k-12/airplane/propth.html>.
- [54] "AERODYNAMIC DRAG ON VARIOUS OBJECTS," n.d.
- [55] Anderson, J., "Fundamentals of Aerodynamics," n.d.
- [56] "UIUC Propeller Data Site," , n.d. URL <https://m-selig.ae.illinois.edu/props/propDB.html>.
- [57] Ihnak, M. S., and Edardar, M. M., "Comparing LQR and PID Controllers for Quadcopter Control Effectiveness and Cost Analysis," *2023 IEEE 11th International Conference on Systems and Control, ICSC 2023*, 2023, pp. 754–759. doi:10.1109/ICSC58660.2023.10449763, URL https://www.researchgate.net/publication/378718779_Comparing_LQR_and_PID_Controllers_for_Quadcopter_Control_Effectiveness_and_Cost_Analysis.
- [58] Härkegård, O., "Dynamic Control Allocation Using Constrained Quadratic Programming," n.d. URL <http://www.control.isy.liu.se/ÅLijola>.

- [59] “Copter Attitude Control — Dev documentation,” , n.d. URL <https://ardupilot.org/dev/docs/apmcopter-programming-attitude-control-2.html>.
- [60] “Materials selection for aerospace,” *Introduction to Aerospace Materials*, 2012, pp. 569–600. doi:10.1533/9780857095152.569.
- [61] Michael F Ashbey, *Materials Selection in Mechanical Design*, second edition ed., Butterworth-Heinemann, 1999.
- [62] “Introduction to Aluminum and Aluminum Alloys,” *Metals Handbook Desk Edition*, 1998, pp. 417–423. doi:10.31399/ASM.HB.MHDE2.A0003121, URL <https://dl.asminternational.org/handbooks/edited-volume/49/chapter/598582/Introduction-to-Aluminum-and-Aluminum-Alloys>.
- [63] “Aluminum 2024-T6,” , n.d. URL <https://matweb.com/search/DataSheet.aspx?MatGUID=ecf8530875cb4ded9675b827f77bfac5&ckck=1>.
- [64] T.H.G. Megson, *Aircraft Structures for Engineering Students*, 7th ed., 2022.
- [65] George C. Marshall Space Flight Center, “(NASA-TM-X-73306) Astronautic Structures Manual, Volume 2,” Tech. rep., NASA, 8 1975.
- [66] Curtis, H. D., *Fundamentals of Aircraft Structural Analysis*, 1996.
- [67] “Why helical gear racks are (often) our preference,” , n.d. URL <https://www.apexdyna.nl/en/news/why-helical-racks>.
- [68] Robert P, and Tata, P, “Introduction to Gear Design,” Tech. rep., Woodcliff Lake, 2020.
- [69] “Pressure Angle,” , n.d. URL https://khkgears.net/new/gear_knowledge/introduction_to_gears/pressure_angle.html.
- [70] “Lewis Factor Equation and Calculator for Gear Tooth,” , n.d. URL <https://www.engineersedge.com/gears/lewis-factor.htm>.
- [71] “Know About Type and Strength of Gear Material,” , n.d. URL https://khkgears.net/new/gear_knowledge/the-first-step-of-mechanism-design-using-gears/know-about-type-and-strength-of-gear-material.html.
- [72] “1FW6050-0TB15-1JC3,” , n.d. URL <https://mall.industry.siemens.com/mall/en/WW/Catalog/Product/1FW6050-0TB15-1JC3>.
- [73] Snorri Gudmundsson, *General Aviation Aircraft Design*, n.d.
- [74] Oliviero, F, “Systems Engineering and Aerospace Design: Lateral and Ground,” , n.d.
- [75] Vos, R., and Hooghreef, M., “Aerospace Systems and Engineering Elements: Empenage and Undercarriage Design,” , 2022.
- [76] Roskam, J., and Edward Lan, C.-T., *Airplane Aerodynamics and Performance*, Vol. 12, Design, Analysis and Research Corporation, Kansas, n.d.
- [77] EASA, “Flight Envelope,” Tech. rep., EASA, 3 2016.
- [78] ANSYS, “Ansys Fluent 2022R1,” 2022.
- [79] Delft High Performance Computing Centre (DHPC), “DelftBlue Supercomputer,” , 2024. URL <https://www.tudelft.nl/dhpc/ark:/44463/DelftBluePhase2>.
- [80] Angelica Giovingo, D., “RAMS and Maintenance cost assessment in a Multidisciplinary Design Optimization environment,” Ph.D. thesis, Politecnico di Torino, Torino, 2019.
- [81] Fosnight, D. S., “Rams Engineering, Advancement of Avionic Equipment Tesi di Laurea Magistrale in Ingegneria Aeronautica,” n.d.
- [82] Allen Hamilton, B., “Final Report Urban Air Mobility (UAM) Market Study,” 2018.

- [83] "CO2 emissions per kWh in Germany - Nowtricity," , n.d. URL <https://www.nowtricity.com/country/germany/>.
- [84] Zhou, J., Zhou, X., Yu, W., Shang, Z., and Xu, S., "Towards Greener Recycling: Direct Repair of Cathode Materials in Spent Lithium-Ion Batteries," *Electrochemical Energy Reviews* 2024 7:1, Vol. 7, No. 1, 2024, pp. 1–30. doi:10.1007/S41918-023-00206-5, URL <https://link.springer.com/article/10.1007/s41918-023-00206-5>.
- [85] "Car Recycling Statistics and Facts," , n.d. URL https://www.liveabout.com/auto-recycling-facts-and-figures-2877933?utm_source=chatgpt.com.
- [86] "Aircraft recycling: up to the challenge - Airport Technology," , n.d. URL https://www.airport-technology.com/features/featureaircraft-recycling-up-to-the-challenge-5710942/?utm_source=chatgpt.com&cf-view.
- [87] "Here's what science says about electric cars and their impact on noise pollution - Fast Company," , n.d. URL <https://www.fastcompany.com/90774779/heres-what-science-says-about-electric-cars-and-their-impact-on-noise-pollution>.
- [88] "'Cobalt Red' describes the 'horror show' of mining the element in the DRC : Goats and Soda : NPR," , n.d. URL <https://www.npr.org/sections/goatsandsoda/2023/02/01/1152893248/red-cobalt-congo-drc-mining-siddharth-kara>.
- [89] "Wayback Machine," , n.d. URL https://web.archive.org/web/20220403072425/http://www.witten.de/fileadmin/user_upload/Dokumente/sta10/orecht/or3/314.pdf.
- [90] "Wer zahlt den Rettungseinsatz?" , n.d. URL https://www.ra-meimann.de/b/%E2%80%8Bwer-zahlt-den-rettungseinsatz?utm_source=chatgpt.com.
- [91] Finger, D. F., Goetten, E., Braun, C., and Bil, C., "Cost Estimation Methods for Hybrid-Electric General Aviation Aircraft," *11th Asia-Pacific International Symposium of Aerospace Technology*, 2019.
- [92] Fair Lifts, "A Guide to 2025 Helicopter Prices: What to Expect When Purchasing Your Own Chopper," , 1 2025. URL <https://www.fairlifts.com/helicopters/guide-to-2025-helicopter-prices/>.
- [93] Manatu Aorere, "German Health Market: Hospital Care Reform," 2024. URL <https://www.mfat.govt.nz/assets/Trade-General/Trade-Market-reports/German-Health-Market-Hospital-Care-Reform.pdf#:~:text=A%20Transformation%20Fund%20of%20up%20to%20%E2%82%AC50,has%20been%20controversial%2C%20politically%20and%20among%20stakeholders>.
- [94] Moller, P. S., and Eng, M., "REVIEW OF SELECTED ADVANCED AIR MOBILITY AIRCRAFT," n.d.
- [95] Liliium, "Analyst Presentation," Tech. rep., 6 2021. URL https://web.archive.org/web/20250616153646/https://liliium.com/files/redaktion/refresh_feb2021/investors/20210615_Liliium_Analyst%20Presentation.pdf.
- [96] NASA, "NASA Crash Tests eVTOL Concept," , 12 2022. URL <https://www.nasa.gov/centers-and-facilities/langley/nasa-crash-tests-evtol-concept/>.
- [97] Sinke, J., "AE 3211-II Production of Aerospace Systems (Reader)," , 2023.
- [98] Zagorchev, H., "Sheet metal rolling, or how to make custom-sized pipes and cones," , 11 2020. URL <https://myeusteel.com/sheet-metal-rolling/>.
- [99] Benavides, S., Li, Y., Murr, L., Brown, D., and McClure, J., "Low-temperature friction-stir welding of 2024 aluminum," *Scripta Materialia*, Vol. 41, No. 8, 1999, pp. 809–815. doi:10.1016/S1359-6462(99)00226-2.